Radiative Corrections to W+Jet Production at Hadron Colliders with a Leptonic Decay of the W Boson

Tobias Kasprzik

Freiburg 2009

Radiative Corrections to W+Jet Production at Hadron Colliders with a Leptonic Decay of the W Boson

Tobias Kasprzik

Dissertation

zur Erlangung des Doktorgrades
an der Fakultät für Mathematik und Physik
der
Albert-Ludwigs-Universität
Freiburg im Breisgau

vorgelegt von

Tobias Kasprzik

aus Hamburg

Freiburg, den 31. August 2009

Dekan: Prof. Dr. Kay Königsmann
Erstgutachter: Prof. Dr. Stefan Dittmaier
Zweitgutachter: Prof. Dr. Jürgen Reuter
Tag der mündlichen Prüfung: 15. Oktober 2009

Contents

Zusammenfassung

Die Produktion von W-Bosonen und zusätzlichen QCD-Jets am LHC ist von großem phänomenologischen Interesse. Da diese Prozesse sehr große Wirkungsquerschnitte besitzen, können sie, auch wegen der klaren leptonischen Zerfalls-Signatur des W-Bosons, beispielsweise für eine präzise Bestimmung der W-Masse oder zur Kalibrierung der Kollider-Luminosität verwendet werden. Ein profundes theoretisches Verständnis dieser Prozessklasse ist daher erstrebenswert.

Um die Präzision der theoretischen Vorhersagen voranzutreiben, werden in dieser Arbeit die elektroschwachen Strahlungskorrekturen in nächst-führender Ordnung der Kopplungskonstanten α im Rahmen des Standard-Modells zur W+jet-Produktion am LHC und am Tevatron berechnet und die resultierenden Effekte diskutiert. Da die Korrekturen zunächst in einem perturbativen Zugang auf Parton-Niveau ausgewertet werden, arbeiten wir im Parton-Modell, in dem die perturbativen Anteile mit den nicht-perturbativen Parton-Verteilungsfunktionen gefaltet werden, um realistische hadronische Wirkungsquerschnitte zu erhalten.

Die Rechnung wird sowohl für ein stabiles W-Boson auf seiner Massen-Schale durchgeführt, als auch für ein intermediäres, leptonisch zerfallendes W-Boson. Neben virtuellen Schleifen-Korrekturen müssen hierbei auch reelle Bremsstrahlungs-Korrekturen, verursacht durch die Abstrahlung eines zusätzlichen Photons, berücksichtigt werden, wobei in beiden Anteilen sogenannte Massen-Singularitäten auftreten, die in der numerischen Auswertung sorgfältig behandelt werden müssen. Für die Rechnung mit stabilem W-Boson verwenden wir die Methode des *Phase-Space-Slicings*, um diese Singularitäten von der numerischen Phasenraum-Integration auszuschließen und sie in den problematischen Bereichen des Phasenraumes analytisch auszuwerten. In der Rechnung mit instabilem W-Boson hingegen werden die singulären Strukturen mittels der Methode der Dipol-Subtraktion auf dem Niveau des Bremsstrahlungs-Integranden subtrahiert, um eine stabile numerische Auswertung zu garantieren. Um eine konsistente Berechnung auch von nicht-kollinear-sicheren Observablen zu ermöglichen, haben wir diese Subtraktions-Methode im Rahmen der vorliegenden Arbeit entsprechend erweitert.

Neben dem Auftreten von Massen-Singularitäten beinhaltet die Berechnung der Strahlungskorrekturen zu Prozessen mit instabilem W-Boson die Schwierigkeit, dass eine endliche Zerfallsbreite in die Rechnung eingeführt werden muss. Geschieht dies in unüberlegter Weise, kann schon in führender Ordnung die Eichinvarianz der Amplitude verletzt sein. Wir arbeiten daher im *Complex-Mass-Scheme*, das eine konsistente und eichinvariante Behandlung der endlichen Lebensdauer des W-Bosons garantiert und in allen Regionen des Phasenraumes angewendet werden kann.

Unsere Resultate sind in einem flexiblen Monte-Carlo Programm implementiert, das es ermöglicht – neben totalen Wirkungsquerschnitten – alle physikalisch motivierten differentiellen Wirkungsquerschnitte in Form von Histogrammen zu generieren. Es kann daher zukünftig als Analyse-Tool für LHC-Daten verwendet werden, zumal die numerische Auswertung – neben großen negativen elektroschwachen Korrekturen bei hohen Transversal-Impulsen – wichtige Korrekturen zur Verteilung der transversalen Masse des Lepton-Paares in der Resonanz-Region ergibt, die für eine präzise Bestimmung der W-Masse berücksichtigt werden sollten.

Abstract

The production of W bosons and additional jets at hadron colliders is a topic of great phenomenological interest, because such processes have large cross sections and, owing to the clear decay signature of the W boson, can for instance be used to monitor and calibrate the collider's luminosity, as well as for a precise determination of the W-boson mass and width. Thus, a profound theoretical understanding of this process class is mandatory.

In order to improve the accuracy of the theoretical predictions, this thesis is devoted to the calculation of the electroweak radiative corrections to the production of one W boson with one associated jet at the LHC and the Tevatron within the Standard Model. Since these corrections are at first evaluated on the parton level in a perturbative approach, we work in the parton model, where the hadronic cross section is obtained by folding the partonic contributions with the parton distribution functions that contain the non-perturbative information of the proton structure and have to be determined by experiment.

We provide results for a stable W boson that is produced on its mass shell as well as for an intermediate (off-shell) W boson decaying into a charged lepton and a neutrino. For a consistent calculation of the next-to-leading order corrections, we have to take into account the virtual one-loop contributions, as well as the real bremsstrahlung corrections caused by radiation of one additional photon. Within both contributions, mass singularities appear that have to be treated with care within the numerical evaluation. In the calculation with a stable W boson in the final state, we use the method of phase-space slicing in order to exclude such singularities from the numerical phase-space integration and calculate them analytically in the problematic phase-space regions. For the off-shell calculation, however, we use the more sophisticated dipole subtraction technique to subtract the infrared-singular structures on the integrand level to allow for a stable numerical evaluation. Within this thesis, we extend this method to also enable the consistent treatment of non-collinear-safe observables related to photon radiation off muons.

Additionally, the calculation of radiative corrections to processes involving an unstable W boson leads to the problem that a finite particle width has to be consistently introduced in the calculation. If this is done carelessly, gauge invariance might be destroyed even at the leading order of the perturbative series. Thus, we work in the complex-mass scheme to account for a proper inclusion of a finite W-boson width in our calculation. This particular scheme respects gauge invariance and can be applied in all phase-space regions.

Our results are implemented into a flexible Monte Carlo code that allows for the calculation of total cross sections and differential distributions, where in principle any event-selection criteria that might be of physical interest can be applied. In the numerical analysis we observe large negative electroweak corrections at large transverse momenta that can be attributed to universal Sudakov logarithms. Moreover, relevant deviations in the shape of the transverse-mass distribution of the final-state lepton pair near the resonance are induced that are important with regard to a precise determination of the W mass. Thus, our code can provide crucial information as a tool for the analysis of LHC data.

Chapter 1

Motivation and introduction

The production of electroweak (EW) W and Z^0 bosons with subsequent leptonic decays is one of the most prominent Standard Model (SM) processes at present and future hadron colliders like the Fermilab Tevatron and the CERN Large Hadron Collider (LHC). The signatures are clean owing to the final-state leptons, and the cross sections are large. In particular, the cross section for W-boson production at the LHC will be about ten times as big as for Z^0 production, corresponding to 200 events per second with a leptonic decay of the W boson, when the collider operates at its design luminosity of $\mathcal{L}_{\mathrm{LHC}} = 10^{34}\ \mathrm{cm}^{-2}/\mathrm{s}$.

Due to the large cross sections and the resulting high statistics even at lower-luminosity runs, the investigation of the charged-current Drell–Yan process

$$\mathrm{pp} \to \mathrm{W} + X \to l\nu_l + X \tag{1.0.1}$$

at the LHC will provide the possibility to directly measure the mass (M_{W}) and width (Γ_{W}) of the W boson with the highest accuracy ever. For this purpose, the distributions of the lepton transverse momentum ($p_{\mathrm{T},l}$) or the transverse mass of the lepton pair ($M_{\mathrm{T},l\nu_l}$) that are obtained by experiment are compared to the theoretical predictions in a fitting procedure [1, 2], since those leptonic observables exhibit a sensitive dependence on M_{W} and Γ_{W} and are also well-suited for experimental reconstruction.

As pointed out in Ref. [2], a precise knowledge of M_{W} and Γ_{W}—which are essential parameters of the SM—is desirable, since a comparison of direct measurements in single-W production at the LHC with indirect measurements from a global fit to EW precision data measured at LEP1/SLD [3], will provide a powerful test of the validity of the SM, i.e. any significant disagreement could be interpreted as a hint to new physics beyond the Standard Model (BSM). Aside, a precise determination of M_{W} and the top-quark mass m_{t} will also allow us to further indirectly constrain the bounds on the mass M_{H} of a SM Higgs boson.

The current values for M_{W} and Γ_{W} stated by the Particle Data Group [4] are

$$M_{\mathrm{W}} = 80.398 \pm 0.025\,\mathrm{GeV}, \quad \Gamma_{\mathrm{W}} = 2.141 \pm 0.041\,\mathrm{GeV}\,. \tag{1.0.2}$$

They are obtained combining results from direct measurements at LEP and the Tevatron. At the LHC, the (expected) experimental accuracy is so excellent that one hopes to further improve the precision measurement of M_{W} to an accuracy of $\delta_{M_{\mathrm{W}}} = 15\,\mathrm{MeV}$ [5], where generally the highest precision for the determination of the W mass can be achieved by fitting

the $M_{\mathrm{T},l\nu_l}$ distribution near the Jacobian peak. In Ref. [1], the ATLAS collaboration even states that for each exploitable leptonic W-boson decay channel ($\mathrm{W} \to \mathrm{e}\nu_\mathrm{e}$, $\mathrm{W} \to \mu\nu_\mu$), and for an integrated luminosity[1] of 10 fb^{-1}, an accuracy of $\delta_{M_\mathrm{W}} = 7\,\mathrm{MeV}$ on the W-boson mass is aspired in the high-precision mass determination. Additionally, the line-shape of the $M_{\mathrm{T},l\nu_l}$ distribution in the off-shell region will give access to an accurate direct determination of Γ_W that might lead to a reduction of the corresponding uncertainty to $\delta_{\Gamma_\mathrm{W}} = 30\,\mathrm{MeV}$ after an accumulated luminosity of 10 fb^{-1} is reached [2].

In addition to its relevance for mass determination, W-boson production can provide important information in the fit of the parton distribution functions (PDFs) for valence- and sea quarks by investigating the W-boson charge asymmetry [2]

$$A(y_l) = \frac{\mathrm{d}\sigma^+/\mathrm{d}y_l - \mathrm{d}\sigma^-/\mathrm{d}y_l}{\mathrm{d}\sigma^+/\mathrm{d}y_l + \mathrm{d}\sigma^-/\mathrm{d}y_l}\,, \tag{1.0.3}$$

at the LHC and the Tevatron, where

$$\mathrm{d}\sigma^\pm = \mathrm{d}\sigma(\mathrm{pp}/\mathrm{p\bar{p}} \to l^\pm\nu_l + X)\,, \tag{1.0.4}$$

and y_l denotes the rapidity of the charged lepton. Due to the high production rates, W events may also serve as a luminosity monitor at the LHC, and they will help to understand the detector performance in the early stage of data analysis [6]. Moreover, at high energies, W bosons deliver background to searches for new heavy charged W' gauge bosons that are predicted in several extensions of the SM [7].

At hadron colliders, the EW gauge bosons are (almost) always produced together with additional QCD radiation. The production cross section of W bosons in association with a hard, visible jet,

$$\mathrm{pp}/\mathrm{p\bar{p}} \to \mathrm{W} + \mathrm{jet} + X \to l\nu_l + \mathrm{jet} + X, \tag{1.0.5}$$

is still large. Moreover, the intermediate W boson recoils against the jet leading to a new kinematical situation with boosted W bosons. For large p_T of the jet the corresponding events contain charged leptons and/or neutrinos with large p_T. In fact, in the SM, $\mathrm{W} + \mathrm{jet(s)}$ production is the largest source for events with large missing transverse momentum where also a charged lepton is present for triggering. Hence, $\mathrm{W} + \mathrm{jet(s)}$ production is not only a SM candle process. It is also an important background for a large class of new-physics searches based on missing transverse momentum. In particular, $\mathrm{W} + \mathrm{jet(s)}$ production plays a crucial role—besides $\mathrm{Z}^0 + \mathrm{jet(s)}$ production and $\mathrm{t\bar{t}}$ events—in the one-lepton search mode for $\mathcal{R}$-parity-conserving supersymmetry (SUSY) scenarios at the LHC [8]. Apart from BSM-physics searches, $\mathrm{W} + 2\,\mathrm{jets}$ production also has to be considered as a background process to the possible discovery channel

$$\mathrm{pp} \to \mathrm{W} + \mathrm{H}^0 \to l\nu_l + \mathrm{b\bar{b}} \tag{1.0.6}$$

for a light SM Higgs boson which is produced via Higgs Strahlung and subsequently decays into a $\mathrm{b\bar{b}}$ pair [9, 10].

To match the prospects and experimental importance of W+jet(s) production at hadron colliders, excellent theoretical predictions are mandatory. The differential cross section for

[1] The value of 10 fb^{-1} will be reached after one year of stable running at a luminosity of $\mathcal{L} = 10^{33}\ \mathrm{cm}^{-2}/\mathrm{s}$, corresponding to about $4{\cdot}10^7$ W events with a leptonic decay in the exploitable channels.

W-boson production is known at NNLO accuracy with respect to QCD corrections [11] and even up to N^{3}LO in the soft-plus-virtual approximation [12]. The next-to-leading-order (NLO) QCD corrections have been matched with parton showers [13] and combined with a summation of soft gluon radiation (see ,e.g., Ref. [14]), which is particularly important to reliably predict the transverse-momentum distribution of the W bosons for small p_{T}. A theoretical study of the QCD uncertainties in the determination of the W cross section at hadron colliders has been presented in Ref. [15]. Concerning EW corrections, the full NLO [16, 17, 18, 19] and leading higher-order effects, in particular due to multi-photon final-state radiation [19, 20, 21, 22], have been calculated. The contributions of photon-induced processes have been discussed in Refs. [22, 23, 24]. First steps towards combining QCD and EW higher-order effects have been taken in Refs. [25, 26]. The NLO QCD and EW corrections have also been calculated within the Minimal Supersymmetric Standard Model (MSSM) [22].

The cross section for $\mathrm{W}+1\,\mathrm{jet}$ [27, 28] and $\mathrm{W}+2\,\mathrm{jets}$ [28] production is known at NLO QCD, and the calculation of the NLO QCD corrections for the $\mathrm{W}+3\,\mathrm{jets}$ cross section has recently been completed [29, 30].

Since there has been such a great progress with respect to precision calculations for $\mathrm{W}+\mathrm{jet(s)}$ production on the QCD side, it is an important task to match this high accuracy also in the EW sector. Since the NLO QCD corrections to $\mathrm{W}+\mathrm{jet}$ production formally provide a perturbative accuracy of $\mathcal{O}(\alpha^2\alpha_{\mathrm{s}}^2)$, a logical next step is to press ahead with the calculation of the corresponding EW corrections that will deliver an even higher accuracy of $\mathcal{O}(\alpha^3\alpha_{\mathrm{s}})$. For this reason, within this thesis we will present the calculation of the full EW corrections to the hadronic process (1.0.5) within the SM, and provide a substantial discussion of the numerical results.

As a reasonable starting point, we first present a fixed-order calculation of the EW radiative corrections to the hadroproduction of an on-shell W boson with one associated jet at the LHC and the Tevatron, where we put a special focus on a physically sensible definition of jet observables. Within this on-shell approach, we are not forced to deal with subtleties according to the finite width of the W boson, but, on the other hand, are also not capable of describing observables that are related to its leptonic decay products. The on-shell calculation presented in this work is an extension of my Diploma thesis [31] that was elaborated at the University of Hamburg under the supervision of Bernd Kniehl.

The largest part of the thesis is then devoted to the calculation of the NLO EW corrections to $\mathrm{W}+\mathrm{jet}$ hadroproduction with a leptonic final state as in (1.0.5). Since the inclusion of a finite particle width within a fixed-order perturbative calculation is a non-trivial task, we describe how the W resonance can be treated consistently using the complex-mass scheme [32, 33]. Another important topic we discuss in detail is—as in the on-shell calculation—the definition of physically meaningful jet observables.

We want to point out that all off-shell effects due to the finite width of the W boson are included in our calculation. Our results have been implemented in a fully flexible Monte Carlo code which is able to calculate binned distributions for all physically relevant $\mathrm{W}+1\,\mathrm{jet}$ observables at NLO accuracy.

As will be discussed later, in real-emission events we are confronted with a soft-gluon singularity that appears in the phase-space integration if the energy of a radiated gluon

becomes arbitrarily small. This singularity will destroy the perturbative result if not treated with special care. To solve this problem, we distinguish W + jet and W + photon production by a cut on the photon energy fraction inside the jet, employing a measured quark-to-photon fragmentation function [34], if the photon and the jet are collinear in phase space.

To reach the accuracy of $\mathcal{O}(\alpha_s\alpha^3)$ throughout the calculation we have also included the photon-induced partonic processes and the respective NLO QCD corrections. Also non-trivial interference terms between EW and QCD diagrams within the real corrections have been included at this order. Moreover, we have recalculated the NLO QCD corrections at $\mathcal{O}(\alpha_s^2\alpha^2)$ in a fully flexible way, supporting a phase-space dependent choice for the factorization and renormalization scales.

Our calculation is completely generic in the sense that it can predict observables that are dominated by W bosons close to their mass shell as well as observables for which the exchanged W boson is far off-shell. The calculation of the EW corrections for W-boson production in association with a hard jet is also a step towards a better understanding of the interplay between QCD and EW corrections for W production in general. This understanding—including a full treatment of off-shell W bosons—is important to match the envisaged experimental accuracy for the W-mass measurement at the Tevatron and the LHC [26].

In the calculation of radiative corrections to SM processes including light or massless particles, one has to face the problem of so-called mass singularities. Such singularities have to be treated carefully in the evaluation of cross sections. Over the last decades, different techniques have been developed to handle these singularities in such a way that they can be controlled on the analytical level. One possibility to extract the mass singularities from the numerical evaluation is to exclude the problematic phase-space regions by means of *slicing* parameters, and to evaluate the singular structures analytically using appropriate regulators. The non-singular structures of the phase-space integrals can then be computed analytically without regulators. This method is known as *phase-space slicing*. We have applied the slicing approach within the on-shell calculation outlined above.

Besides the well-known slicing prescriptions, there are several *subtraction techniques* in the literature that follow a different strategy. Within this approach, an auxiliary function is subtracted from the singular integrand that is constructed in such a way that it cancels all mass-singular structures of the integrand pointwise during the numerical integration. This auxiliary function is then integrated analytically over the singular phase-space structures using proper regulators, and readded to the result afterwards. In the end, the same contribution is readded that has been subtracted before, but the mass singularities are excluded from the involved numerical integration. Specifically, the treatment of mass singularities connected to photon radiation off fermions using the *dipole subtraction method* has been worked out in Ref. [35].

However, attacking the challenge of the calculation of EW corrections to W + jet hadroproduction including a leptonic decay of the W boson, we are facing the problem of collinear singularities related to photon emission off final-state muons. To allow for the calculation of observables where a collinear photon–muon pair can be separated by experiment, we extend the dipole subtraction technique for so-called non-collinear-safe observables within this thesis.

This thesis is organized as follows:

- In Chapter 2 we first discuss the most important features of the Standard Model of particle physics. Then we address the topic of a finite particle width in a fixed-order NLO calculation, where we put special emphasis on the complex-mass scheme for unstable particles. Finally, we outline how hadronic cross sections can be calculated from partonic cross sections that are obtained in a perturbative approach.

- Chapter 3 is devoted to the important topic of infrared (IR) or mass singularities in QED and QCD. The origin of such singularities is explained, and we discuss in detail how the different types of IR singularities have to be dealt with to obtain consistent physical results.

- Chapter 4 contains a rather technical discussion of the dipole subtraction method in NLO QED and QCD that was developed to enable the treatment of IR singularities within real radiative corrections in a general and straight-forward way. Building on these concepts, we have extended the dipole subtraction method to the treatment of non-collinear-safe observables in QED [36].

- In Chapter 5 we present a detailed discussion of the calculation of the EW corrections to on-shell W + jet production at hadron colliders, closely following Ref. [37]. This chapter is in principle self-contained and can be read as a preparation to the more-involved off-shell calculation. Results for the same class of corrections have also been published in Refs. [38, 39], where a slightly different definition of jet observables was used. For a discussion of virtual SUSY effects on W + jet production we refer the reader to Ref. [40].

- Chapter 6 contains a discussion of our general strategy for the calculation of the radiative corrections to W + jet hadroproduction including a leptonic decay of the W boson. We list the different contributions to the NLO cross section and present the relevant physical concepts that are applied within the computation of the radiative corrections, always referring to the parts of the thesis where those problems are elaborated in more detail.

- In Chapter 7, we list the amplitudes that contribute to process (1.0.5) on the parton level at LO, using the Weyl–van-der-Waerden spinor formalism that is outlined at the beginning of the chapter.

- In Chapter 8, we provide the contributions explicitly that have to be calculated within the real-radiation processes, covering the EW and QCD corrections as well as the interference contributions of QCD and EW diagrams.

- Chapter 9 contains a discussions of the virtual EW and QCD corrections, including the counterterm contributions that have to be taken into account to absorb the ultraviolet (UV) divergences that appear in the one-loop amplitudes.

- In Chapter 10 we define the recombination procedure and the event-selection cuts we apply to define physical observables from final-state momenta. Additionally, we present the explicit formulae that are needed to calculate the hadronic cross

sections from the partonic ones, including an explicit prescription of how the NLO contributions have to be included into the hadronic calculation.

- Before we conclude in Chapter 12, we provide a discussion of the numerical results in Chapter 11. The contents presented in Chapters 6 – 11 have been published in Ref. [41].

Chapter 2

Theoretical background

2.1 The Standard Model of particle physics

The Standard Model of particle physics (SM) describes the electroweak (EW) and the strong interactions of elementary particles as a relativistic quantum field theory (QFT) which is formulated in terms of a local non-abelian gauge theory with the underlying gauge group

$$\mathrm{SU(3)_C} \times \mathrm{SU(2)_W} \times \mathrm{U(1)_Y}\,. \tag{2.1.1}$$

Here, the colour group $\mathrm{SU(3)_C}$ denotes the internal symmetry group of the strong interaction that is described by the theory of *Quantum Chromodynamics* (QCD) [42, 43, 44]. In the EW part of the SM, the group $\mathrm{SU(2)_W}$ represents the symmetry group of the weak isospin with the three generators I^a, $a = 1, 2, 3$, and the group $\mathrm{U(1)_Y}$ is generated by the weak hypercharge Y.

The fermionic matter fields transform in the fundamental representation of the symmetry group (2.1.1), while the bosonic gauge fields that mediate the forces between particles live in the adjoint representation. The classical Lagrangian $\mathcal{L}_\mathrm{C}$ that governs the physical interactions of massless fermions and gauge bosons is constructed in such a way that it is invariant under local gauge transformations of the symmetry group (2.1.1). Some basic definitions for gauge groups and Lie algebras can be found in Appendix A.2.

Unfortunately, explicitly introducing mass terms for the weak vector bosons or the fermions would violate the local gauge symmetry of the Lagrangian. Therefore, within the EW part of the SM, vector-boson masses and fermion masses are generated via the Higgs mechanism [45]: By introducing an additional complex scalar field (the Higgs field) with a non-vanishing vacuum expectation value (vev) in the EW sector, the local $\mathrm{SU(2)_W} \times \mathrm{U(1)_Y}$ symmetry is spontaneously broken, and only the electromagnetic gauge symmetry $\mathrm{U(1)_{em}}$ is preserved. As a result, three of the four vector bosons receive masses, and only one degree of freedom that later can be identified with the photon field stays massless, as it is observed in experiment.

Spontaneous symmetry breaking also generates fermion masses through the Yukawa couplings of the Higgs field to the fermion fields. Nevertheless, those Yukawa terms have to be inserted into the classical Lagrangian by hand, while the couplings of the Higgs field to the massive gauge bosons are generated by the covariant derivative. In the QCD sector

of the SM the gauge symmetry remains unbroken, and the eight vector bosons (gluons) that correspond to the eight generators of $\mathrm{SU}(3)_\mathrm{C}$ are exactly massless.

To allow for a correct quantization of a non-abelian gauge theory via the path-integral formalism, one has to solve the problem of divergences in the corresponding functional integral that are caused by the integration over physically equivalent configurations which are related by gauge transformations. Following the ansatz of Faddeev and Popov [46], one introduces a gauge-fixing condition into the functional integral and rewrites the underlying *effective Lagrangian* according to

$$\mathcal{L}_\mathrm{eff} = \mathcal{L}_\mathrm{C} + \mathcal{L}_\mathrm{fix} + \mathcal{L}_\mathrm{FP}\,, \tag{2.1.2}$$

where the gauge-fixing Lagrangian $\mathcal{L}_\mathrm{fix}$ contains the gauge parameter ξ, and the Faddeev–Popov contribution $\mathcal{L}_\mathrm{FP}$ describes the interactions of gauge bosons and the Grassmann-valued *Faddeev–Popov ghost fields*. These anticommuting scalar fields violate the spin-statistics theorem. However, this does not raise any problems, because they are unphysical degrees of freedom which occur in perturbative calculations only inside loops.

We will now briefly discuss the matter content of the SM and the overall structure of the EW and the strong interaction, both to fix our notation and to provide the reader with the concepts that build the framework of this thesis.

2.1.1 The EW part of the SM

We now outline the most important ingredients and principles that govern the EW interactions of elementary particles, following the presentation of [47]. For an extensive discussion of this subject we refer the reader to Chapter 4 of [48].

The EW sector of the SM (EWSM), also known as the Glashow–Salam–Weinberg (GSW) model [49], describes the fundamental EW interactions of all known elementary spin-$\frac{1}{2}$ fermions. To ensure local gauge symmetry of the Lagrangian that determines the free propagation of those fermions, one introduces bosonic degrees of freedom into the theory that couple to the fermion fields by means of a covariant derivative.

In nature one observes three generations of left-handed quarks and leptons that transform as $\mathrm{SU}(2)_\mathrm{W}$ doublets,

$$L_j'^\mathrm{L} = \begin{pmatrix} \nu_j'^\mathrm{L} \\ l_j'^\mathrm{L} \end{pmatrix}\,, \quad Q_j'^\mathrm{L} = \begin{pmatrix} u_j'^\mathrm{L} \\ d_j'^\mathrm{L} \end{pmatrix}\,, \tag{2.1.3}$$

where $j = 1, 2, 3$ is the generation index. The right-handed leptons, up-, and down-type quarks $l_j'^\mathrm{R}$, $u_j'^\mathrm{R}$, and $d_j'^\mathrm{R}$ transform as $\mathrm{SU}(2)_\mathrm{W}$ singlets. In contrast to the leptons, the quarks also take part in the strong interaction that will be discussed in Section 2.1.2. In (2.1.3), the prime indicates that we assume the fermions to be eigenstates of the EW interaction. The elementary fermions can be classified according to the third component I^3 of the weak isospin and their weak hypercharge Y, and the electric charge Q of a fermion is given by the Gell-Mann–Nishijima formula,

$$Q = I^3 + \frac{Y}{2}\,. \tag{2.1.4}$$

As a classical field theory, the EW interactions are described by the classical Lagrangian $\mathcal{L}_{\mathrm{C}}$ that is given by the sum of a Yang–Mills part, a fermionic part, a Higgs part, and a Yukawa part,

$$\mathcal{L}_{\mathrm{C}} = \mathcal{L}_{\mathrm{gauge}} + \mathcal{L}_{\mathrm{ferm}} + \mathcal{L}_{\mathrm{Higgs}} + \mathcal{L}_{\mathrm{Yukawa}}\,, \tag{2.1.5}$$

where all contributions are separately gauge invariant. We will now discuss the different contributions in some detail.

Interactions of fermions and weak gauge bosons

The Yang–Mills part $\mathcal{L}_{\mathrm{gauge}}$ governs the kinematic properties of the weak gauge fields W_μ^a, $a = 1, 2, 3$, and B_μ that can be associated with the connections of $\mathrm{SU}(2)_{\mathrm{W}}$ and $\mathrm{U}(1)_{\mathrm{Y}}$, respectively. We define the field-strength tensors

$$\begin{aligned} B_{\mu\nu} &= \partial_\mu B_\nu - \partial_\nu B_\mu\,, \\ W_{\mu\nu}^a &= \partial_\mu W_\nu^a - \partial_\nu W_\mu^a + g_2 \epsilon^{abc} W_\mu^b W_\nu^c\,, \end{aligned} \tag{2.1.6}$$

where the ϵ^{abc} denote the total-antisymmetric structure functions of $\mathrm{SU}(2)_{\mathrm{W}}$, and g_2 is the corresponding coupling constant. The gauge contribution to the Lagrangian can now be written as

$$\mathcal{L}_{\mathrm{gauge}} = -\frac{1}{4} W_{\mu\nu}^a W^{\mu\nu,a} - \frac{1}{4} B_{\mu\nu} B^{\mu\nu}\,. \tag{2.1.7}$$

We also introduce the covariant derivative

$$D_\mu = \partial_\mu - \mathrm{i} g_2 I^a W_\mu^a + \mathrm{i} g_1 \frac{Y}{2} B_\mu\,, \tag{2.1.8}$$

where g_1 is the $\mathrm{U}(1)_{\mathrm{Y}}$ coupling constant. Employing (2.1.8), the fermionic Lagrangian that describes the physics of the free massless fermion fields and the interactions of fermions with gauge bosons can be specified as

$$\mathcal{L}_{\mathrm{ferm}} = \sum_{i=1}^{3} \left(\overline{L'}_i^{\mathrm{L}} \mathrm{i} \not{D} L_i'^{\mathrm{L}} + \overline{Q'}_i^{\mathrm{L}} \mathrm{i} \not{D} Q_i'^{\mathrm{L}} + \overline{l'}_i^{\mathrm{R}} \mathrm{i} \not{D} l_i'^{\mathrm{R}} + \overline{u'}_i^{\mathrm{R}} \mathrm{i} \not{D} u_i'^{\mathrm{R}} + \overline{d'}_i^{\mathrm{R}} \mathrm{i} \not{D} d_i'^{\mathrm{R}} \right)\,. \tag{2.1.9}$$

Spontaneous symmetry breaking – the Higgs mechanism

Until now, the fermion and gauge-boson fields that are part of the gauge theory with unbroken EW symmetry are exactly massless. To generate particle masses, in $\mathcal{L}_{\mathrm{Higgs}}$ we introduce a single complex scalar field

$$\Phi(x) = \begin{pmatrix} \phi^+(x) \\ \phi^0(x) \end{pmatrix} \tag{2.1.10}$$

with hypercharge $Y_\Phi = 1$ that transforms as an $\mathrm{SU}(2)_{\mathrm{W}}$ doublet and is coupled to the gauge fields of the theory via the covariant derivative (2.1.8),

$$\mathcal{L}_{\mathrm{Higgs}} = (D_\mu \Phi)^\dagger (D^\mu \Phi) - V(\Phi)\,. \tag{2.1.11}$$

The so-called Higgs potential

$$V(\Phi) = \frac{\lambda}{4}(\Phi^\dagger\Phi)^2 - \mu^2(\Phi^\dagger\Phi)\,, \quad \lambda,\, \mu^2 > 0\,, \tag{2.1.12}$$

where λ denotes the Higgs self coupling, and μ^2 is a mass parameter, initiates the spontaneous symmetry breaking in the following way:

The minimum of the potential $V(\Phi)$ is degenerate, i.e. all field configurations that fulfill the condition

$$|\Phi|^2 = \frac{v^2}{2}\,, \quad v = 2\mu/\lambda\,, \tag{2.1.13}$$

minimize the potential $V(\Phi)$, and the non-vanishing vev of the Higgs potential is given by $|\langle 0|\Phi|0\rangle| = v/\sqrt{2}$. While different vacuum states that obey the condition (2.1.13) are mapped onto each other by $\mathrm{SU(2)_W}$ transformations, a specific ground state does not exhibit $\mathrm{SU(2)_W}$ symmetry anymore. Therefore, choosing

$$\Phi_0 = \frac{1}{\sqrt{2}}\begin{pmatrix} 0 \\ v \end{pmatrix} \tag{2.1.14}$$

as vacuum state, the $\mathrm{SU(2)_W \times U(1)_Y}$ symmetry is spontaneously broken, since Φ_0 is in general not invariant under the corresponding gauge transformations. However, the invariance with respect to transformations of the electromagnetic gauge group $\mathrm{U(1)_{em}}$ is preserved, because the non-vanishing vev only affects the ϕ^0 component of Φ that is electrically neutral.

In perturbation theory, the scalar doublet Φ has to be expanded around its vev according to

$$\Phi(x) = \begin{pmatrix} \phi^+(x) \\ \frac{1}{\sqrt{2}}\left[v + H(x) + \mathrm{i}\,\chi(x)\right] \end{pmatrix}, \quad \phi^-(x) = \left[\phi^+(x)\right]^*. \tag{2.1.15}$$

The fields $\phi^\pm$ and χ can be eliminated by an adequate gauge transformation and therefore are not related to physical particles, whereas the real scalar field $H(x)$ corresponds to the neutral scalar Higgs particle H^0 that contributes to the particle content of the SM. The mass of the Higgs particle,

$$M_\mathrm{H} = \sqrt{2}\mu\,, \tag{2.1.16}$$

is a free parameter of the SM that cannot be derived from other known quantities.

The Yukawa contributions to the SM Lagrangian are obtained by introducing interaction terms of fermions with the field Φ in the theory,

$$\mathcal{L}_\mathrm{Yukawa} = \sum_{i,j=1}^{3}\left(\overline{L'}_i^\mathrm{L} G^l_{ij} l'^\mathrm{R}_j \Phi + \overline{Q'}_i^\mathrm{L} G^u_{ij} u'^\mathrm{R}_j \tilde{\Phi} + \overline{Q'}_i^\mathrm{L} G^d_{ij} d'^\mathrm{R}_j \Phi + \mathrm{h.c}\right), \tag{2.1.17}$$

where $\tilde{\Phi} = [\phi^{0*}, -\phi^-]^\mathrm{T}$, and the 3×3 Yukawa coupling matrices for leptons, up-, and down-type quarks are denoted with G^l_{ij}, G^u_{ij}, and G^d_{ij}, respectively.

Mass and charge eigenstates in the SM

In any experiment one will not observe particles that correspond to eigenstates of the EW interaction, but to mass and charge eigenstates. Since the physical gauge bosons have vanishing hypercharge, the charge eigenstates can be found by the determination of the eigenstates of the isospin generator I^3 that are given by the four contributions

$$W_\mu^\pm(x) = \frac{1}{\sqrt{2}}[W_\mu^1 \mp W_\mu^2]\,, \quad W_\mu^3(x)\,, \quad B_\mu(x)\,. \tag{2.1.18}$$

Reformulating $\mathcal{L}_{\text{Higgs}}$ by using the fields $W_\mu^\pm$ instead of W_μ^1 and W_μ^2, one finds that the fields $W_\mu^\pm$ already correspond to mass eigenstates and can therefore be associated with the charged physical vector bosons $\text{W}^\pm$ with masses

$$M_\text{W} = \frac{1}{2} g_2\, v\,. \tag{2.1.19}$$

Diagonalizing the mass matrix of the fields W_μ^3 and B_μ within $\mathcal{L}_{\text{Higgs}}$, one finds that the neutral vector-boson fields Z_μ and A_μ are given by

$$\begin{pmatrix} Z_\mu \\ A_\mu \end{pmatrix} = \begin{pmatrix} c_\text{W} & s_\text{W} \\ -s_\text{W} & c_\text{W} \end{pmatrix} \begin{pmatrix} W_\mu^3 \\ B_\mu \end{pmatrix}\,, \tag{2.1.20}$$

where we have defined the weak mixing angle θ_W,

$$c_\text{W} = \cos\theta_\text{W} = \frac{g_2}{\sqrt{g_1^2 + g_2^2}}\,, \quad s_\text{W} = \sin\theta_\text{W}\,. \tag{2.1.21}$$

The mass of the neutral Z^0 boson that corresponds to the field Z_μ reads

$$M_\text{Z} = \frac{v}{2}\sqrt{g_1^2 + g_2^2}\,, \tag{2.1.22}$$

and the massless field A_μ is identified with the photon. Using Eqs. (2.1.19), (2.1.21), and (2.1.22), the weak mixing angle can be written as

$$c_\text{W} = \frac{M_\text{W}}{M_\text{Z}}\,. \tag{2.1.23}$$

The fermion fields associated to physical particles are obtained from the EW eigenstates according to

$$f_i^\text{L} = \sum_k U_{ik}^{f,\text{L}} f_k'^\text{L}\,, \quad f_i^\text{R} = \sum_k U_{ik}^{f,\text{R}} f_k'^\text{R}\,, \tag{2.1.24}$$

where the matrices $U_{ik}^{f,\text{L/R}}$ diagonalize the Yukawa coupling matrices, so that the fermion masses that are induced by spontaneous symmetry breaking are given by

$$m_{f,i} = \frac{v}{\sqrt{2}} \sum_{k,m} U_{ik}^{f,\text{L}} G_{km}^f U_{mi}^{f,\text{R}\dagger}\,. \tag{2.1.25}$$

After diagonalizing the fermion-mass matrices and rewriting the Lagrangian $\mathcal{L}_{\mathrm{C}}$ in terms of physical fields, one observes that the coupling of $\mathrm{W}^{\pm}$ bosons to one up- and down-type quark receives an additional factor

$$V_{ij} = \sum_k U_{ik}^{u,\mathrm{L}} U_{kj}^{d,\mathrm{L}\dagger} \,. \tag{2.1.26}$$

The unitary quark-mixing matrix V_{ij} is known as the Cabibbo–Kobayashi–Maskawa (CKM) matrix that quantifies the mixing of different quark families in charged-current processes. Since all neutrinos are assumed massless and thus are degenerate in mass with each other, the matrix $U_{ik}^{\nu,\mathrm{L}}$ can be chosen freely, and the neutrino fields

$$\nu_i^{\mathrm{L}} = \sum_k U_{ik}^{l,\mathrm{L}} \nu_k'^{\mathrm{L}} \tag{2.1.27}$$

are defined in such a way that the lepton–W-boson interaction is diagonal at tree level.

The electrical charge $e = \sqrt{4\pi\alpha}$ is defined as the coupling constant multiplying the fermion–photon vertex and can be expressed in terms of the fundamental gauge couplings as

$$e = \frac{g_1 g_2}{\sqrt{g_1^2 + g_2^2}} \,. \tag{2.1.28}$$

After we have identified all input parameters and all fields that can be assigned to physical particles within the EW part of the SM, we can now rewrite the SM Lagrangian $\mathcal{L}_{\mathrm{C}}$ in terms of those fields and the independent parameters

$$e, M_{\mathrm{W}}, M_{\mathrm{Z}}, M_{\mathrm{H}}, m_{f,i}, V_{ij} \,, \tag{2.1.29}$$

that are not fixed by the theory, but have to be determined by experiment.

Gauge fixing and ghost fields

As stated above, we add a gauge-fixing Lagrangian

$$\mathcal{L}_{\mathrm{fix}} = -\frac{1}{2\xi_A}[F^A(x)]^2 - \frac{1}{2\xi_Z}[F^Z(x)]^2 - \frac{1}{\xi_W} F^+(x) F^-(x) \tag{2.1.30}$$

to the classical expression $\mathcal{L}_{\mathrm{C}}$ to enable the proper quantization of the theory, where we choose the linear gauge-fixing functionals

$$\begin{aligned} F^{\pm}(x) &= \partial^\mu W_\mu^{\pm}(x) \mp \mathrm{i} M_{\mathrm{W}} \xi_W' \phi^{\pm}(x) \,, \\ F^Z(x) &= \partial^\mu Z_\mu(x) - \mathrm{i} M_{\mathrm{Z}} \xi_Z' \chi(x) \,, \\ F^A(x) &= \partial^\mu A_\mu(x) \,. \end{aligned} \tag{2.1.31}$$

It is convenient to work in the *'t Hooft gauge* that is defined via $\xi_W = \xi_W'$ and $\xi_Z = \xi_Z'$, respectively. For this special choice, the terms involving the *would-be Goldstone fields* $\phi^{\pm}$ and χ in (2.1.31) will exactly cancel the mixing terms $V^\mu \partial_\mu \phi^{\pm}$ and $V^\mu \partial_\mu \chi$ of the physical vector bosons and the unphysical fields in $\mathcal{L}_{\mathrm{C}}$ that are induced by spontaneous symmetry breaking.

Additionally, the ghost-field Lagrangian

$$\mathcal{L}_{\mathrm{FP}} = \bar{u}^a(x)\,\frac{\delta F^a}{\delta\theta^b(x)}\,u^b(x) \tag{2.1.32}$$

has to be added to the theory that contains the Faddeev–Popov ghosts $u^a(x)$, $\bar{u}^a(x)$ ($a = \pm, A, Z$), and the variations δF^a of the gauge-fixing operators under infinitesimal group transformations quantified by the group parameters $\delta\theta^b(x)$. The choice $\xi_W = \xi_Z = \xi_A = 1$ defines the so called *'t Hooft–Feynman gauge*. In this gauge, the masses that correspond to physical fields equal those that are associated to unphysical fields, and the $k^\mu k^\nu$ terms in the propagators are absent. Therefore, this choice is especially convenient for the calculation of higher-order corrections.

Taking gauge-fixing terms and Faddeev–Popov terms into account, the full Lagrangian of the GSW theory can be written as

$$\mathcal{L}_{\mathrm{GSW}} = \mathcal{L}_{\mathrm{C}} + \mathcal{L}_{\mathrm{fix}} + \mathcal{L}_{\mathrm{FP}}\,, \tag{2.1.33}$$

where $\mathcal{L}_{\mathrm{C}}$ is given by (2.1.5). The corresponding Feynman rules that follow from (2.1.33) can be taken from Appendix A of [47].

2.1.2 The QCD Lagrangian

The strong interaction of colour-charged particles (quarks and gluons) is described by QCD, the quantum theory of the unbroken local $\mathrm{SU}(3)_{\mathrm{C}}$ gauge symmetry. Here, we briefly sketch the construction of the corresponding Lagrangian. For a detailed discussion of the various features of QCD see, e.g., Chapter 3 of [48].

For simplicity, we now switch off the EW interactions and rewrite the Lagrangian for free massive quarks $\boldsymbol{q}_i$ in terms of mass eigenstates,

$$\mathcal{L}_{\text{free quarks}} = \sum_{q=u,d}\sum_{j=1}^{3}\bar{\boldsymbol{q}}_j(x)\left(\mathrm{i}\partial\!\!\!/ - m_j\right)\boldsymbol{q}_j(x)\,, \tag{2.1.34}$$

where $j = 1, 2, 3$ assigns the generation of u- and d-type quarks, and each quark field

$$\boldsymbol{q}_j = \begin{pmatrix} q_j^1 \\ q_j^2 \\ q_j^3 \end{pmatrix} \tag{2.1.35}$$

transforms as a triplet in colour space, since it belongs to the fundamental representation of $\mathrm{SU}(3)_{\mathrm{C}}$. The Lagrangian (2.1.34) is invariant with respect to global $\mathrm{SU}(3)_{\mathrm{C}}$ transformations, but violates local gauge invariance. Therefore, we introduce a bosonic eight-component gluon field $G_\mu^a(x)$, $a = 1, \ldots, 8$, via minimal substitution by means of a covariant derivative, i.e. we replace the bare derivative ∂_μ according to

$$\partial_\mu \to \boldsymbol{D}_\mu = \partial_\mu + \mathrm{i}g_{\mathrm{s}}\boldsymbol{G}_\mu(x)\,, \tag{2.1.36}$$

with the strong coupling constant $g_\mathrm{s} = \sqrt{4\pi\alpha_\mathrm{s}}$, and the traceless hermitian 3×3 matrix $\boldsymbol{G}_\mu(x) = G^a_\mu(x)\boldsymbol{T}^a$, where the matrices $\boldsymbol{T}^a$ denote the eight generators of $\mathrm{SU}(3)_\mathrm{C}$. The gluonic field-strength tensor

$$G^a_{\mu\nu}(x) = \partial_\mu G^a_\nu(x) - \partial_\nu G^a_\mu(x) - \mathrm{i}\, g_\mathrm{s} f^{abc}\, G^b_\mu(x) G^c_\nu(x)\,, \tag{2.1.37}$$

where the f^{abc} are the structure functions of $\mathrm{SU}(3)_\mathrm{C}$, is needed to express the Lagrangian

$$\mathcal{L}_\mathrm{gluon} = -\frac{1}{4} G^a_{\mu\nu}(x) G^{\mu\nu,a}(x)\,, \tag{2.1.38}$$

that governs the dynamics and self interactions of the gluon fields. Defining the colour-space matrix $\boldsymbol{G}_{\mu\nu}(x) = G^a_{\mu\nu}(x)\boldsymbol{T}^a$, the full QCD Lagrangian can be written in a compact form as

$$\mathcal{L}_\mathrm{QCD} = -\frac{1}{2}\mathrm{Tr}\left[\boldsymbol{G}_{\mu\nu}(x)\boldsymbol{G}^{\mu\nu}(x)\right] + \sum_{q=u,d}\sum_{j=1}^{3} \bar{\boldsymbol{q}}_j(x)\left(\mathrm{i}\not{\boldsymbol{D}} - m_j\right)\boldsymbol{q}_j(x)\,. \tag{2.1.39}$$

Gauge fixing and ghost fields

As in the EW case, we introduce gauge-fixing terms and ghost fields into the classical Lagrangian $\mathcal{L}_\mathrm{QCD}$ to allow for a consistent quantization of QCD via the Faddeev–Popov formalism, resulting in the expression

$$\mathcal{L}_\mathrm{QCD,\,eff} = \mathcal{L}_\mathrm{QCD} + \mathcal{L}_\mathrm{fix,QCD} + \mathcal{L}_\mathrm{FP,QCD}\,, \tag{2.1.40}$$

for the effective Lagrangian of QCD. The gauge-fixing Lagrangian explicitly reads

$$\mathcal{L}_\mathrm{fix,QCD} = \frac{1}{2\xi_G}\left[\partial^\mu G^a_\mu(x)\right]\left[\partial^\nu G^a_\nu(x)\right], \tag{2.1.41}$$

and the ghost-field contribution is given by

$$\mathcal{L}_\mathrm{FP,QCD} = -\bar{u}^a(x)\,\partial^\mu D^{ab}_\mu\, u^b(x)\,, \tag{2.1.42}$$

where we have introduced the derivative

$$D_{\mu,ab} = \partial_\mu \delta_{ab} - \mathrm{i}\, g_\mathrm{s}\,(T^c_\mathrm{adj})_{ab}\, G^c_\mu(x) \tag{2.1.43}$$

in the adjoint representation. The Feynman rules that are deduced from (2.1.40) can ,e.g., be found in Section 2.4.2.2 of [48].

2.1.3 Renormalization of the SM: the on-shell scheme

The independent input parameters (2.1.29) that enter the SM Lagrangian (2.1.33) are equivalent to the experimentally determined physical quantities only at tree level. Taking higher-order corrections into account, the simple tree-level definitions of the input parameters do not match their original physical meaning anymore, and the so-called "bare" parameters have to be redefined to predict the experimental results properly. This procedure is called *renormalization*. For instance, at tree level, the particle mass equals the

zero of the corresponding propagator that describes the free propagation of the particle. Including higher-order effects, the position of the zero will be slightly shifted, and the tree-level mass cannot be regarded as a physical quantity anymore.

After renormalization, physical predictions have to be formulated in terms of a set of independent renormalized input parameters, and their actual values have to be determined by experiment. The procedure of renormalization has to be specified by certain renormalization conditions that fix the physical input parameters. Those renormalization conditions can be formulated in different ways, and accordingly different so-called *renormalization schemes* exist.

Dimensional regularization

The calculation of higher-order effects comprises the necessity of calculating loop integrals, where four-momenta of internal particles are not fixed by the external momenta and therefore have to be integrated over all accessible momentum configurations. For one-loop corrections as considered in this thesis, such integrals will be of the form $\int \mathrm{d}^4q\,(\ldots)$ with $\mathrm{d}^4q \equiv \mathrm{d}q^0\mathrm{d}^3\mathbf{q}$, i.e. the one independent loop four-momentum q has to be integrated over the complete Minkowski space. The loop integrals that appear in one-loop corrections to SM processes may diverge if components of the integration momentum q get too large, resulting in so-called ultraviolet (UV) divergences. Those divergences may be cured by introducing a large cut-off scale Λ_{UV} that will work as a regulator. However, since introducing a cut-off scale in loop integrals is a non-Lorentz-invariant approach, we will use the method of *dimensional regularization* [50, 51] that respects Lorentz- as well as gauge invariance of the theory. In dimensional regularization, loop integrals are evaluated in $d = 4 - 2\epsilon$ space-time dimensions, where ϵ is an in principle arbitrary complex quantity. In dimensional regularization, we have to replace the four-dimensional integrals according to

$$\int \mathrm{d}^4q\,(\ldots)|_{4\text{ dim.}} \to (2\pi\mu)^{4-d} \int \mathrm{d}^dq\,(\ldots)|_{d\text{ dim.}}\,, \tag{2.1.44}$$

where the reference-mass scale μ was introduced to preserve the correct mass dimension of the integral, and the subscripts indicate that the Lorentz- and Dirac structures that appear within $(\ldots)$ also have to be evaluated in d dimensions. In d space-time dimensions, the UV divergences are calculable and will appear as regular $1/\epsilon$ poles in the underlying expressions.

After the application of an adequate renormalization procedure, any physical result has to be UV finite, i.e. the $1/\epsilon$ poles will be absorbed in the relations of bare and renormalized parameters. After the cancellation of UV divergences, the limit $\epsilon \to 0$ can easily be achieved, and the theoretical predictions can be formulated in four space-time dimensions.

A theory is called *renormalizable* if its theoretical predictions are UV finite after the redefinition of a finite number of input parameters at any perturbative order. It was proven by 't Hooft [52, 53] that non-abelian gauge theories with spontaneous symmetry breaking, such as the SM, are renormalizable theories. Therefore, within the SM we can provide meaningful theoretical predictions that can be compared to experimental data.

The on-shell renormalization scheme

For the calculation of the EW radiative corrections to on-shell W bosons and one jet which is described in Chapter 5, we will use the *on-shell renormalization scheme* [54] for the renormalization of the Lagrangian at the one-loop order, as described in detail in Chapter 3 of [47]. This scheme is defined in such a way that the redefined parameters of the underlying theory match the physical quantities that are measured by experiment.

For the technical application of the on-shell renormalization scheme we follow the counterterm approach, applying a multiplicative renormalization, where the bare, unrenormalized parameters (denoted by a subscript 0) are given as a product of the renormalized ones and adequate renormalization constants Z that are fixed by the corresponding renormalization conditions. These renormalization constants are then Taylor expanded in the one-loop approximation, $Z = 1 + \delta Z + \mathcal{O}(\alpha^2)$, where δZ denotes the counterterm contribution. In the following, we will sketch the renormalization procedure as far as it is needed for our explicit calculation. Thus, we will not discuss the renormalization prescriptions for the Higgs mass and the Higgs field, and there will also be no discussion of the renormalization of an external photon field.

In case of an external on-shell vector boson there is no need to renormalize the vector-boson mass. However, the renormalization of the vector-boson masses will be of special interest when we consider the more realistic case of a leptonically decaying vector boson. For this reason, we also list the corresponding expression in the on-shell scheme, although the mass renormalization for unstable vector bosons will finally be carried out in the complex-mass scheme that will be discussed in detail in Section 2.2.4.

We first split the bare vector-boson masses $M^2_{V,0}$ according to

$$M^2_{V,0} = M^2_V + \delta M^2_V\,, \quad V = \mathrm{W},\, \mathrm{Z}\,, \tag{2.1.45}$$

and the counterterm contributions explicitly read

$$\delta M^2_{\mathrm{W}} = \mathrm{Re}\Sigma^W_{\mathrm{T}}(M^2_{\mathrm{W}})\,, \quad \delta M^2_{\mathrm{Z}} = \mathrm{Re}\Sigma^{ZZ}_{\mathrm{T}}(M^2_{\mathrm{Z}})\,, \tag{2.1.46}$$

where Σ_{T} denotes the transverse parts of the corresponding unrenormalized self-energies. To derive (2.1.46), we have demanded that the real part of the renormalized vector-boson 2-point function, projected on a physical state $\varepsilon_\mu(k)$, equals zero if the particle is on its mass shell, i.e. $k^2 = M^2_V$ is valid.

Since we will neglect light fermion masses in our calculation whenever possible, we do not have to perform a mass renormalization for light quarks and leptons, because the corresponding counterterm contributions are suppressed by factors of the small mass parameters. We also do not renormalize the quark-mixing matrix V_{ij} and assume that it is diagonal within the calculation of the one-loop corrections, since the off-diagonal effects as well as the counterterm contributions are expected to be negligible.

The bare weak mixing angle

$$c^2_{\mathrm{w},0} = 1 - s^2_{\mathrm{w},0} = \frac{M^2_{\mathrm{W},0}}{M^2_{\mathrm{Z},0}} \tag{2.1.47}$$

is renormalized via

$$c_{\mathrm{w},0} = c_{\mathrm{w}} + \delta c_{\mathrm{w}}\,, \quad s_{\mathrm{w},0} = s_{\mathrm{w}} + \delta s_{\mathrm{w}}\,, \tag{2.1.48}$$

and the counterterms are directly related to the counterterms of the weak gauge-boson masses, yielding

$$\frac{\delta c_{\mathrm{W}}}{c_{\mathrm{W}}} = -\frac{s_{\mathrm{W}}^2}{c_{\mathrm{W}}^2}\frac{\delta s_{\mathrm{W}}}{s_{\mathrm{W}}} = \frac{1}{2}\mathrm{Re}\left(\frac{\Sigma_{\mathrm{T}}^{W}(M_{\mathrm{W}}^2)}{M_{\mathrm{W}}^2} - \frac{\Sigma_{\mathrm{T}}^{ZZ}(M_{\mathrm{Z}}^2)}{M_{\mathrm{Z}}^2}\right). \tag{2.1.49}$$

Note that this renormalization prescription preserves the relation $c_{\mathrm{W}}^2 = M_{\mathrm{W}}^2/M_{\mathrm{Z}}^2$ for the renormalized quantities.

Following the idea of the multiplicative renormalization, we rewrite the bare vector-boson fields according to

$$W_0^{\pm} = (1 + \tfrac{1}{2}\delta Z_W)\, W^{\pm}, \quad \begin{pmatrix} Z_0 \\ A_0 \end{pmatrix} = \begin{pmatrix} 1 + \frac{1}{2}\delta Z_{ZZ} & \frac{1}{2}\delta Z_{ZA} \\ \frac{1}{2}\delta Z_{AZ} & 1 + \frac{1}{2}\delta Z_{AA} \end{pmatrix} \begin{pmatrix} Z \\ A \end{pmatrix}, \tag{2.1.50}$$

where W and Z denote the fields of the two massive weak vector bosons, and A is the photon field, respectively. The vector-boson and fermion fields are renormalized in such a way that the residues of the particle propagators are equal to one for on-shell particles, leading us to the explicit expressions

$$\delta Z_W = -\mathrm{Re}\,\Sigma_{\mathrm{T}}'^{W}(M_{\mathrm{W}}^2), \quad \delta Z_{ZZ} = -\mathrm{Re}\,\Sigma_{\mathrm{T}}'^{ZZ}(M_{\mathrm{Z}}^2) \tag{2.1.51}$$

for the counterterms of the massive vector-boson fields, where $\Sigma'(x) \equiv \partial\Sigma(p^2)/\partial p^2|_{p^2=x}$. The bare external left(L)- and right(R)-handed fermion fields are redefined as

$$f_0^{\sigma} = (1 + \tfrac{1}{2}\delta Z_{f\bar{f}}^{\sigma})\, f^{\sigma}, \quad \sigma = \mathrm{R}, \mathrm{L}, \tag{2.1.52}$$

and the field renormalization constants $\delta Z_{f\bar{f}}^{\mathrm{R/L}}$ are explicitly given by

$$\delta Z_{f\bar{f}}^{\sigma} = -\mathrm{Re}\,\Sigma_{\sigma}^{f\bar{f}}(m_f^2) - m_f^2\,\mathrm{Re}\left[\Sigma_{\mathrm{R}}'^{f\bar{f}}(m_f^2) + \Sigma_{\mathrm{L}}'^{f\bar{f}}(m_f^2) + 2\,\Sigma_{\mathrm{S}}'^{f\bar{f}}(m_f^2)\right], \tag{2.1.53}$$

which is a function of the left-/right-handed and the scalar (S) part of the unrenormalized fermion self-energies.

The bare electric charge

$$e_0 = (1 + \delta Z_e)\, e, \tag{2.1.54}$$

which parametrizes the QED coupling at tree level, is renormalized in such a way that the one-loop expression for the QED vertex $\gamma f \bar{f}$ matches its tree-level definition in the Thomson limit of vanishing four-momentum transfer by the photon. This renormalization prescription leads to the expression

$$\delta Z_e = \frac{1}{2}\Sigma_{\mathrm{T}}'^{AA}(0) - \frac{s_{\mathrm{W}}}{c_{\mathrm{W}}}\frac{\Sigma_{\mathrm{T}}^{AZ}(0)}{M_{\mathrm{Z}}^2}, \tag{2.1.55}$$

for the charge renormalization constant.

Applying the multiplicative renormalization as pointed out above, the bare Lagrangian $\mathcal{L}_0$ that is formulated in terms of bare parameters, can be rewritten according to

$$\mathcal{L}_0 = \mathcal{L} + \delta\mathcal{L}, \tag{2.1.56}$$

where we have neglected two-loop contributions. The renormalized Lagrangian $\mathcal{L}$ is a function of the renormalized input parameters with the same functional dependence as $\mathcal{L}_0$ on the bare parameters. The term $\delta\mathcal{L}$ contains all counterterm contributions which are expressed in terms of (potentially UV divergent) unrenormalized self-energies. Equation (2.1.56) can be used to derive Feynman rules for the counterterm contributions. Within a consistent one-loop calculation in the EW SM, the UV divergences which emerge in the specific one-loop corrections will cancel against universal counterparts that arise from $\delta\mathcal{L}$ already at the amplitude level.

2.2 Resonances in QFT – unstable particles

Unstable particles play an important role in high-energy physics, since many SM particles (like the scalar Higgs boson, the weak vector bosons, and the top quark) have a very short lifetime and can only be identified in any experiment via their decay products. The distribution of the invariant mass $\sqrt{Q^2}$ of those decay products will typically follow a Breit–Wigner shape around the mass m of the decaying particle,

$$\frac{\mathrm{d}\sigma}{\mathrm{d}Q^2} \propto \frac{1}{(Q^2-m^2)^2+m^2\Gamma^2}\,, \tag{2.2.1}$$

where Γ denotes the *total decay width* of the resonant particle which is directly related to its lifetime τ by

$$\Gamma = \frac{1}{\tau}\,, \tag{2.2.2}$$

according to the energy–time uncertainty in quantum mechanics. For reasons of simplicity, one often works in the approximation that unstable particles are produced on their mass shell and have an infinite lifetime. This assumption usually strongly reduces the complexity of the problem under consideration, since one only investigates the production of the particle and does not take into account its possible decay channels. For instance, in Chapter 5 of this thesis we will examine the production of on-shell W bosons at hadron colliders. At tree level, the treatment of resonances as stable particles does not raise any problems. By contrast, at next-to-leading order (NLO) this procedure may for instance result in the appearance of unphysical Landau singularities, as can be observed in the $\mathrm{Z}^0\mathrm{Z}^0 \to \mathrm{Z}^0\mathrm{Z}^0$ scattering process [55].

We wish to perform an NLO calculation for a realistic physical process involving resonant vector bosons that decay into leptons. Therefore, and to avoid the conceptual problems stated above, we need a proper treatment of the finite width of the vector boson to allow for a consistent computation of quantum corrections within a field-theoretical framework.

2.2.1 Naive inclusion of a finite width

One could naively introduce the finite width Γ into the calculation via the replacement

$$m^2 \to m^2 - \mathrm{i}m\Gamma \tag{2.2.3}$$

in the propagator $P(p^2)$ of the resonant particle,

$$P(p^2) \propto \frac{1}{p^2 - m^2} \to \frac{1}{p^2 - m^2 + \mathrm{i}m\Gamma}\,. \tag{2.2.4}$$

This procedure seems very promising, since the replacement (2.2.3) will yield the typical Breit–Wigner shape (2.2.1) for the cross section. Unfortunately, however, in gauge theories the naive inclusion of a finite width may destroy gauge invariance already at the Born level, since the Dyson summation (see next subsection) effectively leads to a mixing of perturbative orders so that incomplete gauge-dependent higher-order contributions enter the calculation.

At NLO, the situation is even more involved. On the one hand, the particles' masses have to be redefined in a renormalization procedure to absorb the UV-singular contributions in the relation between the bare parameters and the renormalized, physical quantities. On the other hand, the introduction of a finite width at leading order (LO) may implicitly include certain NLO contributions that have to be subtracted from the perturbative NLO contributions again to avoid double counting.

We will first discuss the implementation of a finite width within the on-shell renormalization scheme and point out the severe problems arising in this approach. Afterwards, we will present the pole definition of the mass that is considerably better suited to handle resonances in the framework of NLO calculations.

2.2.2 Mass and width in the on-shell scheme

In standard perturbation theory, propagators do not contain the decay width explicitly; in fact, the particle width enters the perturbative calculation via the Dyson summation of one-particle-irreducible (1PI) self-energy insertions $\Sigma(p^2)$ of its propagator. For instance, the inverse propagator of a scalar particle at any perturbative order is given by

$$P^{-1}(p^2) = p^2 - m_0^2 + \Sigma(p^2)\,, \tag{2.2.5}$$

where $\Sigma(p^2)$ for unstable particles in general is a complex quantity near the particle pole. In the on-shell (OS) renormalization scheme (see Section 2.1.3), the renormalized mass of the particle is determined by the zero of the inverse propagator on the real axis, i.e. by

$$0 = P_{\mathrm{OS}}^{-1}(m_{\mathrm{OS}}^2) = m_{\mathrm{OS}}^2 - m_0^2 + \mathrm{Re}\,\Sigma(m_{\mathrm{OS}}^2)\,. \tag{2.2.6}$$

Using $m_0^2 = m_{\mathrm{OS}}^2 + \mathrm{Re}\Sigma(m_{\mathrm{OS}}^2)$, the expression (2.2.5) for $P_{\mathrm{OS}}^{-1}(p^2)$ can be expanded[1] in the vicinity of $p^2 = m_{\mathrm{OS}}^2$,

$$\begin{aligned} P_{\mathrm{OS}}^{-1}(p^2) &= p^2 - m_{\mathrm{OS}}^2 - \mathrm{Re}\,\Sigma(m_{\mathrm{OS}}^2) + \mathrm{Re}\,\Sigma(p^2) + \mathrm{i}\,\mathrm{Im}\,\Sigma(p^2) \\ &= R_{\mathrm{OS}}^{-1}\left[p^2 - m_{\mathrm{OS}}^2 + \mathrm{i}R_{\mathrm{OS}}\,\mathrm{Im}\,\Sigma(p^2)\right] + \mathcal{O}\left((p^2 - m_{\mathrm{OS}}^2)^2\right)\,, \end{aligned} \tag{2.2.7}$$

where

$$R_{\mathrm{OS}} = \frac{1}{1 + \mathrm{Re}\,\Sigma'(m_{\mathrm{OS}}^2)} \tag{2.2.8}$$

[1] Usually, Γ will be much smaller than m, and all relevant contributions to the cross section will emerge from kinematic regions where $p^2 \sim m^2$ is valid.

denotes the residue of the on-shell propagator. Now we define the on-shell width according to the Breit–Wigner expression (2.2.1) as

$$m_{\mathrm{OS}}\Gamma_{\mathrm{OS}} = \frac{\mathrm{Im}\,\Sigma(m^2_{\mathrm{OS}})}{1+\mathrm{Re}\,\Sigma'(m^2_{\mathrm{OS}})}\,. \tag{2.2.9}$$

This equation can be used to perturbatively determine the finite on-shell width Γ_{OS} of the particle at a given perturbative order.

However, using the on-shell renormalization scheme for unstable vector bosons turns out to be a questionable approach, because the on-shell renormalization condition for the W-boson mass (2.1.46) is given by

$$M^2_{\mathrm{W},0} - M^2_{\mathrm{W,OS}} = \mathrm{Re}\,\Sigma^W_{\mathrm{T}}\left(M^2_{\mathrm{W,OS}}\right), \tag{2.2.10}$$

and the real part of the transverse (T) part of the W-boson self-energy $\mathrm{Re}\,\Sigma^W_{\mathrm{T}}(M^2_{\mathrm{W,OS}})$ is not a gauge-independent quantity beyond one-loop order [56]. As a result, $M_{\mathrm{W,OS}}$ and $\Gamma_{\mathrm{W,OS}}$ will receive gauge-dependent contributions at $\mathcal{O}(\alpha^2)$. Thus, one is urged to find a gauge-independent renormalization condition for the masses of unstable particles. This requirement is respected applying the pole-mass definition that will be discussed now.

2.2.3 Gauge-independent description of a finite width: the pole mass

The pole mass μ^2 of an unstable scalar particle is defined as the pole position of the particle's propagator in the complex p^2-plane,

$$0 = P^{-1}_{\mathrm{Pole}}(\mu^2) = \mu^2 - m_0^2 + \Sigma(\mu^2)\,. \tag{2.2.11}$$

As shown in [57], this expression is gauge independent at any order in perturbation theory. Using (2.2.11) as a renormalization condition, the renormalized propagator reads

$$\begin{aligned} P^{-1}_{\mathrm{Pole}}(p^2) &= p^2 - \mu^2 - \Sigma(\mu^2) + \Sigma(p^2) \\ &= R^{-1}_{\mathrm{Pole}}(\mu^2)\left(p^2-\mu^2\right) + \mathcal{O}\left((p^2-\mu^2)^2\right)\,, \end{aligned} \tag{2.2.12}$$

with the residue

$$R_{\mathrm{Pole}} = \frac{1}{1+\Sigma'(\mu^2)}\,. \tag{2.2.13}$$

Equation (2.2.12) implies the definition

$$\mu^2 \equiv m^2 - \mathrm{i}m\Gamma \tag{2.2.14}$$

for the physical mass and width of the particle that have to be determined by experiment.

2.2.4 The complex-mass scheme

Using the pole-mass definitions (2.2.11) and (2.2.14), we have found a gauge-independent way to define the total width of a resonance. Nevertheless, we have not yet attacked the problem of properly inserting a finite width into a fixed-order perturbative calculation. As

mentioned before, the naive approach of introducing a width in the resonant propagators includes an implicit Dyson summation that will lead to a mixing of different perturbative orders. Accordingly, the SM gauge invariance will be violated in this approach, possibly resulting in wrong predictions. To solve this problem, in our computation of the radiative corrections to W+jet production we work in the complex-mass scheme (CMS) [32, 33], because it is probably the most elegant and straight-forward way to account for resonances in perturbative NLO calculations. Within this scheme, gauge invariance and all corresponding Ward- and Slavnov–Taylor identities are respected. Moreover, the CMS includes all off-shell effects and is applicable in all regions of phase space. In spite of all these nice features, its implementation is in principle remarkably easy.

The CMS is a renormalization scheme that is based on the pole definition (2.2.11) of the complex particle mass. For instance, the physical vector-boson masses

$$\mu_{\mathrm{V}}^2 = M_{\mathrm{V}}^2 - \mathrm{i}M_{\mathrm{V}}\Gamma_{\mathrm{V}}\,, \quad \mathrm{V} = \mathrm{W},\mathrm{Z}\,, \tag{2.2.15}$$

are consequently defined as the position of the poles of the renormalized propagators in the complex plane. This definition is applied everywhere in the physical amplitudes whenever the vector-boson masses appear in the propagators or in the SM couplings. All related quantities have to be adjusted according to this definitions to preserve gauge invariance. Especially, the weak mixing angle becomes a complex parameter,

$$\cos^2\theta_{\mathrm{W}} \equiv c_{\mathrm{w}}^2 = 1 - s_{\mathrm{w}}^2 = \frac{\mu_{\mathrm{W}}^2}{\mu_{\mathrm{Z}}^2}\,. \tag{2.2.16}$$

Since c_{w}^2 receives an imaginary part, in tree-level calculations this definition will lead to spurious terms that do not necessarily have a physical implication. However, those effects will be of the order $\mathcal{O}(\Gamma_V/M_V) = \mathcal{O}(\alpha)$ with respect to the lowest-order term, both in the resonant and the non-resonant regions of phase space, and therefore are formally part of an NLO contribution.

The general strategy of the CMS is to introduce complex vector-boson mass parameters directly on the level of the Lagrangian by splitting the real bare mass into the complex renormalized mass and a complex mass counterterm,

$$M_{V,0}^2 = \mu_V^2 + \delta\mu_V^2\,. \tag{2.2.17}$$

We also split the bare vector boson fields into complex fields and complex renormalization constants according to

$$W_0^{\pm} = (1 + \tfrac{1}{2}\delta\mathcal{Z}_W)\,W^{\pm}\,, \quad \begin{pmatrix} Z_0 \\ A_0 \end{pmatrix} = \begin{pmatrix} 1+\frac{1}{2}\delta\mathcal{Z}_{ZZ} & \frac{1}{2}\delta\mathcal{Z}_{ZA} \\ \frac{1}{2}\delta\mathcal{Z}_{AZ} & 1+\frac{1}{2}\delta\mathcal{Z}_{AA} \end{pmatrix} \begin{pmatrix} Z \\ A \end{pmatrix}\,. \tag{2.2.18}$$

As a result, the bare Lagrangian can be expressed as $\mathcal{L}_0 = \mathcal{L} + \delta\mathcal{L}$, where $\mathcal{L}$ and the counterterm contributions $\delta\mathcal{L}$ are formulated using complex mass parameters for unstable particles. The Feynman rules that are deduced from this Lagrangian can be applied in the usual way to perform perturbative calculations. This approach avoids double-counting, because the perturbative series is just rearranged, but the bare Lagrangian and so the theory is unchanged.

We now present a short summary of the complex renormalization procedure concerning the vector-boson masses, the associated fields, the weak mixing angle, and the electric charge, because those quantities will be needed for the explicit calculation. A detailed derivation of the renormalization of the EWSM within the CMS can be found in Chapter 4 of Ref. [33], and a compact review of the method is also presented in [58].

In the CMS, the renormalized transverse (T) parts of the self-energies for massive vector bosons at the one-loop level are given by

$$\begin{aligned}\hat{\Sigma}_{\mathrm{T}}^{W}(k^2) &= \Sigma_{\mathrm{T}}^{W}(k^2) - \delta\mu_{\mathrm{W}}^2 + (k^2-\mu_{\mathrm{W}}^2)\,\delta\mathcal{Z}_W\,,\\ \hat{\Sigma}_{\mathrm{T}}^{ZZ}(k^2) &= \Sigma_{\mathrm{T}}^{ZZ}(k^2) - \delta\mu_{\mathrm{Z}}^2 + (k^2-\mu_{\mathrm{Z}}^2)\,\delta\mathcal{Z}_{ZZ}\,,\end{aligned} \tag{2.2.19}$$

and the renormalization conditions are formulated as a generalization of the expressions in the on-shell scheme (see Section 2.1.3) as

$$\begin{aligned}\hat{\Sigma}_{\mathrm{T}}^{W}(\mu_{\mathrm{W}}^2) &= 0\,, \qquad \hat{\Sigma}_{\mathrm{T}}^{\prime W}(\mu_{\mathrm{W}}^2) = 0\,,\\ \hat{\Sigma}_{\mathrm{T}}^{ZZ}(\mu_{\mathrm{Z}}^2) &= 0\,, \qquad \hat{\Sigma}_{\mathrm{T}}^{\prime ZZ}(\mu_{\mathrm{Z}}^2) = 0\,,\end{aligned} \tag{2.2.20}$$

taking into account the pole-mass definition. The field renormalization constants will drop out in any physical S-matrix element involving only virtual unstable vector bosons.[2] Nevertheless, including those field renormalization constants into the calculation, all renormalized vertex functions can be defined in an UV-finite way. The obvious solutions to (2.2.20) read

$$\begin{aligned}\delta\mu_{\mathrm{W}}^2 &= \Sigma_{\mathrm{T}}^{W}(\mu_{\mathrm{W}}^2)\,, \qquad \delta\mathcal{Z}_W = -\Sigma_{\mathrm{T}}^{\prime W}(\mu_{\mathrm{W}}^2)\,,\\ \delta\mu_{\mathrm{Z}}^2 &= \Sigma_{\mathrm{T}}^{ZZ}(\mu_{\mathrm{Z}}^2)\,, \qquad \delta\mathcal{Z}_{ZZ} = -\Sigma_{\mathrm{T}}^{\prime ZZ}(\mu_{\mathrm{Z}}^2)\,,\end{aligned} \tag{2.2.21}$$

fixing the mass- and field renormalization constants. However, the calculations of $\Sigma_{\mathrm{T}}^{VV}(\mu_{\mathrm{V}}^2)$ enforces an analytic continuation of 2-point functions to the unphysical Riemann sheet. To circumvent this problem, one expands the self-energy expressions around the real mass M_V^2,

$$\begin{aligned}\Sigma_{\mathrm{T}}^{W}(\mu_{\mathrm{W}}^2) &= \Sigma_{\mathrm{T}}^{W}(M_{\mathrm{W}}^2) + (\mu_{\mathrm{W}}^2 - M_{\mathrm{W}}^2)\Sigma_{\mathrm{T}}^{\prime W}(M_{\mathrm{W}}^2) + \mathcal{O}(\alpha^3)\,,\\ \Sigma_{\mathrm{T}}^{ZZ}(\mu_{\mathrm{Z}}^2) &= \Sigma_{\mathrm{T}}^{ZZ}(M_{\mathrm{Z}}^2) + (\mu_{\mathrm{Z}}^2 - M_{\mathrm{Z}}^2)\Sigma_{\mathrm{T}}^{\prime ZZ}(M_{\mathrm{Z}}^2) + \mathcal{O}(\alpha^3)\,,\end{aligned} \tag{2.2.22}$$

exploiting the fact that formally Γ_{V} is an $\mathcal{O}(\alpha)$ correction with respect to M_{V}. Note that the expansion (2.2.22) does not affect the structure of UV divergences in $\Sigma_{\mathrm{T}}^{VV}(\mu_{\mathrm{V}}^2)$. Now the mass- and field renormalization constants can be rewritten according to

$$\begin{aligned}\delta\mu_{\mathrm{W}}^2 &= \Sigma_{\mathrm{T}}^{W}(M_{\mathrm{W}}^2) + (\mu_{\mathrm{W}}^2 - M_{\mathrm{W}}^2)\Sigma_{\mathrm{T}}^{\prime W}(M_{\mathrm{W}}^2)\,, \qquad \delta\mathcal{Z}_W = -\Sigma_{\mathrm{T}}^{\prime W}(M_{\mathrm{W}}^2)\,,\\ \delta\mu_{\mathrm{Z}}^2 &= \Sigma_{\mathrm{T}}^{ZZ}(M_{\mathrm{Z}}^2) + (\mu_{\mathrm{Z}}^2 - M_{\mathrm{Z}}^2)\Sigma_{\mathrm{T}}^{\prime ZZ}(M_{\mathrm{Z}}^2)\,, \qquad \delta\mathcal{Z}_{ZZ} = -\Sigma_{\mathrm{T}}^{\prime ZZ}(M_{\mathrm{Z}}^2)\,.\end{aligned} \tag{2.2.23}$$

Since the weak mixing angle is deduced from the vector-boson masses, its renormalization constant introduced in (2.1.48) can simply be derived from the definition (2.2.16),

$$\frac{\delta s_{\mathrm{W}}}{s_{\mathrm{W}}} = \frac{c_{\mathrm{W}}^2}{s_{\mathrm{W}}^2}\frac{\delta c_{\mathrm{W}}}{c_{\mathrm{W}}} = -\frac{c_{\mathrm{W}}^2}{2s_{\mathrm{W}}^2}\left(\frac{\delta\mu_{\mathrm{W}}^2}{\mu_{\mathrm{W}}^2} - \frac{\delta\mu_{\mathrm{Z}}^2}{\mu_{\mathrm{Z}}^2}\right)\,. \tag{2.2.24}$$

[2] In the CMS, unstable particles must not appear as external states.

The charge renormalization constant in the CMS, given by

$$\delta\mathcal{Z}_e = \frac{1}{2}\Sigma_{\mathrm{T}}'^{AA}(0) - \frac{s_{\mathrm{w}}}{c_{\mathrm{w}}}\frac{\Sigma_{\mathrm{T}}^{AZ}(0)}{\mu_{\mathrm{Z}}^2}\,, \tag{2.2.25}$$

can directly be carried over from the on-shell expression (2.1.55). One has to keep in mind that the self-energies entering (2.2.24) and (2.2.25) are calculated with complex mass parameters for unstable particles in the loops.

In our calculation we treat the light external fermions (namely the electron, the muon and all quark flavours other than the top) as massless, stable particles. Small fermion masses are only introduced to regularize collinear singularities and assumed to be real parameters. Thus, we do not have to perform a renormalization of the corresponding masses, since all related contributions are suppressed by powers of m_f. Moreover, the light-fermion self-energies in the renormalization constants do not have any absorptive contributions arising from decay possibilities into lighter particles. Nevertheless, the self energies have to be calculated with complex vector-boson masses and a complex weak mixing angle and therefore become complex quantities themselves. Taking this into account, it is necessary to perform a complex renormalization of the bare right- and left-handed fermion fields $f_0^{\mathrm{R/L}}$ according to

$$f_0^\sigma = (1 + \tfrac{1}{2}\delta\mathcal{Z}_{f\bar{f}}^\sigma)\, f^\sigma\,, \quad \sigma = \mathrm{R}\,,\mathrm{L}\,, \tag{2.2.26}$$

where the complex field renormalization constants $\delta\mathcal{Z}_{f\bar{f}}^{\mathrm{R/L}}$ are given by

$$\delta\mathcal{Z}_{f\bar{f}}^\sigma = -\Sigma_\sigma^{f\bar{f}}(m_f^2) - m_f^2\left[\Sigma_{\mathrm{R}}'^{f\bar{f}}(m_f^2) + \Sigma_{\mathrm{L}}'^{f\bar{f}}(m_f^2) + 2\,\Sigma_{\mathrm{S}}'^{f\bar{f}}(m_f^2)\right]. \tag{2.2.27}$$

In this equation, the complex functions $\Sigma_{\mathrm{R/L}}^{f\bar{f}}(m_f^2)$ and $\Sigma_{\mathrm{S}}^{f\bar{f}}(m_f^2)$ denote the right-/left-handed and the scalar parts of the fermion self-energies, respectively.

The CMS can also be applied to the renormalization of the masses and fields of the Higgs boson and the top quark. Since those quanta only enter our calculation at NLO, we will not discuss the related renormalization procedure in this thesis. Details concerning this topic can be found in [33]. Nevertheless, we should point out that one could easily introduce a complex mass for the top quark and the Higgs within the loop corrections. This treatment will lead to tiny deviations in the result that are formally of NNLO accuracy and therefore do not necessarily have to be taken into account.

2.3 The parton model and QCD

Scattering processes at hadron colliders pose the problem that hadrons are strongly-coupled, composite objects and therefore refuse access to a purely perturbative description. Therefore, we work in the *parton model* [59, 60] that comprises the possibility of perturbative predictability for hadronic scattering processes, since hadronic cross sections can be factorized into universal non-perturbative contributions and the perturbative description of the hard scattering event.

The parton model is valid for highly-relativistic fast-moving hadrons with a four-momentum that is distributed to the constituting partons (gluons and (anti)quarks).

Those massless partons are all moving in the same direction, and their transverse momenta are negligible. One further assumes that partonic reactions in hadronic collisions take place between two partons, whereas the remaining partons serve as spectators. The parton model is valid if the scale Q^2 of the hard process is large compared to the typical QCD scale Λ^2_{QCD}. In this situation $\alpha_{\mathrm{s}}(Q^2)$ is small and the partons in the hadron can be treated as perturbatively free particles. As a result, the partonic cross section can be computed using standard perturbation theory. One should keep in mind that the parton model only works fine in high-energy processes for large transverse momenta where a large momentum transfer is ensured.

2.3.1 Definition of partonic cross sections

The differential cross section $\mathrm{d}\sigma_{i\to f}$ plays an important role in high-energy collider physics, because it can be formulated as a purely phenomenological quantity, and, on the other hand, has a well-defined counterpart on the theory side. Thus, it can be employed to test theoretical predictions in an appropriate experimental approach.

On the experimental side, $\mathrm{d}\sigma_{i\to f}$ is defined as the ratio of the numbers of events per time n_f that contribute to a certain final state f, and the luminosity $\mathcal{L}_{\mathrm{in}}$ of the incoming particles in the initial state i undergoing the collisions,

$$\frac{\mathrm{d}\sigma_{i\to f}}{\mathrm{d}\mathcal{O}} = \frac{1}{\mathcal{L}_{\mathrm{in}}}\frac{\mathrm{d}n_f(\mathcal{O})}{\mathrm{d}\mathcal{O}}\,. \tag{2.3.1}$$

The final state f will usually be defined via its particle content, and the quantity $\mathcal{O}$ symbolizes a certain physically well-defined observable that has to be constructible from the momenta of the final-state (FS) particles. The total number of events per time n_f is accordingly given by

$$n_f = \mathcal{L}_{\mathrm{in}} \int \mathrm{d}\mathcal{O}\left[\frac{\mathrm{d}\sigma_{i\to f}}{\mathrm{d}\mathcal{O}}\right] \equiv \mathcal{L}_{\mathrm{in}}\;\sigma_{i\to f}\,, \tag{2.3.2}$$

defining the integrated cross section $\sigma_{i\to f}$, where usually event-selection cuts will be applied in the evaluation of (2.3.2).

In QFT, the integrated partonic (indicated by a hat) unpolarized cross section for a process with two massless QCD partons a and b in the initial state is described theoretically by the convolution of the square of the scattering amplitude,

$$\overline{|\mathcal{M}_{ab\to f}|^2} = \frac{1}{n(c_a)\,n(c_b)\;n(\sigma_a)\,n(\sigma_b)} \sum_{c_a,c_b}\sum_{c_f}\sum_{\sigma_a,\sigma_b}\sum_{\sigma_f} |\mathcal{M}_{ab\to f}|^2\,, \tag{2.3.3}$$

averaged over the number of colours $n(c_{a/b})$ and helicities $n(\sigma_{a/b})$ of initial-state (IS) particles and summed over the FS colours and polarizations, and the differential phase space $\mathrm{d}\Phi_{(n)}$ representing the kinematical degrees of freedom of the n-particle final state f,

$$\hat{\sigma}_{ab\to f}(p_a,p_b) = \frac{1}{2\hat{s}}\int \mathrm{d}\Phi_{(n)}(p_a,p_b;k_1\ldots,k_n)\,\overline{|\mathcal{M}_{ab\to f}(p_a,p_b;k_1,\ldots,k_n)|^2}\;F^{(n)}(\{\mathcal{O}_j\})\,. \tag{2.3.4}$$

Here, p_a and p_b are the momenta of the IS partons, $k_1,\ldots,k_n$ depict the FS momenta, and $\hat{s} = (p_a+p_b)^2$ denotes the partonic center-of-mass (cm) energy squared. If there are m

identical particles in the final state f, the cross section additionally has to be multiplied with a factor $(1/m!)$. The cut function $F^{(n)}$ equals zero if the event does not pass certain event-selection cuts defined using a set of observables $\{\mathcal{O}_j\}$, and it is one otherwise. The differential phase space in 4 dimensions reads

$$\mathrm{d}\Phi_{(n)}(p_a, p_b; k_1 \ldots, k_n) \equiv (2\pi)^{4-3n} \left[\prod_{i=1}^{n} \mathrm{d}^4 k_i \, \delta(k_i^2 - m_i^2)\theta(k_i^0)\right] \delta^{(4)}\left(p_a + p_b - \sum_{i=1}^{n} k_i\right), \tag{2.3.5}$$

where $m_i = \sqrt{k_i^2}$ denotes the mass of particle i in the final state.

2.3.2 Hadronic cross sections

Now we consider a collision of two hadrons A and B in the so called *infinite-momentum frame* where the hadrons are moving fast in the x^3-direction, and their masses are small compared to their energies. In this special situation the transverse momenta of the partons can be neglected, and the four-momentum $p_{a(b)}$ of a parton belonging to hadron $A(B)$ is related to the hadronic four-momentum $p_{A(B)}$ via

$$p_{a(b)} = x_{a(b)} p_{A(B)} \,, \tag{2.3.6}$$

with $0 < x_{a(b)} < 1$. Now we can provide the hadronic cross section for the process

$$A(p_A) + B(p_B) \quad \to \quad f + X \,, \tag{2.3.7}$$

where f symbolizes the final state of the hard scattering event, and X denotes the remnants of the two IS hadrons which are destroyed in the hadronic collision. The hadronic cross section is given by

$$\mathrm{d}\sigma_{AB\to f}(p_A, p_B) = \sum_{a,b} \int_0^1 \mathrm{d}x_a \int_0^1 \mathrm{d}x_b \left[f_{a/A}(x_a)\, f_{b/B}(x_b)\, \mathrm{d}\hat{\sigma}_{ab\to f}(p_a, p_b)\right] , \tag{2.3.8}$$

where we have to sum over all relevant pairs $\{a, b\}$ of partons. The functions $f_{a/A}(x_a)$ are called *parton distribution functions* (PDFs). The expression $f_{a/A}(x_a)\,\mathrm{d}x_a$ gives the total number of partons a in a momentum interval $(x_a, x_a + \mathrm{d}x_a)$ within the hadron A. The PDFs cannot be computed from first principles since they are non-perturbative quantities for hadrons; nevertheless, they can be measured by fitting experimental data of deep-inelastic lepton-nucleon scattering (DIS) or hadron–hadron scattering processes. Note that in (2.3.8) we have to perform the convolution over the PDFs and the phase-space integration of (2.3.4) at the same time to allow for the proper calculation of differential cross sections. An illustration of the hadronic process $AB \to \mathrm{W} + \mathrm{jet} + \gamma + X \to l\nu_l + \mathrm{jet} + \gamma + X$ that is discussed in this thesis can be found in Fig. 2.1.

The squared hadronic cm energy is $s = (p_A + p_B)^2$. In the laboratory (lab) frame the IS four-momenta can be expresses via

$$p_A^\mu = \frac{\sqrt{s}}{2}(1, 0, 0, +1) \,, \quad p_B^\mu = \frac{\sqrt{s}}{2}(1, 0, 0, -1) \,, \tag{2.3.9}$$

and according to their definition the partonic momenta read

$$p_a^\mu = x_a \, \frac{\sqrt{s}}{2}(1, 0, 0, +1) \,, \quad p_b^\mu = x_b \, \frac{\sqrt{s}}{2}(1, 0, 0, -1) \,. \tag{2.3.10}$$

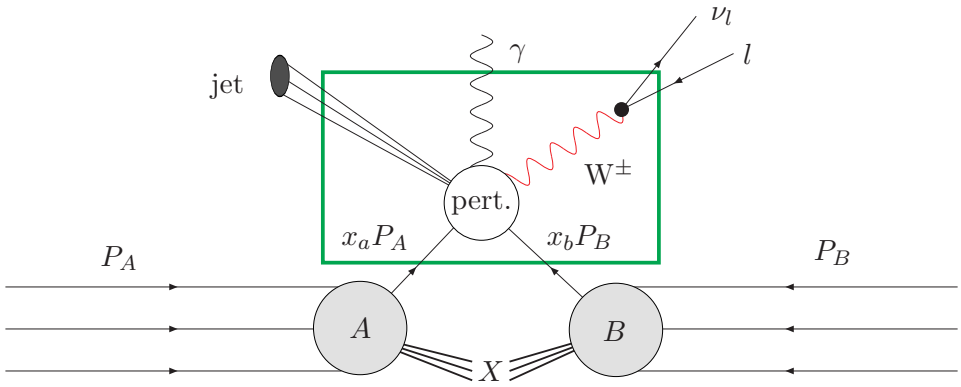

Figure 2.1: Schematic illustration for the hadronic process $AB \to \mathrm{W}{+}\mathrm{jet}{+}\gamma{+}X \to l\nu_l{+}\mathrm{jet}{+}\gamma{+}X$. The perturbative partonic cross section is indicated by a green box.

In the partonic cm frame we find the expression

$$\hat{p}_a^\mu = \frac{\sqrt{\hat{s}}}{2}(1,0,0,+1)\,, \quad \hat{p}_b^\mu = \frac{\sqrt{\hat{s}}}{2}(1,0,0,-1)\,, \tag{2.3.11}$$

for the partonic four-momenta, with $\hat{s} = x_a x_b\, s \equiv \tau s$.

Note that the partonic cross section $\mathrm{d}\hat{\sigma}_{ab\to f}$ is often calculated using momenta defined in the partonic cm frame. Whenever one wants to apply event-selection cuts or sort events into histogram bins, one has to boost the momenta along the beam axis into the lab frame that coincides with the cm frame of the hadrons A and B. The boost parameter of the partonic cm frame for parton a moving in positive x^3-direction is given by

$$\beta_{ab} = \frac{x_a - x_b}{x_a + x_b}\,, \tag{2.3.12}$$

and the FS momenta k_i^μ in the lab frame can be obtained from the ones in the partonic cm frame $\hat{k}_i^\mu$ via the boost

$$\begin{aligned} k_i^0 &= \gamma_{ab}\left(\hat{k}_i^0 - \beta_{ab}\hat{k}_i^3\right)\,, \\ k_i^1 &= \hat{k}_i^1\,, \\ k_i^2 &= \hat{k}_i^2\,, \\ k_i^3 &= \gamma_{ab}\left(\hat{k}_i^3 - \beta_{ab}\hat{k}_i^0\right)\,, \end{aligned} \tag{2.3.13}$$

where we have used $\gamma_{ab} = 1/\sqrt{1-\beta_{ab}^2}$.

2.3.3 The QCD improved parton model

In Section 3.3 we will see that the inclusion of higher-order QCD corrections into the calculation of hadronic cross sections enforces a redefinition of the bare PDFs in Eq. (2.3.8) in an appropriate *factorization* procedure to absorb residual collinear singularities that arise in the perturbative calculation of the partonic cross section. Those singularities can be explained by the fact that in the collinear regime perturbative QCD is not anymore suited for

a proper description of the underlying physics. However, the problematic singular structures turn out to be universal, i.e. they factorize from the hard scattering cross section and can be ascribed to the non-perturbative contributions contained in the PDF of the incoming QCD parton. After the redefinition of the PDFs—which can be understood as a renormalization procedure—the cross section of the perturbatively-defined hard scattering event is infrared safe, and the hadronic cross section can be evaluated consistently.

The possibility of factorizing universal collinear-singular long-distance effects into the non-perturbative part of the hadronic cross section is a fundamental property of the theory which turns QCD into a reliable calculational tool with controllable approximations. For DIS and Drell–Yan-like processes this factorization in universal non-perturbative and process-dependent perturbative parts has proven to be possible at any order of perturbation theory [61].

The "naive" parton model introduced at the beginning of this section that is extended by the strong interaction of partons and the factorization of non-perturabtive IS contributions is known as the *QCD improved parton model* (see, e.g., Ref. [62]). The technical details of the factorization procedure at NLO QCD will be discussed in Section 3.3.

Chapter 3

Infrared singularities in NLO corrections

3.1 Infrared singularities in QED & QCD

Infrared (IR) singularities appear in phase-space integrals of real-emission processes as well as in loop integrals appearing in virtual radiative corrections. In contrast to UV divergences that emerge at large loop momenta within virtual corrections, the IR singularities are related to low-momentum and small-angle regions in real and virtual corrections. We can distinguish two types of IR singularities (see ,e.g., Ref. [63]):

- A *soft* singularity arises if the energy of a massless real vector boson (photon or gluon) that is radiated off an external on-shell particle approaches zero, or if a virtual massless vector boson is exchanged between two on-shell lines within a 1PI loop diagram.

- One can distinguish two types of *collinear singularities*, connected to certain splittings in the initial state or the final state of a hard scattering event. We now briefly describe the collinear-singular situations that appear in real and virtual NLO corrections (four-momenta of particles are given in brackets).

  We observe a *FS collinear singularity* if a virtual light particle (light fermions or massless vector bosons) $\widetilde{ij}(p_{ij})$ in the final state splits into two external light particles $i(p_i)$ and $j(p_j)$ that are collinear (i.e. $(p_i p_j) \to 0$). On the other hand, *IS collinear singularities* appear if a light on-shell particle $a(p_a)$ in the initial state collinearly emits another light on-shell particle $i(p_i)$ (i.e. $(p_a p_i) \to 0$), while the second particle $\widetilde{ai}(p_a - p_i)$ of the splitting undergoes a hard scattering process. If a light on-shell particle splits into two light particles within a 1PI loop diagram, there will also be a collinear singularity. The collinear-singular structures that may appear in radiative processes are depicted in Fig. 3.1.

Note that soft and collinear singularities also arise within on-shell derivatives of certain self-energy contributions that appear in the field renormalization constants in the on-shell renormalization scheme (see Section 2.1.3).

Soft- and collinear-singular situations in loop integrals are shown in Fig. 3.2. Since IR singularities only appear when the involved particles are light or exactly massless, IR

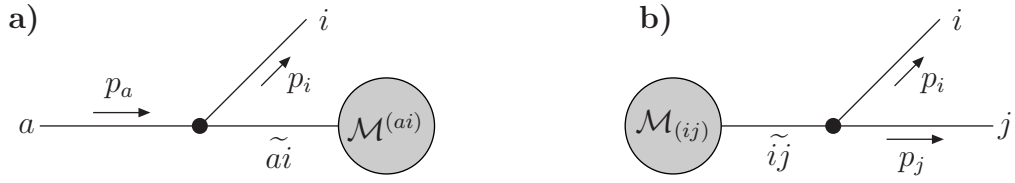

Figure 3.1: Collinear singularities in IS (a) and FS (b) splittings within a radiative process. An IS collinear singularity occurs if the scalar product $(p_a p_i)$ gets small, and we observe FS collinear singularities for $(p_i p_j) \to 0$. The underlying hard scattering processes are represented by their amplitudes $\mathcal{M}^{(ai)}$ and $\mathcal{M}_{(ij)}$, respectively.

singularities are also called *mass singularities*. In real-emission processes, they emerge because the phase-space integral over the propagator of the particle initiating the problematic splitting will diverge logarithmically if the singular structure is not regularized properly. In case of a collinear divergence, the problematic singular structure arises in expressions of the form $\int_0^1 \mathrm{d}\cos\theta/(1-\cos\theta)$ within the integration of the angle θ between the two collinear particles. In soft-singular situations, we are confronted with integrals as $\int_0^{E_{\max}} \mathrm{d}E/E$ that exhibit a logarithmic divergence if the energy E of the emitted photon/gluon goes to zero.

3.1.1 Infrared singularities in QED

All IR singularities related to the $\gamma f \bar{f}$-vertex, where f indicates a light fermion, can be found in Table 3.1. Of course, a photon that is radiated off an external (on-shell) W boson will also cause a soft singularity. This situation will be discussed in detail in Chapter 5. However, in a realistic physical situation the W boson will decay into a quark or lepton pair, and the soft singularity eventually can be ascribed to soft photon radiation off light fermions. If a photon is radiated off an external top quark, we will only observe a soft-singular contribution, because there is no collinearly-divergent propagator due to the large top-quark mass.

We regularize the soft singularity by introducing an infinitesimal photon mass λ and keep small fermion-mass parameters m_f to regularize the collinear-singular situations in the calculation of the real and virtual EW corrections. Working out the singular integrals, one obtains terms $\propto \alpha \ln(\lambda^2/Q^2)$ in the soft-singular situations, and terms $\propto \alpha \ln(m_f^2/Q^2)$ for the collinear singularities, where Q denotes the typical scale of the hard process. If the two singularities overlap in phase space, we observe contributions $\propto \alpha \ln(m_f^2/Q^2)\left[\ln(m_f^2/Q^2) + \ln(\lambda^2/Q^2)\right]$.

It is important to stress that collinear lepton–photon splittings are not literally inducing a singularity, because the lepton mass regularizes the singular structure in a physically meaningful way. Nevertheless, in high-energy processes at hadron colliders the lepton-mass parameters m_l are small compared to the reference scale Q of the underlying hard scattering events. Thus, it is wise to handle the lepton mass as if it was a regulator in the numerical evaluation to ensure numerical stability. This means that the logarithmic lepton-

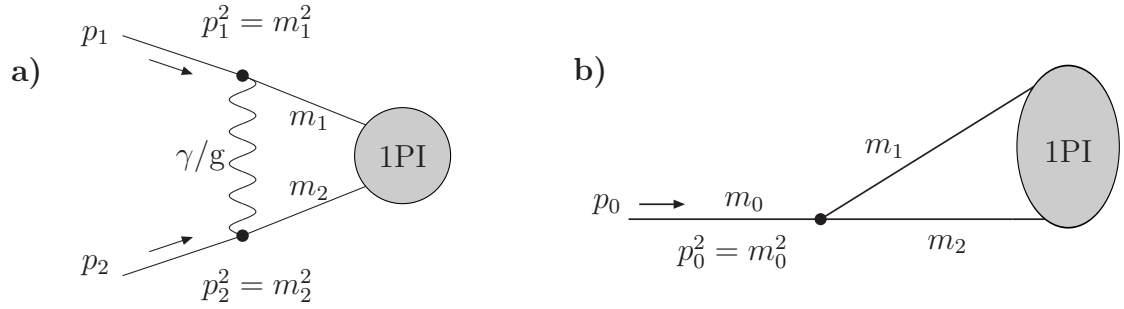

Figure 3.2: Soft singularities (a) and collinear singularities (b) in virtual corrections. A collinear singularity only occurs if m_0, m_1, and m_2 are small compared to typical other scales of the considered process or exactly zero. If particles 1 and 2 in diagram (b) are fermions, there is no collinear singularity due to the coupling structure in the collinear limit [48].

mass dependences in a cross section should be extracted from the numerical evaluation and be isolated as analytical terms $\propto \ln(m_l^2/Q^2)$.

A consistent calculation of NLO EW corrections enforces the computation of real radiative corrections with an additional bremsstrahlung photon in the final state. However, at NLO the unphysical logarithmic photon-mass dependence caused by radiation of a soft photon will drop out in the sum of real and virtual contributions according to the Bloch–Nordsieck theorem [64] if the real photon radiation is treated sufficiently inclusive. Practically this means that the full soft-photon phase space must be covered in the computation of the bremsstrahlung integral. This is consistent with the experimental demands, since it is not possible to apply cuts to kinematical configurations with arbitrarily soft photons.

3.1.2 Infrared singularities in QCD

In QCD it is not convenient to introduce an infinitesimal gluon mass to regularize the soft gluon pole or the collinear pole that arises in the $g \to gg$ splitting. Since we work in the QCD improved parton model, we also have to assume all light quarks that contribute to the parton content of the proton as massless. Therefore, we use dimensional regularization (see Section 2.1.3) to enable the calculation of IR-singular contributions.[1] Within this framework, soft or collinear singularities will arise as $1/\epsilon$ poles. If the singularities overlap, we observe poles of $1/\epsilon^2$. In Table 3.2 we show IR-singular scenarios that can appear in real-emission and one-loop processes in QCD.

[1] As in the QED case, one could also safely insert small quark-mass parameters to properly regularize the collinear-singular structures that appear due to the $gq\bar{q}$-vertex.

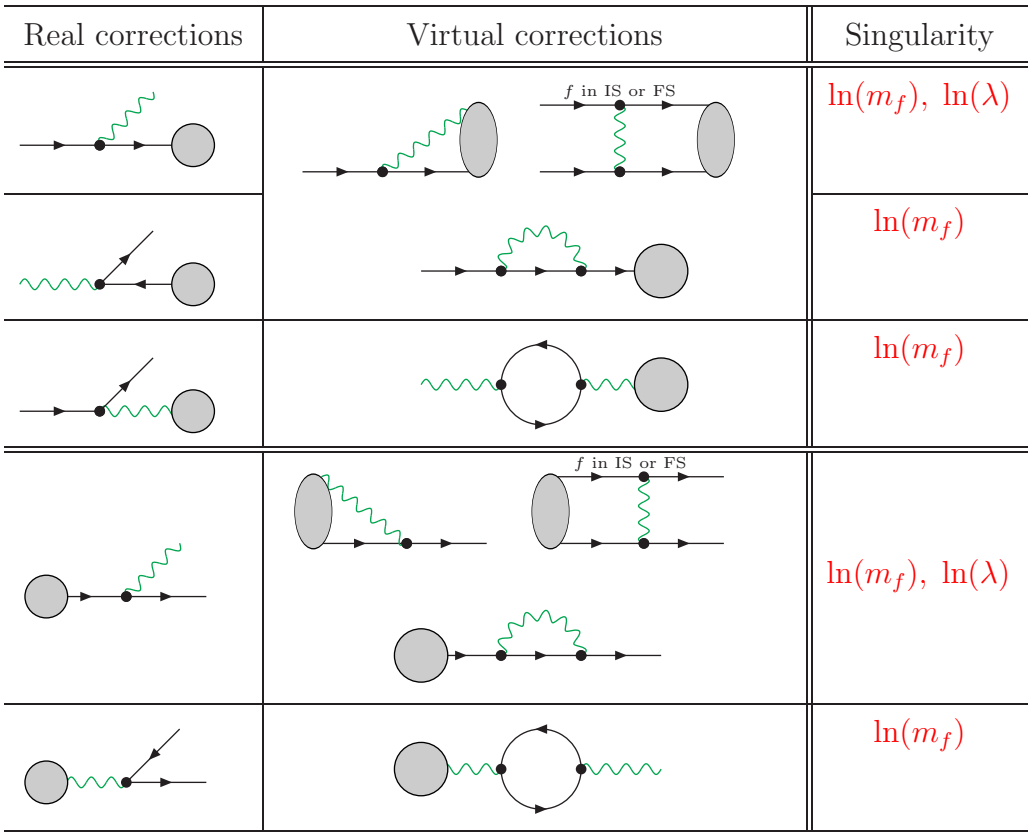

Table 3.1: Relevant graphs for IR singularities in real and virtual corrections within NLO QED corrections. Diagrams in one row contribute to the same LO process indicated by the grey blob. The collinear singularities can arise from IS or FS splittings and appear as terms of $\ln(m_f)$. In case of soft singularities, there will be terms of $\ln(\lambda)$ and $\ln(m_f)\ln(\lambda)$. There will also be a soft singularity if a photon is exchanged between FS and IS fermions. The arrows depicting the fermion-number flow may also be reversed.

3.2 Squared amplitudes in the IR limit

We will now discuss some general factorization properties of squared physical amplitudes in the soft or collinear limit and present the structure of those factorized expressions. Doing so, we will focus on soft and collinear photon radiation in QED, since these formulae are very important in the calculation of EW radiative corrections. On should mention that the existence of such factorization properties is the basis for any general method that allows for the analytical extraction of IR singularities from the numerical phase-space integration, as e.g. achieved in slicing and subtraction techniques.

3.2.1 Factorization in the soft limit – the eikonal approximation

Consider a partonic scattering process with n FS particles with four-momenta $p_1, \ldots, p_n$ and one additional bremsstrahlung photon with momentum k. If the energy $E_\gamma = k^0$ of

Real corrections	Virtual corrections	Singularity
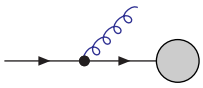	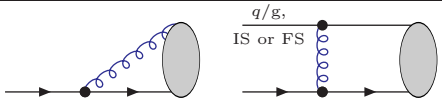	$1/\epsilon,\ 1/\epsilon^2$
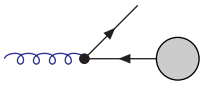	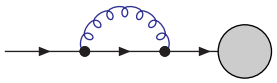	$1/\epsilon$
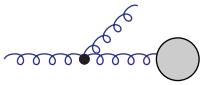	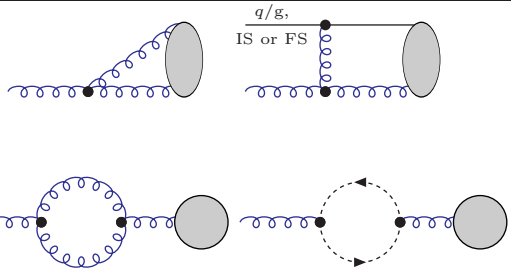	$1/\epsilon,\ 1/\epsilon^2$
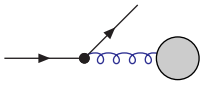	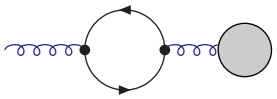	$1/\epsilon$
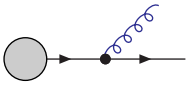	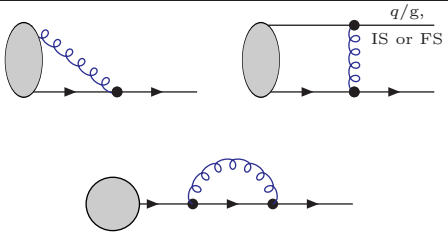	$1/\epsilon,\ 1/\epsilon^2$
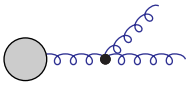	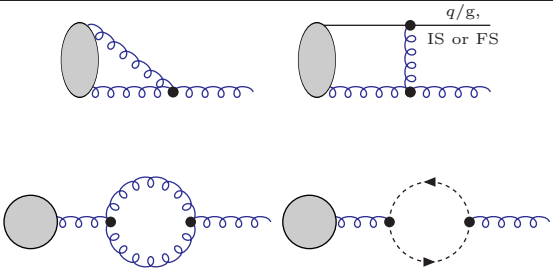	$1/\epsilon,\ 1/\epsilon^2$
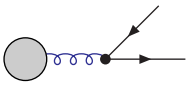	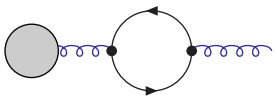	$1/\epsilon$

Table 3.2: Situations for IR singularities in real and virtual corrections within NLO QCD corrections. Diagrams in one row contribute to the same LO process indicated by they grey blob. The singularities can arise from IS and FS splittings and show up as poles of $1/\epsilon$ or $1/\epsilon^2$. Soft and collinear singularities also appear if a gluon is interchanged between external IS and FS quarks or gluons. The arrows depicting the fermion-number flow may also be reversed.

the radiated photon becomes small, the corresponding squared bremsstrahlung amplitude $|\mathcal{M}_{n+\gamma}|^2$, summed over the photon polarizations, factorizes into an *eikonal factor* and the squared amplitude $|\mathcal{M}_n|^2$ without additional photon radiation [65],

$$\sum_{\lambda_\gamma} |\mathcal{M}_{n+\gamma}(p_a, p_b; p_1, \ldots, k, \ldots, p_n)|^2$$
$$\widetilde{E_\gamma \to 0} \; -\sum_{i,j} Q_i \sigma_i Q_j \sigma_j e^2 \frac{p_i p_j}{(p_i k)(p_j k)} \, |\mathcal{M}_n(p_a, p_b; p_1, \ldots, p_n)|^2 + \mathcal{O}(1)\,, \quad (3.2.1)$$

where we have suppressed terms that do not contribute in the soft limit after phase-space integration. The indices i and j run over all external charged particles that carry the electrical charges $Q_i e$ and $Q_j e$, respectively. The sign factors σ_i and σ_j define the charge flow of i and j into or out of the diagram. We define $\sigma_f = +1$ for incoming fermions and outgoing antifermions, and $\sigma_f = -1$ for outgoing fermions and incoming antifermions. For an incoming charged W^- boson or an outgoing W^+ boson we define $\sigma_\mathrm{W} = +1$. Since the W^+ is defined to be the antiparticle, the charge of the W boson is $Q_\mathrm{W} = -1$. Charge conservation implies

$$\sum_i Q_i \sigma_i = 0\,, \quad (3.2.2)$$

if we sum over all external charged particles. A formula similar to (3.2.1) can be deduced for soft-gluon radiation in QCD (See, e.g., Eq. (4.3) in [66]).

3.2.2 Asymptotic behaviour in the collinear limit

Consider a real-emission process

$$a(p_a) + b(p_b) \to c_1(p_1) + \ldots + c_{n+1}(p_{n+1})\,, \quad (3.2.3)$$

which is described by the scattering amplitude $\mathcal{M}_{n+1}$. The particle momenta are given in parentheses. It is possible to find general factorization formulae for any splitting depicted in the left columns of Table 3.1 and Table 3.2, respectively, if the kinematical configuration approaches the collinear limit, i.e. the scalar product of the two collinear particles becomes small. Schematically, all those formulae can be expressed as

$$|\mathcal{M}_{n+1}(p_a, p_b)|^2 \;\widetilde{p_a p_i \to 0}\; \boldsymbol{g}^{a,i}(p_i, p_a, x_a) \otimes |\mathcal{M}_n^{(ai)}(p_{ai} = x_a p_a, p_b)|^2\,, \quad (3.2.4a)$$

$$|\mathcal{M}_{n+1}(p_a, p_b; \ldots, p_i, \ldots, p_j, \ldots)|^2$$
$$\widetilde{p_i p_j \to 0}\; \boldsymbol{g}_{i,j}(p_i, p_j, z_i) \otimes |\mathcal{M}_{n,(ij)}(p_a, p_b; \ldots, p_{ij} = p_i + p_j, \ldots)|^2, \quad (3.2.4b)$$

for IS and FS collinear singularities. We will now discuss those expressions in some detail. The variable

$$x_a = \frac{p_a^0 - p_i^0}{p_a^0} \quad (3.2.5)$$

denotes the energy fraction of p_a that enters the hard scattering process without splitting specified by the amplitude $\mathcal{M}_n^{(ai)}$ as indicated in Fig. 3.1(a), and

$$z_i = \frac{p_i^0}{p_i^0 + p_j^0} \quad (3.2.6)$$

is the energy fraction that is carried away by particle i in the collinear FS splitting. The information of the hard subprocess before the collinear splitting is contained in $\mathcal{M}_{n,(ij)}$ (see Fig. 3.1(b)). The universal prefactors $\boldsymbol{g}^{ai}(x_a)$ and $\boldsymbol{g}_{ij}(z_i)$ are independent of the underlying hard process and contain the physical information of the corresponding splitting in the collinear limit. The symbol $\otimes$ in (3.2.4) indicates that, besides normal factorization, spin correlations appear for certain splittings, namely if a vector boson enters the hard scattering.

Collinear photon radiation

In case of collinear photon radiation off light (anti)fermions, the general formulae for the squared averaged amplitudes in the collinear limit (3.2.4) explicitly read [35]

$$\begin{aligned}
\overline{|\mathcal{M}_{n+\gamma}(p_f,p_b)|^2} &\underset{p_f k\to 0}{\sim} g^{f,\gamma}(k,p_f,x_f)\,\overline{\left|\mathcal{M}_n^{(f)}(x_f p_f,p_b)\right|^2}\,,\\
\overline{|\mathcal{M}_{n+\gamma}(p_a,p_b;\ldots,k,\ldots,p_f,\ldots)|^2} &\underset{k p_f\to 0}{\sim} g_{\gamma,f}(k,p_f,z_f)\,\overline{|\mathcal{M}_{n,(f)}(p_a,p_b;\ldots,k+p_f,\ldots)|^2},
\end{aligned} \tag{3.2.7}$$

and—up to terms that are finite in the collinear limit—the unpolarized splitting kernels are given by

$$\begin{aligned}
g_{\gamma,f}(k,p_f,x_f) &= \frac{1}{p_f k}\left[P_{ff}(z_f)-\frac{m_f^2}{p_f k}\right],\\
g^{f,\gamma}(k,p_f,z_f) &= \frac{1}{x_f\,(p_f k)}\left[P_{ff}(x_f)-\frac{x_f\,m_f^2}{p_f k}\right],
\end{aligned} \tag{3.2.8}$$

with the splitting function

$$P_{ff}(\xi)=\frac{1+\xi^2}{1-\xi}\,. \tag{3.2.9}$$

3.3 Factorization of initial-state singularities in QCD

In NLO QCD calculation all soft singularities and collinear singularities due to FS splittings will drop out of any properly-defined jet observable as a consequence of the KLN theorem [67]. Nevertheless, in the calculation of perturbative corrections to hadronic scattering processes residual IR singularities arise that are caused by (real and virtual) collinear parton radiation from IS (anti)quarks or gluons. These singularities are the consequence of the fact that the collinear scenario is not describable in a perturbative approach anymore, since the collinear radiation is settled at a low scale where QCD is strongly coupled.

These collinear singularities turn out to be universal, i.e. they are independent of the hard scattering event. Thus, one can factorize them for all processes in the same way into the renormalized PDFs. As a trade-off one has to introduce a *factorization scale* μ_{F} into the calculation that separates the perturbative from the non-perturbative regime.

In NLO QCD factorization can be described as a replacement of the bare PDF of parton a according to

$$f_{a/A}(x) \to f^{\text{F.S.}}_{a/A}(x,\mu_{\text{F}}^2) + \sum_{a'} \int_x^1 \frac{\mathrm{d}z}{z} f^{\text{F.S.}}_{a'/A}\left(\frac{x}{z},\mu_{\text{F}}^2\right) \frac{\alpha_{\text{s}}}{2\pi} \left[\frac{P^{a'a}(z)}{\Gamma(1-\epsilon)\epsilon}\left(\frac{4\pi\mu^2}{\mu_{\text{F}}^2}\right)^{\epsilon} - K^{a'a}_{\text{F.S.}}(z)\right], \tag{3.3.1}$$

where the $P^{a'a}(z)$ denote the renormalized Altarelli–Parisi splitting functions in four dimensions that can be found in Appendix C of [66]. The terms $K^{a'a}_{\text{F.S.}}$ contain the finite terms that are shifted to the renormalized PDFs, i.e. they depend on the choice for the so-called *factorization scheme* (F.S.). In our calculation of the NLO QCD corrections we use the modified minimal-subtraction ($\overline{\text{MS}}$) scheme where the contribution in (3.3.1) proportional to

$$\Delta_1^{\text{IR}} \equiv \frac{1}{\epsilon}\frac{(4\pi)^{\epsilon}}{\Gamma(1-\epsilon)} = \frac{1}{\epsilon} - \gamma_{\text{E}} + \ln 4\pi + \mathcal{O}(\epsilon)\,, \tag{3.3.2}$$

which is typical for dimensional regularization, is absorbed into $f^{\overline{\text{MS}}}_{a/A}(x,\mu_{\text{F}}^2)$. For this special choice we find $K^{a'a}_{\overline{\text{MS}}}(z) \equiv 0$. In (3.3.2), γ_{E} is the Euler–Mascheroni constant.

Technically, the factorization can be arranged by adding a universal collinear counterterm $\mathrm{d}\hat{\sigma}^{\text{C}}$ to the partonic cross section and replacing the PDFs according to $f_{a/A}(x) \to f^{\text{F.S.}}_{a/A}(x,\mu_{\text{F}})$. For a two-parton initial state the collinear counterterm reads

$$\begin{aligned}
\mathrm{d}\hat{\sigma}^{\text{C}}_{ab}(p_a,p_b;\mu_{\text{F}}) = {} & -\frac{\alpha_s}{2\pi}\frac{1}{\Gamma(1-\epsilon)}\sum_{c,d}\int_0^1 \mathrm{d}z \int_0^1 \mathrm{d}\bar{z}\; \mathrm{d}\hat{\sigma}^0_{cd}(zp_a,\bar{z}p_b) \\
& \times \left\{\delta_{bd}\,\delta(1-\bar{z})\left[-\frac{1}{\epsilon}\left(\frac{4\pi\mu^2}{\mu_{\text{F}}^2}\right)^{\epsilon} P^{ac}(z) + K^{ac}_{\text{F.S.}}(z)\right]\right. \\
& \left. + \delta_{ac}\,\delta(1-z)\left[-\frac{1}{\epsilon}\left(\frac{4\pi\mu^2}{\mu_{\text{F}}^2}\right)^{\epsilon} P^{bd}(\bar{z}) + K^{bd}_{\text{F.S.}}(\bar{z})\right]\right\}.
\end{aligned} \tag{3.3.3}$$

If one investigates partonic processes with just one IS QCD parton, like DIS or photon-induced contributions at hadron colliders, the collinear counterterm is given by

$$\mathrm{d}\hat{\sigma}^{\text{C}}_{a}(p_a;\mu_{\text{F}}) = -\frac{\alpha_s}{2\pi}\frac{1}{\Gamma(1-\epsilon)}\sum_{b}\int_0^1 \mathrm{d}z \left[-\frac{1}{\epsilon}\left(\frac{4\pi\mu^2}{\mu_{\text{F}}^2}\right)^{\epsilon} P^{ab}(z) + K^{ab}_{\text{F.S.}}(z)\right]\mathrm{d}\hat{\sigma}^0_b(zp_a)\,. \tag{3.3.4}$$

Taking NLO factorization into account, the partonic NLO cross section can be summarized as

$$\hat{\sigma}^{\text{NLO}}_{ab} = \int_{n+1}\mathrm{d}\hat{\sigma}^{\text{R}}_{ab} + \int_n \mathrm{d}\hat{\sigma}^{\text{V}}_{ab} + \int_n \mathrm{d}\hat{\sigma}^{\text{C}}_{ab}\,, \tag{3.3.5}$$

where the cross sections $\int_{n+1}\mathrm{d}\hat{\sigma}^{\text{R}}_{ab}$ and $\int_n \mathrm{d}\hat{\sigma}^{\text{V}}_{ab}$ of the real and virtual corrections will be formally defined in Section 4.4.1. Using the dipole subtraction formalism for the calculation of the real QCD corrections (see Section 4.4), the collinear counterterm will automatically be included when the subtracted contributions are added to the cross section again.

3.4 Factorization of initial-state singularities in QED

Similar to the procedure in QCD, the residual $\ln(m_q)$-dependence resulting from IS QED splittings can be factorized into renormalized PDFs according to the replacement [68]

$$\begin{aligned} f_{q/A}(x) \to f_{q/A}^{\text{F.S.}}(x,\mu_\text{F}^2) &- \int_x^1 f_{q/A}^{\text{F.S.}}\left(\frac{x}{z},\mu_\text{F}^2\right)\frac{\alpha}{2\pi}Q_q^2 \\ &\times\left\{\ln\left(\frac{\mu_\text{F}^2}{m_q^2}\right)\left[P_{ff}(z)\right]_+ - \left[P_{ff}(z)\left(2\ln(1-z)+1\right)\right]_+ + C_{ff}^{\text{F.S.}}(z)\right\} \\ &- \int_x^1 f_{\gamma/A}^{\text{F.S.}}\left(\frac{x}{z},\mu_\text{F}^2\right)\frac{\alpha}{2\pi}3Q_q^2\left\{\ln\left(\frac{\mu_\text{F}^2}{m_q^2}\right)P_{f\gamma}(z) + C_{f\gamma}^{\text{F.S.}}(z)\right\}, \end{aligned} \tag{3.4.1}$$

with

$$P_{f\gamma}(\xi) = \xi^2 + (1-\xi)^2\,. \tag{3.4.2}$$

Equation (3.4.1) accounts for both the case in which an IS quark radiates a collinear photon and for the case of an incoming photon splitting into a collinear $q\bar{q}$-pair where the q initiates the hard scattering process. It is also valid for antiquarks if one replaces q by $\bar{q}$. Again, the process of factorization introduces a scheme dependence since we can absorb in principle arbitrary finite parts into the renormalized PDFs. This scheme dependence is contained in the structure functions $C_{ij}^{\text{F.S.}}(z)$.

In the calculation of the EW corrections to off-shell W + jet production we will apply the so-called DIS scheme that is defined in such a way that the DIS structure function F_2 is unchanged at NLO. We make this choice, because the `MRSTQED2004` PDF set we apply in our calculation is defined in a DIS factorization scheme with respect to QED corrections [68].

In analogy to QCD, one can furthermore define the $\overline{\text{MS}}$ factorization scheme for IS collinear QED singularities at NLO in the following way: First, the logarithmic quark-mass divergences in (3.4.1) are expressed as $1/\epsilon$ poles in d dimensions. In a second step, one demands that—as in QCD—the terms proportional to (3.3.2) are absorbed into the renormalized PDFs, thereby defining the finite parts of $C_{ij}^{\overline{\text{MS}}}(z)$. The coefficient functions $C_{ij}^{\text{F.S.}}(x)$ for the $\overline{\text{MS}}$ and the DIS scheme are then given by

$$\begin{aligned} C_{ff}^{\overline{\text{MS}}}(z) &= C_{f\gamma}^{\overline{\text{MS}}}(z) = 0\,, \\ C_{ff}^{\text{DIS}}(z) &= \left[P_{ff}(z)\left(\ln\left(\frac{1-z}{z}\right) - \frac{3}{4}\right) + \frac{9+5z}{4}\right]_+, \\ C_{f\gamma}^{\text{DIS}}(z) &= P_{f\gamma}(z)\ln\left(\frac{1-z}{z}\right) - 8z^2 + 8z - 1\,. \end{aligned} \tag{3.4.3}$$

3.5 Infrared safety – definition of jet observables

A proper definition of jet observables is a very important topic, since it addresses the question of how to construct physical jets from partons in perturbation theory. First of all, it is mandatory to ensure that jet quantities are defined in an *IR-safe* way. This means that at NLO an n-parton final state must not be identified as an $(n+1)$-parton final state

if one adds one additional parton that is either collinear to another parton, or arbitrarily soft.

There are two reasons for demanding IR safety, one is more of practical nature, while the other has its origin in the underlying theory.

On the experimental side, it is not possible to separate two sufficiently collinear partons in any realistic detector configuration, since the partons will in reality first undergo a parton shower and afterwards hadronize, leaving a multi-hadron signal in the hadronic calorimeter. If the energy of a jet is too low, however, it will not lead to a signal in the detector at all. Therefore, no experimental setup is sensitive to any ultra-soft parton activity.

On the theory side, soft and collinear parton configurations connected to an additional parton arising from real radiation lead to IR singularities in the real-emission cross section $\mathrm{d}\hat{\sigma}^{\mathrm{R}}$. These unphysical singularities will only drop out in the full NLO cross section if all collinear and soft contributions are treated fully inclusively, simulating the experimental demands. This request can be translated to certain properties of the jet function $F_J^{(\mathcal{R}+k)}$. This quantity defines the jet observables for a k-parton final state, i.e. it contains a prescription how to construct physical jets from k distinct partons. It also includes event selection cuts that apply to the FS jets as well as to the non-strongly-interacting particles in the final state, symbolized by $\mathcal{R}$.

In order to respect IR safety in the soft limit, we demand [66]

$$F_J^{(\mathcal{R}+n+1)}(p_1,\ldots,p_j=\lambda q,\ldots,p_{n+1};p_a,p_b)\to F_J^{(\mathcal{R}+n)}(p_1,\ldots,p_{n+1};p_a,p_b)\quad\text{if}\quad\lambda\to 0\,, \tag{3.5.1}$$

for the $(n+1)$-parton jet function. To ensure collinear safety, the jet function has to fulfill

$$F_J^{(\mathcal{R}+n+1)}(p_1,\ldots,p_i,\ldots,p_j,\ldots,p_{n+1};p_a,p_b)\to F_J^{(\mathcal{R}+n)}(p_1,\ldots,p,\ldots,p_{n+1};p_a,p_b)$$
$$\text{if}\quad p_i\to zp\quad\text{and}\quad p_j\to(1-z)p\,. \tag{3.5.2}$$

In a realistic situation, the partons i and j have to be merged in a well-defined way if they cannot be separated in a sensible experimental setup. This is done by so-called *jet algorithms* that construct a new quasi-particle $\widetilde{ij}$ with momentum $\tilde{p}_{ij}$ from the partons i and j. This procedure is called *recombination*. There are many different jet algorithms in the literature (see ,e.g., Refs. [69]). In the actual calculation of the real QCD corrections to off-shell W + jet production we apply the Tevatron Run II k_{T}-algorithm [70] to construct physical jets from partons.

Of course, at LO the n-parton final state has to be defined in such a way that it contains n genuine jets. This implies the conditions

$$F_J^{(\mathcal{R}+n)}(p_1,\ldots,p_n;p_a,p_b)\to 0\quad\text{if}\quad p_i\cdot p_j\to 0\quad\text{or if}\quad p_i\cdot p_a\to 0\ \text{or}\ p_i\cdot p_b\to 0\,. \tag{3.5.3}$$

3.6 Non-collinear-safe observables in QED

Collinear-safe observables

In case of leptons in the final state the situation is somewhat different from the case of QCD partons. If an electron ($\mathrm{e}^{\pm}$) in the final state radiates a photon, these two particles will be detected as a shower in the electromagnetic calorimeter, a separation is impossible

and the scenario is in some sense "QCD-like". On the theory side this means that we have to define *collinear-safe* observables for this special situation. This is achieved by recombining electron and photon if they are sufficiently close to each other. As a result, any perturbative corrections that are defined in such a way will not be enhanced by $\ln(m_e)$-terms, but, since the electron mass is a physical parameter, this cancellation does not have to be demanded for theoretical consistency. In case of collinear photon radiation off FS light quarks, however, recombination is also mandatory from a theoretical point of view, because an exclusive treatment of a collinear quark–photon system will lead to residual unphysical quark-mass logarithms in the perturbative result for the cross section, unless non-perturbative effects are carefully taken into account (see Section 3.7.1).

Non-collinear-safe observables

By contrast, the configuration with a muon ($\mu^\pm$) in the final state can be treated differently. In a scenario where the muon emits a collinear photon, the photon will be detected in the calorimeter, while the muon escapes this detector and will lead to a signal in the muon chambers. Therefore, we can experimentally distinguish photons and muons that are emitted collinearly in phase space and we can apply event-selection cuts to the bare muon, i.e. we do not have to perform a recombination for final states in which photons are very close to muons. On the theory side this means that the $\ln(m_\mu)$-terms that are related to the collinear splitting will not drop out of the NLO cross section, which leads to an enhancement of the relative EW corrections. Observables that exhibit this logarithmic enhancement are called *non-collinear-safe* observables.

3.7 IR safety within W + jet production

The calculation of EW NLO corrections to W + jet production comprises a conceptual problem. In the treatment of FS collinear singularities caused by the parallel emission of a photon from an outgoing (anti)quark line, one is led to introduce a cut in an appropriate separation variable. Within the collinear phase-space region thus defined, the (anti)quark-photon system is effectively treated as one particle whose momentum is identified with the jet momentum and thus subject to an acceptance cut—e.g. a cut in transverse momentum, $p_\mathrm{T}(\mathrm{jet}) > p_\mathrm{T}^\mathrm{min}(\mathrm{jet})$—that has to be applied to ensure the experimental observation of the jet. This includes phase-space configurations where the photon essentially carries all the momentum, while the (anti)quark can, in principle, be arbitrarily soft.

This will not generate any soft IR singularities, and the recombination procedure will lead to a proper cancellation of unphysical quark-mass logarithms (see previous section). However, since (anti)quark and gluon jets can, in general, not be distinguished experimentally on an event-by-event basis, the same recombination procedure needs to be applied to a gluon–photon system in the final state as well. This time, a soft gluon will produce an IR singularity. Formally, this soft-gluon singularity could be avoided by applying the $p_\mathrm{T}^\mathrm{min}(\mathrm{jet})$ cut just to the transverse momentum of the gluon, even if it is accompanied by a collinear photon. However, such a prescription is purely academic and quite unsuitable for experimental implementation because (anti)quark and gluon jets are treated on different footings. In this thesis we will follow two different strategies to treat the problem of photon–gluon recombination in a theoretically consistent way.

- The IR singularities related to soft gluon emission can be cancelled within the NLO QCD corrections to $\mathrm{W} + \gamma$ production, so that those contributions are also taken into account in the calculation of radiative corrections to on-shell W+jet production that is discussed in Chapter 5.

- In the off-shell situation with a leptonic final state we exclude the soft gluon pole in a collinear gluon–photon configuration from our calculation by means of phase-space cuts, i.e. we discard events where the energy of the gluon in a collinear gluon–photon system gets too small. Since situations with collinear photons and quarks in the final state have to be treated analogously, this non-inclusive definition of observables will lead to residual unphysical quark-mass logarithms in the cross sections. These logarithms are subsequently absorbed into the non-perturbative parts of the quark-to-photon fragmentation function that will be discussed in the next subsection.

3.7.1 Quark-to-photon fragmentation at NLO

In contrast to the QCD situation where two collinear partons cannot be separated in any experimental setup, the situation with a collinear jet–photon pair in the final state is slightly different. If the energy fraction carried by a hard, isolated photon in a collinear photon–jet configuration is sufficiently high, the origin of this photon may be attributed to FS radiation emitted at an early stage of the QCD parton evolution process [34]. Thus, those events may be considered as a contribution to prompt-photon production and therefore be discarded from the jet cross section. The possibility of resolving collinear parton–photon pairs comprises a theoretical problem within a perturbative calculation, since any observable that is defined in such a way that it is sensitive to a single photon in a collinear photon–quark pair, will destroy IR safety: if a photon is radiated collinearly to a FS quark and we apply a cut solely to the photon, the situation is not inclusive anymore, leading to residual unphysical $\ln(m_q)$-terms in the cross section. This problem can be attacked similarly to the factorization of IS IR singularities.

As in case of the unphysical IS singularities, the logarithmic quark-mass dependence arising from the exclusive treatment of quark–photon pairs can be absorbed into the non-perturbative parts of an NLO definition of a quark-to-photon fragmentation function [72].

Consider a situation in which a light FS quark with four-momentum p splits into a collinear quark–photon pair, $q(p) \to q(\tilde{p}) + \gamma(k_\gamma)$. After the splitting the photon carries away the momentum fraction $z_\gamma p$, where z_γ is defined as the ratio of the photon energy and the energy of the quark–photon system,

$$z_\gamma = \frac{k_\gamma^0}{k_\gamma^0 + \tilde{p}^0}\,, \quad 0 < z_\gamma < 1\,. \tag{3.7.1}$$

As worked out in [72], the cross section $\sigma_{q\to\gamma}(p, z_\gamma)$ for a situation in which a FS quark emits a collinear photon can be expressed as a product of the cross section for the bare quark $\sigma_q(p)$ and the quark-to-photon fragmentation function $\mathscr{D}_{q\to\gamma}(z_\gamma)$,

$$\sigma_{q\to\gamma}(p, z_\gamma) = \sigma_q(p)\, \mathscr{D}_{q\to\gamma}(z_\gamma)\,. \tag{3.7.2}$$

The function $\mathscr{D}_{q\to\gamma}(z_\gamma)$ contains the full perturbative and non-perturbative information of the fragmentation process. At NLO,[2] the collinear quark-to-photon splitting can be calculated in dimensional regularization, using a slicing approach. We integrate out the collinear cone if $p^2 = (\tilde{p} + k_\gamma)^2 < s_{\min}$, where $s_{\min}$ is small compared to all relevant scales of the process. Now we can decompose the fragmentation function into this singular perturbative fraction and the bare non-perturbative fragmentation function $D_{q\to\gamma}(z_\gamma)$,

$$\mathscr{D}_{q\to\gamma}(z_\gamma) = D_{q\to\gamma}(z_\gamma) - \frac{1}{\epsilon}\left(\frac{4\pi\mu^2}{s_{\min}}\right)^{\epsilon}\frac{1}{\Gamma(1-\epsilon)}\left(\frac{\alpha Q_q^2}{2\pi}\right)[z_\gamma(1-z_\gamma)]^{-\epsilon}P_{q\to\gamma}(z_\gamma;\epsilon)\,, \quad (3.7.3)$$

where the quark-to-photon splitting function in d dimensions is given by

$$P_{q\to\gamma}(z;\epsilon) = \frac{1+(1-z)^2-\epsilon z}{z}\,. \quad (3.7.4)$$

The collinear pole can be absorbed into the bare parameter $D_{q\to\gamma}(z_\gamma)$ using an $\overline{\text{MS}}$ fragmentation prescription in dimensional regularization (DR),

$$D_{q\to\gamma}(z_\gamma) \to D^{(\text{DR})}_{q\to\gamma}(z_\gamma,\epsilon) = D^{\overline{\text{MS}}}_{q\to\gamma}(z_\gamma,\mu_\text{F}) + \frac{1}{\epsilon}\left(\frac{4\pi\mu^2}{\mu_\text{F}^2}\right)^{\epsilon}\frac{1}{\Gamma(1-\epsilon)}\left(\frac{\alpha Q_q^2}{2\pi}\right)\left[\frac{1+(1-z)^2}{z}\right], \quad (3.7.5)$$

where the fragmentation scale μ_F separates the perturbative from the non-perturbative regime. After this redefinition, the function $\mathscr{D}_{q\to\gamma}(z_\gamma)$ is finite; $D^{\overline{\text{MS}}}_{q\to\gamma}(z_\gamma,\mu_\text{F})$ has to be determined by experiment.

In our calculation we need (3.7.5) in the mass-regularization (MR) scheme with a quark-mass regulator m_q. The prescription then reads

$$D_{q\to\gamma}(z_\gamma) \to D^{(\text{MR})}_{q\to\gamma}(z_\gamma,m_q) = D^{\overline{\text{MS}}}_{q\to\gamma}(z_\gamma,\mu_\text{F}) + \frac{\alpha Q_q^2}{2\pi}P_{q\to\gamma}(z_\gamma)\left(\ln\frac{m_q^2}{\mu_\text{F}^2} + 2\ln z_\gamma + 1\right), \quad (3.7.6)$$

with the four-dimensional splitting

$$P_{q\to\gamma}(z) = \frac{1+(1-z)^2}{z}\,. \quad (3.7.7)$$

Note that (3.7.5) and (3.7.6) define the same finite perturbative parts that are absorbed into the bare fragmentation function $D_{q\to\gamma}$.

In our perturbative calculation for off-shell W + jet production, we will discard events where the energy fraction z_γ of the photon in a collinear parton–photon configuration after recombination is larger than a certain cut-off z_0. Doing so, the problematic soft gluon pole is explicitly excluded from our computation. However, if the parton is a quark, we will thereby effectively subtract IR singular contributions from the perturbatively well-defined inclusive configuration, leading to a perturbatively ill-defined result. However, for a consistent treatment of the fragmentation physics, we additionally have to take into account the analogous non-perturbative contributions to the fragmentation process that

[2]The quark-to-photon fragmentation function does not exist at LO.

are parametrized by $D_{q\to\gamma}(z_\gamma)$. On the technical side this means that we additionally have to subtract the expression

$$\Delta_{q\to\gamma}(m_q, z_0) \equiv \sigma_q(p_q) \int_{z_0}^{1} \mathrm{d}z_\gamma \, D_{q\to\gamma}^{(\mathrm{MR})}(z_\gamma, m_q) \tag{3.7.8}$$

from the NLO cross section. As a consequence, the residual quark-mass dependence in the NLO result will vanish.

Fortunately, the non-perturbative contribution to the class of events we want to exclude has been measured at LEP in photon+jet events. In these events a photon carries almost all the energy of a radiating quark in a hadronic Z^0-boson decay. In our explicit calculation we use the bare fragmentation function

$$D_{q\to\gamma}^{(\mathrm{MR})}(z_\gamma, m_q) = D_{q\to\gamma}^{\mathrm{ALEPH},\overline{\mathrm{MS}}}(z_\gamma, \mu_\mathrm{F}) + \frac{\alpha Q_q^2}{2\pi} P_{q\to\gamma}(z_\gamma) \left(\ln \frac{m_q^2}{\mu_\mathrm{F}^2} + 2 \ln z_\gamma + 1 \right) , \tag{3.7.9}$$

where we employ the parametrization of the renormalized fragmentation function used by the ALEPH collaboration to fit the data [34],

$$D_{q\to\gamma}^{\mathrm{ALEPH},\overline{\mathrm{MS}}}(z_\gamma, \mu_\mathrm{F}) = \frac{\alpha Q_q^2}{2\pi} \left(P_{q\to\gamma}(z_\gamma) \ln \frac{\mu_\mathrm{F}^2}{(1-z_\gamma)^2 \mu_0^2} + C \right) . \tag{3.7.10}$$

Here, the constants μ_0^2 and C are fit parameters and the dependence of the complete fragmentation function on the fragmentation scale μ_F cancels by construction. We use the result of a one-parameter fit where C is constraint to $C = -1 - \ln(M_\mathrm{Z}^2/(2\mu_0^2))$ resulting in

$$\mu_0 = 0.14\,\mathrm{GeV} \quad \text{and} \quad C = -13.26\,. \tag{3.7.11}$$

Details on the specific recombination- and cut procedure we have applied in our calculation can be found in Section 10.1.

Chapter 4

Dipole subtraction in NLO calculations

In this chapter we present an overview about the *dipole subtraction method* as it is applied in our calculation of the NLO QCD and EW corrections to the off-shell W+jet production. We do not claim to provide all technical details that are necessary to actually implement the method into a computer code. For this purpose, one actually has to work carefully through the papers where the procedure was originally developed.

In Section 4.1 we start with a short motivation and afterwards discuss the underlying principles of the method on the basis of its relevance for the calculation of IR QED singularities. Then we will—building on earlier work by Stefan Dittmaier—discuss in detail the construction of the subtraction formulae for the calculation of non-collinear-safe observables in QED that were defined in Section 3.6.

In Section 4.4 we give a brief description of dipole subtraction within NLO QCD calculations. We sketch the general procedure and comprise the most important formulae.

4.1 Dipole subtraction in QED

The calculation of real NLO QED corrections gives rise to several IR or mass singularities in the phase-space integral $\int \mathrm{d}\Phi_{\mathrm{LO+1}}|\mathcal{M}_{\mathrm{real}}|^2$ of real-emission processes (see Table 3.1, left column). These mass singularities have to be regularized to make them calculable. As stated in Section 3.1.1, we include small fermion masses m_f to regularize the collinear singularities and an infinitesimal photon mass λ to regularize the soft singularity.

If we naively introduced small regulator masses everywhere in a real-radiation amplitude $|\mathcal{M}_{\mathrm{real}}|^2$ of a physical process that happens at a typical energy scale Q, the numerical evaluation would be significantly slowed down by terms of order $\mathcal{O}(m^2_{\mathrm{reg}}/Q^2, m^4_{\mathrm{reg}}/Q^4, \ldots)$ that are irrelevant for the final result anyway. Moreover, the presence of many different scales could spoil the numerical accuracy and—as a consequence—the reliability of the result. The mass-singular logarithmic terms would be piled up as a purely-numerical contribution, and the cancellation against the analytic counterparts from the virtual corrections would be a tedious and delicate task. Additionally, the numerically-evaluated and potentially huge singular terms could superimpose the finite contributions and jeopardize the accuracy of the evaluation. Consequently, one has to work out a strategy which offers

a fast and stable numerical evaluation on the one hand and analytical control over the mass-singular terms on the other.

As a solution to this problem we now discuss the dipole subtraction formalism. In the following, we try to be as general as possible and to present the keynote of the procedure. All presented formulae are understood in such a way that they have to be specified for the calculation of a particular process.

The general idea of any subtraction formalism is to subtract an auxiliary function $|\mathcal{M}_{\text{sub}}|^2$ from the real-emission amplitude $|\mathcal{M}_{\text{real}}|^2$ that pointwise cancels all IR-singular contributions in $|\mathcal{M}_{\text{real}}|^2$. The IR-singular structures in this auxiliary function can then be integrated out analytically before the subtracted contribution is added to the cross section again. The subtraction function $|\mathcal{M}_{\text{sub}}|^2$ should be a general function in a sense that its IR-singular structures should factorize from the hard process without IR-singular splitting. This can in principle be achieved, since—as explained in Section 3.2—any given QED amplitude exhibits a universal factorization behaviour in any IR-singular limit, resulting in a convolutive expression of a general splitting term and the squared amplitude $|\mathcal{M}_{\text{LO}}|^2$ of the underlying process without IR-singular splitting. The subtraction function should also be simple enough that the singular parts allow for an analytical integration over the IR-singular subspace $[\mathrm{d}\phi_{\text{IR}}]$ of $\mathrm{d}\Phi_{\text{LO+1}}$ to attain analytical control over the singularities. For this purpose, one needs an adequate phase-space decomposition, symbolically denoted as

$$\mathrm{d}\Phi_{\text{LO+1}} = \mathrm{d}\tilde{\Phi}_{\text{LO}} \otimes [\mathrm{d}\phi_{\text{IR}}]\,, \tag{4.1.1}$$

where the symbol $\otimes$ abbreviates multiplications and adequate phase-space convolutions. Following the preceding considerations, we can schematically reformulate the phase-space integration of a real-emission amplitude containing problematic IR splittings according to

$$\int \mathrm{d}\Phi_{\text{LO+1}} |\mathcal{M}_{\text{real}}|^2 = \int \mathrm{d}\Phi_{\text{LO+1}} \Big(|\mathcal{M}_{\text{real}}|^2 - |\mathcal{M}_{\text{sub}}|^2 \Big) + \int \mathrm{d}\tilde{\Phi}_{\text{LO}} \otimes \left(\int [\mathrm{d}\phi_{\text{IR}}] |\mathcal{M}_{\text{sub}}|^2 \right). \tag{4.1.2}$$

Since in the subtraction integral all IR singularities are neutralized pointwise, the evaluation of $\int \mathrm{d}\Phi_{\text{LO+1}} (|\mathcal{M}_{\text{real}}|^2 - |\mathcal{M}_{\text{sub}}|^2)$ is possible without any mass regulators. The three-fold integration $[\mathrm{d}\phi_{\text{IR}}]$ covers all mass-singular structures and can be done analytically once and for all, employing mass regulators. Finally, we are left with a trivial numerical convolution over a LO phase space $\mathrm{d}\tilde{\Phi}_{\text{LO}}$. Of course the problematic task is now

1. to construct the subtraction function $|\mathcal{M}_{\text{sub}}|^2$, and

2. to perform the analytical integration of $[\mathrm{d}\phi_{\text{IR}}]$.

At NLO, different subtraction techniques have been proposed in the literature [35, 36, 66, 71, 73, 74, 75] that tackle this problem in different ways. Probably the most common approach is the dipole subtraction method that constructs $|\mathcal{M}_{\text{sub}}|^2$ as an appropriate sum of so-called "dipoles" $\mathfrak{g}^{\text{sub}}_{ij,K}$ and $\mathfrak{g}^{\text{sub}}_{ai,K}$,

$$\begin{aligned} |\mathcal{M}_{\text{sub}}(\Phi_{\text{LO+1}}(\ldots,p_a,p_i,p_j,p_K,\ldots))|^2 = {} & \sum \mathfrak{g}^{\text{sub}}_{\widetilde{ij},K}(p_i,p_j,p_K) \otimes \Big| \mathcal{M}_{\text{LO}}(\tilde{\Phi}_{\text{LO}}(\tilde{p}_{ij},\tilde{p}_K)) \Big|^2 \\ & + \sum \mathfrak{g}^{\text{sub}}_{\widetilde{ai},K}(p_a,p_i,p_K) \otimes \Big| \mathcal{M}_{\text{LO}}(\tilde{\Phi}_{\text{LO}}(\tilde{p}_{ai},\tilde{p}_K)) \Big|^2 . \end{aligned} \tag{4.1.3}$$

The dipoles $\mathfrak{g}^{\text{sub}}_{ij,K}$ and $\mathfrak{g}^{\text{sub}}_{ai,K}$ are built from *emitter-spectator* pairs corresponding to IR-singular IS and FS splittings of the form $a \to \widetilde{ai} + i$ and $\widetilde{ij} \to i + j$ that are illustrated in Fig. 3.1. The particles $\widetilde{ai}$ and $\widetilde{ij}$ that enter the hard scattering event are denoted as emitters, while the spectator particles K are needed to construct the reduced LO phase space $\mathrm{d}\tilde{\Phi}_{\text{LO}}$ that enters the subtraction integral and to correctly match the asymptotic behaviour of $|\mathcal{M}_{\text{real}}|^2$ in case of soft-photon radiation.

For the readers convenience, we summarize the relevant properties of (4.1.3):

- $|\mathcal{M}_{\text{sub}}|^2$ matches the asymptotic behaviour of $|\mathcal{M}_{\text{real}}|^2$ in any soft or collinear limit, i.e. its asymptotic behaviour is given by (3.2.4a), (3.2.4b), and (3.2.1), respectively.

- The dipoles $\mathfrak{g}^{\text{sub}}_{ij,K}$ and $\mathfrak{g}^{\text{sub}}_{ai,K}$ are general functions, i.e. they are independent of the LO process and can be constructed once and for all for every collinear-singular splitting.

- Since the matrix elements in (4.1.3) have to be evaluated with physical momenta of Φ_{LO}, one needs an adequate prescription to map the momenta of the radiative process to the momenta of the auxiliary phase space $\tilde{\Phi}_{\text{LO}}$ of the underlying LO contribution.

- The functions $\mathfrak{g}^{\text{sub}}_{ij,K}$ and $\mathfrak{g}^{\text{sub}}_{ai,K}$ have to be simple enough that they can be integrated analytically over the IR-singular degrees of freedom in $[\mathrm{d}\phi_{\text{IR}}]$.

The dipole subtraction approach was first developed in [66] for IR singularities related to splittings of massless QCD partons. In Ref. [75] people have also worked out the dipole subtraction formalism for massive QCD partons, for instance allowing for the application of the method for cross sections involving external top quarks. The technique was extended in [35] to the treatment of photon radiation off fermions with arbitrary masses, following the ideas and principles of [66]. In the progress of this thesis we have broadened the procedure to non-collinear-safe photon radiation off FS fermions and to all other possible collinear splittings that might show up in NLO EW calculations [36] (see Table 3.1, left column). In that paper, we present subtraction formulae for polarized external particles and allow for the inclusion of truly massive FS spectators.

However, in this thesis we calculate unpolarized cross sections and do not have to take into account massive spectators in the initial or final state. Therefore, we restrict ourselves to the treatment of strictly massless spectators and only present results that are summed (averaged) over FS (IS) emitters, respectively.

In the next section we will provide a detailed discussion of the dipole subtraction procedure for photon radiation off FS fermions in processes with non-collinear-safe observables, building on the conventions and results of [35]. In Section 4.3, we will also describe the dipole subtraction approach for collinear IS $\gamma \to f\bar{f}^*$ splittings, since these techniques will be needed for the calculation of the photon-induced processes listed in Section 6.3.2.

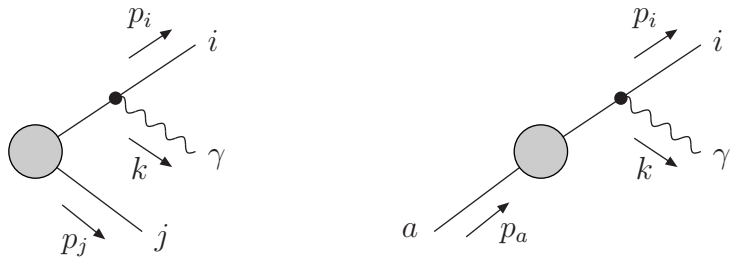

Figure 4.1: Generic diagrams for photonic FS radiation off an emitter i with a spectator j or a in the final or initial state, respectively.

4.2 Dipole subtraction for non-collinear-safe observables

The schematic form of the subtraction procedure to integrate the squared matrix element $\sum_{\lambda_\gamma} |\mathcal{M}_{n+\gamma}|^2$ (summed over photon polarizations λ_γ) for real photon radiation over the $(n+1)$-particle phase space $\mathrm{d}\Phi_\gamma$ reads

$$\int \mathrm{d}\Phi_\gamma \sum_{\lambda_\gamma} |\mathcal{M}_{n+\gamma}|^2 = \int \mathrm{d}\Phi_\gamma \left(\sum_{\lambda_\gamma} |\mathcal{M}_{n+\gamma}|^2 - |\mathcal{M}_{\mathrm{sub}}|^2 \right) + \int \mathrm{d}\tilde{\Phi}_0 \otimes \left(\int [\mathrm{d}k] \, |\mathcal{M}_{\mathrm{sub}}|^2 \right), \tag{4.2.1}$$

where $\mathrm{d}\tilde{\Phi}_0$ is a phase-space element of the corresponding non-radiative process and $[\mathrm{d}k]$ includes the photonic phase space that leads to the soft and collinear singularities. The two contributions involving the subtraction function $|\mathcal{M}_{\mathrm{sub}}|^2$ have to cancel each other, however, they will be evaluated separately.

In the dipole subtraction formalism for photon radiation, the subtraction function is explicitly given by [35]

$$|\mathcal{M}_{\mathrm{sub}}(\Phi_\gamma)|^2 = -\sum_{f \neq f'} Q_f \sigma_f Q_{f'} \sigma_{f'} e^2 g^{(\mathrm{sub})}_{ff'}(p_f, p_{f'}, k) \left| \mathcal{M}_n \left(\tilde{\Phi}_{0,ff'} \right) \right|^2, \tag{4.2.2}$$

where the sum runs over all dipoles that can be constructed from emitter–spectator pairs ff'. In (4.2.2), which is a specification of (4.1.3), we implicitly assume summation over polarizations of IS and FS fermions. The subtraction kernels $g^{(\mathrm{sub})}_{ff'}$ are constructed in such a way that (4.2.2) will exactly match the bremsstrahlung amplitude $\sum_{\lambda_\gamma} |\mathcal{M}_{n+\gamma}|^2$ in the soft and collinear limits that are given by Eqs. (3.2.1) and (3.2.7), respectively. The auxiliary momenta defined on the phase-space sets $\tilde{\Phi}_{0,ff'}$ respect momentum conservation and all on-shell conditions in the calculation of $|\mathcal{M}_n|^2$.

For a FS emitter (FS radiation), the two possible dipoles are illustrated in Fig. 4.1. The relative charges are denoted Q_f, $Q_{f'}$, and the sign factors σ_f and $\sigma_{f'}$ were defined in Section 3.2.1. The singular behaviour of the subtraction function is contained in the radiator functions $g^{(\mathrm{sub})}_{ff'}(p_f, p_{f'}, k)$, which depend on the emitter, spectator, and photon momenta p_f, $p_{f'}$, and k, respectively. The squared lowest-order matrix element $|\mathcal{M}_n|^2$ of the corresponding non-radiative process enters the subtraction function with modified emitter and spectator momenta $\tilde{p}_f^{(ff')}$ and $\tilde{p}_{f'}^{(ff')}$. For a FS emitter f, the momenta are

related by $p_f + k \pm p_{f'} = \tilde{p}_f^{(ff')} \pm \tilde{p}_{f'}^{(ff')}$, where $\pm$ refers to a spectator f' in the final or initial state, and the same set $\{k_n\}$ of remaining particle momenta enters $|\mathcal{M}_\gamma|^2$ and $|\mathcal{M}_n|^2$. The modified momenta are constructed in such a way that $\tilde{p}_f^{(ff')} \to p_f + k$ in the collinear limit ($p_f k \to 0$).

In collinear-safe observables (w.r.t. FS radiation), and only those are considered for light fermions in Ref. [35], a collinear fermion–photon system is treated as one quasi-particle, i.e., in the limit where f and γ become collinear only the sum $p_f + k$ enters the procedures of implementing phase-space selection cuts or of sorting an event into a histogram bin of a differential distribution. Therefore, it is guaranteed that for each photon radiation cone around a charged particle f the energy fraction

$$z_f = \frac{p_f^0}{p_f^0 + k^0} \tag{4.2.3}$$

is fully integrated over. According to the KLN theorem, no mass singularity connected with FS radiation remains. Collinear safety facilitates the actual application of the subtraction procedure as indicated in Eq. (4.2.1). In this case the events resulting from the contributions of $|\mathcal{M}_{\text{sub}}|^2$ can be consistently regarded as n-particle final states of the non-radiative process with particle momenta as going into $\left|\mathcal{M}_n\left(\tilde{\Phi}_{0,ff'}\right)\right|^2$, i.e. the emitter and spectator momenta are given by $\tilde{p}_f^{(ff')}$, $\tilde{p}_{f'}^{(ff')}$, respectively. Owing to $\tilde{p}_f^{(ff')} \to p_f + k$ in the collinear limits, the difference $\sum_{\lambda_\gamma} |\mathcal{M}_\gamma|^2 - |\mathcal{M}_{\text{sub}}|^2$ can be integrated over all collinear regions, because all events that differ only in the value of z_f enter cuts or histograms in the same way. The implicit *full* integration over all z_f in the collinear cones, on the other hand, implies that in the analytical integration of $|\mathcal{M}_{\text{sub}}|^2$ over $[\mathrm{d}k]$ the z_f integrations can be carried out over the whole z_f range.

In non-collinear-safe observables as defined in Section 3.6 (w.r.t. FS radiation) not all photons within arbitrarily narrow collinear cones around outgoing charged particles are treated inclusively. For a fixed cone axis the integration over the corresponding variable z_f is constrained by a phase-space cut or by the boundary of a histogram bin. Consequently, mass-singular contributions of the form $\alpha \ln m_f$ remain in the integral. Technically this means that the information on the variables z_f has to be exploited in the subtraction procedure of Eq. (4.2.1). The variables that take over the role of z_f in the individual dipole contributions in $|\mathcal{M}_{\text{sub}}|^2$ are called z_{ij} and z_{ia} in Ref. [35], where $f = i$ is a FS emitter and j/a a FS/IS spectator. In the collinear limit they behave as $z_{ij} \to z_i$ and $z_{ia} \to z_i$. Thus, the integral $\int \mathrm{d}\Phi_\gamma \left(\sum_{\lambda_\gamma} |\mathcal{M}_\gamma|^2 - |\mathcal{M}_{\text{sub}}|^2\right)$ can be performed over the whole phase space if the events associated with $|\mathcal{M}_{\text{sub}}|^2$ are treated as $(n+1)$-particle events with momenta $p_f \to z_{ff'} \tilde{p}_f^{(ff')}$, $p_{f'} \to \tilde{p}_{f'}^{(ff')}$, and $k \to (1 - z_{ff'}) \tilde{p}_f^{(ff')}$. This can be formalized by introducing a step function $\Theta_{\text{cut}}(p_f, k, p_{f'}, \{k_n\})$ on the $(n+1)$-particle phase space which is 1 if the event passes the cuts and 0 otherwise. The set $\{k_n\}$ simply contains the momenta of the remaining particles in the process. Making the dependence on Θ_{cut} explicit, the first term on the r.h.s. of Eq. (4.2.1) reads

$$\int \mathrm{d}\Phi_\gamma \left[\sum_{\lambda_\gamma} |\mathcal{M}_\gamma|^2 \Theta_{\text{cut}}(p_f, k, p_{f'}, \{k_n\})\right.$$

$$- \sum_{f \neq f'} |\mathcal{M}_{\text{sub},ff'}|^2 \Theta_{\text{cut}}\Big(z_{ff'}\tilde{p}_f^{(ff')}, (1-z_{ff'})\tilde{p}_f^{(ff')}, \tilde{p}_{f'}^{(ff')}, \{k_n\}\Big)\Bigg], \quad (4.2.4)$$

where we have decomposed the subtraction function $|\mathcal{M}_{\text{sub}}|^2$ into its subcontributions

$$|\mathcal{M}_{\text{sub},ff'}|^2 = -Q_f \sigma_f Q_{f'} \sigma_{f'} e^2 g_{ff'}^{(\text{sub})}(p_f, p_{f'}, k) \left|\mathcal{M}_n\left(\tilde{\Phi}_{0,ff'}\right)\right|^2 \quad (4.2.5)$$

of specific emitter–spectator pairs ff'. Apart from this refinement of the cut prescription in the subtraction part for non-collinear-safe observables, no modification in $|\mathcal{M}_{\text{sub}}|^2$ is needed. Since its construction exactly proceeds as described in Sections 3 and 4 of Ref. [35], we do not repeat the individual steps in this thesis. However, we will list all subtraction contributions explicitly in Appendix C that are needed for the calculation of the real photonic corrections to the process (1.0.5).

The modification of the cut procedure requires a generalization of the evaluation of the second subtraction term on the r.h.s. of Eq. (4.2.1), because now the integral over $z_{ff'}$ implicitly contained in $[\mathrm{d}k]$ depends on the cuts that define the observable. In the following two sections we work out the form of the necessary modifications, where we set up the formalism in such a way that it reduces to the procedure described in Ref. [35] for a collinear-safe situation, while the non-collinear-safe case is covered upon including extra contributions.

4.2.1 Final-state emitter and final-state spectator

For a FS emitter i with mass m_i and a massless FS spectator j the integral of $g_{ij}^{(\text{sub})}(p_i, p_j, k)$ over the photonic subspace $[\mathrm{d}k(P_{ij}^2, y_{ij}, z_{ij})]$ defined in Eq. (4.7) of Ref. [35] is proportional to

$$G_{ij}^{(\text{sub})}(P_{ij}^2) = \frac{\bar{P}_{ij}^4}{2(P_{ij}^2 - m_i^2)} \int_{y_1}^{y_2} \mathrm{d}y_{ij}\,(1-y_{ij}) \int_{z_1(y_{ij})}^{z_2(y_{ij})} \mathrm{d}z_{ij}\, g_{ij}^{(\text{sub})}(p_i, p_j, k)\,. \quad (4.2.6)$$

Here, the definitions of Sections 3.1 and 4.2 of Ref. [35] for a massless spectator are used, i.e.

$$P_{ij}^\mu = p_i^\mu + p_k^\mu + k^\mu\,, \quad \bar{P}_{ij}^2 = P_{ij}^2 - m_i^2 - \lambda^2\,, \quad (4.2.7)$$

and the subtraction kernel

$$g_{ij}^{(\text{sub})}(p_i, p_j, k) = \frac{1}{(p_i k) R_{ij}(y_{ij})} \left[\frac{2}{1 - z_{ij}(1-y_{ij})} - 1 - z_{ij} - \frac{m_i^2}{p_i k}\right], \quad (4.2.8)$$

with the shorthand

$$R_{ij}(y) = \frac{\bar{P}_{ij}^2 (1-y)}{\bar{P}_{ij}^2 + \lambda^2}\,, \quad (4.2.9)$$

is given as a function of the auxiliary variables

$$y_{ij} = \frac{p_i k}{p_i p_j + p_i k + p_j k}\,, \quad z_{ij} = \frac{p_i p_j}{p_i p_j + p_j k}\,, \quad (4.2.10)$$

which are constructed from the momenta of the full bremsstrahlung phase space. In order to leave the integration over z_{ij} open, the order of the two integrations has to be interchanged, and the integral solely taken over y_{ij} is needed. Therefore, we define

$$\bar{\mathcal{G}}_{ij}^{(\mathrm{sub})}(P_{ij}^2, z_{ij}) = \frac{\bar{P}_{ij}^2}{2(P_{ij}^2 - m_i^2)} \int_{y_1(z_{ij})}^{y_2(z_{ij})} \mathrm{d}y_{ij}\,(1 - y_{ij})\, g_{ij}^{(\mathrm{sub})}(p_i, p_j, k). \tag{4.2.11}$$

For practical purposes, we can safely neglect the photon-mass dependence in the function $\bar{\mathcal{G}}_{ij}^{(\mathrm{sub})}(P_{ij}^2, z)$, because the soft singularity appearing at $z \to 1$ can be split off by employing a $[\dots]_+$ prescription in the variable z,

$$\bar{\mathcal{G}}_{ij}^{(\mathrm{sub})}(P_{ij}^2, z) = G_{ij}^{(\mathrm{sub})}(P_{ij}^2)\delta(1 - z) + \left[\bar{\mathcal{G}}_{ij}^{(\mathrm{sub})}(P_{ij}^2, z)\right]_+ . \tag{4.2.12}$$

This procedure shifts the soft singularity into the quantity $G_{ij}^{(\mathrm{sub})}(P_{ij}^2)$ which is already known from Ref. [35]. Moreover, the generalization to non-collinear-safe integrals simply reduces to the extra term $\left[\bar{\mathcal{G}}_{ij}^{(\mathrm{sub})}(P_{ij}^2, z)\right]_+$, which cancels out for collinear-safe integrals where the full z-integration is carried out.

In the limit $m_i \to 0$ and $\lambda = 0$ the boundary of the y_{ij} integration is asymptotically given by

$$y_1(z) = \frac{m_i^2(1 - z)}{P_{ij}^2 z}\,, \quad y_2(z) = 1\,, \tag{4.2.13}$$

and the splitting kernel $g_{ij}^{(\mathrm{sub})}$ is expressed via the integration variables y_{ij} and z_{ij} according to

$$g_{ij}^{(\mathrm{sub})}(p_i, p_j, p_k) = \frac{2}{P_{ij}^2\, y_{ij}(1 - y_{ij})} \left[\frac{2}{1 - z_{ij}(1 - y_{ij})} - 1 - z_{ij} - \frac{2m_i^2}{y_{ij} P_{ij}^2}\right] . \tag{4.2.14}$$

The evaluation of Eq. (4.2.11) yields

$$\bar{\mathcal{G}}_{ij}^{(\mathrm{sub})}(P_{ij}^2, z) = P_{ff}(z) \left[\ln\left(\frac{P_{ij}^2 z}{m_i^2}\right) - 1\right] + (1 + z)\ln(1 - z) + 1 - z\,, \tag{4.2.15}$$

where $P_{ff}(z)$ is the splitting function (3.2.9). Equation (4.2.15) is correct up to terms suppressed by factors of m_i. For completeness, we repeat the form of the full integral $G_{ij}^{(\mathrm{sub})}(P_{ij}^2)$ in the case of a light emitter mass m_i,

$$G_{ij}^{(\mathrm{sub})}(P_{ij}^2) = \mathcal{L}(P_{ij}^2, m_i^2) - \frac{\pi^2}{3} + \frac{3}{2}\,, \tag{4.2.16}$$

with the auxiliary function

$$\mathcal{L}(P^2, m^2) = \ln\left(\frac{m^2}{P^2}\right)\ln\left(\frac{\lambda^2}{P^2}\right) + \ln\left(\frac{\lambda^2}{P^2}\right) - \frac{1}{2}\ln^2\left(\frac{m^2}{P^2}\right) + \frac{1}{2}\ln\left(\frac{m^2}{P^2}\right), \tag{4.2.17}$$

which are taken from Eqs. (3.7) and (3.8) of Ref. [35].

Finally, we give the explicit form of the ij contribution $|\mathcal{M}_{\text{sub},ij}(\Phi_\gamma)|^2$ to the phase-space integral of the subtraction function,

$$\begin{aligned}\int \mathrm{d}\Phi_\gamma \, |\mathcal{M}_{\text{sub},ij}(\Phi_\gamma)|^2 = -\frac{\alpha}{2\pi} Q_i \sigma_i Q_j \sigma_j \int \mathrm{d}\tilde{\Phi}_{0,ij} \int_0^1 \mathrm{d}z \\ \times \left\{ G_{ij}^{(\text{sub})}(P_{ij}^2)\delta(1-z) + \left[\bar{\mathcal{G}}_{ij}^{(\text{sub})}(P_{ij}^2, z)\right]_+ \right\} \\ \times |\mathcal{M}_n(\tilde{p}_i, \tilde{p}_j)|^2 \, \Theta_{\text{cut}}\Big(p_i = z\tilde{p}_i, k = (1-z)\tilde{p}_i, \tilde{p}_j, \{k_n\}\Big),\end{aligned} \tag{4.2.18}$$

generalizing Eq. (3.6) of Ref. [35]. While $\tilde{p}_i, \tilde{p}_j, \{k_n\}$ are the momenta corresponding to the generated phase-space point in $\tilde{\Phi}_{0,ij}$, the momenta p_i and k result from $\tilde{p}_i$ via a simple rescaling with the independently generated variable z. The invariant P_{ij}^2 is calculated via $P_{ij}^2 = (\tilde{p}_i + \tilde{p}_j)^2$ independently of z. The arguments of the step function $\Theta_{\text{cut}}(p_i, k, \tilde{p}_j, \{k_n\})$ indicate on which momenta phase-space cuts are imposed.

4.2.2 Final-state emitter and initial-state spectator

For the treatment of a FS emitter i and an IS spectator a, we consistently make use of the definitions of Sections 3.2 and 4.2 of Ref. [35]. In this thesis we only consider light particles in the initial state, because we assume the incoming quarks as massless within our calculation. Therefore, the spectator mass m_a can be set to zero from the beginning, which simplifies the formulae considerably.

Before we consider the non-collinear-safe situation, we briefly repeat the concept of the collinear-safe case described in Ref. [35]. Following Eqs. (4.24) and (4.27) from there, adopting the definitions

$$P_{ia}^\mu = p_i^\mu + k^\mu - p_a^\mu \,, \quad \bar{P}_{ia}^2 = P_{ia}^2 - m_i^2 - \lambda^2 \,, \tag{4.2.19}$$

and using the auxiliary variables

$$x_{ia} = \frac{p_a p_i + p_a k - p_i k}{p_a p_i + p_a k} \,, \quad z_{ia} = \frac{p_a p_i}{p_a p_i + p_a k} \,, \tag{4.2.20}$$

respectively, the inclusive integral of the subtraction kernel

$$g_{ia}^{(\text{sub})}(p_i, p_a, k) = \frac{2}{\bar{P}_{ia}^2 (x_{ia} - 1)} \left[\frac{2}{2 - x_{ia} - z_{ia}} - 1 - z_{ia} - \frac{2\, m_i^2\, x_{ia}}{\bar{P}_{ia}^2 (x_{ia} - 1)} \right] \tag{4.2.21}$$

over $[\mathrm{d}k(P_{ia}^2, x_{ia}, z_{ia})]$ (See Eq. (4.20) of Ref. [35]) is proportional to

$$G_{ia}^{(\text{sub})}(P_{ia}^2) = \int_0^{x_1} \mathrm{d}x \, \mathcal{G}_{ia}^{(\text{sub})}(P_{ia}^2, x) \,, \tag{4.2.22}$$

with

$$\mathcal{G}_{ia}^{(\text{sub})}(P_{ia}^2, x_{ia}) = -\frac{\bar{P}_{ia}^2}{2} \int_{z_1(x_{ia})}^{z_2(x_{ia})} \mathrm{d}z_{ia} \, g_{ia}^{(\text{sub})}(p_i, p_a, k) \,. \tag{4.2.23}$$

In (4.2.22) we can set the lower limit x_0 of the x_{ia}-integration to zero because of $m_a = 0$, and the upper bound is given by

$$x_1 = 1 - \frac{2m_i\lambda}{|\bar{P}_{ia}^2|}\,, \tag{4.2.24}$$

that can be derived from the limits of the z_{ia}-integration,

$$z_{1,2}(x) = \frac{[\bar{P}_{ia}^2 - x(\bar{P}_{ia}^2 + 2m_i^2)] \mp \sqrt{\bar{P}_{ia}^4(1-x)^2 - 4m_i^2\lambda^2x^2}}{2[\bar{P}_{ia}^2 - xP_{ia}^2]}\,. \tag{4.2.25}$$

Since, however, the squared lowest-order matrix element $|\mathcal{M}_n|^2$ multiplying $g_{ia}^{(\mathrm{sub})}$ in Eq. (4.2.2) depends on the variable x_{ia}, the integration of $|\mathcal{M}_{\mathrm{sub}}|^2$ over $x = x_{ia}$ is performed employing a $[\dots]_+$ prescription,

$$\begin{aligned} &-\frac{\bar{P}_{ia}^2}{2}\int_0^{x_1}\mathrm{d}x_{ia}\int_{z_1(x_{ia})}^{z_2(x_{ia})}\mathrm{d}z_{ia}\,g_{ia}^{(\mathrm{sub})}(p_i,p_a,k)\cdots \\ &\quad = \int_0^1\mathrm{d}x\left\{G_{ia}^{(\mathrm{sub})}(P_{ia}^2)\,\delta(1-x) + \Big[\mathcal{G}_{ia}^{(\mathrm{sub})}(P_{ia}^2,x)\Big]_+\right\}\cdots\,. \end{aligned} \tag{4.2.26}$$

This integration, where the ellipses stand for x-dependent functions such as the squared lowest-order matrix elements and flux factors, is usually done numerically. Since the soft and collinear singularities occur at $x \to x_1 = 1 - \mathcal{O}(\lambda)$, the singular parts are entirely contained in $G_{ia}^{(\mathrm{sub})}(P_{ia}^2)$ in Eq. (4.2.26), and the upper limit x_1 could be replaced by 1 in the actual x-integration. For completeness we give the explicit form of the functions $G_{ia}^{(\mathrm{sub})}$ and $\mathcal{G}_{ia}^{(\mathrm{sub})}$ in the limit $m_i \to 0$,

$$\begin{aligned} G_{ia}^{(\mathrm{sub})}(P_{ia}^2) &= \mathcal{L}(|P_{ia}^2|,m_i^2) - \frac{\pi^2}{2} + \frac{3}{2}\,, \\ \mathcal{G}_{ia}^{(\mathrm{sub})}(P_{ia}^2,x) &= \frac{1}{1-x}\left[2\ln\left(\frac{2-x}{1-x}\right) - \frac{3}{2}\right]\,, \end{aligned} \tag{4.2.27}$$

which are obtained from Eqs. (3.19) and (3.20) Ref. [35].

In a non-collinear-safe situation, the ellipses on the l.h.s. of Eq. (4.2.26) also involve z_{ia}-dependent functions, as e.g. θ-functions for cuts or event selection. Thus, also the integration over z_{ia} has to be performed numerically in this case, and we have to generalize Eq. (4.2.26) in an appropriate way. Introducing a double $[\dots]_+$ prescription in $x = x_{ia}$ and $z = z_{ia}$,

$$\begin{aligned} \int_0^1\mathrm{d}x\int_0^1\mathrm{d}z\big[g(x,z)\big]_+^{(x,z)}f(x,z) &\equiv \int_0^1\mathrm{d}x\int_0^1\mathrm{d}z\left[[g(x,z)]_+^{(x)}\right]_+^{(z)}f(x,z) \\ &= \int_0^1\mathrm{d}x\int_0^1\mathrm{d}z\,g(x,z)\Big(f(x,z) - f(x,1) - f(1,z) + f(1,1)\Big)\,, \end{aligned} \tag{4.2.28}$$

defined with an appropriate test function $f(x,z)$, we can reformulate Eq. (4.2.26) according to

$$\begin{aligned}
&-\frac{\bar{P}_{ia}^2}{2}\int_0^{x_1}\mathrm{d}x\int_{z_1(x)}^{z_2(x)}\mathrm{d}z\,g_{ia}^{(\mathrm{sub})}(p_i,p_a,k)\cdots\\
&\quad=\int_0^1\mathrm{d}x\int_0^1\mathrm{d}z\,\Bigg\{G_{ia}^{(\mathrm{sub})}(P_{ia}^2)\,\delta(1-x)\,\delta(1-z)+\Big[\mathcal{G}_{ia}^{(\mathrm{sub})}(P_{ia}^2,x)\Big]_+\delta(1-z)\\
&\qquad\qquad+\Big[\bar{\mathcal{G}}_{ia}^{(\mathrm{sub})}(P_{ia}^2,z)\Big]_+\delta(1-x)+\Big[\bar{g}_{ia}^{(\mathrm{sub})}(x,z)\Big]_+^{(x,z)}\Bigg\}\cdots\,. \qquad (4.2.29)
\end{aligned}$$

If the functions hidden in the ellipses do not depend on z, the last two terms within the curly brackets do not contribute and the formula reduces to Eq. (4.2.26). In (4.2.29) we have introduced the abbreviations

$$\begin{aligned}
\bar{g}_{ia}^{(\mathrm{sub})}(x,z)&=-\frac{\bar{P}_{ia}^2}{2}\,g_{ia}^{(\mathrm{sub})}\Big|_{\substack{\lambda=0\\m_i=0}},\\
\mathcal{G}_{ia}^{(\mathrm{sub})}(P_{ia}^2,x)&=-\frac{\bar{P}_{ia}^2}{2}\int_0^1\mathrm{d}z\,g_{ia}^{(\mathrm{sub})}\Big|_{\substack{\lambda=0\\m_i=0}},\\
\bar{\mathcal{G}}_{ia}^{(\mathrm{sub})}(P_{ia}^2,z)&=-\frac{\bar{P}_{ia}^2}{2}\int_0^{x_1(z)}\mathrm{d}x\,g_{ia}^{(\mathrm{sub})}\Big|_{\lambda=0},\\
G_{ia}^{(\mathrm{sub})}(P_{ia}^2)&=-\frac{\bar{P}_{ia}^2}{2}\int_0^1\mathrm{d}z\int_0^{x_1(z)}\mathrm{d}x\,g_{ia}^{(\mathrm{sub})}\,, \qquad (4.2.30)
\end{aligned}$$

with the upper integration boundary

$$x_1(z)=\frac{\bar{P}_{ia}^2x}{\bar{P}_{ia}^2z-m_i^2(1-z)}\,. \qquad (4.2.31)$$

The explicit results for $\mathcal{G}_{ia}^{(\mathrm{sub})}(P_{ia}^2,x)$ and $G_{ia}^{(\mathrm{sub})}(P_{ia}^2)$ have already been given above in Eq. (4.2.27), and the two remaining functions are easily evaluated to

$$\begin{aligned}
\bar{g}_{ia}^{(\mathrm{sub})}(x,z)&=\frac{1}{1-x}\left(\frac{2}{2-x-z}-1-z\right),\\
\bar{\mathcal{G}}_{ia}^{(\mathrm{sub})}(P_{ia}^2,z)&=P_{ff}(z)\left[\ln\left(\frac{-P_{ia}^2z}{m_i^2}\right)-1\right]-\frac{2\ln(2-z)}{1-z}+(1+z)\ln(1-z)+1-z\,.
\end{aligned} \qquad (4.2.32)$$

The collinear singularity $\propto\ln m_i$ that appears in non-collinear-safe observables is contained in the function $\bar{\mathcal{G}}_{ia}^{(\mathrm{sub})}(P_{ia}^2,z)$. A detailed derivation of (4.2.29) can be found in Ref. [36].

The resulting ia contribution $|\mathcal{M}_{\mathrm{sub},ia}(\Phi_\gamma)|^2$ to the phase-space integral of the subtraction function reads

$$\begin{aligned}
&\int\mathrm{d}\Phi_\gamma\,|\mathcal{M}_{\mathrm{sub},ia}(\Phi_\gamma)|^2=-\frac{\alpha}{2\pi}Q_a\sigma_aQ_i\sigma_i\int_0^1\mathrm{d}x\int\mathrm{d}\tilde{\Phi}_{0,ia}(P_{ia}^2,x)\int_0^1\mathrm{d}z\\
&\quad\times\Theta_{\mathrm{cut}}\Big(p_i=z\tilde{p}_i(x),k=(1-z)\tilde{p}_i(x),\{\tilde{k}_n(x)\}\Big)\\
&\quad\times\frac{1}{x}\Bigg\{G_{ia}^{(\mathrm{sub})}(P_{ia}^2)\,\delta(1-x)\,\delta(1-z)+\Big[\mathcal{G}_{ia}^{(\mathrm{sub})}(P_{ia}^2,x)\Big]_+\delta(1-z)
\end{aligned}$$

$$+\left[\bar{\mathcal{G}}_{ia}^{(\mathrm{sub})}(P_{ia}^2,z)\right]_+\delta(1-x)+\left[\bar{g}_{ia}^{(\mathrm{sub})}(x,z)\right]_+^{(x,z)}\Bigg\}\left|\mathcal{M}_n\Big(\tilde{p}_i(x),\tilde{p}_a(x)\Big)\right|^2, \quad (4.2.33)$$

which generalizes Eq. (3.18) of Ref. [35]. Again, the arguments of the step function $\Theta_{\mathrm{cut}}(p_i,k,\{\tilde{k}_n\})$ indicate on which momenta phase-space cuts are imposed. We recall that $\tilde{\Phi}_{0,ia}$ is the phase space of momenta $\tilde{p}_i(x)$ and $\{\tilde{k}_n(x)\}$ (without FS radiation) with rescaled incoming momentum $\tilde{p}_a(x)=xp_a$ instead of the original incoming momentum p_a. In the actual evaluation of Eq. (4.2.33), thus, the two phase-space points $\tilde{\Phi}_{0,ia}(P_{ia}^2,x)$ and $\tilde{\Phi}_{0,ia}(P_{ia}^2,x=1)$ have to be generated for each value of x owing to the plus prescription in x. The relevant value of the invariant P_{ia}^2 is then calculated separately via $P_{ia}^2=(\tilde{p}_i-\tilde{p}_a)^2$ for each of the two points, so that P_{ia}^2 results from the momenta entering the matrix element $\mathcal{M}_n$ in both cases. The variable z, however, is generated independently of the phase-space points and does not influence the kinematics in the matrix element.

4.3 Dipole subtraction for photon-induced processes

4.3.1 Asymptotics in the collinear limit

We consider a generic scattering process

$$\gamma(k)+a(p_a)\to f(p_f)+X(k_X), \quad (4.3.1)$$

where the momenta of the particles are given in parentheses. Here a is any massless incoming particle and f is an outgoing light fermion or antifermion. The remainder X may contain additional light fermions which can be treated in the same way as f. For later use, we define the squared cm energy s,

$$s=(p_a+k)^2=2p_ak. \quad (4.3.2)$$

The collinear singularity in the squared matrix element $|\mathcal{M}_{\gamma a\to fX}|^2$ occurs if the angle θ_f between f and the incoming γ becomes small; in this limit the scalar product (kp_f) is of $\mathcal{O}(m_f^2)$, where m_f is the small mass of f. Neglecting terms that are irrelevant in the limit $m_f\to 0$ the squared matrix element $\overline{|\mathcal{M}_{\gamma a\to fX}(k,p_a,p_f)|^2}$, averaged over the polarizations of a and γ and summed over the polarizations of f, asymptotically behaves like

$$\overline{|\mathcal{M}_{\gamma a\to fX}(k,p_a,p_f)|^2}\ \underset{kp_f\to 0}{\sim}\ Q_f^2e^2\,h^{\gamma f}(k,p_f)\,\overline{|\mathcal{M}_{\bar{f}a\to X}(p_{\bar{f}}=xk,p_a)|^2}, \quad (4.3.3)$$

where $x=1-p_f^0/k^0$ and Q_fe is the electric charge of f. The matrix element $\mathcal{M}_{\bar{f}a\to X}$ corresponds to the related process $\bar{f}a\to X$ that results from $\gamma a(\to f\bar{f}^*a)\to fX$ upon cutting the $\bar{f}^*$ line in all diagrams involving the splitting $\gamma\to f\bar{f}^*$ (see also Fig. 4.2). Here and in the following, asterisks indicate virtual particles, and the momenta relevant in the different matrix elements are given in parentheses. It is reasonable to stress that Eq. (4.3.3) is also a specification of Eq. (3.2.4a). The function $h^{\gamma f}(k,p_f)$, which rules the structure of the collinear singularity, is given by

$$h^{\gamma f}(k,p_f)=\frac{1}{x(kp_f)}\left(P_{f\gamma}(x)+\frac{xm_f^2}{kp_f}\right) \quad (4.3.4)$$

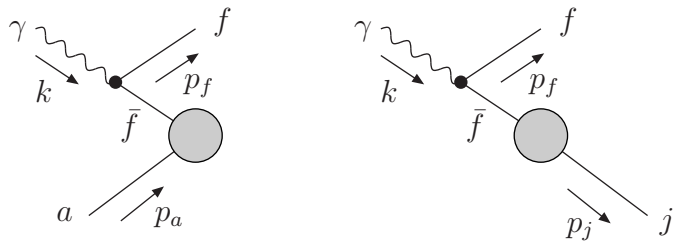

Figure 4.2: Generic diagrams for the splittings $\gamma \to f\bar{f}^*$ with an IS spectator a or a FS spectator j.

with the splitting function $P_{f\gamma}(x)$ from (3.4.2). The derivation of this result is carried out in Appendix B.1 of [36].

Note that the collinear singularity for $kp_f \to 0$ can be attributed to a single external leg (namely $\bar{f}$) of the related hard process $\bar{f}a \to X$. Thus, there is no need to construct the subtraction function $|\mathcal{M}_{\text{sub}}|^2$ from several dipole contributions $\propto Q_f Q_{f'}$. Instead we can construct $|\mathcal{M}_{\text{sub}}|^2$ as a single term $\propto Q_f^2$. Nevertheless we select a spectator f' to the emitter f for the phase-space construction, which proceeds in complete analogy to the photon radiation case. We have the freedom to choose any particle in the initial or final state as spectator. In the following we describe the dipole formalism in two variants: one with a spectator from the initial state, another with a spectator from the final state. The two situations are illustrated in Fig. 4.2.

4.3.2 Initial-state spectator

Subtraction function

The function that is subtracted from the integrand $\overline{|\mathcal{M}_{\gamma a\to fX}(k,p_a,p_f)|^2}$ is defined as follows,

$$\overline{|\mathcal{M}_{\text{sub}}|^2} = Q_f^2 e^2\, h^{\gamma f,a}(k,p_f,p_a)\, \overline{\left|\mathcal{M}_{\bar{f}a\to X}\left(\tilde{p}_{\bar{f}},p_a,\{\tilde{k}_n\}\right)\right|^2}, \tag{4.3.5}$$

with the unpolarized radiator function

$$h^{\gamma f,a}(k,p_f,p_a) = \frac{1}{x_{f,\gamma a}(kp_f)}\left(P_{f\gamma}(x_{f,\gamma a}) + \frac{x_{f,\gamma a}m_f^2}{kp_f}\right), \tag{4.3.6}$$

and the auxiliary quantity

$$x_{f,\gamma a} = \frac{p_a k - p_f k - p_a p_f}{p_a k}. \tag{4.3.7}$$

Here we kept the dependence on a finite m_f, because it is needed in the analytical treatment of the singular phase-space integration below. The modified momenta $\tilde{p}_{\bar{f}}$ and $\{\tilde{k}_n\}$ entering the squared matrix element on the r.h.s. of Eq. (4.3.5) will only be needed for $m_f = 0$ in applications with small values of m_f. In this limit they can be chosen as

$$\tilde{p}_{\bar{f}}^{\,\mu}(x) = xk^\mu, \qquad \tilde{p}_{\bar{f}}^{\,\mu} = \tilde{p}_{\bar{f}}^{\,\mu}(x_{f,\gamma a}), \qquad \tilde{k}_n^\mu = \Lambda^\mu{}_\nu\, k_n^\nu \tag{4.3.8}$$

with the Lorentz transformation matrix $\Lambda^\mu{}_\nu$ given by

$$\Lambda^\mu{}_\nu = g^\mu{}_\nu - \frac{(P+\tilde{P})^\mu (P+\tilde{P})_\nu}{P^2 + P\tilde{P}} + \frac{2\tilde{P}^\mu P_\nu}{P^2}, \tag{4.3.9}$$

$$P^\mu = p_a^\mu + k^\mu - p_f^\mu, \qquad \tilde{P}^\mu(x) = p_a^\mu + \tilde{p}_{\bar{f}}^\mu(x), \qquad \tilde{P}^\mu = p_a^\mu + \tilde{p}_{\bar{f}}^\mu. \tag{4.3.10}$$

It is straight-forward to check that $\overline{|\mathcal{M}_{\text{sub}}|^2}$ possesses the same asymptotic behaviour as $\overline{|\mathcal{M}_{\gamma a \to fX}|^2}$ in Eq. (4.3.3) in the collinear limit with $m_f \to 0$. Thus, the difference $\overline{|\mathcal{M}_{\gamma a \to fX}|^2} - \overline{|\mathcal{M}_{\text{sub}}|^2}$ can be integrated numerically for $m_f = 0$.

Readded counterpart

The correct dependence of $\overline{|\mathcal{M}_{\text{sub}}|^2}$ (and the related kinematics) on a finite m_f is, however, needed when this function is integrated over θ_f leading to the collinear singularity for $\theta_f \to 0$. The actual analytical integration can be done as described in Section 4.4 of Ref. [35] (even for finite m_a and m_f). Here we only sketch the individual steps and give the final result. The $(n+1)$-particle phase space is first split into the corresponding n-particle phase space of the process

$$\bar{f}(\tilde{p}_{\bar{f}}(x)) + a(p_a) \to X(k_X)\,, \tag{4.3.11}$$

and the integral over the remaining degrees of freedom that contain the singularity,

$$\int \mathrm{d}\Phi_{(n+1)}(k, p_a; P, p_f, k_X) = \int_0^{x_1} \mathrm{d}x \int \mathrm{d}\Phi_{(n)}\Big(\tilde{p}_{\bar{f}}(x), p_a; \tilde{P}(x), k_X\Big) \int [\mathrm{d}p_f(s, x, y_{f,\gamma a})], \tag{4.3.12}$$

with the explicit parametrization

$$\int [\mathrm{d}p_f(s, x, y_{f,\gamma a})] = \frac{s}{4(2\pi)^3} \int_{y_1(x)}^{y_2(x)} \mathrm{d}y_{f,\gamma a} \int \mathrm{d}\phi_f. \tag{4.3.13}$$

The upper kinematical limit of the parameter $x = x_{f,\gamma a}$ is given by

$$x_1 = 1 - \frac{2m_f}{\sqrt{s}}, \tag{4.3.14}$$

but in the limit $m_f \to 0$ we can set $x_1 = 1$. While the integration of the azimuthal angle ϕ_f of f simply yields a factor 2π, the integration over the auxiliary parameter

$$y_{f,\gamma a} = \frac{kp_f}{kp_a} = \frac{2kp_f}{s} \tag{4.3.15}$$

with the boundaries

$$y_{1,2}(x) = \frac{1}{2}\left[1 - x \mp \sqrt{(1-x)^2 - \frac{4m_f^2}{s}}\right] \tag{4.3.16}$$

is less trivial. Defining

$$\mathcal{H}^{\gamma f,a}(s, x) = \frac{xs}{2} \int_{y_1(x)}^{y_2(x)} \mathrm{d}y_{f,\gamma a}\, h^{\gamma f,a}(k, p_f, p_a), \tag{4.3.17}$$

the result of the integration (for $m_f \to 0$) is

$$\mathcal{H}^{\gamma f,a}(s,x) = P_{f\gamma}(x) \ln\left(\frac{s(1-x)^2}{m_f^2}\right) + 2x(1-x)\,. \tag{4.3.18}$$

For clarity we finally give the contribution $\sigma^{\text{sub}}_{\gamma a\to fX}$ that has to be added to the result for the cross section obtained from the integral of the difference $\overline{|\mathcal{M}_{\gamma a\to fX}|^2} - \overline{|\mathcal{M}_{\text{sub}}|^2}$,

$$\sigma^{\text{sub}}_{\gamma a\to fX}(k,p_a) = N_{\text{C},f}\,\frac{Q_f^2\alpha}{2\pi}\int_0^1 \mathrm{d}x\,\mathcal{H}^{\gamma f,a}(s,x)\,\sigma_{\bar f a\to X}(p_{\bar f} = xk, p_a)\,, \tag{4.3.19}$$

where $N_{\text{C},f}$ denotes the colour factor of the fermion f. Although formulated for integrated cross sections, the previous formula can be used to calculate any differential cross section after obvious modifications.

4.3.3 Final-state spectator

As an alternative to the case of an IS spectator described in the previous section, we here present the treatment with a massless FS spectator j, i.e. we consider the process

$$\gamma(k) + a(p_a) \to f(p_f) + j(p_j) + X(k_X). \tag{4.3.20}$$

The IS particle a is also assumed massless in the following, but all formulas can be generalized to $m_a \neq 0$ following closely the treatment of phase space described in Section 4.2 of Ref. [35].

Subtraction function

The subtraction function now is constructed as follows,

$$\overline{|\mathcal{M}_{\text{sub}}|^2} = Q_f^2 e^2\, h_j^{\gamma f}(k,p_f,p_j)\,\overline{|\mathcal{M}_{\bar f a\to jX}(\tilde p_{\bar f}, p_a, \tilde p_j)|^2}, \tag{4.3.21}$$

with the unpolarized radiator function

$$h_j^{\gamma f}(k,p_f,p_j) = \frac{1}{x_{fj,\gamma}(kp_f)}\left(P_{f\gamma}(x_{fj,\gamma}) + \frac{x_{fj,\gamma}m_f^2}{kp_f}\right), \tag{4.3.22}$$

and the auxiliary parameter

$$x_{fj,\gamma} = \frac{kp_j + kp_f - p_f p_j}{kp_j + kp_f}. \tag{4.3.23}$$

The momenta $\tilde p_{\bar f}$ and $\tilde p_j$ are given by

$$\tilde p^\mu_{\bar f}(x) = xk^\mu, \quad \tilde p^\mu_{\bar f} = \tilde p^\mu_{\bar f}(x_{fj,\gamma}), \quad \tilde p^\mu_j = P^\mu + \tilde p^\mu_{\bar f}, \quad P^\mu = p^\mu_f + p^\mu_j - k^\mu, \tag{4.3.24}$$

while the momenta of the other particles are unaffected. Note that this construction of momenta is based on the restriction $m_f = 0$, which is used in the integration of the difference $\overline{|\mathcal{M}_{\gamma a\to fjX}|^2} - \overline{|\mathcal{M}_{\text{sub}}|^2}$.

Readded counterpart

In the integration of $\overline{|\mathcal{M}_{\rm sub}|^2}$ over the collinear-singular phase space $\int[{\rm d}\phi]$, of course, the correct dependence on a finite m_f is required. The auxiliary momenta defined for a non-zero fermion mass m_f read

$$\begin{aligned}\tilde{p}^\mu_{\bar{f}}(x) &= xk^\mu - \frac{m_f^2}{P^2}P^\mu\,, \quad \tilde{p}^\mu_{\bar{f}} = \tilde{p}^\mu_{\bar{f}}(x_{fj,\gamma})\,,\\ \tilde{p}^\mu_{j}(x) &= P^\mu + \tilde{p}^\mu_{\bar{f}}(x)\,, \quad \tilde{p}^\mu_{j} = \tilde{p}^\mu_{j}(x_{fj,\gamma})\,.\end{aligned} \tag{4.3.25}$$

The phase space $\int {\rm d}\Phi_{(n+1)}(k,p_a;p_f,p_j,k_X)$ of the $(n+1)$-particle scattering process (4.3.20) can be decomposed according to

$$\int {\rm d}\Phi_{(n+1)}(k,p_a;p_f,p_j,k_X) = \int_0^1 {\rm d}x \int {\rm d}\Phi_{(n)}(\tilde{p}_{\bar{f}}(x),p_a;\tilde{p}_j(x),k_X)\int[{\rm d}\phi(P^2,x,z_{fj,\gamma})]\,, \tag{4.3.26}$$

where $\Phi_{(n)}(\tilde{p}_{\bar{f}}(x),p_a;\tilde{p}_j(x),k_X)$ denotes the phase-space measure of the underlying hard process

$$\bar{f}(\tilde{p}_{\bar{f}}(x)) + a(p_a) \to j(\tilde{p}_j(x)) + X(k_X)\,, \tag{4.3.27}$$

and the effective phase space of the collinear-singular structure is given by

$$\int[{\rm d}\phi(P^2,x,z_{fj,\gamma})] = \frac{1}{2(2\pi)^3}\frac{-(P^2-m_f^2)(p_a\tilde{p}_{\bar{f}}(x))}{x^2 s}\int_{z_1(x)}^{z_2(x)}{\rm d}z_{fj,\gamma}\int_0^{2\pi}{\rm d}\phi_f\,, \tag{4.3.28}$$

where we have introduced the auxiliary variable

$$z_{fj,\gamma} = \frac{kp_j}{kp_f + kp_j}\,, \tag{4.3.29}$$

and ϕ_f denotes the azimuthal angle of the outgoing fermion. The boundaries of the $z_{fj,\gamma}$ integration are given by

$$z_1(x) = 0\,, \quad z_2(x) = \frac{-(P^2-m_f^2)(1-x)}{-P^2(1-x)+m_f^2}\,. \tag{4.3.30}$$

Defining

$$\mathcal{H}_j^{\gamma f}(P^2,x) = -\frac{(P^2-m_f^2)}{2}\int_{z_1(x)}^{z_2(x)}{\rm d}z_{fj,\gamma}h_j^{\gamma f}(k,p_f,p_j)\,, \tag{4.3.31}$$

the cross-section contribution $\sigma^{\rm sub}_{\gamma a\to fjX}$ that has to be added to the integrated difference $\overline{|\mathcal{M}_{\gamma a\to fX}|^2} - \overline{|\mathcal{M}_{\rm sub}|^2}$ is given by

$$\sigma^{\rm sub}_{\gamma a\to fjX}(k,p_a) = N_{{\rm C},f}\,\frac{Q_f^2\alpha}{2\pi}\int_0^1 {\rm d}x\,\mathcal{H}_j^{\gamma f}(P^2,x)\,\sigma_{\bar{f}a\to jX}(p_{\bar{f}} = xk, p_a)\,, \tag{4.3.32}$$

where the integrated subtraction kernel containing the collinear singularity explicitly reads

$$\mathcal{H}_j^{\gamma f}(P^2,x) = -P_{f\gamma}(x)\ln\left[\frac{m_f^2\,x}{-P^2(1-x)}\right] + 2x(1-x)\,. \tag{4.3.33}$$

Of course, the singular contributions $\propto \ln m_f$ have the same form as in the case of an IS spectator discussed in the previous section.

4.4 Dipole subtraction for NLO QCD corrections

As mentioned before, the dipole subtraction formalism was first introduced in [66] to enable the calculation of NLO QCD corrections involving exactly massless partons. This approach is well motivated, because masses of light quarks do not have a well-defined meaning in perturbative QCD. Thus, in QCD one uses dimensional regularization to regularize IR singularities in the phase-space integration, posing the necessity to perform phase-space integrals in $d = 4 - 2\epsilon$ dimensions.

4.4.1 Partonic cross sections at NLO QCD

Here, we provide the contributions to the NLO QCD cross section, establishing the notation we will use for the discussion of the dipole subtraction technique in the next subsection.

We examine a process with two massless QCD partons a and b in the initial state and n partons $c_1, \ldots, c_n$ in the final state,

$$a(p_a) + b(p_b) \to c_1(p_1) + \ldots + c_n(p_n) + \mathcal{R}(Q)\,. \tag{4.4.1}$$

Particles in the final state that are not strongly interacting, like γ, $\mathrm{W}^{\pm}$, Z^0, or the leptons are denoted as "rest" $\mathcal{R}$. In our special case, $\mathcal{R}$ represents a leptonically decaying W boson. The four-momenta of the particles are given in parentheses. The momenta p_a and p_b are incoming while all other momenta are defined as outgoing. Moreover, we employ a factorization of the differential phase space of the partonic n-particle system

$$\begin{aligned}&\mathrm{d}\phi_n(p_1, \ldots, p_n; p_a + p_b - Q)\\ &\quad\equiv \left[\prod_{l=1}^{n} \frac{\mathrm{d}^d p_l}{(2\pi)^{d-1}} \theta(p_l^0)\delta(p_l^2)\right] (2\pi)^d \delta^{(d)}(p_l + \ldots + p_n + Q - p_a - p_b)\,,\end{aligned} \tag{4.4.2}$$

defined in d space-time dimensions, and the phase space $\mathrm{d}\phi_{\mathcal{R}}$ of the system $\mathcal{R}$,

$$\mathrm{d}\Phi_{(\mathcal{R}+n)} = \frac{\mathrm{d}Q^2}{(2\pi)^4}\, \mathrm{d}\phi_{\mathcal{R}}(Q)\, \mathrm{d}\phi_n\,, \tag{4.4.3}$$

where $\mathrm{d}\Phi_{(\mathcal{R}+n)}$ denotes the fully differential phase space of the process (4.4.1). When we discuss the phase-space parametrization for off-shell W-boson production in Chapters 7 and 8, we will present explicit formulae for the factorization in (4.4.3).

The total partonic cross section at NLO accuracy in QCD is given by

$$\hat{\sigma}_{ab} = \hat{\sigma}_{ab}^{\mathrm{LO}} + \hat{\sigma}_{ab}^{\mathrm{NLO}}\,, \tag{4.4.4}$$

where the LO cross section for a final state with n partons results from integrating the fully exclusive cross section $\mathrm{d}\hat{\sigma}_{ab}^0$ in the Born approximation,

$$\hat{\sigma}_{ab}^{\mathrm{LO}} = \int \frac{\mathrm{d}Q^2}{(2\pi)^4} \int_{\mathcal{R}} \int_n \mathrm{d}\hat{\sigma}_{ab}^0\,. \tag{4.4.5}$$

The differential cross section at the Born level reads

$$\begin{aligned}\mathrm{d}\hat{\sigma}^{0}_{ab}(p_a,p_b) = {}& \frac{\mathrm{d}\phi_{\mathcal{R}}(Q)}{2\hat{s}} \sum_{\{n\}} \mathrm{d}\phi_n(p_1,\ldots,p_n;p_a+p_b-Q) \\ & \times \frac{1}{S_{\{n\}}} \overline{\left|\mathcal{M}^{0}_{n,ab}(p_1,\ldots,p_n,Q;p_a,p_b)\right|^2} F_J^{(\mathcal{R}+n)}(Q,p_1,\ldots,p_n;p_a,p_b)\,,\end{aligned} \tag{4.4.6}$$

where $\mathcal{M}^{0}_{n,ab}$ is the tree-level amplitude of process (4.4.1). The symmetry factors $S_{\{n\}}$ account for identical partons in the final state, and the basic properties of the jet function $F_J^{(\mathcal{R}+n)}$ have been discussed in Section 3.5. Note that we have to sum over all possible sets of FS partons $\{c_1,\ldots,c_n\}$ to cover all LO contributions.

The perturbative part of the NLO cross section consists of the sum of real and virtual corrections, and moreover includes the collinear counterterm that was introduced in Section 3.3,

$$\hat{\sigma}^{\mathrm{NLO}}_{ab} = \int \frac{\mathrm{d}Q^2}{(2\pi)^4} \int_{\mathcal{R}} \left[\int_{n+1} \mathrm{d}\hat{\sigma}^{\mathrm{R}}_{ab} + \int_n \mathrm{d}\hat{\sigma}^{\mathrm{V}}_{ab} + \int_n \mathrm{d}\hat{\sigma}^{\mathrm{C}}_{ab} \right], \tag{4.4.7}$$

where

$$\begin{aligned}\mathrm{d}\hat{\sigma}^{\mathrm{R}}_{ab}(p_a,p_b) = {}& \frac{\mathrm{d}\phi_{\mathcal{R}}(Q)}{2\hat{s}} \sum_{\{n+1\}} \mathrm{d}\phi_{n+1}(p_1,\ldots,p_{n+1};p_a+p_b-Q) \\ & \times \frac{1}{S_{\{n+1\}}} \overline{\left|\mathcal{M}^{0}_{n+1,ab}(p_1,\ldots,p_{n+1},Q;p_a,p_b)\right|^2} F_J^{(\mathcal{R}+n+1)}(Q,p_1,\ldots,p_{n+1};p_a,p_b)\end{aligned} \tag{4.4.8}$$

arises from (4.4.6) by simply replacing $\{n\}$ by $\{n+1\}$. The expression for the virtual contributions is

$$\mathrm{d}\hat{\sigma}^{\mathrm{V}}_{ab}(p_a,p_b) = \frac{\mathrm{d}\phi_{\mathcal{R}}(Q)}{2\hat{s}} \sum_{\{n\}} \frac{\mathrm{d}\phi_n}{S_{\{n\}}}\, 2\,\mathrm{Re}\,\overline{\left[\mathcal{M}^{1}_{n,ab}\,(\mathcal{M}^{0}_{n,ab})^{*}\right]}\, F_J^{(\mathcal{R}+n)}\,, \tag{4.4.9}$$

with the renormalized one-loop amplitude $\mathcal{M}^{1}_{n,ab}$. In (4.4.9), we have omitted the dependence on the external momenta, since it is given by (4.4.6).

4.4.2 General procedure of the subtraction formalism

In this subsection we present a brief and formal summary of the basic ideas of the dipole subtraction method for the calculation of NLO corrections in QCD, following the notation of [66]. The technical details about the explicit construction of the dipole formulae and about the integration of the universal IR-singular parts can also be found in this paper. The following general statements hold for any scattering process involving massless QCD partons (i.e. gluons, quarks, or antiquarks) in the final and/or initial state. Nevertheless, for simplicity we neglect the dependence on the non-strongly-interacting system $\mathcal{R}(Q)$ we have introduced in Section 4.4.1 in this subsection, since the following explanations only affect the QCD sector of the examined process. We also remark that we demand collinear

safety with respect to the definition of physical jets. Since we do not specify the initial state, we always assume parton-level cross sections in the following.

As explained in Sections 3.3 and 4.4.1, the NLO part of any cross section is defined as the sum of the real corrections $\int_{n+1} \mathrm{d}\hat{\sigma}^{\mathrm{R}}$, arising from one additional parton in the FS, the virtual corrections $\int_n \mathrm{d}\hat{\sigma}^{\mathrm{V}}$ and the collinear counterterm $\int_n \mathrm{d}\hat{\sigma}^{\mathrm{C}}$ that removes the residual IS collinear singularities connected to radiative QCD corrections to IS partons. As a result of general factorization properties of QCD amplitudes in the soft and the collinear limit (see Section 3.2), one is able to construct a *local counterterm* $\mathrm{d}\hat{\sigma}^{\mathrm{A}}$ that exactly matches the IR-singular structure of $\mathrm{d}\hat{\sigma}^{\mathrm{R}}$. This local counterterm can be composed from the underlying hard process $\mathrm{d}\hat{\sigma}^{0}$ and the dipoles $\mathrm{d}V_{\mathrm{dipole}}$ by summing over all possible dipole contributions,

$$\mathrm{d}\hat{\sigma}^{\mathrm{A}} = \sum_{\mathrm{dipoles}} \mathrm{d}\hat{\sigma}^{0} \otimes \mathrm{d}V_{\mathrm{dipole}} \,. \tag{4.4.10}$$

Note that this notation is symbolic and just visualizes the general procedure. The symbol $\otimes$ denotes adequately defined phase-space convolutions and the sums over colour and spin indices, and $\mathrm{d}\hat{\sigma}^{0}$ is a particular spin and colour projection of the exclusive Born-level cross section. The dipoles $\mathrm{d}V_{\mathrm{dipole}}$ do not depend on the underlying hard process and can be computed once and for all.

No we can rearrange the NLO cross section (4.4.7) as

$$\hat{\sigma}^{\mathrm{NLO}} = \int_{n+1} (\mathrm{d}\hat{\sigma}^{\mathrm{R}} - \mathrm{d}\hat{\sigma}^{\mathrm{A}}) + \int_n \mathrm{d}\hat{\sigma}^{\mathrm{V}} + \int_{n+1} \mathrm{d}\hat{\sigma}^{\mathrm{A}} + \int_n \mathrm{d}\hat{\sigma}^{\mathrm{C}} \,. \tag{4.4.11}$$

Since $\mathrm{d}\hat{\sigma}^{\mathrm{A}}$ acts as a local counterterm that cancels all IR singularities in $\mathrm{d}\hat{\sigma}^{\mathrm{R}}$, the first subtraction integral can be computed numerically in four dimensions over the whole $(n+1)$-parton phase space. The IR-singular subspace of the emitted parton in $\mathrm{d}\hat{\sigma}^{\mathrm{A}}$ can be integrated analytically in $d = 4 - 2\epsilon$ dimensions,

$$\int_{n+1} \mathrm{d}\hat{\sigma}^{\mathrm{A}} = \sum_{\mathrm{dipoles}} \int_n \mathrm{d}\hat{\sigma}^{0} \otimes \int_1 \mathrm{d}V_{\mathrm{dipole}} \,, \tag{4.4.12}$$

exploiting the general factorization properties of the jet amplitudes mentioned before. This procedure results in a convolution of the general, process-independent operators $\boldsymbol{I}(\epsilon)$, $\boldsymbol{P}$, and $\boldsymbol{K}$ with the leading order cross section $\mathrm{d}\hat{\sigma}^{0}$ specifying the underlying hard process without additional parton radiation. Finally, one finds that the NLO cross section can be decomposed according to the n- and the $(n+1)$-parton kinematics in the following way,

$$\begin{aligned}
\hat{\sigma}^{\mathrm{NLO}}(p) = \int_{n+1} & \left[\left(\mathrm{d}\hat{\sigma}^{\mathrm{R}}(p)\right)_{\epsilon=0} - \left(\sum_{\mathrm{dipoles}} \mathrm{d}\hat{\sigma}^{0}(p) \otimes \mathrm{d}V_{\mathrm{dipole}} \right)_{\epsilon=0} \right] \\
& + \int_n \left[\mathrm{d}\hat{\sigma}^{\mathrm{V}}(p;\epsilon) + \mathrm{d}\hat{\sigma}^{0}(p) \otimes \boldsymbol{I}(\epsilon) \right]_{\epsilon=0} \\
& + \int_0^1 \mathrm{d}x \int_n \left[\mathrm{d}\hat{\sigma}^{0}(xp) \otimes \left(\boldsymbol{P}(x, xp, \mu_{\mathrm{F}}) + \boldsymbol{K}(x) \right) \right]_{\epsilon=0} \,,
\end{aligned} \tag{4.4.13}$$

where the argument "p" includes the schematic dependence of the cross section on the momenta of the IS partons.

The $\boldsymbol{I}$-operator contains all IR-singular $1/\epsilon$ and $1/\epsilon^2$ poles arising from the collinear splitting of a FS parton into two collinear partons. It additionally contains the endpoint contributions of gluon radiation from IS partons, corresponding to a situation in which the radiated gluon becomes soft. All these IR singularities have to be cancelled against antipodal contributions from the virtual corrections $\mathrm{d}\hat{\sigma}^{\mathrm{V}}$ according to the KLN theorem as already stated in Section 3.3.

The $\boldsymbol{P}$- and the $\boldsymbol{K}$-operator, respectively, are related to collinear parton radiation from IS partons. In the collinear limit, the emitted parton carries away the four-momentum $(1-x)p$ from the incoming parton, reducing the momentum of the hard process from p to xp. This qualitatively explains why we have to perform a convolution of the LO cross section $\mathrm{d}\hat{\sigma}^0(xp)$, allowing for all possible momentum configurations after parton emission for x between $x=0$ (soft emission) and $x=1$ (hard emission).

The $\boldsymbol{P}$-operator exhibits a dependence on the factorization scale μ_{F} and the momentum p, since it contains the regular remnant resulting from the cancellation of the universal IS collinear singularities against the $1/\epsilon$ terms in the collinear counterterm $\mathrm{d}\hat{\sigma}^{\mathrm{C}}$. In contrast, the $\boldsymbol{K}$-operator includes the factorization–scheme-dependent finite contributions $K^{ab}_{\mathrm{F.S.}}(z)$ introduced in (3.3.1).

4.4.3 The dipole subtraction formulae for two initial-state partons

Here we provide the explicit formulae that allow one to calculate a NLO QCD cross section at hadron colliders using the dipole subtraction method. This section summarizes the results of Chapter 10 in Ref. [66].

Consider a partonic process with two incoming partons of flavours a and b with momenta p_a and p_b, and n QCD partons in the final state. The full NLO cross section for this process is given by

$$\begin{aligned}\hat{\sigma}^{\mathrm{NLO}}_{ab}(p_a,p_b;\mu_{\mathrm{F}}) = &\int_{n+1}\left(\mathrm{d}\hat{\sigma}^{\mathrm{R}}_{ab}(p_a,p_b)-\mathrm{d}\hat{\sigma}^{\mathrm{A}}_{ab}(p_a,p_b)\right)\\ &+\left[\int_{n+1}\mathrm{d}\hat{\sigma}^{\mathrm{A}}_{ab}(p_a,p_b)+\int_n\mathrm{d}\hat{\sigma}^{\mathrm{V}}_{ab}(p_a,p_b)+\int_n\mathrm{d}\hat{\sigma}^{\mathrm{C}}_{ab}(p_a,p_b)\right]. \qquad (4.4.14)\end{aligned}$$

Following the ideas of the last subsection, the second line of this equation can be turned into a simple convolution of Born-level cross sections with the all-purpose operators $\boldsymbol{I}(\epsilon)$, $\boldsymbol{P}$, and $\boldsymbol{K}$,

$$\begin{aligned}&\int_{n+1}\mathrm{d}\hat{\sigma}^{\mathrm{A}}_{ab}(p_a,p_b)+\int_n\mathrm{d}\hat{\sigma}^{\mathrm{V}}_{ab}(p_a,p_b)+\int_n\mathrm{d}\hat{\sigma}^{\mathrm{C}}_{ab}(p_a,p_b)\\ &=\int_n\left[\mathrm{d}\hat{\sigma}^0_{ab}(p_a,p_b)\,\boldsymbol{I}(\epsilon)+\mathrm{d}\hat{\sigma}^{\mathrm{V}}_{ab}(p_a,p_b;\epsilon)\right]\,F_J^{(n)}(p_1,\ldots,p_n;p_a,p_b)\\ &+\sum_{a'}\int_0^1\mathrm{d}x\int_n\left[\boldsymbol{K}^{a,a'}(x)+\boldsymbol{P}^{a,a'}(xp_a,x;\mu_{\mathrm{F}}^2)\right]\mathrm{d}\hat{\sigma}^0_{a'b}(xp_a,p_b)\,F_J^{(n)}(p'_1,\ldots,p'_n;xp_a,p_b)\\ &+\sum_{b'}\int_0^1\mathrm{d}x\int_n\left[\boldsymbol{K}^{b,b'}(x)+\boldsymbol{P}^{b,b'}(xp_b,x;\mu_{\mathrm{F}}^2)\right]\mathrm{d}\hat{\sigma}^0_{ab'}(p_a,xp_b)\,F_J^{(n)}(p''_1,\ldots,p''_n;p_a,xp_b)\,,\end{aligned} \qquad (4.4.15)$$

where the FS momenta p_i' and p_i'' are generated with the reduced squared cm energy $x\hat{s}$. The explicit expressions of the three contributing operators can be found in Section 10.1 of [66]. We will discuss this equation in some detail. Since the $\boldsymbol{I}$-operator contains the full IR structure of the real corrections, the cancellation against the virtual corrections can be done analytically, resulting in a straight-forward numerical integration of a Born-level phase space. All non-singular contributions to the NLO cross section are given by simple convolutions of smooth functions with Born-level differential cross sections, also allowing for a numerically stable evaluation.

The expression $\mathrm{d}\hat{\sigma}^{\mathrm{A}}_{ab}(p_a,p_b)$ in the subtraction integral is given by a sum over all dipoles that can be constructed from all partonic processes with $(n+1)$ partons in the final state, contributing as real corrections to the cross section $\mathrm{d}\hat{\sigma}^{0}_{ab}(p_a,p_b)$:

$$
\begin{aligned}
\mathrm{d}\hat{\sigma}^{\mathrm{A}}_{ab}(p_a,p_b) &= \frac{1}{n_s(a)n_s(b)\,2\hat{s}} \sum_{\{n+1\}} \mathrm{d}\phi_{n+1}(p_1,\dots,p_{n+1};p_a+p_b)\frac{1}{S_{\{n+1\}}} \\
&\times \Bigg\{ \sum_{\substack{\text{pairs}\\ i,j}} \sum_{k\neq i,j} \mathcal{D}_{ij,k}(p_1,\dots,p_{n+1};p_a,p_b) F_J^{(n)}(p_1,\dots,\tilde{p}_{ij},\tilde{p}_k,\dots,p_{n+1};p_a,p_b) \\
&+ \sum_{\substack{\text{pairs}\\ i,j}} \Big[\mathcal{D}^{a}_{ij}(p_1,\dots,p_{n+1};p_a,p_b) F_J^{(n)}(p_1,\dots,\tilde{p}_{ij},\dots,p_{n+1};\tilde{p}_a,p_b) + (a\leftrightarrow b) \Big] \\
&+ \sum_{i} \sum_{k\neq i} \Big[\mathcal{D}^{ai}_{k}(p_1,\dots,p_{n+1};p_a,p_b) F_J^{(n)}(p_1,\dots,\tilde{p}_{k},\dots,p_{n+1};\tilde{p}_{ai},p_b) + (a\leftrightarrow b) \Big] \\
&+ \sum_{i} \Big[\mathcal{D}^{ai,b}(p_1,\dots,p_{n+1};p_a,p_b) F_J^{(n)}(\tilde{p}_1,\dots,\tilde{p}_{n+1};\tilde{p}_{ai},p_b) + (a\leftrightarrow b) \Big] \Bigg\}, \qquad (4.4.16)
\end{aligned}
$$

where i, j, and k depict QCD partons in the final state, and $n_s(a/b)$ denotes the number of polarizations of the IS partons a and b.

The dipoles $\mathcal{D}^{ai,b}$ and $\mathcal{D}^{ai}_{k}$ that are constructed with the IS spectator b or the FS spectator c_k according to (4.4.10) are composed in such a way that the sum $\sum_{b,k}(\mathcal{D}^{ai,b}+\mathcal{D}^{ai}_{k})$ will cancel the collinear singularity that arises due to the IS splitting $a\to\widetilde{ai}+i$, where the parton $\widetilde{ai}$ enters the hard scattering process depicted by the amplitude $\mathcal{M}^{0,(ai)}$, in which parton c_i is absent (see Fig. 3.1(a)). The structure of the dipoles is given by

$$
\begin{aligned}
\mathcal{D}^{ai}_{k}(p_1,\dots,p_{n+1};p_a,p_b) &= \frac{1}{2\,(p_a p_i)} \boldsymbol{G}^{ai}_{k}(p_a,p_i,p_k) \\
&\otimes \left|\mathcal{M}^{0,(ai)}\big(\widetilde{ai}(\tilde{p}_{ai})+b(p_b)\to c_1(p_1)+\dots+c_k(\tilde{p}_k)+\dots+c_n(p_n)\big)\right|^2, \qquad (4.4.17a) \\
\mathcal{D}^{ai,b}(p_1,\dots,p_{n+1};p_a,p_b) &= \frac{1}{2\,(p_a p_i)} \boldsymbol{G}^{ai,b}(p_a,p_b,p_i,) \\
&\otimes \left|\mathcal{M}^{0,(ai)}\big(\widetilde{ai}(\tilde{p}_{ai})+b(\tilde{p}_b)\to c_1(\tilde{p}_1)+\dots+c_n(\tilde{p}_n)\big)\right|^2, \qquad (4.4.17b)
\end{aligned}
$$

where the matrices $\boldsymbol{G}^{ai,\cdots}_{\cdots}$ contain the process-independent information about the singular splitting, and the so-called auxiliary momenta indicated by a "$\sim$" have to be constructed from the full radiative phase space in such a way that momentum conservation and all mass-shell conditions are fulfilled within the calculation of $\mathcal{M}^{0,(ai)}$. Note that the matrices

$\boldsymbol{G}$ normally do not factorize from the squared LO matrix element, but act as operators on the colour structure of the the LO amplitude $\mathcal{M}^0$ (see Section 4.4.5) and employ spin correlations.

On the other hand, the dipoles $\mathcal{D}_{ij,k}$ and $\mathcal{D}^a_{ij}$ that are constructed with the IS spectator a or the FS spectator c_k are composed in such a way that the sum $\sum_{a,k}(\mathcal{D}_{ij,k}+\mathcal{D}^a_{ij})$ cancels the collinear singularity in $\hat{\sigma}^{\mathrm{R}}_{ab}$ originating from the FS splitting $\widetilde{ij}\to i+j$, where the parton $\widetilde{ij}$ leaves the hard scattering process and splits into the collinear pair of partons i and j (see Fig. 3.1(b)). The kernels now read

$$\begin{aligned}\mathcal{D}_{ij,k}(p_1,\dots,p_{n+1};p_a,p_b) &= \frac{1}{2\,(p_ip_j)}\boldsymbol{G}_{ij,k}(p_i,p_j,p_k)\\ &\otimes\left|\mathcal{M}^0_{(ij)}\big(a(p_a)+b(p_b)\to c_1(p_1)+\dots+c_{\widetilde{ij}}(\tilde{p}_{ij})+\dots+c_k(\tilde{p}_k)+\dots+c_n(p_n)\big)\right|^2,\end{aligned} \tag{4.4.18a}$$

$$\begin{aligned}\mathcal{D}^a_{ij}(p_1,\dots,p_{n+1};p_a,p_b) &= \frac{1}{2\,(p_ip_j)}\boldsymbol{G}^a_{ij}(p_a,p_i,p_j)\\ &\otimes\left|\mathcal{M}^0_{(ij)}\big(a(\tilde{p}_a)+b(p_b)\to c_1(p_1)+\dots+c_{\widetilde{ij}}(\tilde{p}_{ij})+\dots c_n(p_n)\big)\right|^2,\end{aligned} \tag{4.4.18b}$$

with the adequate matrices $\boldsymbol{G}^{\dots}_{ij,\dots}$, and the auxiliary momenta $\tilde{p}_{ij}$, $\tilde{p}_k$, and $\tilde{p}_a$ that again have to be physical external momenta of the amplitude $\mathcal{M}^0_{(ij)}$ without collinear splitting. In accordance with [66], we assume summation over helicities and colours of external particles as well as colour-averaged IS particles in the squared LO amplitudes in (4.4.17) and (4.4.18), respectively.

Although it is possible to cancel different collinear singularities in different regions of the phase space independently, the soft singularities in $\hat{\sigma}^{\mathrm{R}}_{ab}$ are not related to a single external splitting. Thus, all contributions in (4.4.16) are needed to match the soft-singular structure of the radiative process properly.

A detailed technical discussion of the construction of the dipole kernels $\mathcal{D}$ is carried out in Chapter 5 of [66]. It is important to stress that the FS momenta that enter the cut function $F^{(n)}_J$ or are used to calculate a phase-space dependent scale parameter should be identical with the auxiliary momenta entering the reduced LO amplitudes $\mathcal{M}^0$ within the subtraction kernels. Otherwise, it could become very intricate to consistently readd the correct contributions in the analytically integrated counterparts.

4.4.4 The dipole subtraction formulae for one initial-state parton

Here we list the subtraction formulae for a situation with just one QCD parton a in the initial state. This description for example accounts for processes with one photon in the initial state that arise due to the photon content of the proton. In this case, the subtraction function $\mathrm{d}\hat{\sigma}^{\mathrm{A}}_a$ reads

$$\begin{aligned}\mathrm{d}\hat{\sigma}^{\mathrm{A}}_a(p_a) = \frac{1}{n_s(a)\,2\hat{s}}\sum_{\{n+1\}}\mathrm{d}\phi_{n+1}(p_1,\dots,p_{n+1};p_a+p_b)\frac{1}{S_{\{n+1\}}}\\ \times\left\{\sum_{\substack{\text{pairs}\\ i,j}}\sum_{k\neq i,j}\mathcal{D}_{ij,k}(p_1,\dots,p_{n+1};p_a,p_b)F^{(n)}_J(p_1,\dots,\tilde{p}_{ij},\tilde{p}_k,\dots,p_{n+1};p_a,p_b)\right.\end{aligned}$$

$$+\sum_{\substack{\text{pairs}\\ i,j}} \mathcal{D}_{ij}^{a}(p_1,\dots,p_{n+1};p_a,p_b) F_J^{(n)}(p_1,\dots,\tilde{p}_{ij},\dots,p_{n+1};\tilde{p}_a,p_b)$$

$$+\sum_i \sum_{k\neq i} \mathcal{D}_{k}^{ai}(p_1,\dots,p_{n+1};p_a,p_b) F_J^{(n)}(p_1,\dots,\tilde{p}_{k},\dots,p_{n+1};\tilde{p}_{ai},p_b)\Bigg\}, \quad (4.4.19)$$

and the readded counterpart is given by

$$\begin{aligned}
&\int_{n+1} \mathrm{d}\hat{\sigma}_a^{\mathrm{A}}(p_a) + \int_n \mathrm{d}\hat{\sigma}_a^{\mathrm{V}}(p_a) + \int_n \mathrm{d}\hat{\sigma}_a^{\mathrm{C}}(p_a) \\
&= \int_n \left[\mathrm{d}\hat{\sigma}_a^{0}(p_a)\boldsymbol{I}(\epsilon) + \mathrm{d}\hat{\sigma}_a^{\mathrm{V}}(p_a;\epsilon)\right] F_J^{(n)}(p_1,\dots,p_n;p_a,p_b) \\
&+ \sum_b \int_0^1 \mathrm{d}x \int_n \left[\boldsymbol{K}^{a,b}(x) + \boldsymbol{P}^{a,b}(xp_a,x;\mu_{\mathrm{F}}^2)\right] \mathrm{d}\hat{\sigma}_b^{0}(xp_a)\, F_J^{(n)}(p_1',\dots,p_n';xp_a,p_b)\,,
\end{aligned} \quad (4.4.20)$$

where the operators $\boldsymbol{I}(\epsilon)$, $\boldsymbol{K}(x)$, and $\boldsymbol{P}(xp_a,x;\mu_{\mathrm{F}}^2)$ are listed in Section 8.1 of [66].

4.4.5 Colour-correlated amplitudes

For the implementation of the QCD subtraction kernels and their integrated counterparts, one is confronted with the calculation of colour-correlated squared amplitudes at the Born level. Establishing the notation

$$|\mathcal{M}_n|^2 \equiv \langle 1,\dots,n|1,\dots,n\rangle\,, \quad (4.4.21)$$

for an n-parton amplitude, the colour-correlated squared amplitude is defined via

$$|\mathcal{M}_n^{I,J}|^2 = \langle 1,\dots,I,J,\dots,n|\boldsymbol{T}_I\cdot\boldsymbol{T}_J|1,\dots,I,J,\dots,n\rangle\,, \quad (4.4.22)$$

where the colour charges $\boldsymbol{T}_{I/J}$ that act as operators in colour space are associated with the emission of a gluon from parton I or J, respectively. We will not discuss the explicit calculation of colour-correlated amplitudes in detail, because this is not necessary in our special case, as will be pointed out now.

The matrices $\boldsymbol{T}$ obey the colour-charge algebra

$$\boldsymbol{T}_i\cdot\boldsymbol{T}_j = \boldsymbol{T}_i\cdot\boldsymbol{T}_j \quad \text{if} \quad i\neq j, \quad \boldsymbol{T}_i^2 = C_i\,, \quad (4.4.23)$$

where C_i is the Casimir operator of parton i, i.e. $C_i = C_{\mathrm{A}} = N_{\mathrm{C}}$ if the parton is a gluon, and $C_i = C_{\mathrm{F}} = (N_{\mathrm{C}}^2-1)/2N_{\mathrm{C}}$ if the parton i is a quark or antiquark. Note that the expression $\boldsymbol{T}_i^2$ is diagonal in colour space. Since any physical amplitude corresponds to a colour-singlet state, conservation of colour charge implies

$$\sum_{i=1}^{n} \boldsymbol{T}_i|1,\dots,n\rangle = 0\,. \quad (4.4.24)$$

In our explicit calculation we have to consider processes with three QCD partons at the Born level, namely two quarks and a gluon. In such cases, colour conservation (4.4.24) can be used to express any colour-correlator $\boldsymbol{T}_I \cdot \boldsymbol{T}_J$ in terms of Casimir operators. Using

$$\begin{aligned} 0 &= \left(\sum_{i=1}^{3} \boldsymbol{T}_i \right)^2 |1,2,3\rangle \\ &= \left[\boldsymbol{T}_1^2 + \boldsymbol{T}_2^2 + \boldsymbol{T}_3^2 + 2(\boldsymbol{T}_1 \cdot \boldsymbol{T}_2 + \boldsymbol{T}_1 \cdot \boldsymbol{T}_3 + \boldsymbol{T}_2 \cdot \boldsymbol{T}_3) \right] |1,2,3\rangle \,, \end{aligned} \tag{4.4.25}$$

and

$$\begin{aligned} (\boldsymbol{T}_1 \cdot \boldsymbol{T}_2 + \boldsymbol{T}_1 \cdot \boldsymbol{T}_3) \, |1,2,3\rangle &= -\boldsymbol{T}_1^2 \, |1,2,3\rangle \,, \\ (\boldsymbol{T}_2 \cdot \boldsymbol{T}_1 + \boldsymbol{T}_2 \cdot \boldsymbol{T}_3) \, |1,2,3\rangle &= -\boldsymbol{T}_2^2 \, |1,2,3\rangle \,, \\ (\boldsymbol{T}_3 \cdot \boldsymbol{T}_1 + \boldsymbol{T}_3 \cdot \boldsymbol{T}_2) \, |1,2,3\rangle &= -\boldsymbol{T}_3^2 \, |1,2,3\rangle \,, \end{aligned} \tag{4.4.26}$$

one obtains

$$\langle 1,2,3|\boldsymbol{T}_i \cdot \boldsymbol{T}_j|1,2,3\rangle = (C_k^2 - C_i^2 - C_j^2) \, |\mathcal{M}_3|^2 \,, \tag{4.4.27}$$

for any permutation $\{i,j,k\}$ of $\{1,2,3\}$. This expression gives the prescription how to express colour-correlated amplitudes in terms of a simple factorization in any three-parton process.

For the calculation of the QCD corrections to photon-induced processes (see Section 8.1) we will also apply the dipole subtraction procedure. In this particular situation, the Born-level processes only contain two partons, and one simply obtains

$$\langle 1,2|\boldsymbol{T}_1 \cdot \boldsymbol{T}_2|1,2\rangle = C_1^2 \, |\mathcal{M}_2|^2 = C_2^2 \, |\mathcal{M}_2|^2 \,, \tag{4.4.28}$$

for the colour-correlated amplitudes.

Chapter 5

Production of on-shell W bosons in association with a jet

In this chapter we present the full NLO EW corrections to hadroproduction of one on-shell (stable) W boson with one associated parton that will subsequently hadronize to a hadron jet which will be denoted as j in the following. At LO, we take into account the dominant partonic channels with two QCD partons in the initial state, but we will also have a closer look at the contributions via photoproduction. Due to the conceptual problems discussed in Section 3.7, we also include $\mathrm{W} + \gamma$ production and the associated QCD corrections in our calculation.

This chapter is organized as follows. First, we outline the different contributions that can be assigned to photon-induced processes. In Section 5.2, we list the relevant partonic cross sections at LO and explain how to evaluate the hadronic cross section from them. In Section 5.3, we discuss in detail the structure of the NLO corrections. In Section 5.4, we present our numerical results for $\mathrm{p\bar{p}}$ collisions with cm energy $\sqrt{s} = 1.96$ TeV at the Fermilab Tevatron and pp collisions with $\sqrt{s} = 14$ TeV at the CERN LHC.

5.1 Photon-induced contributions

By crossing external lines, the LO partonic subprocesses of $\mathrm{W} + \gamma$ hadroproduction can be converted to those of $\mathrm{W} + j$ photoproduction with one incoming photon participating directly in the hard scattering via direct photoproduction. The emission of photons off the proton can happen either elastically or inelastically, i.e. the proton stays intact or is destroyed, respectively. In both cases, an appropriate PDF can be evaluated in the Weizsäcker–Williams approximation [76, 77, 78]. Since the PDFs are of $\mathcal{O}(\alpha)$, these direct photoproduction contributions are of $\mathcal{O}(\alpha^3)$. Although photoproduction contributions are parametrically suppressed by a factor of α/α_s relative to the dominant EW $\mathcal{O}(\alpha^2\alpha_\mathrm{s})$ corrections, we shall include them in our analysis because we want to investigate their phenomenological relevance compared to the EW NLO corrections to $\mathrm{W} + j$ production.

5.2 Conventions and LO results

We consider the hadronic process

$$A(p_A) + B(p_B) \to \mathrm{W}(p) + X, \tag{5.2.1}$$

where the four-momentum assignments are indicated in parentheses. We work in the QCD improved parton model (see Section 2.3) with $n_f = 5$ massless quark flavours $q = \mathrm{u}, \mathrm{d}, \mathrm{s}, \mathrm{c}, \mathrm{b}$, neglect the masses of the incoming hadrons, A and B, and impose the acceptance cut $p_\mathrm{T} > p_\mathrm{T}^\mathrm{cut}$ on the transverse momentum p_T of the W boson. (We assign masses to the partons $\gamma, \mathrm{g}, q, \overline{q}$ only to regulate soft and collinear IR singularities in intermediate steps of our calculation, as explained in Section 3.1.)

Specifically, denoting $\mathrm{u}_1 = \mathrm{u}$, $\mathrm{u}_2 = \mathrm{c}$, $\mathrm{d}_1 = \mathrm{d}$, $\mathrm{d}_2 = \mathrm{s}$, and $\mathrm{d}_3 = \mathrm{b}$, the relevant partonic subprocesses include

$$\mathrm{u}_i\, \overline{\mathrm{d}}_j \to \mathrm{W}^+ + \mathrm{g}, \tag{5.2.2}$$
$$\mathrm{u}_i\, \mathrm{g} \to \mathrm{W}^+ + \mathrm{d}_j, \tag{5.2.3}$$
$$\overline{\mathrm{d}}_j\, \mathrm{g} \to \mathrm{W}^+ + \overline{\mathrm{u}}_i, \tag{5.2.4}$$

at $\mathcal{O}(\alpha\alpha_\mathrm{s})$,

$$\mathrm{u}_i\, \overline{\mathrm{d}}_j \to \mathrm{W}^+ + \gamma, \tag{5.2.5}$$
$$\mathrm{u}_i\, \gamma \to \mathrm{W}^+ + \mathrm{d}_j, \tag{5.2.6}$$
$$\overline{\mathrm{d}}_j\, \gamma \to \mathrm{W}^+ + \overline{\mathrm{u}}_i, \tag{5.2.7}$$

at $\mathcal{O}(\alpha^2)$, and

$$\mathrm{u}_i\, \overline{\mathrm{d}}_j \to \mathrm{W}^+ + \mathrm{g} + \gamma, \tag{5.2.8}$$
$$\mathrm{u}_i\, \mathrm{g} \to \mathrm{W}^+ + \mathrm{d}_j + \gamma, \tag{5.2.9}$$
$$\overline{\mathrm{d}}_j\, \mathrm{g} \to \mathrm{W}^+ + \overline{\mathrm{u}}_i + \gamma, \tag{5.2.10}$$

at $\mathcal{O}(\alpha^2\alpha_\mathrm{s})$. The partonic subprocesses involving a W^- boson emerge through a $\mathcal{CP}$ transformation on the parton level. Processes (5.2.2) – (5.2.5) must be treated also at one loop, $\mathcal{O}(\alpha^2\alpha_\mathrm{s})$. The Processes (5.2.6) and (5.2.7) contribute to direct photoproduction. Since photon emission off protons happens at $\mathcal{O}(\alpha)$, it is a good starting point to deal with photoproduction at tree level. In summary, we calculate the cross section of process (5.2.1) at NLO as the sum

$$\sigma_{AB\to\mathrm{W}X} = \sigma^0_{\mathrm{W}j} + \sigma^0_{\mathrm{W}\gamma} + \sigma^{\mathcal{O}(\alpha)}_{\mathrm{W}j} + \sigma^{\mathcal{O}(\alpha_\mathrm{s})}_{\mathrm{W}\gamma} + \sigma^0_{\mathrm{W}j\gamma} + \sigma^\gamma_{\mathrm{W}j}, \tag{5.2.11}$$

where $\sigma^0_{\mathrm{W}j}$ and $\sigma^{\mathcal{O}(\alpha)}_{\mathrm{W}j}$ are due to processes (5.2.2) – (5.2.4) at tree level and one loop, $\sigma^0_{\mathrm{W}\gamma}$ and $\sigma^{\mathcal{O}(\alpha_\mathrm{s})}_{\mathrm{W}\gamma}$ are due to process (5.2.5) at tree level and one loop, $\sigma^0_{\mathrm{W}j\gamma}$ is due to processes (5.2.8) – (5.2.10) at tree level, and $\sigma^\gamma_{\mathrm{W}j}$ is due to processes (5.2.6) and (5.2.7) via direct photoproduction at tree-level.

We demand a minimum p_T for the jet, i.e. $p_\mathrm{T}(j) > p_\mathrm{T}^\mathrm{cut}$, to ensure that we observe a visible jet at LO. As discussed in Section 2.3.2, the cross section $\sigma_{AB\to\mathrm{W}X}$ of the hadronic process (5.2.1) is related to the cross sections $\hat{\sigma}_{ab\to\mathrm{W}c(d)}$ of the partonic subprocesses,

$$a(p_a) + b(p_b) \to \mathrm{W}(p) + c(p_c)(+d(p_d)), \tag{5.2.12}$$

where $a, b, c, d = \gamma, \mathrm{g}, q, \overline{q}$ and $p_a = x_a p_A$, $p_b = x_b p_B$ with scaling parameters x_a, x_b, as the incoherent sum

$$\sigma_{AB\to \mathrm{W}X}(s, p_\mathrm{T} > p_\mathrm{T}^\mathrm{cut}) = \sum_{a,b,c(,d)} \int_{\tau_0}^1 \mathrm{d}\tau\, \mathcal{L}_{AB}^{ab}(\tau) \hat{\sigma}_{ab\to \mathrm{W}c(d)}(\hat{s}, p_\mathrm{T} > p_\mathrm{T}^\mathrm{cut}), \tag{5.2.13}$$

where

$$\mathcal{L}_{AB}^{ab}(\tau) = \int_\tau^1 \frac{\mathrm{d}x_a}{x_a} f_{a/A}(x_a, \mu_\mathrm{F}^2) f_{b/B}\left(\frac{\tau}{x_a}, \mu_\mathrm{F}^2\right), \tag{5.2.14}$$

is the parton luminosity defined in terms of the PDFs. In (5.2.13), we have to sum over all combination of partons a, b, c, and d that contribute to the processes (5.2.2) – (5.2.10). Introducing the shorthand notation $w = M_\mathrm{W}^2$, we have

$$\tau_0 = \frac{\left(p_\mathrm{T}^\mathrm{cut} + \sqrt{w + (p_\mathrm{T}^\mathrm{cut})^2}\right)^2}{s}. \tag{5.2.15}$$

In order to obtain $\hat{\sigma}_{ab\to \mathrm{W}c(d)}$, we have to evaluate the transition matrix elements $\mathcal{M}_{ab\to \mathrm{W}c(d)}$ of processes (5.2.12), square them, average them over the IS spins and colours, and sum them over the FS ones, which leads to $\overline{|\mathcal{M}_{ab\to \mathrm{W}c(d)}|^2}$. To the order of our calculation, $\mathcal{M}_{ab\to \mathrm{W}cd}$ is calculated at tree level, while $\mathcal{M}_{ab\to \mathrm{W}c}$ may receive also one-loop contributions, $\mathcal{M}_{ab\to \mathrm{W}c} = \mathcal{M}^0_{ab\to \mathrm{W}c} + \mathcal{M}^1_{ab\to \mathrm{W}c}$, so that

$$\overline{|\mathcal{M}_{ab\to \mathrm{W}c}|^2} = \overline{|\mathcal{M}^0_{ab\to \mathrm{W}c}|^2} + 2\mathrm{Re}\overline{\left[(\mathcal{M}^0_{ab\to \mathrm{W}c})^* \mathcal{M}^1_{ab\to \mathrm{W}c}\right]}. \tag{5.2.16}$$

Then we have to integrate over the partonic phase spaces constrained by the minimum-p_T cut. In the following two subsections, we describe how this is done for the two- and three-particle final states, respectively.

Since we are dealing with charged-current interactions of quarks, u_i and d_j, the quark-mixing matrix V_{ij} (see Eq. (2.1.26)) appears. At tree level, the cross sections of processes (5.2.2) – (5.2.10) contain the overall factor $|V_{ij}|^2$. Since we assume the CKM matrix as diagonal in the one-loop corrections, we can absorb the residual appearances of $|V_{ij}|^2$ at LO into a redefinition of the down-quark PDFs, as [38, 39]

$$\tilde{f}_{\mathrm{d}_i/A}(x, \mu_\mathrm{F}^2) = \sum_{j=1}^3 |V_{ij}|^2 f_{\mathrm{d}_j/A}(x, \mu_\mathrm{F}^2), \tag{5.2.17}$$

and similarly for down antiquarks. Therefore, it is sufficient to calculate the partonic cross sections for the flavour-diagonal case, with $V_{ij} = \delta_{ij}$. The replacement (5.2.17) in particular restores the correct CKM dependences for the $\mathrm{u}\bar{\mathrm{d}}$ and $\bar{\mathrm{u}}\mathrm{d}$ annihilation channels.

5.2.1 Two-particle final states

If parton d is absent in process (5.2.12), we supplement $\hat{s}$ by two more Mandelstam variables, $t = (p_a - p)^2$ and $u = (p_b - p)^2$. Four-momentum conservation implies that $\hat{s} + t + u = w$, and we have $p_\mathrm{T}^2 = tu/\hat{s}$. The partonic cross section entering Eq. (5.2.13) is evaluated as

$$\hat{\sigma}_{ab\to \mathrm{W}c}(\hat{s}, p_\mathrm{T} > p_\mathrm{T}^\mathrm{cut}) = \int_{p_\mathrm{T}^\mathrm{cut}}^{p_\mathrm{T}^\mathrm{max}} \mathrm{d}p_\mathrm{T} \frac{\mathrm{d}\hat{\sigma}_{ab\to Wc}}{\mathrm{d}p_\mathrm{T}}, \tag{5.2.18}$$

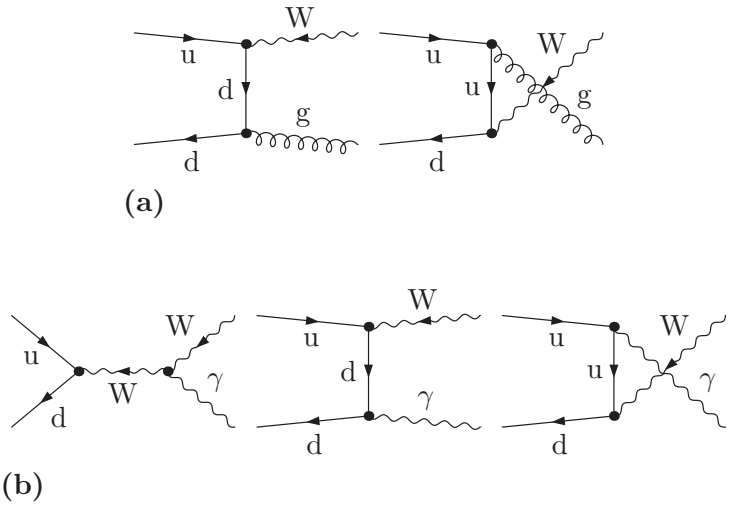

Figure 5.1: Tree-level diagrams of (a) process (5.2.2) and (b) process (5.2.5). The tree-level diagrams of processes (5.2.3), (5.2.4), (5.2.6), and (5.2.7) emerge through crossing.

where $p_{\mathrm{T}}^{\max} = (\hat{s} - w)/(2\sqrt{\hat{s}})$ and

$$\frac{\mathrm{d}\hat{\sigma}_{ab\to \mathrm{W}c}}{\mathrm{d}p_{\mathrm{T}}} = \frac{p_{\mathrm{T}}}{8\pi\hat{s}\sqrt{(\hat{s}-w)^2 - 4\hat{s}p_{\mathrm{T}}^2}}\overline{|\mathcal{M}_{ab\to \mathrm{W}c}|^2}. \tag{5.2.19}$$

For the reader's convenience, we list the differential cross sections of processes (5.2.2) – (5.2.7), in the conventional form

$$\frac{\mathrm{d}\hat{\sigma}_{ab\to \mathrm{W}c}}{\mathrm{d}t} = \frac{1}{16\pi\hat{s}^2}\overline{|\mathcal{M}_{ab\to \mathrm{W}c}|^2}, \tag{5.2.20}$$

at LO. The Feynman diagrams contributing to processes (5.2.2) and (5.2.5) are displayed in Figs. 5.1(a) and (b), respectively. We have

$$\begin{aligned}
\frac{\mathrm{d}\hat{\sigma}_{\mathrm{u}\bar{\mathrm{d}}\to \mathrm{W}^+\mathrm{g}}}{\mathrm{d}t} &= \frac{2\pi\alpha\alpha_{\mathrm{s}}}{9s_{\mathrm{W}}^2}\,\frac{\hat{s}^2 + w^2 - 2tu}{\hat{s}^2 tu}, \\
\frac{\mathrm{d}\hat{\sigma}_{\mathrm{u}\bar{\mathrm{d}}\to \mathrm{W}^+\gamma}}{\mathrm{d}t} &= \frac{\alpha}{12\alpha_{\mathrm{s}}}\left(1 + \frac{3t}{\hat{s}-w}\right)^2 \frac{\mathrm{d}\hat{\sigma}_{\mathrm{u}\bar{\mathrm{d}}\to \mathrm{W}^+\mathrm{g}}}{\mathrm{d}t},
\end{aligned} \tag{5.2.21}$$

where $s_{\mathrm{W}} = \sin\theta_{\mathrm{W}}$ is the sine of the weak mixing angle θ_{W} defined in (2.1.21). We use the G_{F} scheme for the definition of the electromagnetic coupling α, i.e. we derive α from the Fermi constant G_{F} according to

$$\alpha_{G_{\mathrm{F}}} = \frac{\sqrt{2}}{\pi} G_{\mathrm{F}} s_{\mathrm{W}}^2 w. \tag{5.2.22}$$

In this scheme, the weak corrections to muon decay Δr are included in the charge renormalization constant (see e.g. Ref. [17]). As a consequence, the EW corrections are independent

of logarithms of the light-quark masses. Moreover, this definition effectively resums the contributions associated with the running of α from zero to the W-boson mass and absorbs leading universal corrections $\propto G_\mathrm{F} m_\mathrm{t}^2$ from the ρ parameter into the LO amplitude. The implementation of the G_F scheme at one loop is explained in Section 5.3.1.

The cross sections of processes (5.2.3), (5.2.4), (5.2.6), and (5.2.7) may be obtained from Eq. (5.2.21) by exploiting crossing symmetries, leading to

$$\begin{aligned}
\hat{s}^2 \frac{\mathrm{d}\hat{\sigma}_{\mathrm{ug}\to\mathrm{W^+d}}}{\mathrm{d}t} &= -\frac{3}{8}\left[\hat{s}^2 \frac{\mathrm{d}\hat{\sigma}_{\mathrm{u\bar{d}}\to\mathrm{W^+g}}}{\mathrm{d}t}\right]_{\hat{s}\leftrightarrow u}, \\
\hat{s}^2 \frac{\mathrm{d}\hat{\sigma}_{\bar{\mathrm{d}}\mathrm{g}\to\mathrm{W^+}\bar{\mathrm{u}}}}{\mathrm{d}t} &= \left[\hat{s}^2 \frac{\mathrm{d}\hat{\sigma}_{\mathrm{ug}\to\mathrm{W^+d}}}{\mathrm{d}t}\right]_{\hat{s}\leftrightarrow t}, \\
\hat{s}^2 \frac{\mathrm{d}\hat{\sigma}_{\mathrm{u}\gamma\to\mathrm{W^+d}}}{\mathrm{d}t} &= -3\left[\hat{s}^2 \frac{\mathrm{d}\hat{\sigma}_{\mathrm{u\bar{d}}\to\mathrm{W^+}\gamma}}{\mathrm{d}t}\right]_{\hat{s}\leftrightarrow u}, \\
\hat{s}^2 \frac{\mathrm{d}\hat{\sigma}_{\bar{\mathrm{d}}\gamma\to\mathrm{W^+}\bar{\mathrm{u}}}}{\mathrm{d}t} &= \left[\hat{s}^2 \frac{\mathrm{d}\hat{\sigma}_{\mathrm{u}\gamma\to\mathrm{W^+d}}}{\mathrm{d}t}\right]_{\hat{s}\leftrightarrow t}.
\end{aligned} \tag{5.2.23}$$

5.2.2 Three-particle final states

If parton d is present in process (5.2.12), then the partonic cross section entering Eq. (5.2.13) may be obtained through a four-fold phase-space integration along the lines of Ref. [79]. We work in the partonic cm frame and choose our coordinate system so that $\mathbf{p}_a$ points along the x^3 direction and $\mathbf{p}_d$ lies in the x^2–x^3 plane. We denote the polar angle of $\mathbf{p}_d$ by ϑ and the azimuthal angle of $\mathbf{p}_c$ by φ. As the first three independent variables, we select p_d^0, ϑ, and φ, which take the values

$$0 < p_d^0 < \frac{\hat{s}-w}{2\sqrt{\hat{s}}}, \qquad 0 < \vartheta < \pi, \qquad 0 < \varphi < 2\pi. \tag{5.2.24}$$

In the case of process (5.2.8), which contains two massless gauge bosons in the final state, it is convenient to take the fourth variable to be p_c^0, with values

$$\frac{1}{2}\left(\sqrt{\hat{s}} - 2p_d^0 - \frac{w}{\sqrt{\hat{s}}}\right) < p_c^0 < \frac{1}{2}\left(\sqrt{\hat{s}} - \frac{w}{\sqrt{\hat{s}}-2p_d^0}\right). \tag{5.2.25}$$

We then have

$$\left.\frac{\mathrm{d}^4\hat{\sigma}_{\mathrm{u\bar{d}}\to\mathrm{W^+g}\gamma}}{\mathrm{d}p_c^0\mathrm{d}p_d^0\mathrm{d}\cos\vartheta\mathrm{d}\varphi}\right|_{p_\mathrm{T}>p_\mathrm{T}^\mathrm{cut}} = \frac{1}{8(2\pi)^4}\overline{\left|\mathcal{M}_{\mathrm{u\bar{d}}\to\mathrm{W^+g}\gamma}\right|^2}\,\theta\left(p_\mathrm{T}-p_\mathrm{T}^\mathrm{cut}\right). \tag{5.2.26}$$

On the other hand, in the case of processes (5.2.9) and (5.2.10), which only contain one massless gauge boson in the final state, it is more useful to choose the fourth variable to be the angle ψ enclosed between $\mathbf{p}_c$ and $\mathbf{p}_d$, with values

$$0 < \psi < \pi. \tag{5.2.27}$$

We then have

$$\left.\frac{\mathrm{d}^4\hat{\sigma}_{\mathrm{ug}\to\mathrm{W^+d}\gamma}}{\mathrm{d}p_d^0\mathrm{d}\cos\vartheta\mathrm{d}\varphi\mathrm{d}\psi}\right|_{p_\mathrm{T}>p_\mathrm{T}^\mathrm{cut}} = \frac{p_d^0\left[\sqrt{\hat{s}}\left(\sqrt{\hat{s}}-2p_d^0\right)-w\right]}{16(2\pi)^4\left[\sqrt{\hat{s}}-2p_d^0\sin^2(\psi/2)\right]}\overline{\left|\mathcal{M}_{\mathrm{ug}\to\mathrm{W^+d}\gamma}\right|^2}\,\theta\left(p_\mathrm{T}-p_\mathrm{T}^\mathrm{cut}\right), \tag{5.2.28}$$

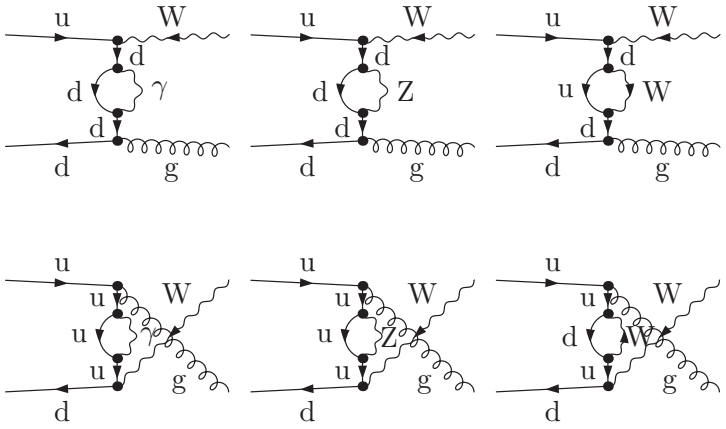

Figure 5.2: $\mathcal{O}(\alpha)$ self-energy diagrams of process (5.2.2).

and similarly for process (5.2.10). In order to implement the minimum-p_{T} cut, p_{T} can be expressed in terms the integration variables, which is conveniently done with the help of Eqs. (5.40) and (5.42) of Ref. [79] and starting from

$$p_{\mathrm{T}} = \sqrt{(p_c^1 + p_d^1)^2 + (p_c^2 + p_d^2)^2}. \tag{5.2.29}$$

5.3 NLO results

We now describe the calculation of the NLO contributions $\sigma_{\mathrm{W}j}^{\mathcal{O}(\alpha)}$, $\sigma_{\mathrm{W}\gamma}^{\mathcal{O}(\alpha_{\mathrm{s}})}$, and $\sigma_{\mathrm{W}j\gamma}^{0}$ of Eq. (5.2.11) in some detail.

We employ the following tools. We generate the relevant Feynman diagrams using the symbolic program package FeynArts [80, 81], carry out the spin and colour sums using the program package FormCalc [82], and perform the Passarino–Veltman reduction of the tensor one-loop integrals [83] using the program package FeynCalc [84]. Subsequently, the analytical results are implemented in a *Fortran* program. The standard scalar one-loop integrals contained in the purely weak corrections (i.e. corrections due to diagrams without photon exchange) are evaluated using the program package LoopTools [85], which incorporates the program library FF [86]. The numerical integrations are performed using a version of the adaptive Monte Carlo algorithm Vegas [87] that is part of the program package Cuba [88].

5.3.1 Virtual EW corrections to W + j production

The virtual EW corrections of $\mathcal{O}(\alpha)$ to processes (5.2.2) – (5.2.4) arise from self-energy, triangle, box, and counterterm diagrams. They are shown for process (5.2.2) in Figs. 5.2 – 5.5, respectively.

Evaluating the transition matrix element $\mathcal{M}_{\mathrm{W}j}^{\mathcal{O}(\alpha)}$ from these loop diagrams, we encounter both UV and IR singularities, which need to be regularized and properly cancelled. As outlined in Section 2.1.3, we use dimensional regularization, with $d = 4 - 2\epsilon$ space-time

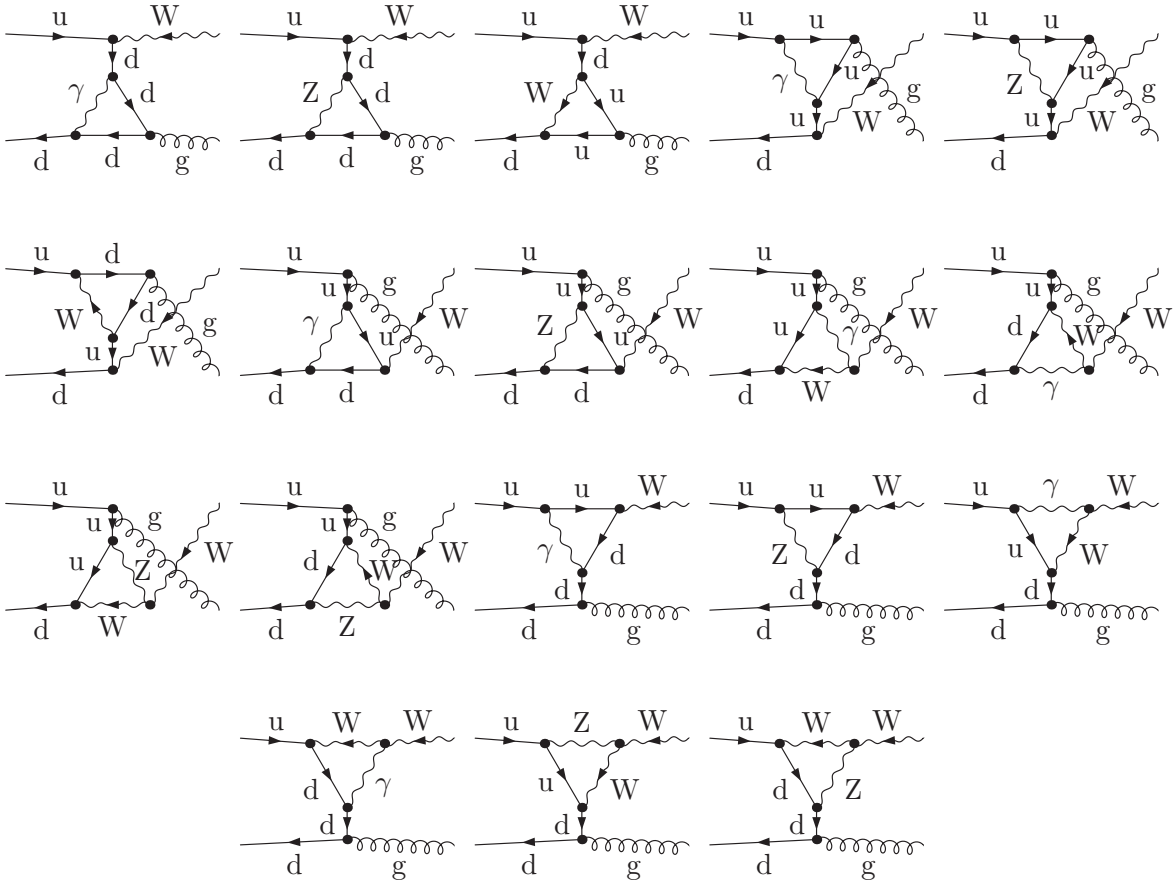

Figure 5.3: $\mathcal{O}(\alpha)$ triangle diagrams of process (5.2.2).

dimensions and 't Hooft mass scale μ, to extract the UV singularities as single poles in ϵ. These poles vanish after renormalizing the parameters and wave functions of the LO transition matrix element $\mathcal{M}^0_{\mathrm{W}j}$, which leads to the counterterm contribution (see Fig. 5.5),

$$\mathcal{M}^{\mathrm{CT}}_{\mathrm{W}j} = \mathcal{M}^0_{\mathrm{W}j}\, \delta^{\mathrm{CT}}_{\mathrm{W}j}. \tag{5.3.1}$$

Owing to the renormalizability of the SM, the UV singularities in $\mathcal{M}^{\mathcal{O}(\alpha)}_{\mathrm{W}j}$ cancel, and the physical limit $\epsilon \to 0$ can be reached smoothly.

As explained in Section 2.1.3, the EW on-shell renormalization scheme uses the fine-structure constant α defined in the Thomson limit and the physical particle masses as basic parameters. In order to avoid the appearance of large logarithms induced by the running of α to the EW scale M_{W} in $\mathcal{M}^{\mathcal{O}(\alpha)}_{\mathrm{W}j}$, it is useful to replace α by G_{F} in the set of basic parameters, using the relation [89]

$$G_{\mathrm{F}} = \frac{\pi\alpha}{\sqrt{2}s^2_{\mathrm{W}}w}\,\frac{1}{1-\Delta r}, \tag{5.3.2}$$

where

$$\Delta r = \Sigma'^{AA}_{\mathrm{T}}(0) - \frac{c^2_{\mathrm{W}}}{s^2_{\mathrm{W}}}\left(\frac{\Sigma^{ZZ}_{\mathrm{T}}(M^2_{\mathrm{Z}})}{M^2_{\mathrm{Z}}} - \frac{\Sigma^{W}_{\mathrm{T}}(M^2_{\mathrm{W}})}{M^2_{\mathrm{W}}}\right) + \frac{\Sigma^{W}_{\mathrm{T}}(0) - \Sigma^{W}_{\mathrm{T}}(M^2_{\mathrm{W}})}{M^2_{\mathrm{W}}}$$

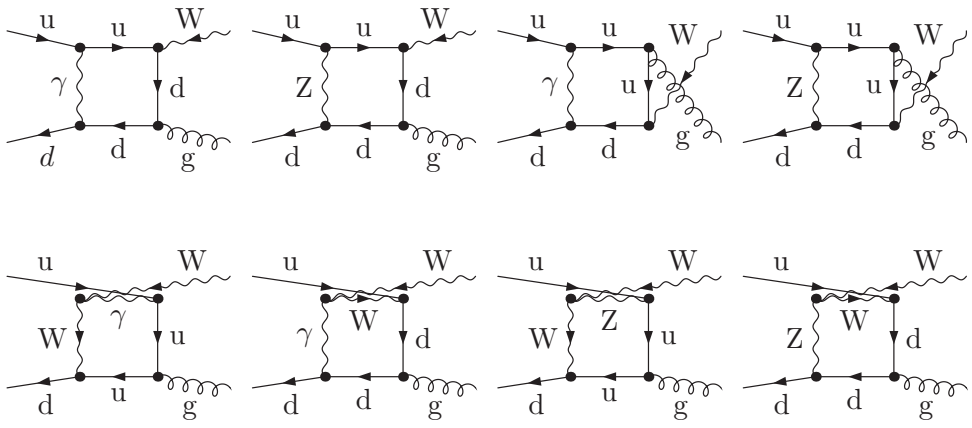

Figure 5.4: $\mathcal{O}(\alpha)$ box diagrams of process (5.2.2).

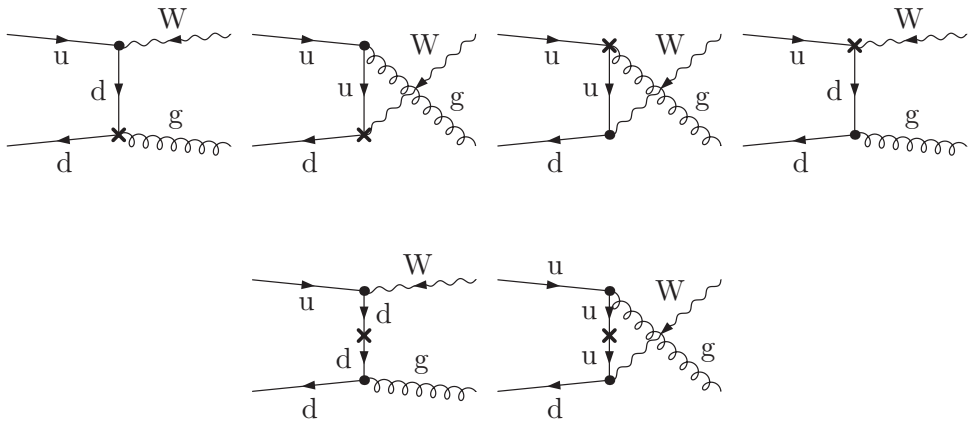

Figure 5.5: $\mathcal{O}(\alpha)$ counterterm diagrams of process (5.2.2).

$$+ 2\frac{c_{\mathrm{W}}}{s_{\mathrm{W}}}\frac{\Sigma_{\mathrm{T}}^{AZ}(0)}{M_{\mathrm{Z}}^2} + \frac{\alpha}{4\pi s_{\mathrm{W}}^2}\left(6 + \frac{7-4s_{\mathrm{W}}^2}{2s_{\mathrm{W}}^2}\ln c_{\mathrm{W}}^2\right) \tag{5.3.3}$$

contains those EW one-loop corrections to the muon lifetime which the SM introduces on top of those derived in the QED improved Fermi model. In the EW on-shell scheme thus modified, we have

$$\delta_{\mathrm{W}j}^{\mathrm{CT}} = \delta Z_e - \frac{\delta s_{\mathrm{W}}}{s_{\mathrm{W}}} + \frac{1}{2}\left(\delta Z_{u\bar{u}}^{\mathrm{L}} + \delta Z_{d\bar{d}}^{\mathrm{L}} + \delta Z_W - \Delta r\right), \tag{5.3.4}$$

where the renormalization constants are defined in Section 2.1.3.

The IR singularities can be of soft or collinear type. The loop diagrams involving virtual photons interchanged between external lines contain soft IR singularities. Owing to the Bloch–Nordsieck theorem [64], they cancel against similar singularities arising from the real emission of soft photons, as discussed in Section 3.1.1. The loop diagrams involving external quark or antiquark lines that split into virtual photons and quarks induce collinear IR singularities. Such singularities also arise from the real emission of collinear photons

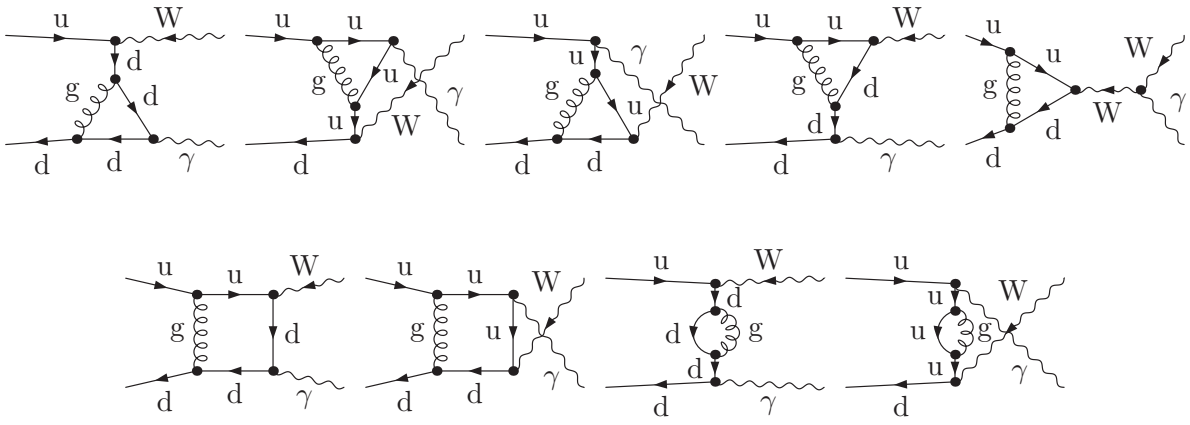

Figure 5.6: $\mathcal{O}(\alpha_s)$ self-energy, triangle, and box diagrams of process (5.2.5).

off external quark or antiquark lines (see Tab. 3.1). According to the KLN theorem [67], collinear IR singularities from FS radiation are completely cancelled in the sum of real and virtual corrections provided that the final state is treated sufficiently inclusive. On the other hand, collinear IR singularities from IS radiation survive and have to be absorbed into the quark and antiquark PDFs according to the replacement (3.4.1). For consistency, the splitting functions in the evolution equations of the PDFs then need to be complemented by their $\mathcal{O}(\alpha)$ terms. IR singularities also arise from the wave-function renormalizations in Eq. (5.3.4). We choose to regularize the IR singularities by assigning infinitesimal masses, λ, m_u, and m_d, to the photon, the light up-type quarks, and the down-type quarks, respectively. This is convenient because the standard scalar one-loop integrals C_0 and D_0 that emerge after the tensor reduction [83] are well established for this regularization prescription [63, 90].

We emphasize that, in the treatment of both the virtual and real corrections, terms depending on λ, m_u, and m_d are extracted analytically and their cancellation is established on the analytical level, so that the expressions used for the numerical analysis do not contain these IR regulators.

5.3.2 Virtual QCD corrections to W + γ production

The virtual QCD corrections of $\mathcal{O}(\alpha_s)$ to process (5.2.5) arise from the self-energy, triangle, and box diagrams shown in Fig. 5.6 and the counterterm contribution,

$$\mathcal{M}^{\mathrm{CT}}_{\mathrm{W}\gamma} = \mathcal{M}^{0}_{\mathrm{W}\gamma}\, \delta^{\mathrm{CT}}_{\mathrm{W}\gamma}. \tag{5.3.5}$$

The latter only receives contributions from the gluon-induced wave-function renormalization of the external quark lines,

$$\delta^{\mathrm{CT}}_{\mathrm{W}\gamma} = \frac{1}{2}\left(\delta Z^{G}_{u\bar{u}} + \delta Z^{G}_{d\bar{d}}\right), \tag{5.3.6}$$

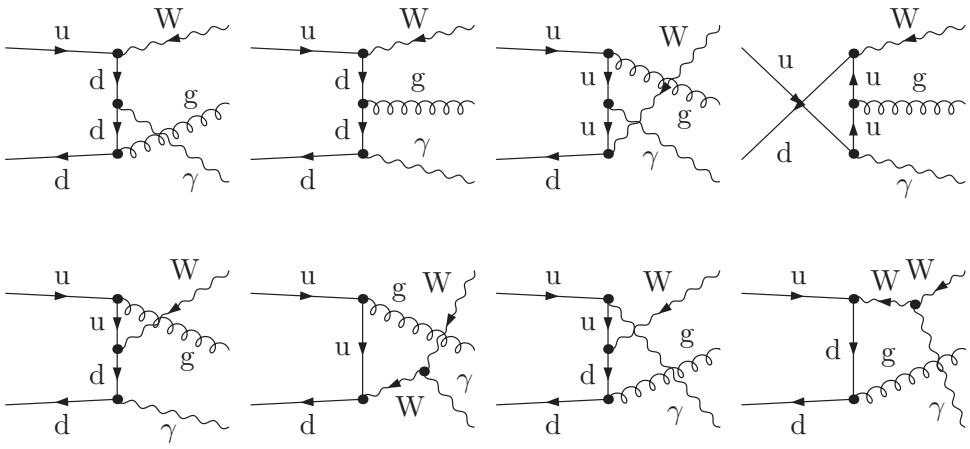

Figure 5.7: Tree-level diagrams of process (5.2.8). The tree-level diagrams of processes (5.2.9) and (5.2.10) emerge through crossing.

where

$$\delta Z_{q\bar{q}}^{G} = -\Sigma_{G,\mathrm{V}}^{q\bar{q}}(m_q^2) - 2m_q^2 \frac{\partial}{\partial q^2}\left[\Sigma_{G,\mathrm{V}}^{q\bar{q}}(q^2) + \Sigma_{G,\mathrm{S}}^{q\bar{q}}(q^2)\right]\Big|_{q^2=m_q^2}, \tag{5.3.7}$$

in analogy to Eq. (2.1.53). Because parity is conserved within QCD, the quark self-energy has just one vector part $\Sigma_{G,\mathrm{V}}^{q\bar{q}} = \Sigma_{G,\mathrm{L}}^{q\bar{q}} = \Sigma_{G,\mathrm{R}}^{q\bar{q}}$. Up to terms that vanish in the limit $m_q \to 0$, we have

$$\delta Z_{q\bar{q}}^{G} = -\frac{\alpha_\mathrm{s} C_\mathrm{F}}{4\pi}\left[\frac{1}{\epsilon} - \gamma_\mathrm{E} + \ln(4\pi) - \ln\frac{m_q^2}{\mu^2} - 2\ln\frac{m_q^2}{\lambda^2} + 4\right] + \mathcal{O}(\epsilon), \tag{5.3.8}$$

where $C_\mathrm{F} = (N_\mathrm{C}^2 - 1)/(2N_\mathrm{C}) = 4/3$ for $N_\mathrm{C} = 3$ quark colours, and λ now represents an infinitesimal gluon mass. Since the $\mathrm{W} + \gamma$ production cross section at LO does not contain a gluon, we can safely employ mass regularization for the soft gluon pole, because the gluon—except for a colour factor—couples to the external quarks like a photon, and potentially gauge-violating terms will vanish in the limit $\lambda \to 0$.

5.3.3 Real corrections due to $\mathrm{W} + j + \gamma$ production – phase-space slicing

The tree-level diagrams for process (5.2.8) are shown in Fig. 5.7. They contribute at the same time to the electromagnetic bremsstrahlung in process (5.2.2) and to the QCD bremsstrahlung in process (5.2.5), which complicates the treatment of the EW corrections to $\mathrm{W} + j$ associated production, as we have detailed in Section 3.7. The diagrams contributing to the electromagnetic bremsstrahlung in processes (5.2.3) and (5.2.4) emerge from Fig. 5.7 by crossing the gluon with the u and $\overline{\mathrm{d}}$ quarks, respectively.

When the cross sections of processes (5.2.8) – (5.2.10) are integrated over their three-particle phase spaces, one encounters IR singularities of both soft and collinear types. The former stem from the emission of soft photons and gluons and cancel against similar contributions from the virtual corrections owing to the Bloch–Nordsieck theorem [64], as

explained in Section 5.3.1. The latter arise when a massless gauge boson is collinearly emitted from an external massless fermion line or when a massless gauge boson splits into two collinear massless fermions. Specifically,

- in process (5.2.8), the photon or the gluon can be emitted collinearly from the incoming u_i and $\overline{\mathrm{d}}_j$ quarks;
- in process (5.2.9), the photon can be emitted collinearly from the incoming u_i quark or the outgoing d_j quark, and the gluon can split into a collinear $\mathrm{d}_j\overline{\mathrm{d}}_j$ quark pair;
- and in process (5.2.10), the photon can be emitted collinearly from the incoming $\overline{\mathrm{d}}_j$ quark or the outgoing $\overline{\mathrm{u}}_i$ quark, and the gluon can split into a collinear $\mathrm{u}_i\overline{\mathrm{u}}_i$ quark pair.

As already mentioned in Section 5.3.1, the collinear IR singularities from FS radiation are cancelled by the virtual corrections according to the KLN theorem [67] if the considered process is treated sufficiently inclusive. By contrast, those from IS radiation survive and have to be absorbed into the PDFs as shown in Sections 3.3 and 3.4.

Due to the minimum-p_{T} cut, the photon and the gluon cannot be soft simultaneously because one of them has to balance the transverse momentum of the W boson. By the same reasoning, there can only be one collinear situation at a time. However, soft and collinear singularities do overlap, and care needs to be exercised to avoid double counting.

For consistency, also the IR singularities in the real corrections need to be regularized by the infinitesimal photon or gluon mass λ and the light-quark masses m_u and m_d introduced in Sections 5.3.1 and 5.3.2. As already mentioned in Section 5.3.1, the cancellation of IR singularities is achieved analytically, so that the expressions underlying the numerical analysis are free of them.

Phase-space slicing

As in Refs. [91, 92], we employ the method of phase-space slicing [93] to separate the soft and collinear regions of the phase space from the one where the momenta are hard and non-collinear, so that the partonic cross section can be written as

$$\mathrm{d}\hat{\sigma}_{\mathrm{W}j\gamma} = \hat{\sigma}^{\mathrm{soft}}_{\mathrm{W}j\gamma} + \mathrm{d}\hat{\sigma}^{\mathrm{coll}}_{\mathrm{W}j\gamma} + \mathrm{d}\hat{\sigma}^{\mathrm{hard}}_{\mathrm{W}j\gamma}. \tag{5.3.9}$$

For definiteness, let us assume that parton d in process (5.2.12) is the soft or collinearly-emitted one and that partons a and c are the ones emitting IS radiation and FS radiation, respectively. In the notation introduced in Section 5.2.2, the soft regions of phase space are then defined by $\lambda < p_d^0 < \Delta E \ll (\hat{s}-w)/(2\sqrt{\hat{s}})$, the collinear ones for IS radiation and FS radiation by $\vartheta < \Delta\vartheta$ and $\psi < \Delta\psi$, respectively, and $p_d^0 > \Delta E$, and the hard and non-collinear one by the rest. The angular slicing cuts $\Delta\vartheta$ and $\Delta\psi$ fulfill the conditions $m_q^2/\hat{s} \ll \Delta\vartheta \ll 1$ and $m_q^2/\hat{s} \ll \Delta\psi \ll 1$, respectively. In the following, we explain how to evaluate $\mathrm{d}\hat{\sigma}^{\mathrm{soft}}_{\mathrm{W}j\gamma}$ and $\mathrm{d}\hat{\sigma}^{\mathrm{coll}}_{\mathrm{W}j\gamma}$ analytically using appropriate approximations. On the other hand, $\mathrm{d}\hat{\sigma}^{\mathrm{hard}}_{\mathrm{W}j\gamma}$ can straight-forwardly be evaluated numerically with high precision. For this purpose, the integration boundaries for p_d^0 and the angles ϑ and ψ in (5.2.26) and (5.2.28) have to be adjusted according to

$$\Delta E < p_d^0 < \frac{\hat{s}-w}{2\sqrt{\hat{s}}}, \qquad \Delta\vartheta < \vartheta < \pi - \Delta\vartheta\,, \tag{5.3.10}$$

and

$$\Delta\psi < \psi < \pi\,, \tag{5.3.11}$$

respectively. Moreover, we apply adequate exponential phase-space mappings for the variables p_d^0, ϑ, and ψ to improve the efficiency of the numerical evaluation. Since ΔE has to be compared to $\sqrt{\hat{s}}/2$, we define $\delta_s = 2\Delta E/\sqrt{\hat{s}}$. The demarcation parameters δ_s, $\Delta\vartheta$, and $\Delta\psi$ must be chosen judiciously. If they are too small, the numerical phase-space integration performed for $\mathrm{d}\hat{\sigma}^{\mathrm{hard}}_{\mathrm{W}j\gamma}$ becomes unstable; if they are too large, the approximations adopted for $\mathrm{d}\hat{\sigma}^{\mathrm{soft}}_{\mathrm{W}j\gamma}$ and $\mathrm{d}\hat{\sigma}^{\mathrm{coll}}_{\mathrm{W}j\gamma}$ become crude. In practice, one varies δ_s, $\Delta\vartheta$, and $\Delta\psi$ to find the respective stability regions. For the problem considered here, this is easily achieved.

Soft singularities

In the soft phase-space regions, $\mathcal{M}_{ab\to\mathrm{W}cd}$ factorizes into $\mathcal{M}_{ab\to\mathrm{W}c}$ times an eikonal factor that depends on $\mathbf{p}_d$. For soft-photon radiation, i.e. $d = \gamma$, the general formula for this eikonal factor is given by (3.2.1). The integration of (3.2.1) over the soft-photon phase space leads to the integrals

$$\mathcal{I}_{ij} \equiv \int_{|\mathbf{k}|\le\Delta E} \frac{\mathrm{d}^3\mathbf{k}}{2k^0}\,\frac{2(p_ip_j)}{(kp_i)(kp_j)}\,, \tag{5.3.12}$$

that can be integrated analytically [65], yielding

$$\begin{aligned}\mathcal{I}_{ij} = \frac{4\pi\eta\,(p_ip_j)}{(\eta\,p_i)^2-p_j^2}\Bigg\{&\frac{1}{2}\ln\frac{(\eta\,p_i)^2}{p_j^2}\,\ln\frac{4\Delta E^2}{\lambda^2}\\ &+\left[\frac{1}{4}\ln^2\frac{u_0-|\mathbf{u}|}{u_0+|\mathbf{u}|}+\mathrm{Li}_2\left(1-\frac{u_0+|\mathbf{u}|}{v}\right)+\mathrm{Li}_2\left(1-\frac{u_0-|\mathbf{u}|}{v}\right)\right]_{u=\eta\,p_j}^{u=\eta\,p_i}\Bigg\}\,,\end{aligned} \tag{5.3.13}$$

where $\mathrm{Li}_2(x) = -\int_0^1 \mathrm{d}t\,\ln(1-tx)/t$ is the dilogarithm, η is implicitly defined through

$$\eta^2p_i^2 - 2\eta\,(p_ip_j) + p_j^2 = 0\,,\quad \frac{\eta\,p_i^0-p_j^0}{p_j^0} > 0\,, \tag{5.3.14}$$

and

$$v = \frac{(\eta\,p_i)^2-p_j^2}{2(\eta\,p_i^0-k_j^0)}\,. \tag{5.3.15}$$

Squaring $\mathcal{M}_{ab\to\mathrm{W}cd}$, performing the spin and colour sums, and integrating over $\mathbf{p}_d$ with the constraint $\lambda < p_d^0 < \Delta E$, one finds

$$\mathrm{d}\hat{\sigma}^{\mathrm{soft}}_{ab\to\mathrm{W}cd}(\lambda,\Delta E) = \delta^{\mathrm{soft}}_{ab\to\mathrm{W}cd}(\lambda,\Delta E)\mathrm{d}\hat{\sigma}_{ab\to\mathrm{W}c}\,, \tag{5.3.16}$$

for the soft part of the bremsstrahlung integral.

In case of soft electromagnetic and QCD bremsstrahlung in process (5.2.8), we then obtain

$$\begin{aligned}\delta^{\mathrm{soft}}_{\mathrm{u\bar{d}}\to\mathrm{W^+g}\gamma}(\lambda,\Delta E) &= -\frac{\alpha}{2\pi}\left(Q_u^2\delta_{\mathrm{uu}}+Q_d^2\delta_{\mathrm{dd}}+\delta_{\mathrm{WW}}+2Q_uQ_d\delta_{\mathrm{ud}}+2Q_u\delta_{\mathrm{uW}}+2Q_d\delta_{\mathrm{dW}}\right),\\ \delta^{\mathrm{soft}}_{\mathrm{u\bar{d}}\to\mathrm{W^+}\gamma\mathrm{g}}(\lambda,\Delta E) &= -\frac{\alpha_{\mathrm{s}}C_{\mathrm{F}}}{2\pi}(\delta_{\mathrm{uu}}+\delta_{\mathrm{dd}}+2\delta_{\mathrm{ud}}),\end{aligned} \tag{5.3.17}$$

where $Q_u = 2/3$ and $Q_d = -1/3$ are the fractional electric charges of the u and d quarks, respectively. Applying (5.3.13), the particular IR-singular contributions read

$$\begin{aligned}
\delta_{\mathrm{uu}} &= \ln\frac{4(\Delta E)^2}{\lambda^2} + \ln\frac{m_u^2}{\hat{s}},\\
\delta_{\mathrm{dd}} &= \delta_{\mathrm{uu}}\big|_{m_u\leftrightarrow m_d}\,,\\
\delta_{\mathrm{ud}} &= \frac{1}{2}\ln\frac{4(\Delta E)^2}{\lambda^2}\ln\frac{m_u^2 m_d^2}{\hat{s}^2} + \frac{1}{4}\left(\ln^2\frac{m_u^2}{\hat{s}} + \ln^2\frac{m_d^2}{\hat{s}}\right) + \frac{\pi^2}{3},\\
\delta_{\mathrm{WW}} &= \ln\frac{4(\Delta E)^2}{\lambda^2} + \frac{\hat{s}+w}{\hat{s}-w}\ln\frac{w}{\hat{s}},\\
\delta_{\mathrm{uW}} &= \frac{1}{2}\ln\frac{4(\Delta E)^2}{\lambda^2}\ln\frac{w m_u^2}{(w-t)^2} + \frac{1}{4}\left(\ln^2\frac{m_u^2}{\hat{s}} + \ln^2\frac{w}{\hat{s}}\right)\\
&\quad + \mathrm{Li}_2\left(\frac{-t}{w-t}\right) + \mathrm{Li}_2\left(\frac{-u}{w-t}\right) + \frac{\pi^2}{6},\\
\delta_{\mathrm{dW}} &= -\,\delta_{\mathrm{uW}}\big|_{t\leftrightarrow u,\, m_u\leftrightarrow m_d}\,,
\end{aligned} \tag{5.3.18}$$

where the hierarchy $\lambda \ll m_q$ was respected,[1] and terms that vanish for $m_u = m_d = 0$ have been omitted.

Furthermore, we find the soft-photon correction factor for process (5.2.9) to be

$$\delta^{\mathrm{soft}}_{\mathrm{ug}\to\mathrm{W^+d}\gamma}(\lambda,\Delta E) = -\frac{\alpha}{2\pi}\left(Q_u^2\delta_{\mathrm{uu}} + Q_d^2\delta_{\mathrm{dd}} + \delta_{\mathrm{WW}} + 2Q_uQ_d\tilde{\delta}_{\mathrm{ud}} + 2Q_u\delta_{\mathrm{uW}} + 2Q_d\tilde{\delta}_{\mathrm{dW}}\right), \tag{5.3.19}$$

in which two terms of Eq. (5.3.18) are modified to be

$$\begin{aligned}
\tilde{\delta}_{\mathrm{ud}} &= \frac{1}{2}\ln\frac{4(\Delta E)^2}{\lambda^2}\ln\frac{m_u^2 m_d^2}{u^2} + \frac{1}{4}\left[\ln^2\frac{m_u^2}{\hat{s}} + \ln^2\frac{\hat{s}m_d^2}{(\hat{s}-w)^2}\right] + \mathrm{Li}_2\left(-\frac{t}{u}\right) + \frac{\pi^2}{3},\\
\tilde{\delta}_{\mathrm{dW}} &= -\frac{1}{2}\ln\frac{4(\Delta E)^2}{\lambda^2}\ln\frac{w m_u^2}{(\hat{s}-w)^2} - \frac{1}{4}\left[\ln^2\frac{w}{\hat{s}} + \ln^2\frac{\hat{s}m_d^2}{(\hat{s}-w)^2}\right] - \mathrm{Li}_2\left(1-\frac{w}{\hat{s}}\right) - \frac{\pi^2}{6}.
\end{aligned} \tag{5.3.20}$$

Finally, the soft-photon correction factor for process (5.2.10) emerges from the one of process (5.2.9) through the simple replacement

$$\delta^{\mathrm{soft}}_{\bar{\mathrm{d}}\mathrm{g}\to\mathrm{W^+}\bar{\mathrm{u}}\gamma}(\lambda,\Delta E) = \delta^{\mathrm{soft}}_{\mathrm{ug}\to\mathrm{W^+d}\gamma}(\lambda,\Delta E)\big|_{m_u\leftrightarrow m_d,\, Q_u\leftrightarrow Q_d}\,. \tag{5.3.21}$$

Collinear singularities

In our calculation collinear singularities arise from three sources:

(1) the emission of a photon or gluon from an incoming quark or antiquark;

(2) the splitting of an incoming gluon into a quark–antiquark pair; and

[1] This assumption is important, since the fermion masses are small physical parameters, while the photon/gluon mass λ is an infinitesimal regulator that has to be neglected with respect to all physical scales of the process.

(3) the emission of a photon from an outgoing quark or antiquark.

In accordance with Eqs. (3.2.4), the resulting contributions to $\mathrm{d}\hat{\sigma}^{\mathrm{coll}}_{\mathrm{W}j\gamma}$ all factorize into the respective LO cross sections without radiation and appropriate collinear radiator functions. For collinear photon radiation off fermions, the factorization formulae for the squared matrix elements are explicitly given by Eq. (3.2.7). While in case of FS radiation the collinear cone can be integrated out analytically, for IS radiation the calculation of $\mathrm{d}\hat{\sigma}^{\mathrm{coll}}_{\mathrm{W}j\gamma}$ involves a convolution with respect to the fraction x of four-momentum that the emitting parton passes on to the one that enters the hard interaction.

Let parton a in process (5.2.12) be the emitting quark q and parton d the emitted photon or gluon. Then we have [79, 94]

$$\mathrm{d}\hat{\sigma}^{\mathrm{coll}}_{qb\to\mathrm{W}c\{\gamma,\mathrm{g}\}}(m_q,\Delta\vartheta) = \frac{\left\{\alpha Q_q^2,\alpha_\mathrm{s}C_\mathrm{F}\right\}}{2\pi}\int_{x_0}^{1-\delta_s}\mathrm{d}x\,R_q^{\mathrm{IS}}(m_q,\Delta\vartheta,x)\mathrm{d}\hat{\sigma}^0_{qb\to\mathrm{W}c}(xp_q,p_b)\,, \tag{5.3.22}$$

where δ_s is introduced to exclude a slice of phase space that is both soft and collinear and is already included in $\hat{\sigma}^{\mathrm{soft}}_{\mathrm{W}j\gamma}$, $x_0=\tau_0 s/\hat{s}$, with τ_0 being defined in Eq. (5.2.15), and

$$R_q^{\mathrm{IS}}(m_q,\Delta\vartheta,x) = P_{qq}(x)\left[\ln\frac{\hat{s}(\Delta\vartheta)^2}{4m_q^2}-\frac{2x}{1+x^2}\right], \tag{5.3.23}$$

with

$$P_{qq}(x) = \frac{1+x^2}{1-x} \tag{5.3.24}$$

being the LO $q\to q^*\gamma$ splitting function [95]. This result is identical to the case when parton a is an antiquark $\overline{q}$. Note that the cm frame is boosted along the beam axis by the collinear emission of the photon or gluon.

Now, let parton a in process (5.2.12) be a gluon that splits into a $q\overline{q}$ pair, with q being outgoing and $\overline{q}$ entering the residual hard scattering. Then we have [68]

$$\mathrm{d}\hat{\sigma}^{\mathrm{coll}}_{\mathrm{g}b\to\mathrm{W}cq}(m_q,\Delta\vartheta) = \frac{\alpha_\mathrm{s}T_\mathrm{F}}{2\pi}\int_{x_0}^{1}\mathrm{d}x\,R_\mathrm{g}^{\mathrm{IS}}(m_q,\Delta\vartheta,x)\mathrm{d}\hat{\sigma}^0_{\overline{q}b\to\mathrm{W}c}(xp_{\bar{q}},p_b)\,, \tag{5.3.25}$$

where $T_\mathrm{F}=1/2$ and

$$R_\mathrm{g}^{\mathrm{IS}}(m_q,\Delta\vartheta,x) = P_{\mathrm{g}q}(x)\ln\frac{\hat{s}(1-x)^2(\Delta\vartheta)^2}{4m_q^2}+2x(1-x), \tag{5.3.26}$$

with

$$P_{\mathrm{g}q}(x) = x^2+(1-x)^2 \tag{5.3.27}$$

being the LO $\mathrm{g}\to q\overline{q}^*$ splitting function. This result is identical to the case when parton d is an antiquark $\overline{q}$.

Finally, let parton c in process (5.2.12) be the emitting quark q and parton d the emitted photon. Then we have [79, 94]

$$\mathrm{d}\hat{\sigma}^{\mathrm{coll}}_{ab\to\mathrm{W}q\gamma}(m_q,\Delta\psi) = \frac{\alpha Q_q^2}{2\pi}\int_0^{1-\tilde{\delta}_s}\mathrm{d}z\,R_q^{\mathrm{FS}}(m_q,\Delta\psi,z)\mathrm{d}\hat{\sigma}^0_{ab\to\mathrm{W}q}, \tag{5.3.28}$$

where $\tilde{\delta}_s = \hat{s}\delta_s/(\hat{s}-w)$ is again to avoid double counting of phase space regions that are both soft and collinear, and

$$R_q^{\mathrm{FS}}(m_q, \Delta\psi, z) = P_{qq}(z)\left[\ln\frac{(\hat{s}-w)^2(\Delta\psi)^2}{4\hat{s}m_q^2} + 2\ln z - \frac{2z}{1+z^2}\right], \tag{5.3.29}$$

with P_{qq} given in Eq. (5.3.24). The same result is obtained in the the case when parton c is an antiquark $\overline{q}$. The integral in Eq. (5.3.28) is not a convolution and can easily be carried out analytically if we recombine the FS quark and the collinearly-radiated photon, yielding

$$\int_0^{1-\tilde{\delta}_s} \mathrm{d}z\, R_q^{\mathrm{FS}}(m_q, \Delta\psi, z) = -\left(2\ln\tilde{\delta}_s + \frac{2}{3}\right)\ln\frac{(\hat{s}-w)^2(\Delta\psi)^2}{4\hat{s}m_q^2} + 2\ln\tilde{\delta}_s - \frac{2}{3}\pi + \frac{9}{2}. \tag{5.3.30}$$

In order to obtain $\mathrm{d}\hat{\sigma}^{\mathrm{coll}}_{\mathrm{W}j\gamma}$ for one of the processes (5.2.8) – (5.2.10), all possible collinear emissions must be taken into account one by one.

While the collinear IR singularities from FS radiation cancel upon combination with the virtual corrections by the KLN theorem [67] within collinear-safe observables, those from IS radiation survive. Since their form is universal (see Sections 3.3 and 3.4), they can be factorized and absorbed into the PDFs [61]. Adopting the $\overline{\mathrm{MS}}$ factorization scheme both for the collinear singularities of relative orders $\mathcal{O}(\alpha)$ and $\mathcal{O}(\alpha_{\mathrm{s}})$, this is achieved by modifying the PDF of quark q inside hadron A as

$$\begin{aligned} f_{q/A}(x) \to \tilde{f}_{q/A}(x,\mu_{\mathrm{F}}^2) = f_{q/A}^{\overline{\mathrm{MS}}}(x,\mu_{\mathrm{F}}^2)\left\{1 - \frac{\alpha Q_q^2 + \alpha_{\mathrm{s}}C_{\mathrm{F}}}{\pi}\left[\left(\ln\delta_s + \frac{3}{4}\right)\ln\frac{\mu_{\mathrm{F}}^2}{m_q^2}\right.\right. \\ \left.\left. - \ln^2\delta_s - \ln\delta_s + 1\right]\right\} - \int_x^{1-\delta_s}\frac{\mathrm{d}z}{z}\, f_{q/A}^{\overline{\mathrm{MS}}}\left(\frac{x}{z},\mu_{\mathrm{F}}^2\right)\frac{\alpha Q_q^2 + \alpha_{\mathrm{s}}C_{\mathrm{F}}}{2\pi}P_{qq}(z) \\ \times\left[\ln\frac{\mu_{\mathrm{F}}^2}{(1-z)^2m_a^2} - 1\right] - \int_x^1\frac{\mathrm{d}z}{z}\, f_{\mathrm{g}/A}^{\overline{\mathrm{MS}}}\left(\frac{x}{z},\mu_{\mathrm{F}}^2\right)\frac{\alpha_{\mathrm{s}}T_{\mathrm{F}}}{2\pi}P_{\mathrm{g}q}(z)\ln\frac{\mu_{\mathrm{F}}^2}{m_q^2}, \end{aligned} \tag{5.3.31}$$

where μ_{F} is the factorization scale, which separates the perturbative and non-perturbative parts of the hadronic cross section. In contrast to the procedure described in Chapters 3.3 and 3.4, where we have applied a $[\ldots]_+$ prescription to extract the soft-photon pole from the z-integration, in (5.3.31) we have used the soft-photon cut-off δ_s for this purpose. Note that the prescription (5.3.31) does not include a redefinition for the photon PDF, because we treat photon-induced processes only at LO.

5.4 Numerical results

We are now in a position to present our numerical results. Our choice of input is specified as follows: We adopt the values

$$\begin{aligned} G_{\mathrm{F}} &= 1.6637\times10^{-5}\,\mathrm{GeV}^{-2}\,, & M_{\mathrm{W}} &= 80.403\,\mathrm{GeV}\,, \\ M_{\mathrm{Z}} &= 91.1876\,\mathrm{GeV}\,, & m_{\mathrm{t}} &= 174.2\,\mathrm{GeV}\,, \end{aligned}$$

that have been quoted by the Particle Data Group [96], take the other $n_f = 5$ quarks to be massless partons, and assume $M_{\mathrm{H}} = 120$ GeV, which is presently compatible with the

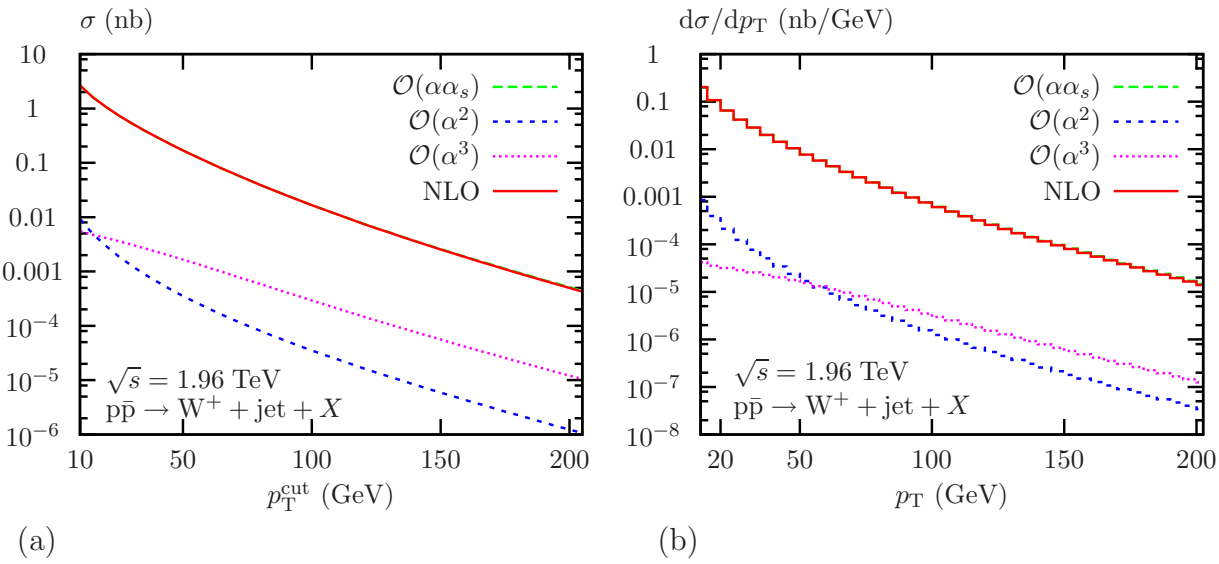

Figure 5.8: (a) Total cross section as a function of $p_{\mathrm{T}}^{\mathrm{cut}}$ and (b) p_{T} distribution of $\mathrm{p\bar{p}} \to \mathrm{W}^+ + X$ for $\sqrt{s} = 1.96$ TeV (Tevatron). The NLO results are compared with those of orders $\mathcal{O}(\alpha\alpha_{\mathrm{s}})$, $\mathcal{O}(\alpha^2)$, and $\mathcal{O}(\alpha^3)$ via photoproduction. In both plots (a) and (b), the curve for the $\mathcal{O}(\alpha\alpha_{\mathrm{s}})$ contribution is covered by the NLO result.

direct search limits and the bounds from the EW precision tests [96]. We take the absolute values of the CKM matrix elements to be [96]

$$\begin{aligned} &|V_{\mathrm{ud}}| = 0.9377, \; |V_{\mathrm{us}}| = 0.2257, \qquad |V_{\mathrm{cd}}| = 0.230, \\ &|V_{\mathrm{cs}}| = 0.957, \quad |V_{\mathrm{cb}}| = 41.6 \times 10^{-3}, \; |V_{\mathrm{ub}}| = 4.31 \times 10^{-3}. \end{aligned} \tag{5.4.1}$$

Since we are working at LO in QCD, we employ the one-loop formula for $\alpha_{\mathrm{s}}^{(n_f),\mathrm{LO}}(\mu_{\mathrm{R}})$,

$$\alpha_{\mathrm{s}}^{(n_f),\mathrm{LO}}(\mu_{\mathrm{R}}^2) = \frac{4\pi}{\beta_0^{(n_f)} \ln \frac{\mu_{\mathrm{R}}^2}{\left(\Lambda_{\mathrm{QCD}}^{(n_f)}\right)^2}}, \tag{5.4.2}$$

with $\beta_0^{(n_f)} = 11/3\, C_{\mathrm{F}} - 2/3\, T_{\mathrm{F}}\, n_f$. We use the LO proton PDF set `CTEQ6L1` by the Coordinated Theoretical-Experimental Project on QCD (CTEQ) [97], with $\Lambda_{\mathrm{QCD}}^{(5)} = 165$ MeV. In the case of photoproduction, we add the photon spectra for elastic [76] and inelastic [77, 78] scattering elaborated in the Weizsäcker–Williams approximation. In the latter case, we use the more recent set by Martin, Roberts, Stirling, and Thorne (`MRSTQED2004`) [78] as our default, and the set by Glück, Stratmann, and Vogelsang (`GSV`) [77] to assess the theoretical uncertainty from this source. We choose the renormalization and factorization scales to be $\mu_{\mathrm{R}} = \mu_{\mathrm{F}} = \xi m_{\mathrm{T}}^{\mathrm{cut}}$, where

$$m_{\mathrm{T}}^{\mathrm{cut}} = \sqrt{(p_{\mathrm{T}}^{\mathrm{cut}})^2 + M_{\mathrm{W}}^2} \tag{5.4.3}$$

is the minimum transverse mass of the produced W boson and ξ is introduced to estimate the residual scale uncertainty. Unless stated otherwise, we use the default value $\xi = 1$.

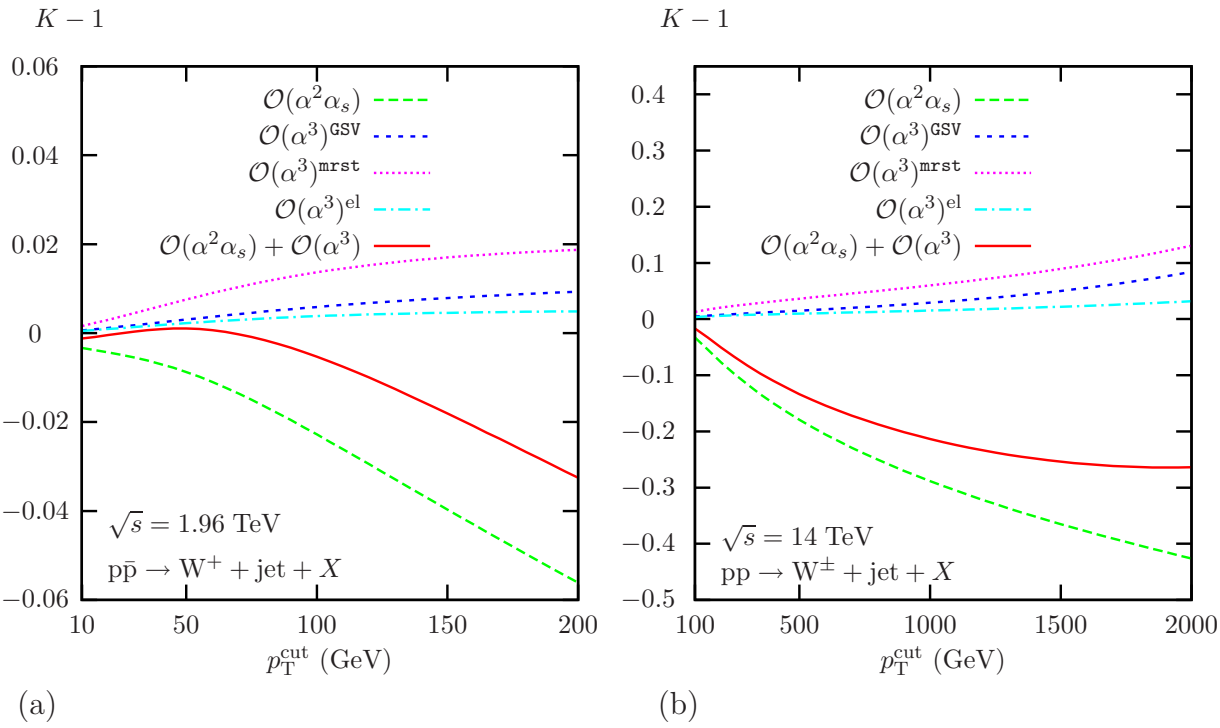

Figure 5.9: NLO corrections $(K-1)$, with and without the photoproduction contributions, to the total cross sections of (a) $\mathrm{p\overline{p}} \to \mathrm{W}^+ + X$ for $\sqrt{s} = 1.96$ TeV (Tevatron run II) and of (b) $\mathrm{pp} \to \mathrm{W}^\pm + X$ for $\sqrt{s} = 14$ TeV (LHC) as functions $p_\mathrm{T}^\mathrm{cut}$. For comparison, also the contributions due to elastic and inelastic photoproduction normalized to the LO results are shown. In the latter case, the evaluation is also performed with the GSV PDFs. The symbol $\mathrm{W}^\pm$ in the LHC plot (b) indicates that we present our results for the sum of W^+ and W^- production.

We consider the total cross sections of $\mathrm{p\bar{p}} \to \mathrm{W}^\pm + X$ at the Tevatron (run II) with $\sqrt{s} = 1.96$ TeV and $\mathrm{pp} \to \mathrm{W}^\pm + X$ at the LHC with $\sqrt{s} = 14$ TeV as functions of $p_\mathrm{T}^\mathrm{cut}$. By numerically differentiating the latter with respect to $p_\mathrm{T}^\mathrm{cut}$, we also obtain the corresponding p_T distributions as $\mathrm{d}\sigma/\mathrm{d}p_\mathrm{T} = -\,\mathrm{d}\sigma(p_\mathrm{T}^\mathrm{cut})/\mathrm{d}p_\mathrm{T}^\mathrm{cut}|_{p_\mathrm{T}^\mathrm{cut}=p_\mathrm{T}}$. Owing to the baryon symmetry of the initial state, the results for W^+ and W^- bosons are identical at the Tevatron, and it is sufficient to study one of them. By contrast, W^+-boson production is favoured at the LHC because the proton most frequently interacts via a u quark. Therefore, it is necessary to study the production of W^+ and W^- bosons separately at the LHC. We compare the contributions of four different orders:

(1) the LO contribution of $\mathcal{O}(\alpha\alpha_\mathrm{s})$ from processes (5.2.2) – (5.2.4), where the system X accompanying the W boson contains a hadron jet;

(2) the LO contribution of $\mathcal{O}(\alpha^2)$ from process (5.2.5), where X contains a prompt photon;

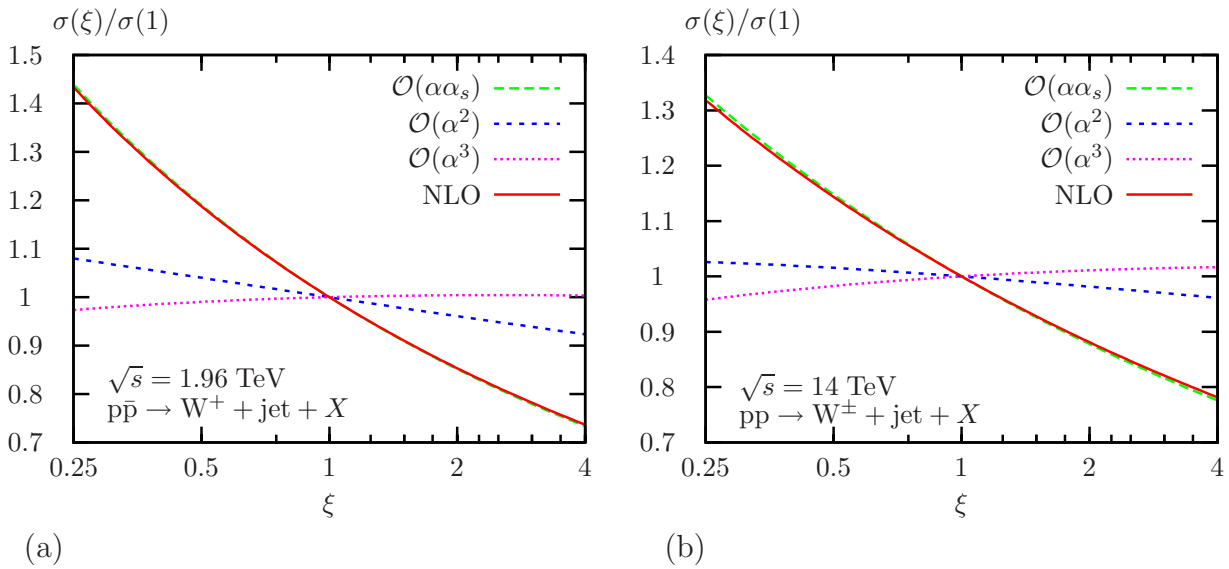

Figure 5.10: Total cross sections of (a) $p\bar{p} \to W^+ + X$ for $\sqrt{s} = 1.96$ TeV and $p_T^{cut} = 20$ GeV (Tevatron run II) and of (b) $pp \to W^\pm + X$ for $\sqrt{s} = 14$ TeV and $p_T^{cut} = 200$ GeV (LHC) as functions of ξ normalized to their default values for $\xi = 1$. The NLO results are compared with those of orders $\mathcal{O}(\alpha\alpha_s)$, $\mathcal{O}(\alpha^2)$, and $\mathcal{O}(\alpha^3)$ via photoproduction. The symbol $W^\pm$ in the LHC plot (b) indicates that we show our results for the sum of W^+ and W^- production.

(3) the NLO contribution of $\mathcal{O}(\alpha^2\alpha_s)$ comprising processes (5.2.2) – (5.2.5) at one loop as well as processes (5.2.8) – (5.2.10) at tree level, where X contains a hadron jet, a prompt photon, or both; and

(4) the LO contributions of $\mathcal{O}(\alpha^3)$ from processes (5.2.6) and (5.2.7) via direct photoproduction, where X contains a hadron jet and, in the case of elastic photoproduction, also the scattered proton or antiproton.

Since we consider inclusive one-particle production, we do not use any information on the composition of X, i.e. we include all possibilities. In the following, we regard the sum of contributions (1) and (2) as LO and sum of contributions (1) – (4) as NLO unless the perturbative orders are explicitly specified in terms of coupling constants. We thus define the correction factor K to be the NLO to LO ratio with this understanding.

Let us now discuss the numerical results and their phenomenological implications in detail. Specifically, Figs. 5.8, 5.9(a), and 5.10(a) refer to the Tevatron, while Figs 5.9(b), 5.10(b), 5.11, 5.12, and 5.13 refer to the LHC. In Fig. 5.8(a) the NLO result for the total cross section as a function of p_T^{cut} is compared with the LO contributions of $\mathcal{O}(\alpha\alpha_s)$ and $\mathcal{O}(\alpha^2)$ as well as with the photoproduction contribution of $\mathcal{O}(\alpha^3)$. The $\mathcal{O}(\alpha\alpha_s)$ and $\mathcal{O}(\alpha^2)$ results exhibit very similar shapes, but the normalization of the latter is suppressed by a factor of about 500. This is qualitatively understood from the partonic cross section formulae in Eq. (5.2.21) and by noticing that the $\mathcal{O}(\alpha\alpha_s)$ contributions from the Compton-like processes (5.2.3) and (5.2.4), which have no counterparts in $\mathcal{O}(\alpha^2)$, are significantly enhanced by the gluon PDF. As a consequence, the LO result is almost entirely exhausted by the $\mathcal{O}(\alpha\alpha_s)$ contribution.

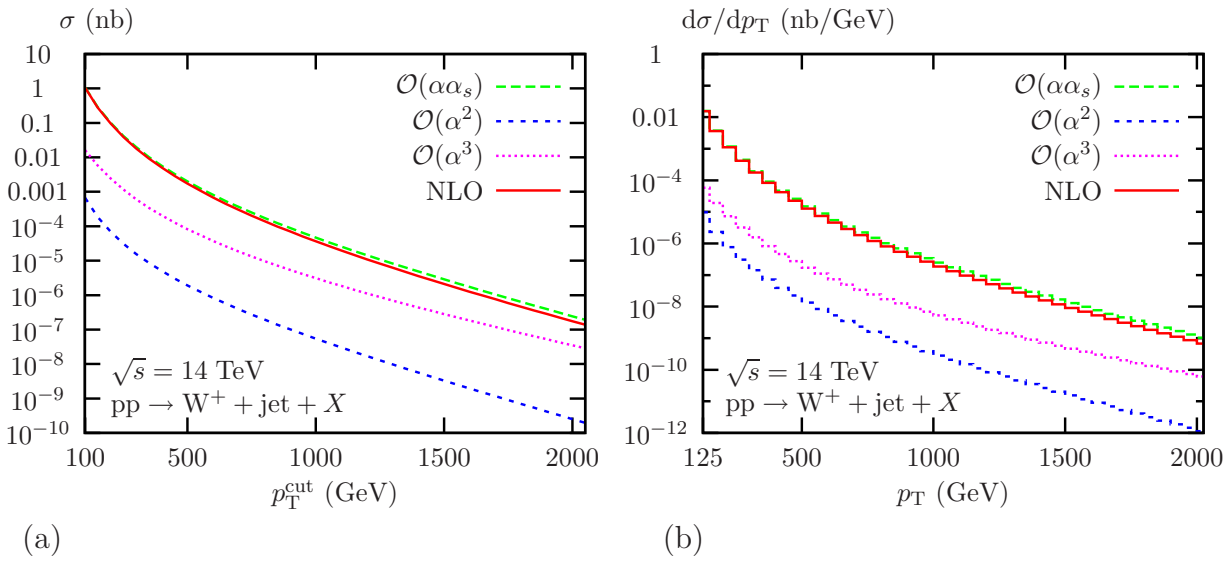

Figure 5.11: (a) Total cross section as a function of $p_{\mathrm{T}}^{\mathrm{cut}}$ and (b) p_{T} distribution of $\mathrm{pp} \to \mathrm{W}^+ + X$ for $\sqrt{s} = 14$ TeV (LHC). The NLO results are compared with those of orders $\mathcal{O}(\alpha\alpha_{\mathrm{s}})$, $\mathcal{O}(\alpha^2)$, and $\mathcal{O}(\alpha^3)$ via photoproduction.

The inclusion of the NLO correction leads to a moderate reduction in cross section, which increases in magnitude with $p_{\mathrm{T}}^{\mathrm{cut}}$, reaching about -4% for $p_{\mathrm{T}}^{\mathrm{cut}} = 200$ GeV, as can be seen from Fig. 5.9(a), where the K factor is depicted.

In Fig. 5.8(a), also the photoproduction contribution is shown. As explained above, we have to distinguish between elastic and inelastic scattering off the proton that both formally contribute at $\mathcal{O}(\alpha^3)$. For the combined photoproduction contribution, we observe from Fig. 5.8(a), that, except for small values of $p_{\mathrm{T}}^{\mathrm{cut}}$, it overshoots the $\mathcal{O}(\alpha^2)$ contribution, although it is formally suppressed by one power of α. Detailed inspection reveals that this unexpected enhancement can be traced to the photoproduction diagram involving the triple-gauge-boson coupling and the space-like W-boson exchange, which significantly contributes at large values of $\sqrt{\hat{s}}$. In fact, for a fixed value of $p_{\mathrm{T}}^{\mathrm{cut}}$, the total cross sections of processes (5.2.6) and (5.2.7) have an asymptotic large-$\hat{s}$ behaviour proportional to $1/(m_{\mathrm{T}}^{\mathrm{cut}})^2$, while those of processes (5.2.2) – (5.2.5) behave as $\ln \hat{s}/\hat{s}$. Consequently, photoproduction appreciably contributes to the K factor, as is apparent from Fig. 5.9(a), which also shows the photoproduction to LO ratios for elastic and inelastic scattering. The freedom in the choice of the inelastic photon content of the proton is likely to be the largest source of theoretical uncertainty in the photoproduction cross section. In order to get an idea of this uncertainty, we display in Fig. 5.9(a) also the inelastic-photoproduction to LO ratio evaluated with the `GSV` photon spectrum for inelastic scattering. The result is roughly a factor of two smaller than our default prediction based on the `MRSTQED2004` spectrum.

In Fig. 5.10(a), we examine the theoretical uncertainties in the $\mathcal{O}(\alpha\alpha_{\mathrm{s}})$, $\mathcal{O}(\alpha^2)$, NLO, and photoproduction results due to the freedom in setting the renormalization and factorization scales by exhibiting their ξ dependences relative to their default values at $\xi = 1$. The ξ dependencies of the $\mathcal{O}(\alpha^2)$ and photoproduction results stem solely from the factorization scale μ_{F} and are rather feeble, while the ξ dependence of the $\mathcal{O}(\alpha\alpha_{\mathrm{s}})$ result is

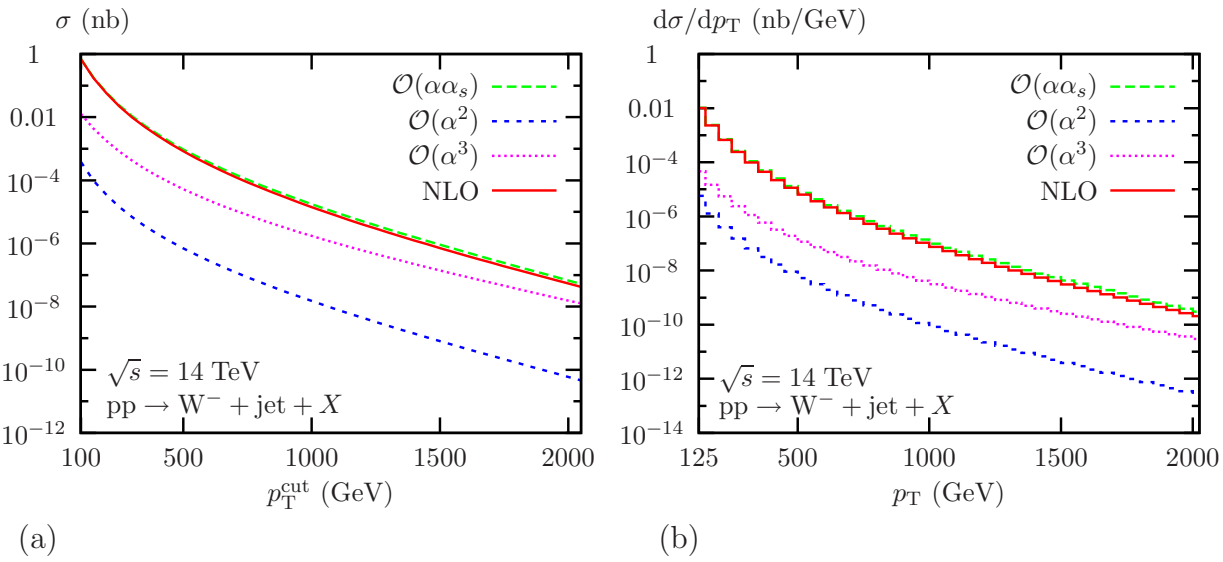

Figure 5.12: (a) Total cross section as a function of $p_{\mathrm{T}}^{\mathrm{cut}}$ and (b) p_{T} distribution of $\mathrm{pp} \to \mathrm{W}^- + X$ for $\sqrt{s} = 14$ TeV (LHC). The NLO results are compared with those of orders $\mathcal{O}(\alpha\alpha_{\mathrm{s}})$, $\mathcal{O}(\alpha^2)$, and $\mathcal{O}(\alpha^3)$ via photoproduction.

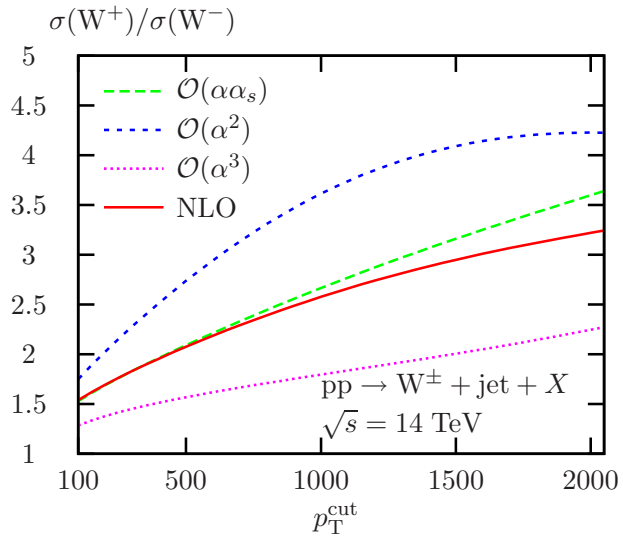

Figure 5.13: Ratios of the respective results for W^+ and W^- bosons shown in Figs. 5.11(a) and 5.12(a).

also linked to the renormalization scale μ_{R} of $\alpha_{\mathrm{s}}(\mu_{\mathrm{R}})$ and is therefore more pronounced, but still not dramatic. The scale variation of the LO result amounts to less than $\pm 15\%$ for $1/2 < \xi < 2$. It is only slightly reduced by the inclusion of the NLO correction. This is expected because the NLO result is still linear in $\alpha_{\mathrm{s}}(\mu_{\mathrm{R}})$, so that the μ_{R} dependence of $\alpha_{\mathrm{s}}(\mu_{\mathrm{R}})$ is not compensated yet. For this reason, we have also included the NLO QCD contributions in the calculation of the radiative corrections to off-shell W-boson production that will be discussed in the following chapters.

In Fig. 5.8(b), the analysis of Fig. 5.8(a) is repeated for the p_T distribution. We observe that the line shapes and relative normalizations of the various distributions are very similar to those in Figs. 5.8(a) and the same comments apply.

Turning to the LHC, we can essentially repeat the above discussion for the Tevatron, except that we have to take into account the difference between W^+ and W^- boson production. Thus, Fig. 5.8 has two LHC counterparts, Figs. 5.11 and 5.12, for the W^+ and W^- bosons, respectively. To illustrate this difference more explicitly, we show in Fig. 5.13 the W^+ to W^- ratios of the respective results from Figs. 5.11 and 5.12. For simplicity, Figs. 5.9(b) and 5.10(b), the LHC counterparts of Figs. 5.9(a) and 5.10(a), refer to the sum of the results for W^+ and W^- bosons. In the following, we only focus on those features which are specific for the LHC. From Figs. 5.11 and 5.12, we observe that the gaps between the $\mathcal{O}(\alpha\alpha_s)$ and $\mathcal{O}(\alpha^2)$ results are increased by about a factor of two, to reach three orders of magnitude. This is mainly because the Compton-like processes (5.2.3) and (5.2.4) benefit from the extended dominance of the gluon PDF at small values of x. Furthermore, the photoproduction contributions now significantly exceed the $\mathcal{O}(\alpha^2)$ ones throughout the entire p_T^{cut} and p_T ranges. From Fig. 5.13, we see that the W^+ to W^- ratios take values in excess of unity, as expected, and strongly increase with increasing values of p_T^{cut}. Comparing Figs. 5.9(a) and (b), we find that the EW K factors are significantly amplified as one passes from the Tevatron to the LHC. This is due to the fact that the typical Sudakov logarithms $\propto \frac{\alpha}{\pi s_W^2} \ln^2(\hat{s}/w)$ [98], which originate from triangle and box diagrams, become quite sizeable at the large values of $\sqrt{\hat{s}}$ and p_T that can be reached at the LHC, as has been dicussed in detail in Refs. [38, 39]. Finally, comparing Fig. 5.10(a) and (b), we conclude that the ξ dependence is generally somewhat larger at the LHC.

Chapter 6

Off-shell W-boson production at NLO accuracy: an overview

6.1 General setup and contributions at Born level

6.1.1 LO contributions via QCD partons

Analogously to the on-shell case discussed in the previous chapter, the hadroproduction of an intermediate W boson in association with one hard jet is governed at LO by quark–antiquark annihilation, where the IS quarks radiate a gluon, and the corresponding crossed channels with a gluon in the initial state. Specifically, for W^+ production the relevant partonic processes are

$$\mathrm{u}_i\ \bar{\mathrm{d}}_j \to \mathrm{W}^+\mathrm{g} \to l^+\nu_l\,\mathrm{g}\,, \tag{6.1.1}$$

$$\mathrm{u}_i\ \mathrm{g} \to \mathrm{W}^+\mathrm{d}_j \to l^+\nu_l\,\mathrm{d}_j\,, \tag{6.1.2}$$

$$\bar{\mathrm{d}}_j\ \mathrm{g} \to \mathrm{W}^+\bar{\mathrm{u}}_i \to l^+\nu_l\,\bar{\mathrm{u}}_i\,, \tag{6.1.3}$$

where u_i and d_j denote an up-type quark of generation i and a down-type quark of generation j, respectively. In contrast to the approach of Chapter 5, we now perform the calculation for the physical final state, i.e. a charged lepton l, the corresponding neutrino ν_l, and a parton which will be seen in the detector as a jet. The corresponding tree-level Feynman diagrams for process (6.1.2) are shown in Fig. 6.1. The intermediate W-boson resonance is described by a complex W-boson mass μ_W via the replacement

$$M_\mathrm{W}^2 \to \mu_\mathrm{W}^2 = M_\mathrm{W}^2 - \mathrm{i}M_\mathrm{W}\Gamma_\mathrm{W} \tag{6.1.4}$$

in the W propagator as dictated by the complex-mass scheme that has been discussed in Section 2.2.4. Hence, all our results correspond to a fixed-width description of the Breit–Wigner resonance.

The dependence on quark mixing, as parametrized in the CKM matrix (2.1.26), factorizes from the tree-level matrix elements. Apart from a global CKM-dependent factor, the tree-level amplitudes do not depend on the specific generations. Hence, for hadronic observables, the summation over the quark generations $i = 1, 2$ and $j = 1, 2, 3$ requires only the evaluation of a single generic amplitude per process type shown in (6.1.1) – (6.1.3) when folding the squared tree-level amplitudes with the corresponding PDFs. The explicit

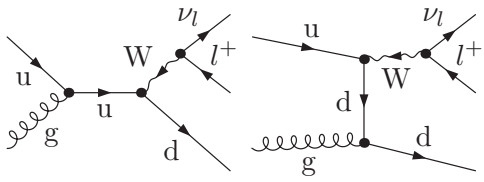

Figure 6.1: Feynman diagrams for the LO process (6.1.2).

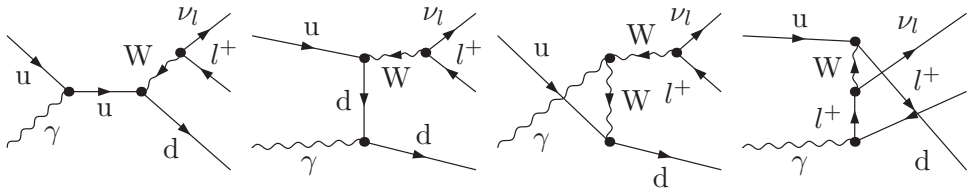

Figure 6.2: Feynman diagrams for the photon-induced process (6.1.5).

calculation of these amplitudes is carried out in Section 7.2.1. Only squares of the absolute value of CKM elements enter the final results. We do not include top quarks in the final state since their decays lead to significantly different signatures. According to Section 3.1.1, the five other quark flavours (including the bottom quark) as well as the FS leptons are treated as massless throughout the calculation, except if small masses are needed to regularize a collinear divergence. Since we neglect the small CKM mixing of the third generation with the first two generations, the PDFs of the bottom quark are irrelevant at tree level but enter the result for the QCD bremsstrahlung cross sections (see Section 6.3).

6.1.2 LO photon-induced contributions

In our approach, we describe W + jet production up to an accuracy of $\mathcal{O}(\alpha^3\alpha_s)$. Hence, we also include the $\mathcal{O}(\alpha^3)$ tree-level processes with a photon in the initial state,

$$\mathrm{u}_i\,\gamma \to \mathrm{W}^+\mathrm{d}_j \to l^+\nu_l\,\mathrm{d}_j\,, \tag{6.1.5}$$

$$\bar{\mathrm{d}}_j\,\gamma \to \mathrm{W}^+\bar{\mathrm{u}}_i \to l^+\nu_l\,\bar{\mathrm{u}}_i\,. \tag{6.1.6}$$

The tree-level Feynman diagrams for process (6.1.5) are shown in Fig. 6.2. The photon content of the proton has been quantified in the `MRSTQED2004` PDFs [78], that was also our default choice in the on-shell calculation. Since the photon also couples to the charged lepton and the intermediate W boson, the amplitude is more involved than its QCD counterpart (see Section 7.2.2). We neglect the effects due to elastic photoproduction in the full off-shell calculation, because they turned out to be small in the on-shell case. Moreover, contrary to the on-shell calculation, we do not consider the crossed processes corresponding to $\mathrm{W} + \gamma$ production at this point, following the approach of Section 3.7.

6.1.3 General setup

As in the on-shell calculation, we use the G_F scheme to define the electromagnetic coupling constant α, i.e. we derive α from the Fermi constant according to (5.2.22).

We employ the Feynman-diagrammatic approach to calculate all relevant amplitudes in the 't Hooft–Feynman gauge defined in Section 2.1.1. For a numerical evaluation at the amplitude level we use the Weyl–van-der-Waerden spinor formalism that is briefly outlined in Section 7.1. To ensure the correctness of the presented results, our team has performed two independent calculations which are in mutual agreement.

Our calculation starts from diagrammatic expressions for the one-loop corrections generated by FeynArts 1.0 [80], and the subsequent evaluation of the amplitudes is carried out with programs that have been derived from code that was usually developed for the computation of the EW one-loop corrections to the process $\mathrm{e^+e^-} \to 3\,\mathrm{jets}$ [99]. The algebraic evaluation of the loop amplitudes is performed with a program written in *Mathematica*, and the results are automatically transferred to *Fortran*. The Born and bremsstrahlung amplitudes are calculated and optimized by hand and directly included into a *Fortran* program for numerical evaluation. A specific parametrization of phase space is used for an adaptive Monte Carlo integration employing the Vegas [87] algorithm. The analytical expressions for all bremsstrahlung amplitudes, as well as the explicit phase-space parametrizations are presented in Chapter 8.

The second calculation carried out by Ansgar Denner and Alexander Mück is based on FeynArts 3.2 [81] and FormCalc version 3.1 [82]. The translation of the amplitudes into the Weyl–van-der-Waerden formalism as presented in Ref. [100] is performed with the program Pole [101]. Pole also provides an interface to the multi-channel phase-space integrator Lusifer [102] which has been extended to use Vegas [87] in order to optimize each phase-space mapping.

6.2 Virtual EW and QCD corrections

We calculate the virtual one-loop QCD and EW corrections for the partonic processes (6.1.1) – (6.1.3) to order $\mathcal{O}(\alpha^2\alpha_\mathrm{s}^2)$ and $\mathcal{O}(\alpha^3\alpha_\mathrm{s})$, respectively, and discuss the calculation in some detail in Chapter 9. Since the partonic processes (6.1.5) and (6.1.6) are already suppressed by α/α_s at LO, we only need to include the NLO QCD corrections for these channels to reach the required accuracy. The QCD corrections are induced by self-energy, vertex, and box (4-point) diagrams only. The NLO EW corrections are more involved and include pentagon (5-point) diagrams. There are $\mathcal{O}(100)$ diagrams per partonic channel, including 6 pentagons and 20 boxes. The generic structure of the contributing diagrams is indicated in Fig. 6.3, and the pentagon diagrams are explicitly given in Fig. 6.4. The different channels are related by crossing symmetry.

In the calculation of the one-loop contributions UV divergences are regularized dimensionally. For the IR, i.e. soft or collinear, divergences we use pure dimensional regularization with massless gluons and (anti)fermions (except for the top quark) to calculate the QCD corrections, or—in case of the EW NLO corrections—pure mass regularization with infinitesimal photon mass and small fermion masses, which are only kept in the mass-singular logarithms. When using dimensional regularization, the rational terms of IR origin are treated as described in Appendix A of Ref. [103].

Self-energy insertions:

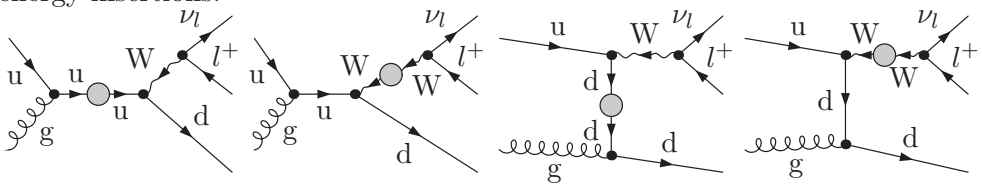

Triangle insertions:

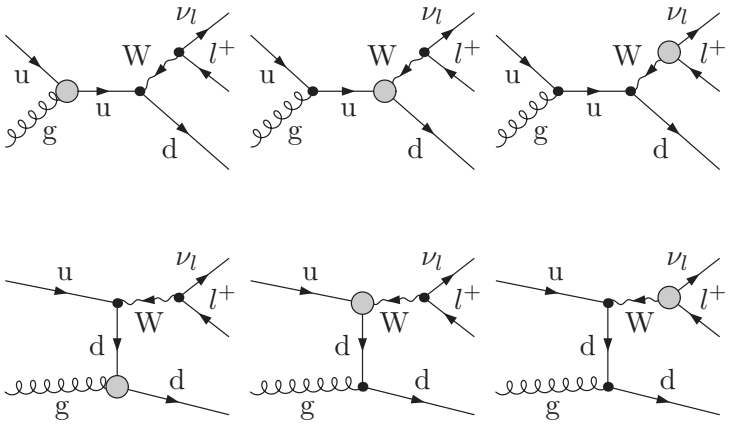

Box and pentagon insertions:

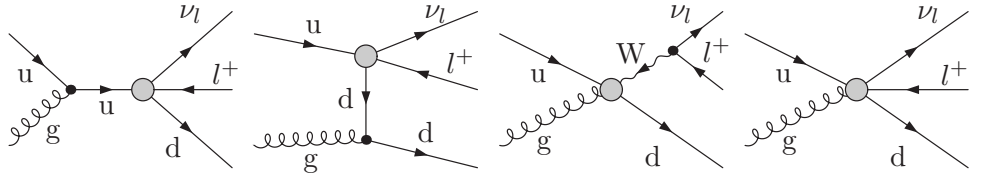

Figure 6.3: Contributions of different one-particle irreducible vertex functions (indicated as blobs) to the LO process (6.1.2); there are contributions from self-energies, triangles, boxes, and pentagon graphs.

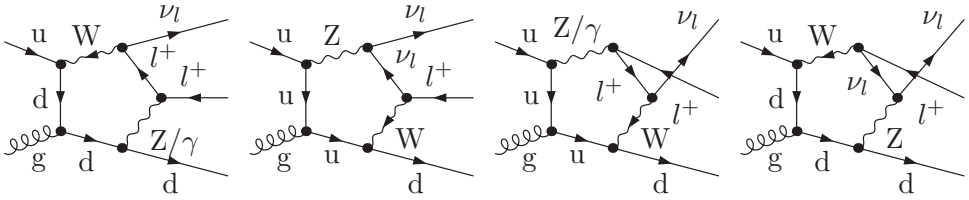

Figure 6.4: Virtual pentagon contributions to the process (6.1.2).

We use the on-shell renormalization prescription for the EW part of the SM as detailed in Section 2.2.4 for the complex-mass scheme. Employing the G_F scheme for the definition of the fine-structure constant (see Sections 5.2.1 and 5.3.1), we include Δr in the counterterm contribution via the replacement

$$\delta\mathcal{Z}_e|_{\alpha(0)} \to \delta\mathcal{Z}_e|_{G_\mathrm{F}} = \delta\mathcal{Z}_e|_{\alpha(0)} - \frac{1}{2}\Delta r \tag{6.2.1}$$

for the charge renormalization constant, as suggested in Ref. [104]. The strong coupling constant is renormalized in the $\overline{\mathrm{MS}}$ scheme with $n_f = 5$ active flavours. Hence, bottom quarks are included everywhere in the calculation as a massless quark flavour.

6.3 Real corrections and interference effects

The evaluation of the real corrections has to be done with care, both for theoretical consistency as well as to match the experimental observables as closely as possible.

6.3.1 Real EW corrections

Let us first focus on the EW real corrections to the partonic processes (6.1.1) – (6.1.3). The emission of an additional photon leads to the processes

$$\mathrm{u}_i\ \bar{\mathrm{d}}_j \to l^+\nu_l\,\mathrm{g}\,\gamma\,, \tag{6.3.1}$$
$$\mathrm{u}_i\ \mathrm{g} \to l^+\nu_l\,\mathrm{d}_j\,\gamma\,, \tag{6.3.2}$$
$$\bar{\mathrm{d}}_j\ \mathrm{g} \to l^+\nu_l\,\bar{\mathrm{u}}_i\,\gamma\,. \tag{6.3.3}$$

The Feynman diagrams contributing to the process (6.3.2) are shown in Fig. 6.5. If the photon and the charged leptons/quarks are recombined into a pseudo-particle (mimicking the start of hadronic or electromagnetic showers) to form IR-safe observables, all the soft singularities and collinear singularities related to FS radiation cancel against the corresponding singularities in the virtual corrections. The collinear singularities arising from IS collinear splittings are absorbed into the PDFs according to (3.4.1). Note that the `MRSTQED2004` PDFs are defined in the DIS scheme with respect to QED corrections, as explained in Ref. [68]. It is implied that all selection cuts for a given observable have to be blind to the distribution of momenta in collinear lepton–photon configurations. We use the dipole subtraction formalism as specified for photon emission in Ref. [35] to isolate the divergences and observe the numerical cancellation. In Appendix C we explicitly list the relevant subtraction functions and the readded counterparts that carry the IR singularities for the processes (6.3.1) – (6.3.3).

For muons in the final state it is, however, experimentally possible to separate collinear photons from the lepton, i.e. to observe so-called "bare" muons (see Section 3.6). Hence, the resulting cross sections are not collinear safe (i.e. the KLN theorem [67] does not apply), and the corresponding collinear singularities show up as logarithms of the small lepton (muon) mass. The lepton mass cuts off the collinear divergence in a physically meaningful way. In this work, we employ the extension of the subtraction formalism that has been illustrated in Section 4.2 which allows one to calculate cross sections for bare leptons, i.e. cross sections defined without any photon recombination. There, the

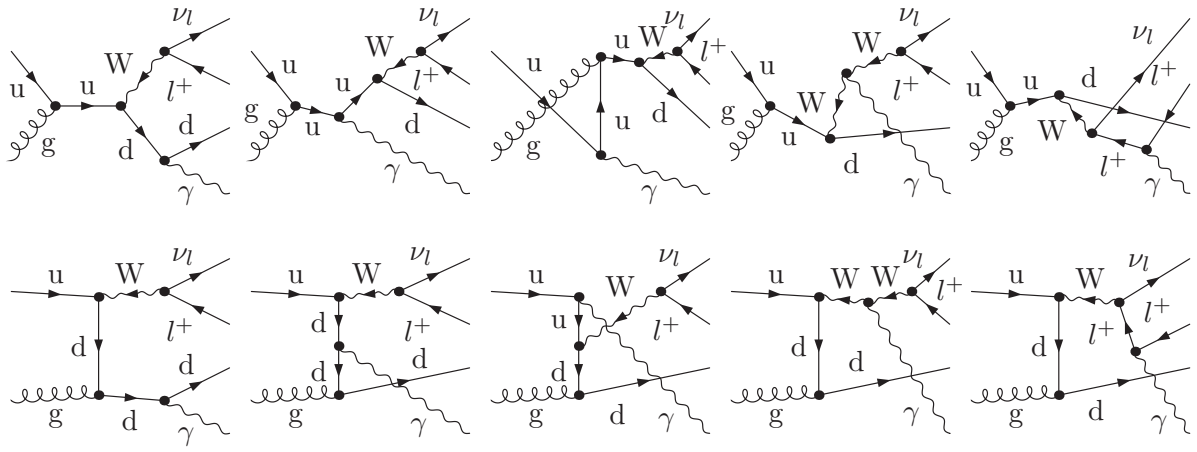

Figure 6.5: Real photonic bremsstrahlung corrections to the LO process (6.1.2).

additional logarithms of the lepton mass in the final result are also isolated analytically. Like in the standard subtraction formalism, it is sufficient to calculate the real matrix elements for the partonic processes in the massless-fermion approximation.

Photons and QCD partons always have to be recombined into a single jet if they are sufficiently collinear. This leads to collinear-safe observables if the selection cuts respect the recombination procedure. However, the recombination induces a problem for subprocess (6.3.1), as we have seen in Section 3.7. If the photon and the gluon are accidentally collinear (of course there is no collinear enhancement for these configurations) arbitrarily soft gluons can still pass the jet selection due to a collinear photon. There is a soft-gluon divergence induced by this simple recombination procedure that can be cancelled by the virtual QCD corrections to $\mathrm{W}+\gamma$ production as demonstrated in Chapter 5. To avoid the singularity, one has to distinguish $\mathrm{W}+\gamma$ and $\mathrm{W}+\mathrm{jet}$ production by means of a more precise event definition employing a cut on the maximal energy or transverse momentum fraction of a photon inside a given jet. However, this procedure spoils the collinear safety of the event definition in subprocesses (6.3.2) and (6.3.3). Using again the subtraction formalism for non-collinear-safe observables to extract the problematic collinear terms, the appearance of an unphysical quark-mass logarithm in the final result signals the necessity to include non-perturbative physics to properly describe the emission of a photon by a quark for exclusive final states. In our calculation, we follow the strategy of Section 3.7.1 and absorb the residual quark-mass dependence in the non-perturbative parts of the quark-to-photon fragmentation function.

6.3.2 Real QCD corrections

The real corrections due to NLO QCD are less subtle, but, in contrast to the EW corrections, new partonic channels contribute to the real-emission processes that have been absent at LO.

Real gluon emission leads to the processes

$$\mathrm{u}_i\ \bar{\mathrm{d}}_j \to l^+\nu_l\,\mathrm{g}\,\mathrm{g}\,, \tag{6.3.4a}$$
$$\mathrm{u}_i\ \mathrm{g} \to l^+\nu_l\,\mathrm{d}_j\,\mathrm{g}\,, \tag{6.3.4b}$$
$$\bar{\mathrm{d}}_j\ \mathrm{g} \to l^+\nu_l\,\bar{\mathrm{u}}_i\,\mathrm{g}\,, \tag{6.3.4c}$$

Additionally, the FS gluon at LO may also split into two quarks, inducing the two partonic channels

$$\mathrm{u}_i\ \bar{\mathrm{d}}_j \to l^+\nu_l\,\mathrm{u}_k\bar{\mathrm{u}}_k\,, \quad k=1,2\,, \tag{6.3.5}$$
$$\mathrm{u}_i\ \bar{\mathrm{d}}_j \to l^+\nu_l\,\mathrm{d}_m\bar{\mathrm{d}}_m\,, \quad m=1,2,3\,. \tag{6.3.6}$$

Application of crossing symmetry to (6.3.5) and (6.3.6) results in the processes

$$\mathrm{u}_i\ \bar{\mathrm{d}}_j \to l^+\nu_l\,q_k\,\bar{q}_k\,, \tag{6.3.7}$$
$$\bar{q}_k\ \bar{\mathrm{d}}_j \to l^+\nu_l\,\bar{\mathrm{u}}_i\,\bar{q}_k\,, \tag{6.3.8}$$
$$q_k\ \bar{\mathrm{d}}_j \to l^+\nu_l\,q_k\,\bar{\mathrm{u}}_i \quad (q_k\neq \mathrm{u}_i, q_k\neq \mathrm{d}_j)\,, \tag{6.3.9}$$
$$\mathrm{u}_i\ \bar{q}_k \to l^+\nu_l\,\mathrm{d}_j\,\bar{q}_k \quad (\bar{q}_k\neq \bar{\mathrm{d}}_j, \bar{q}_k\neq \bar{\mathrm{u}}_i)\,, \tag{6.3.10}$$
$$\mathrm{u}_i\ q_k \to l^+\nu_l\,q_k\,\mathrm{d}_j\,, \tag{6.3.11}$$
$$q_k\ \bar{q}_k \to l^+\nu_l\,\bar{\mathrm{u}}_i\,\mathrm{d}_j\,, \tag{6.3.12}$$

where q_k stands for up-type quarks u_k with $k=1,2$ or for down-type quarks d_k with $k=1,2,3$. Note that the Feynman diagrams are different in the two cases $i=k$ ($j=k$) and $i\neq k$ ($j\neq k$). As in the EW case, we use the dipole subtraction method [66] to extract the IR singularities analytically from the numerical phase-space integration. In Section 4.4 we have presented a brief summary of the relevant formulae that are needed to apply the dipole subtraction method in QCD. Absorbing all the collinear singularities due to IS splittings into the relevant PDFs as prescribed by (3.3.3), the remaining collinear and soft divergences cancel all divergent parts of the one-loop QCD corrections for processes (6.1.1) – (6.1.3). Here, also the bottom-quark PDF enters the NLO prediction. For example a bottom quark from a proton can emit a gluon which subsequently takes part in the hard process.

Turning to the photon-induced contributions, the corresponding real-radiation processes are

$$\mathrm{u}_i\ \gamma \to l^+\nu_l\,\mathrm{d}_j\,\mathrm{g}\,, \tag{6.3.13}$$
$$\bar{\mathrm{d}}_j\ \gamma \to l^+\nu_l\,\bar{\mathrm{u}}_i\,\mathrm{g}\,, \tag{6.3.14}$$
$$\mathrm{g}\ \gamma \to l^+\nu_l\,\bar{\mathrm{u}}_i\,\mathrm{d}_j\,. \tag{6.3.15}$$

All singularities cancel those in the virtual NLO QCD corrections or are absorbed into PDFs as prescribed by Eqs. (3.3.4) and (3.4.1).

6.3.3 Interference of EW and QCD diagrams

There is yet another class of corrections contributing at $\mathcal{O}(\alpha^3\alpha_\mathrm{s})$. For the six-fermion processes (6.3.7) – (6.3.12) with two identical quarks, diagrams with gluon exchange can

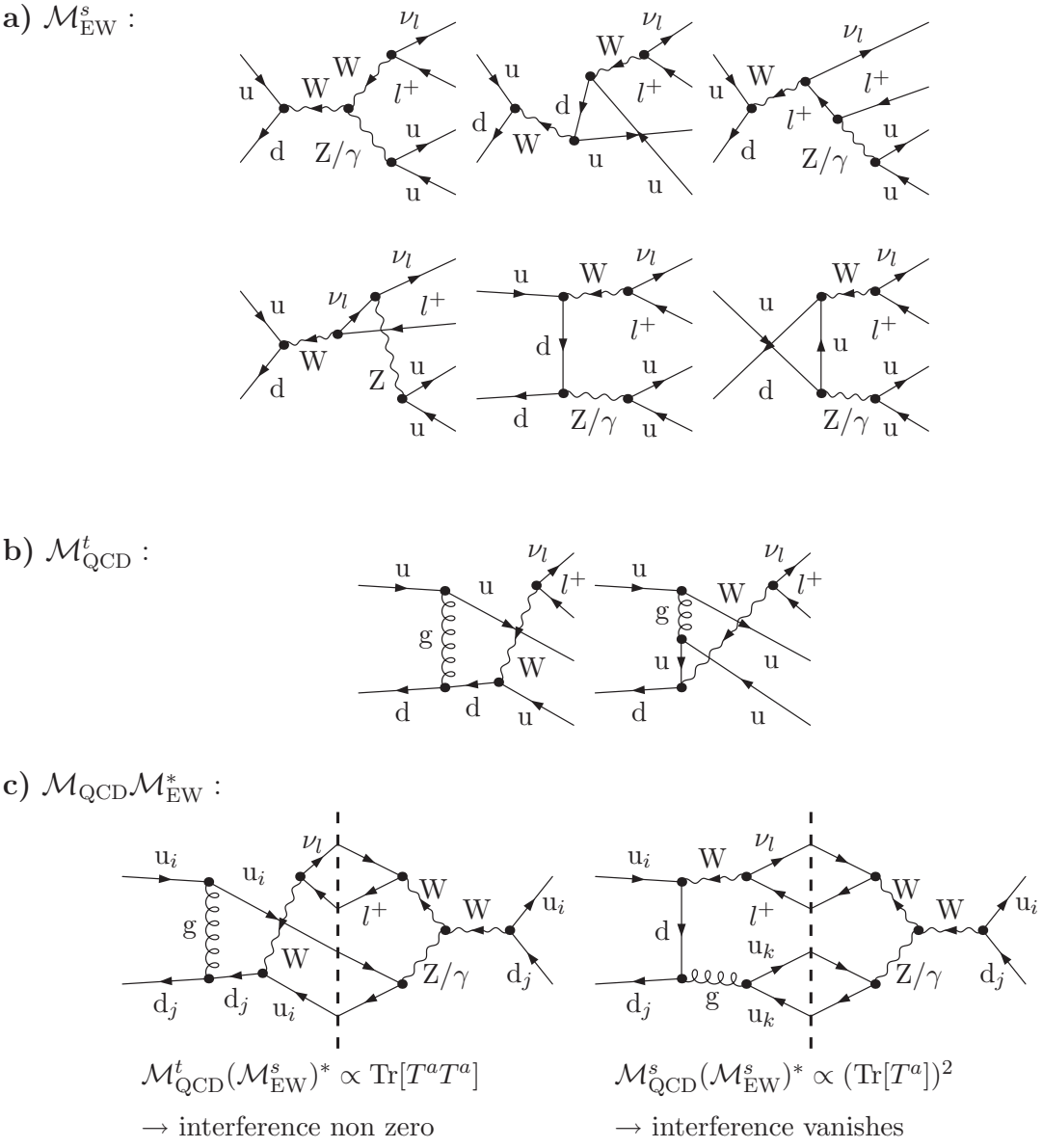

Figure 6.6: The interference between EW and QCD diagrams: a) EW diagrams with s–channel-like colour flow for process (6.3.7) with $q_k = \mathrm{u}_k$. b) QCD diagrams with t–channel-like colour flow. c) EW and QCD diagrams of both s- or t-type do not contribute (right). However, for $i = k$, there is an interference contribution from diagrams of different types that is non-zero. The full interference term for the partonic process (6.3.7) reads $2\,\mathrm{Re}[\mathcal{M}^{t}_{\rm QCD}(\mathcal{M}^{s}_{\rm EW})^{*} + \mathcal{M}^{s}_{\rm QCD}(\mathcal{M}^{t}_{\rm EW})^{*}]$. All other partonic interference contributions with the same flavour structure can be obtained by applying the same crossing procedure to $\mathcal{M}^{s/t}_{\rm QCD}$ and $\mathcal{M}^{s/t}_{\rm EW}$.

interfere with purely EW diagrams. Exemplarily, the relevant diagrams for one of the contributing subprocesses are shown in Fig. 6.6. The result is non-singular due to the restrictions from colour flow, but only if all fermions are distinct the interference contribution vanishes. We have also included these corrections in our calculation. However, their effect turns out to be phenomenologically negligible. Diagrams with an internal top propagator and two W bosons do not contribute if mixing with quarks of the third generation is neglected. The tree-level amplitudes that correspond to the purely weak diagrams for the processes (6.3.7) – (6.3.12) will be listed in Section 8.3, where we will also discuss the calculation of the interference contributions of EW and QCD diagrams.

Chapter 7

Partonic LO contributions to $\mathrm{pp}/\mathrm{p\bar{p}} \to l^+\nu_l + \mathrm{jet}$

7.1 The Weyl–van-der-Waerden spinor formalism

Throughout this thesis, we use the Weyl–van-der-Waerden (WvdW) spinor formalism to express helicity amplitudes in terms of spinor products. The squaring of amplitudes and the summation over helicities of external particles is then performed numerically within the computational processing. The WvdW formalism is discussed in detail in Ref. [100]. Nevertheless, we will now, after a short motivation, expose the underlying principles of the method.

Performing polarization sums numerically, the number of terms that have to be calculated analytically is usually much smaller than the number of contributions that arise when using completeness relations and trace techniques to sum over the external polarizations. Moreover, applying WvdW spinors to express the scattering amplitudes, it is often possible to significantly simplify the intermediate cumbersome expressions and to obtain very compact results. This is especially true if massless external particles are involved. The approach also directly enables the calculation of polarized cross sections without introducing additional helicity projectors, which is another beneficial feature of this method.

In the end, the analytical power of the technique is based on the fact that all physical objects, i.e. fermion spinors, Dirac matrices, four-vectors of physical momenta, and polarization vectors of external vector bosons, can be expressed in terms of the same fundamental mathematical objects.

On the one hand, external (anti)fermions are mathematically described using the covariant and contravariant two-dimensional WvdW-spinors ψ_A and $\psi^{\dot{A}}$ that belong to the two-dimensional irreducible representations $D(\frac{1}{2},0)$ and $D(0,\frac{1}{2})$ of the Lorentz group, respectively. The two components of the spinors are denoted by capital letters, and a dotted index simply means complex conjugation of the particular component,

$$\psi^{\dot{A}} = (\psi^A)^* \,, \quad \psi_{\dot{A}} = (\psi_A)^* \,. \tag{7.1.1}$$

We need the anti-symmetric 2×2 matrix

$$\epsilon^{AB} = \epsilon_{AB} = \epsilon^{\dot{A}\dot{B}} = \epsilon_{\dot{A}\dot{B}} = \begin{pmatrix} 0 & 1 \\ -1 & 0 \end{pmatrix} , \tag{7.1.2}$$

called *spinor metric*, to convert covariant to contravariant spinors, and vice versa,

$$\psi^A = \epsilon^{AB}\psi_B\,, \quad \psi^{\dot{A}} = \epsilon^{\dot{A}\dot{B}}\psi_{\dot{B}}\,, \quad ,\psi_A = \psi^B\epsilon_{BA}\,, \quad \psi_{\dot{A}} = \psi^{\dot{B}}\epsilon_{\dot{B}\dot{A}}\,, \tag{7.1.3}$$

where we assume implicit summation over pairs of identical indices. Note that the two different representations are not mixed by this manipulation.

On the other hand, the description of four-vectors (i.e. momenta and polarization vectors) is done by means of four-dimensional matrices with two spinor indices. The transition matrices

$$\sigma^{\mu,\dot{A}B} = (\sigma^0, \boldsymbol{\sigma})\,, \quad \sigma^{\mu}_{A\dot{B}} = (\sigma^0, -\boldsymbol{\sigma})\,, \tag{7.1.4}$$

where σ^0 denotes the 2×2 unity matrix, and $\boldsymbol{\sigma}$ is a vector of the three Pauli matrices, transform a given four-vector k^μ to the spinor representation $D(\frac{1}{2},\frac{1}{2}) = D(\frac{1}{2},0)\otimes D(0,\frac{1}{2})$ of the Lorentz group via

$$K_{\dot{A}B} = k^\mu\sigma_{\mu,\dot{A}B} = \begin{pmatrix} k^0+k^3 & k^1+\mathrm{i}k^2 \\ k^1-\mathrm{i}k^2 & k^0-k^3 \end{pmatrix}. \tag{7.1.5}$$

Here, $K_{\dot{A}B}$ is a hermitian 2×2 matrix if the components of k^μ are real. If k^μ denotes the physical four-momentum of a massless particle, i.e. $k^2 = 0$, the momentum matrix $K_{\dot{A}B}$ factorizes into a product of two so-called momentum spinors,

$$K_{\dot{A}B} = k_{\dot{A}}k_B\,. \tag{7.1.6}$$

Denoting the polar angle of the massless particle by θ and its azimuthal angle by ϕ, the four-vector reads

$$k^\mu = k^0(1,\, \sin\theta\cos\phi,\, \sin\theta\sin\phi,\, \cos\theta)\,, \tag{7.1.7}$$

and the momentum spinor can be written as

$$k_A = \sqrt{2k^0}\begin{pmatrix} \mathrm{e}^{-\mathrm{i}\phi}\cos\frac{\theta}{2} \\ \sin\frac{\theta}{2}\end{pmatrix}. \tag{7.1.8}$$

According to Chapter 4 of [100], the usual Feynman rules given in terms of four-vectors, Dirac matrices, and Dirac spinors can be systematically translated to the WvdW formalism. Doing so, one finds that—if only massless external particles are involved—any helicity amplitude at tree level can be expressed in terms of so-called spinor products $\langle pk\rangle \equiv p_A k^A$ and ordinary scalar products (pk), which are related to spinor products via $(pk) = |\langle pk\rangle|^2/2$. In the numerical evaluation, the spinor products can be calculated according to the explicit expression

$$\langle pk\rangle = 2\sqrt{p^0k^0}\left(\mathrm{e}^{-\mathrm{i}\phi_p}\cos\frac{\theta_p}{2}\sin\frac{\theta_k}{2} - \mathrm{e}^{-\mathrm{i}\phi_k}\cos\frac{\theta_k}{2}\sin\frac{\theta_p}{2}\right). \tag{7.1.9}$$

7.2 Analytical expressions of LO amplitudes

In this section we list the partonic scattering amplitudes for the LO contributions to W+jet production. For the dominant channels (6.1.1) – (6.1.3), we have to consider processes of the form

$$a^{(c_1)}(p_a,\sigma_a) + b^{(c_2)}(p_b,\sigma_b) \to l^+(k_l,\tau_l) + \nu_l(k_n,-) + c^{(c_3)}(k_c,\sigma_c)\,, \tag{7.2.1}$$

where momenta and polarizations are given in parentheses, and the colours of the strongly interacting partons a, b, and c are depicted as upper indices. The partons a and b initiate the hard scattering process, while the parton c will be seen as a jet in the detector after hadronization has taken place. Accordingly, the momenta p_a and p_b are assumed to be incoming, while the momenta k_l, k_n, and k_c are outgoing.

In addition to the W+jet prduction via two QCD partons, we will also discuss the photon-induced contributions

$$a^{(c_1)}(p_a,\sigma_a) + \gamma(p_b,\sigma_b) \to l^+(k_l,\tau_l) + \nu_l(k_n,-) + c^{(c_2)}(k_c,\sigma_c)\,, \tag{7.2.2}$$

that are given by the processes (6.1.5) and (6.1.6).

7.2.1 Contributions at $\mathcal{O}(\alpha^2\alpha_\mathrm{s})$

Now we provide the amplitudes for the partonic channels at LO listed in (6.1.1) – (6.1.3). We start with the process

$$\mathrm{u}_i^{(l)}(p_a,\sigma_a) + \bar{\mathrm{d}}_j^{(k)}(p_b,\sigma_b) \to l^+(k_l,\tau_l) + \nu_l(k_n,-) + \mathrm{g}^{(a)}(k_c,\sigma_c)\,, \tag{7.2.3}$$

and define the corresponding LO amplitude as

$$\mathrm{i}\mathcal{M}^0_{\mathrm{u}_i\bar{\mathrm{d}}_j\to l^+\nu_l\mathrm{g}} = \mathrm{i}\frac{\sqrt{2}e^2V_{ij}^*}{s_\mathrm{W}^2}\,(g_\mathrm{s}T^a_{kl})\,M^{0,\sigma_a\sigma_b}_{\mathrm{u}\bar{\mathrm{d}}\to l^+\nu_l\mathrm{g}}(\tau_l,\sigma_c)\,. \tag{7.2.4}$$

The dependence on the momenta and the helicities of the external particles is entirely contained in the non-vanishing colour- and CKM-stripped helicity amplitudes,

$$M^{0,-+}_{\mathrm{u}\bar{\mathrm{d}}\to l^+\nu_l\mathrm{g}}(+,+) = -\frac{\langle k_n p_b\rangle^2\langle k_l k_n\rangle^*}{(q_\mathrm{W}^2-\mu_W^2)\langle k_c p_a\rangle\langle k_c p_b\rangle}\,, \tag{7.2.5a}$$

$$M^{0,-+}_{\mathrm{u}\bar{\mathrm{d}}\to l^+\nu_l\mathrm{g}}(+,-) = -\frac{(\langle k_l p_a\rangle^*)^2\,\langle k_n k_l\rangle}{(q_\mathrm{W}^2-\mu_W^2)\langle k_c p_a\rangle^*\langle k_c p_b\rangle^*}\,, \tag{7.2.5b}$$

with $q^\mu_\mathrm{W} = k^\mu_l + k^\mu_n$ being the four-momentum of the virtual W^+ boson. All other helicity combinations vanish or are suppressed by masses of light fermions.

Since the prefactor in (7.2.4) is of course the same for all partonic processes (6.1.1) – (6.1.3), the amplitudes

$$\mathrm{i}\mathcal{M}^0_{\mathrm{u}_i\mathrm{g}\to l^+\nu_l\mathrm{d}_j} = \mathrm{i}\frac{\sqrt{2}e^2V_{ij}^*}{s_\mathrm{W}^2}\,(g_\mathrm{s}T^a_{kl})\,M^{0,\sigma_a\sigma_b}_{\mathrm{ug}\to l^+\nu_l\mathrm{d}}(\tau_l,\sigma_c)\,, \tag{7.2.6}$$

$$\mathrm{i}\mathcal{M}^0_{\bar{\mathrm{d}}_j\mathrm{g}\to l^+\nu_l\bar{\mathrm{u}}_i} = \mathrm{i}\frac{\sqrt{2}e^2V_{ij}^*}{s_\mathrm{W}^2}\,(g_\mathrm{s}T^a_{kl})\,M^{0,\sigma_a\sigma_b}_{\bar{\mathrm{d}}\mathrm{g}\to l^+\nu_l\bar{\mathrm{u}}}(\tau_l,\sigma_c)\,, \tag{7.2.7}$$

for the processes (6.1.2) and (6.1.3) can be obtained applying crossing symmetry to (7.2.5) as explained in Section 4.2 of [100]. The resulting contributions $M^{0,\sigma_a\sigma_b}_{\mathrm{ug}\to l^+\nu_l\mathrm{d}}(\tau_l,\sigma_c)$ and $M^{0,\sigma_a\sigma_b}_{\bar{\mathrm{d}}\mathrm{g}\to l^+\nu_l\bar{\mathrm{u}}}(\tau_l,\sigma_c)$ are given by

$$M^{0,--}_{\mathrm{ug}\to l^+\nu_l\mathrm{d}}(+,-) = \frac{\langle k_n k_c\rangle^2 \langle k_l k_n\rangle^*}{(q^2_{\mathrm{W}}-\mu^2_W)\langle p_a p_b\rangle\langle p_b k_c\rangle}\,, \tag{7.2.8a}$$

$$M^{0,-+}_{\mathrm{ug}\to l^+\nu_l\mathrm{d}}(+,-) = \frac{\left(\langle k_l p_a\rangle^*\right)^2 \langle k_n k_l\rangle}{(q^2_{\mathrm{W}}-\mu^2_W)\langle p_b k_c\rangle^*\langle p_b p_a\rangle^*}\,, \tag{7.2.8b}$$

$$M^{0,++}_{\bar{\mathrm{d}}\mathrm{g}\to l^+\nu_l\bar{\mathrm{u}}}(+,+) = \frac{\left(\langle k_l k_c\rangle^*\right)^2 \langle k_n k_l\rangle}{(q^2_{\mathrm{W}}-\mu^2_W)\langle p_b p_a\rangle^*\langle p_b k_c\rangle^*}\,, \tag{7.2.8c}$$

$$M^{0,+-}_{\bar{\mathrm{d}}\mathrm{g}\to l^+\nu_l\bar{\mathrm{u}}}(+,+) = \frac{\langle k_n p_a\rangle^2 \langle k_l k_n\rangle^*}{(q^2_{\mathrm{W}}-\mu^2_W)\langle p_b k_c\rangle\langle p_b p_a\rangle}\,, \tag{7.2.8d}$$

where the assignment of the momenta and helicities is defined by (7.2.1). Squaring the amplitudes, summing over the external colours and polarizations, and averaging over the IS ones yields

$$\overline{|\mathcal{M}^0_{ab\to l^+\nu_l c,\,(ij)}|^2} = \frac{16}{F_{ab}}(2\pi)^3\frac{\alpha^2|V_{ij}|^2}{|s^2_{\mathrm{W}}|^2}(N^2_{\mathrm{C}}-1)\,\alpha_{\mathrm{s}}\,T_{\mathrm{F}}\sum_{\sigma_a,\sigma_b}\sum_{\tau_l,\sigma_c}\left|M^{0,\sigma_a\sigma_b}_{ab\to l^+\nu_l c}(\tau_l,\sigma_c)\right|^2\,, \tag{7.2.9}$$

where the colour relation

$$\sum_{k,l=1}^{N_{\mathrm{C}}}\sum_{a=1}^{N^2_{\mathrm{C}}-1}(T^a_{kl}T^a_{lk}) = \sum_{a=1}^{N^2_{\mathrm{C}}-1}\mathrm{Tr}(T^aT^a) = (N^2_{\mathrm{C}}-1)\,T_{\mathrm{F}} \tag{7.2.10}$$

was used. Equation (7.2.9) is valid for all partonic channels (6.1.1) – (6.1.3), and the different averaging factors F_{ab} read

$$F_{\mathrm{u}\bar{\mathrm{d}}} = 36\,, \quad F_{\mathrm{ug}} = F_{\bar{\mathrm{d}}\mathrm{g}} = 96\,. \tag{7.2.11}$$

Due to the very simple structure of (7.2.5) it is also easily possible to perform the summation over the helicities in (7.2.9) analytically, yielding

$$\sum_{\sigma_a,\sigma_b}\sum_{\tau_l,\sigma_c}\left|M^{0,\sigma_a\sigma_b}_{\mathrm{u}\bar{\mathrm{d}}\to l^+\nu_l\mathrm{g}}(\tau_l,\sigma_c)\right|^2 = \frac{q^2_{\mathrm{W}}}{|q^2_{\mathrm{W}}-\mu^2_{\mathrm{W}}|^2}\,\frac{(p_bk_n)^2+(p_ak_l)^2}{(p_ak_c)(p_bk_c)} \tag{7.2.12}$$

for process (6.1.1), where we have used the relation $|\langle pk\rangle|^2 = 2(pk)$.

7.2.2 Photon-induced contributions at $\mathcal{O}(\alpha^3)$

The helicity amplitudes for the partonic channels (6.1.5) and (6.1.6) can be obtained from the photon-bremsstrahlung amplitudes of the Drell–Yan process, given by Eqs. (2.28) and (2.29) in Ref. [17], by crossing the photon into the initial state and one quark into the final state at the same time. For instance, the scattering amplitude of the process

$$\mathrm{u}^{(l)}_i(p_a,\sigma_a) + \gamma(p_b,\sigma_b) \to l^+(k_l,\tau_l) + \nu_l(k_n,-) + \mathrm{d}^{(k)}_j(k_c,\sigma_c) \tag{7.2.13}$$

can be written as

$$\mathrm{i}\mathcal{M}^0_{\mathrm{u}_i\gamma\to l^+\nu_l\mathrm{d}_j} = \mathrm{i}\frac{\sqrt{2}e^3V_{ij}^*}{s_{\mathrm{W}}^2}\,\delta_{kl}\,M^{0,\sigma_a\sigma_b}_{\mathrm{u}\gamma\to l^+\nu_l\mathrm{d}}(\tau_l,\sigma_c)\,, \tag{7.2.14}$$

where the dependence on the momenta and the helicities is again solely contained in the following colour- and CKM-stripped amplitudes,

$$\begin{aligned} M^{0,--}_{\mathrm{u}\gamma\to l^+\nu_l\mathrm{d}}(+,-) = \langle k_c k_n\rangle^2\Bigg\{ &- \frac{Q_u\langle k_n k_l\rangle^*}{(q_{\mathrm{W}}^2-\mu_{\mathrm{W}}^2)\langle p_a p_b\rangle\langle k_c p_b\rangle} \\ &+ \frac{1}{(\hat{s}-\mu_{\mathrm{W}}^2)}\left[-\frac{Q_l\langle p_a k_c\rangle^*}{\langle p_b k_n\rangle\langle p_b k_l\rangle} + \frac{(Q_d-Q_u)\langle p_a k_l\rangle^*}{\langle k_c p_b\rangle\langle p_b k_n\rangle}\right] \\ &- \frac{C_{\gamma\mathrm{WW}}(Q_u-Q_d)\langle k_n k_l\rangle^*\langle p_a p_b\rangle^*}{(\hat{s}-\mu_{\mathrm{W}}^2)(q_{\mathrm{W}}^2-\mu_{\mathrm{W}}^2)\langle k_c p_b\rangle}\Bigg\}, \end{aligned} \tag{7.2.15a}$$

$$\begin{aligned} M^{0,-+}_{\mathrm{u}\gamma\to l^+\nu_l\mathrm{d}}(+,-) = (\langle p_a k_n\rangle^*)^2\Bigg\{ &\frac{Q_d\langle k_n k_l\rangle}{(q_{\mathrm{W}}^2-\mu_{\mathrm{W}}^2)\langle p_a p_b\rangle^*\langle k_c p_b\rangle^*} + \frac{(Q_d-Q_u)\langle k_c k_n\rangle}{(\hat{s}-\mu_{\mathrm{W}}^2)\langle p_a p_b\rangle^*\langle p_b k_l\rangle^*} \\ &- \frac{C_{\gamma\mathrm{WW}}(Q_d-Q_u)\langle k_n k_l\rangle\langle k_c p_b\rangle}{(\hat{s}-\mu_{\mathrm{W}}^2)(q_{\mathrm{W}}^2-\mu_{\mathrm{W}}^2)\langle p_a p_b\rangle^*}\Bigg\}. \end{aligned} \tag{7.2.15b}$$

After the trivial colour summation $\sum_{i,j=1}^{N_{\mathrm{C}}}\delta_{ij} = N_{\mathrm{C}}$, the squared averaged amplitudes for both photon-induced contributions (6.1.5) and (6.1.6) at LO are given by the general formula

$$\overline{|\mathcal{M}^0_{a\gamma\to l^+\nu_l c}|^2} = \frac{N_{\mathrm{C}}}{F_{q\gamma}}\frac{16\,(2\pi)^3\,\alpha^3\,|V_{ij}|^2}{|s_{\mathrm{W}}^2|^2}\sum_{\sigma_a,\sigma_b}\sum_{\tau_l,\sigma_c}\left|M^{0,\sigma_a\sigma_b}_{a\gamma\to l^+\nu_l c}(\tau_l,\sigma_c)\right|^2\,, \tag{7.2.16}$$

where $F_{q\gamma} = 12$, and the $M^{0,\sigma_a\sigma_b}_{\bar{\mathrm{d}}\gamma\to l^+\nu_l\bar{\mathrm{u}}}(\tau_l,\sigma_c)$ result from (7.2.15) via crossing.

7.3 Construction of the LO phase space

In accordance with (2.3.4), the partonic cross section for any contributing LO channel $a\,(b/\gamma)\to l^+ + \nu_l + c$ is given by

$$\hat{\sigma}^0_{a\,(b/\gamma)\to l^+\nu_l c}(p_a,p_b) = \frac{1}{2\hat{s}}\int \mathrm{d}\Phi_{(l+\nu_l+c)}\;\overline{|\mathcal{M}^0_{a\,(b/\gamma)\to l^+\nu_l c}|^2}\,. \tag{7.3.1}$$

As explained in Appendix B.2, the three-particle phase space $\int\mathrm{d}\Phi_{(l+\nu_l+c)}$ for a lepton, a neutrino, and a parton c in the final state can be decomposed according to

$$\int\mathrm{d}\Phi_{(l+\nu_l+c)}(p_a,p_b;k_l,k_n,k_c) = \frac{1}{(2\pi)^5}\int_0^{\hat{s}}\mathrm{d}q_{\mathrm{W}}^2\int\mathrm{d}\Omega_d(q_{\mathrm{W}}^2;k_l^2,k_n^2)\int\mathrm{d}\Omega_p(p_a,p_b;\,k_c^2,q_{\mathrm{W}}^2)\,, \tag{7.3.2}$$

where we have constructed the phase space subject to the topology depicted in Fig. 7.1. In (7.3.2), $\mathrm{d}\Omega_d(q_{\mathrm{W}}^2;k_l^2,k_n^2)$ is the two-particle subspace of the decay process $\mathrm{W}^+\to l^+ + \nu_l$, and $\mathrm{d}\Omega_p(p_a,p_b;k_c^2,q_{\mathrm{W}}^2)$ represents the effective two-particle phase space of the preceding

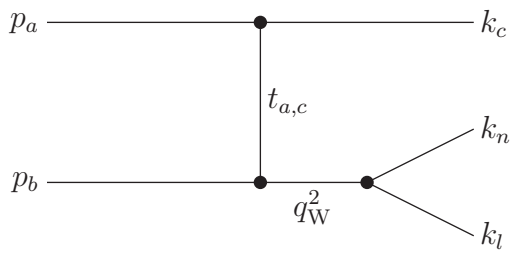

Figure 7.1: Topology for the phase-space construction within the LO calculations.

$2 \to 2$ scattering process $a + b \to \mathrm{W}^+ + c$. The explicit expressions for $\int \mathrm{d}\Omega_d(q^2_{\mathrm{W}}; k^2_l, k^2_n)$ and $\int \mathrm{d}\Omega_p(p_a, p_b; k^2_c, q^2_{\mathrm{W}})$ read

$$\int \mathrm{d}\Omega_d(q^2_{\mathrm{W}}; k^2_l, k^2_n) = \frac{1}{8} \int_0^{2\pi} \mathrm{d}\phi^{\mathrm{W}}_l \int_{-1}^{1} \mathrm{d}\cos\theta^{\mathrm{W}}_l \,, \tag{7.3.3a}$$

$$\int \mathrm{d}\Omega_p(p_a, p_b; k^2_c, q^2_{\mathrm{W}}) = \frac{1}{4\hat{s}} \int_0^{2\pi} \mathrm{d}\phi_c \int_{-\hat{s}+q^2_{\mathrm{W}}}^{0} \mathrm{d}t_{a,c} \,, \tag{7.3.3b}$$

where ϕ^{W}_l and θ^{W}_l are the azimuthal and polar angles of the lepton in the rest frame of the decaying W boson, ϕ_c denotes the azimuthal angle of the parton c in the partonic cm frame, and $t_{a,c} = (p_a - k_c)^2$. Since the process under consideration is invariant with respect to rotations around the beam axis, the corresponding matrix elements exhibit an azimuthal symmetry, and the integration over ϕ_c is trivial, yielding a factor 2π.

The particle momenta in the partonic cm frame can be expressed in terms of the integration variables as follows. The jet momentum is chosen as

$$k^\mu_c = \frac{\hat{s} - q^2_{\mathrm{W}}}{2\sqrt{\hat{s}}} (1, \sin\theta_c, 0, \cos\theta_c) \,, \tag{7.3.4}$$

where the polar angle θ_c of the parton c reads

$$\theta_c = \arccos\left(1 + \frac{2\, t_{a,c}}{\hat{s} - q^2_{\mathrm{W}}}\right) . \tag{7.3.5}$$

We also need the four-momentum of the intermediate W boson,

$$q^\mu_{\mathrm{W}} = \frac{\hat{s} + q^2_{\mathrm{W}}}{2\sqrt{\hat{s}}} (1, -\beta_{\mathrm{W}} \sin\theta_c, 0, -\beta_{\mathrm{W}} \cos\theta_c) \,, \tag{7.3.6}$$

where we have introduced the W-boson velocity $\beta_{\mathrm{W}} = (\hat{s} - q^2_{\mathrm{W}})/(\hat{s} + q^2_{\mathrm{W}})$, to construct the lepton momenta in the cm frame. In the rest frame of the W boson we find

$$k^{\mathrm{W},\mu}_l = \frac{\sqrt{q^2_{\mathrm{W}}}}{2} (1, \sin\theta^{\mathrm{W}}_l \cos\phi^{\mathrm{W}}_l, \sin\theta^{\mathrm{W}}_l \sin\phi^{\mathrm{W}}_l, \cos\theta^{\mathrm{W}}_l) \,, \tag{7.3.7a}$$

$$k^{\mathrm{W},\mu}_n = \frac{\sqrt{q^2_{\mathrm{W}}}}{2} (1, -\sin\theta^{\mathrm{W}}_l \cos\phi^{\mathrm{W}}_l, -\sin\theta^{\mathrm{W}}_l \sin\phi^{\mathrm{W}}_l, -\cos\theta^{\mathrm{W}}_l) \,, \tag{7.3.7b}$$

and we obtain the momenta in the cm frame by applying the boost

$$k_l = \boldsymbol{B}\left(q^0_{\mathrm{W}}, -\mathbf{q}_{\mathrm{W}}\right) k^{\mathrm{W}}_l\,, \quad k_n = \boldsymbol{B}\left(q^0_{\mathrm{W}}, -\mathbf{q}_{\mathrm{W}}\right) k^{\mathrm{W}}_n\,, \tag{7.3.8}$$

with the boost matrix $\boldsymbol{B}$ defined by (B.16).

In the actual numerical analysis we use a Breit–Wigner mapping (see Appendix B.3) to improve the efficiency of the q^2_{W}-integration. The remaining integrations are carried out applying simple linear mappings as prescribed by (B.23) and (B.24).

Chapter 8

Real corrections to partonic cross sections: $\mathrm{pp/p\bar{p}} \to l^+\nu_l + \mathrm{jet} + (\mathrm{jet}/\gamma)$

In this chapter we describe the calculation of real-correction amplitudes $\mathcal{M}^{\mathrm{R}}_{a\,b\to l^+\nu_l+c+(d/\gamma)}$ for processes with four FS particles,

$$\begin{aligned} &a^{(c_1)}(p_a,\sigma_a) + b^{(c_2)}(p_b,\sigma_b) \\ &\quad\to l^+(k_l,\tau_l) + \nu_l(k_n,-) + c^{(c_3)}(k_c,\sigma_c) + [d^{(c_4)}/\gamma](k_d/k_\gamma,\sigma_d/\lambda_\gamma)\,. \end{aligned} \tag{8.0.1}$$

In case of the real EW corrections, we are confronted with an additional bremsstrahlung photon γ in the final state, and for the real QCD corrections a second strongly interacting parton d occurs.

In the following, the assignment of momenta and helicities for processes denoted as $a\,b \to l^+\nu_l + c + (d/\gamma)$ is given by (8.0.1), where colours of partons are indicated by upper indices.

8.1 Real EW corrections and QCD corrections to photon-induced processes

Here, we present the amplitudes for the bremsstrahlung processes listed in (6.3.1) – (6.3.3). Since all these channels are related by crossing symmetry, it is sufficient to discuss the amplitudes for the process (6.3.1),

$$\mathrm{u}_i^{(l)}(p_a,\sigma_a) + \bar{\mathrm{d}}_j^{(k)}(p_b,\sigma_b) \to l^+(k_l,\tau_l) + \nu_l(k_n,-) + \mathrm{g}^{(a)}(k_c,\sigma_c) + \gamma(k_\gamma,\lambda_\gamma)\,. \tag{8.1.1}$$

Again, we use the WvdW formalism to compute the different helicity amplitudes and to simplify the corresponding expressions as far as possible. As in the LO case, the squaring of the amplitudes and the helicity summation is performed numerically afterwards.

The full scattering amplitude $\mathcal{M}^{\mathrm{R,EW}}$ for the process (8.1.1) can be written as

$$\mathrm{i}\mathcal{M}^{\mathrm{R,EW}}_{\mathrm{u}_i\bar{\mathrm{d}}_j\to l^+\nu_l+\mathrm{g}+\gamma} = \mathrm{i}\frac{4\,e^3\,V_{ij}^*}{s_{\mathrm{W}}^2}\,(g_{\mathrm{s}}\,T^a_{kl})\,M^{\sigma_a\sigma_b}_{\mathrm{u}\bar{\mathrm{d}}\to l^+\nu_l\mathrm{g}\gamma}(\tau_l,\sigma_c,\lambda_\gamma)\,. \tag{8.1.2}$$

The colour- and CKM-stripped helicity amplitudes $M^{\sigma_a\sigma_b}_{\mathrm{u\bar{d}}\to l^+\nu_l\mathrm{g}\gamma}(\tau_l,\sigma_c,\lambda_\gamma)$ are given by the following expressions,

$$\begin{aligned}
M^{-+}_{\mathrm{u\bar{d}}\to l^+\nu_l\mathrm{g}\gamma}(+,+,+) &= \frac{\langle p_b k_n\rangle}{\langle p_a k_c\rangle\langle p_b k_\gamma\rangle\langle k_c p_b\rangle}\Bigg\{\frac{1}{[(q_\mathrm{W}+k_\gamma)^2-\mu_\mathrm{W}^2]\,(q_\mathrm{W}^2-\mu_\mathrm{W}^2)}\\
&\times\Bigg[\langle k_\gamma k_l\rangle^*(\langle p_b p_a\rangle\langle p_a|K_n|p_b\rangle-\langle p_b k_c\rangle\langle k_c|K_n|p_b\rangle)\left(1-Q_l\frac{q_\mathrm{W}^2-\mu_\mathrm{W}^2}{(k_\gamma+k_l)^2}\right)\\
&\quad-\langle k_\gamma|K_n|p_b\rangle\langle k_l|K_c-P_a|p_b\rangle\Bigg]-Q_u\frac{\langle p_a p_b\rangle}{\langle p_a k_\gamma\rangle}\frac{\langle k_l|K_n|p_b\rangle}{q_\mathrm{W}^2-\mu_\mathrm{W}^2}\Bigg\}, \qquad (8.1.3a)\\
M^{-+}_{\mathrm{u\bar{d}}\to l^+\nu_l\mathrm{g}\gamma}(+,-,-) &= \frac{\langle k_l p_a\rangle^*}{\langle p_b k_c\rangle^*\langle k_c p_a\rangle^*\langle k_\gamma p_b\rangle^*}\Bigg\{\frac{1}{[(q_\mathrm{W}+k_\gamma)^2-\mu_\mathrm{W}^2]\,(q_\mathrm{W}^2-\mu_\mathrm{W}^2)}\\
&\times\Bigg[\langle p_a|K_c-P_b|k_n\rangle\Bigg(\langle p_b|K_n|k_\gamma\rangle+\langle p_b|K_l|k_\gamma\rangle\left[1-Q_l\frac{q_\mathrm{W}^2-\mu_\mathrm{W}^2}{(k_\gamma+k_l)^2}\right]\Bigg)\\
&\quad+\langle p_a|K_n+K_l|k_\gamma\rangle\langle p_b|K_\gamma|k_n\rangle\Bigg]+\frac{\langle p_b p_a\rangle^*}{\langle k_\gamma p_a\rangle^*}\frac{[\langle p_a|K_\gamma|k_n\rangle+Q_u\langle p_a|K_l|k_n\rangle]}{q_\mathrm{W}^2-\mu_\mathrm{W}^2}\Bigg\}, \qquad (8.1.3b)\\
M^{-+}_{\mathrm{u\bar{d}}\to l^+\nu_l\mathrm{g}\gamma}(+,+,-) &= \frac{1}{\langle p_a k_c\rangle\langle p_b k_c\rangle\langle p_a k_\gamma\rangle^*}\Bigg\{\frac{\mathcal{F}_{\gamma\mathrm{Q}}(+,+,-)}{q_\mathrm{W}^2-\mu_\mathrm{W}^2}+\frac{\mathcal{F}_{\gamma l}(+,+,-)}{(q_\mathrm{W}+k_\gamma)^2-\mu_\mathrm{W}^2}\\
&\quad+\frac{\mathcal{F}_{\gamma\mathrm{W}}(+,+,-)}{(q_\mathrm{W}^2-\mu_\mathrm{W}^2)[(q_\mathrm{W}+k_\gamma)^2-\mu_\mathrm{W}^2]}\Bigg\}, \qquad (8.1.3c)\\
M^{-+}_{\mathrm{u\bar{d}}\to l^+\nu_l\mathrm{g}\gamma}(+,-,+) &= \frac{1}{\langle p_a k_c\rangle^*\langle p_b k_\gamma\rangle\langle p_b k_c\rangle^*}\Bigg\{\frac{\mathcal{F}_{\gamma\mathrm{Q}}(+,-,+)}{q_\mathrm{W}^2-\mu_\mathrm{W}^2}+\frac{\mathcal{F}_{\gamma l}(+,-,+)}{(q_\mathrm{W}+k_\gamma)^2-\mu_\mathrm{W}^2}\\
&\quad+\frac{\mathcal{F}_{\gamma\mathrm{W}}(+,-,+)}{(q_\mathrm{W}^2-\mu_\mathrm{W}^2)[(q_\mathrm{W}+k_\gamma)^2-\mu_\mathrm{W}^2]}\Bigg\}, \qquad (8.1.3d)
\end{aligned}$$

where we use the shorthand notation $\langle\eta|P|\xi\rangle\equiv\eta_{\dot{A}}P^{\dot{A}B}\xi_B$, following the conventions in Chapter 2 of [100]. The expressions for the amplitudes where the photon and the gluon have opposite helicities are quite lengthy. Therefore, we have introduced the form factors

$$\begin{aligned}
\mathcal{F}_{\gamma\mathrm{Q}}(+,+,-) &= \frac{1}{\langle p_b k_\gamma\rangle^*}\Bigg[Q_d\Bigg(\langle k_l|P_a-K_c|p_b\rangle\langle p_a|K_\gamma-P_b|k_n\rangle\\
&\quad-\frac{\langle p_a|K_\gamma|p_b\rangle}{(q_\mathrm{W}-p_a)^2}\langle k_l|P_a|k_c\rangle\langle k_c|P_a-K_l|k_n\rangle\Bigg)+Q_u\frac{\langle p_a|K_c|p_b\rangle}{(q_\mathrm{W}-p_b)^2}\langle k_\gamma|P_b|k_n\rangle\langle k_l|K_n-P_b|k_\gamma\rangle\Bigg], \qquad (8.1.4a)\\
\mathcal{F}_{\gamma l}(+,+,-) &= \frac{Q_l}{\langle k_l k_\gamma\rangle^*}\langle p_a k_l\rangle^*\langle k_n p_b\rangle\langle k_l|P_a-K_c|p_b\rangle, \qquad (8.1.4b)\\
\mathcal{F}_{\gamma\mathrm{W}}(+,+,-) &= \langle k_\gamma p_b\rangle\langle p_a|K_c|p_b\rangle\langle k_l|K_\gamma|k_l\rangle+\langle k_n p_b\rangle\langle p_a|K_l+K_n|k_\gamma\rangle\langle k_l|P_a-K_c|p_b\rangle\\
&\quad-\frac{1}{2}\langle k_\gamma k_n\rangle\big(\langle p_a k_l\rangle^*\langle p_b k_c\rangle\langle k_c|K_\gamma-K_l-K_n|p_b\rangle+\langle k_l|P_a|p_b\rangle\langle p_a|K_\gamma-K_l-K_n|p_b\rangle\big), \qquad (8.1.4c)
\end{aligned}$$

for the $(+,+,-)$ case and

$$\mathcal{F}_{\gamma\mathrm{Q}}(+,-,+)=\frac{1}{\langle k_\gamma p_a\rangle}\Bigg[-Q_u\Bigg(\langle k_l|P_a-K_\gamma|p_b\rangle\langle p_a|K_c-P_b|k_n\rangle$$

$$+\frac{\langle p_a|K_\gamma|p_b\rangle}{(q_\mathrm{W}-p_b)^2}\langle k_c|P_b|k_n\rangle\langle k_l|K_n-P_b|k_c\rangle\Big)+Q_d\frac{\langle p_a|K_c|p_b\rangle}{(q_\mathrm{W}-p_a)^2}\langle k_l|P_a|k_\gamma\rangle\langle k_\gamma|P_a-K_l|k_n\rangle\Big]\,, \tag{8.1.5a}$$

$$\mathcal{F}_{\gamma l}(+,-,+)=-\frac{Q_l}{\langle k_l k_\gamma\rangle\langle}\langle p_a|K_c-P_b|k_n\rangle\langle p_a|K_l+K_\gamma|p_b\rangle\,, \tag{8.1.5b}$$

$$\begin{aligned}\mathcal{F}_{\gamma\mathrm{W}}(+,-,+)&=\langle p_a k_\gamma\rangle^*\langle k_l|K_\gamma|k_n\rangle\langle p_a|K_c|p_b\rangle+\langle k_l p_a\rangle^*\langle k_\gamma|K_l+K_n|p_b\rangle\langle p_a|K_c-P_b|k_n\rangle\\&\quad+\frac{1}{2}\langle k_\gamma k_l\rangle^*\langle p_b k_n\rangle\big(\langle p_a k_c\rangle^*\langle p_a|K_\gamma-K_l-K_n|k_c\rangle-\langle p_a p_b\rangle^*\langle p_a|K_\gamma-K_l-K_n|p_b\rangle\big)\,,\end{aligned} \tag{8.1.5c}$$

for the $(+,-,+)$ combination. As in the LO expressions, the prefactor in (8.1.2) is the same for all bremsstrahlung processes. Thus, the averaged squared amplitudes can generally be written as

$$\begin{aligned}&\overline{\left|\mathcal{M}^{\mathrm{R,EW}}_{ab\to l^+\nu_l+c+\gamma,\,(ij)}\right|^2}\\&\quad=\frac{64}{F_{ab}}\,(2\pi)^4\,\frac{\alpha^3|V_{ij}|^2}{|s_\mathrm{W}^2|^2}\,(N_\mathrm{C}^2-1)\,\alpha_\mathrm{s}\,T_\mathrm{F}\sum_{\sigma_a,\sigma_b}\sum_{\tau_l,\sigma_c,\lambda_\gamma}\left|M^{\gamma,\,\sigma_a\sigma_b}_{ab\to l^+\nu_l c}(\tau_l,\sigma_c,\lambda_\gamma)\right|^2\,,\end{aligned} \tag{8.1.6}$$

with the averaging factors from (7.2.11). For the sake of completeness, we also provide the formula

$$\hat{\sigma}^{\mathrm{R,EW}}_{ab\to l^+\nu_l+c+\gamma,\,(ij)}=\frac{1}{2\hat{s}}\int\mathrm{d}\Phi_{(l\nu_l+c+\gamma)}\,\overline{\left|\mathcal{M}^{\mathrm{R,EW}}_{ab\to l^+\nu_l+c+\gamma,\,(ij)}\right|^2}\,, \tag{8.1.7}$$

for the total bremsstrahlung cross section, where the computation of the phase-space integral $\int\mathrm{d}\Phi_{(l\nu_l+c+\gamma)}$ will be described in detail in Section 8.4.

Crossing the bremsstrahlung photon into the initial state, the amplitudes above also provide the real QCD corrections (6.3.13) – (6.3.15) to the photon-induced processes. For the calculation of the corresponding amplitudes $\overline{\left|\mathcal{M}^{\mathrm{R,QCD}}_{a\gamma\to l^+\nu_l+c,\,(ij)}\right|^2}$, we additionally need the averaging factor

$$F_{\mathrm{g}\gamma}=64\,, \tag{8.1.8}$$

for channels with a photon and a gluon in the initial state. The amplitudes for the photon-induced LO processes (6.1.5) and (6.1.6) were already discussed in Section 7.2.2.

8.2 Real QCD corrections

8.2.1 Generic amplitudes

Corresponding to (6.3.4), (6.3.5), and (6.3.6) there are three generic processes contributing to the real QCD corrections,

$$0\to\bar{\mathrm{d}}_i^{(n)}(p_1,\sigma_1)+\mathrm{d}_j^{(m)}(p_2,\sigma_2)+\mathrm{d}_l^{(q)}(p_3,\sigma_3)+\bar{\mathrm{u}}_k^{(p)}(p_4,\sigma_4)+l^+(k_l,\tau_l)+\nu_l(k_n,-)\,, \tag{8.2.1a}$$

$$0\to\bar{\mathrm{u}}_i^{(n)}(p_1,\sigma_1)+\mathrm{u}_j^{(m)}(p_2,\sigma_2)+\mathrm{d}_l^{(q)}(p_3,\sigma_3)+\bar{\mathrm{u}}_k^{(p)}(p_4,\sigma_4)+l^+(k_l,\tau_l)+\nu_l(k_n,-)\,, \tag{8.2.1b}$$

$$0 \to \mathrm{g}^{(a)}(p_1,\sigma_1) + \mathrm{g}^{(b)}(p_2,\sigma_2) + \mathrm{d}_j^{(l)}(p_3,\sigma_3) + \bar{\mathrm{u}}_i^{(k)}(p_4,\sigma_4) + l^+(k_l,\tau_l) + \nu_l(k_n,-)\,. \tag{8.2.1c}$$

Crossing all possible pairs of partons into the initial state, one obtains all partonic channels that enter the real QCD corrections. To give examples for a six- and a four-quark process, respectively, we list the Feynman diagrams for the processes $\mathrm{u}\bar{\mathrm{d}} \to l\nu_l + \mathrm{gg}$ and $\mathrm{u}\bar{\mathrm{d}} \to l\nu_l + \mathrm{u}\bar{\mathrm{u}}$ in Figs. 8.1 and 8.2. The generic amplitudes $\mathcal{T}^{\mathrm{R,QCD}}$ for the real QCD corrections are given by the expressions

$$\mathcal{T}^{\mathrm{R,QCD}}_{0\to \mathrm{W}+\bar{\mathrm{d}}_i\mathrm{d}_j\mathrm{d}_l\bar{\mathrm{u}}_k} = \frac{2\,g_\mathrm{s}^2 e^2}{s_\mathrm{W}^2(q_\mathrm{W}^2-\mu_\mathrm{W}^2)}\left[(\delta_{ij}V_{kl}^*)\sum_a (T^a_{mn}T^a_{qp})\,A_{\mathrm{dddu}} + (\delta_{il}V_{kj}^*)\sum_a (T^a_{mp}T^a_{qn})\,B_{\mathrm{dddu}}\right], \tag{8.2.2a}$$

$$\mathcal{T}^{\mathrm{R,QCD}}_{0\to \mathrm{W}+\bar{\mathrm{u}}_i\mathrm{u}_j\mathrm{d}_l\bar{\mathrm{u}}_k} = \frac{2\,g_\mathrm{s}^2 e^2}{s_\mathrm{W}^2(q_\mathrm{W}^2-\mu_\mathrm{W}^2)}\left[(\delta_{ij}V_{kl}^*)\sum_a (T^a_{mn}T^a_{qp})\,A_{\mathrm{uudu}} + (\delta_{jk}V_{il}^*)\sum_a (T^a_{mp}T^a_{qn})\,B_{\mathrm{uudu}}\right], \tag{8.2.2b}$$

$$\mathcal{T}^{\mathrm{R,QCD}}_{0\to \mathrm{W}+\mathrm{gg}\mathrm{d}_j\bar{\mathrm{u}}_i} = -\frac{g_\mathrm{s}^2 e^2}{s_\mathrm{W}^2(q_\mathrm{W}^2-\mu_\mathrm{W}^2)}\,V_{ij}^*\left[-\mathrm{i}\sum_c f^{abc}T^c_{lk}\,\tilde{G}_{\mathrm{ggdu}} + (T^aT^b)_{lk}\,\tilde{A}_{\mathrm{ggdu}} + (T^bT^a)_{lk}\,\tilde{B}_{\mathrm{ggdu}}\right], \tag{8.2.2c}$$

where the colour- and CKM structures have been separated. In (8.2.2) we have omitted the explicit helicity dependence of the helicity amplitudes $A_{\ldots}$ and $B_{\ldots}$ in the notation,

$$A_{\ldots} = A^{\tau_l}_{\ldots}(\sigma_1,\sigma_2,\sigma_3,\sigma_4)\,, \quad B_{\ldots} = B^{\tau_l}_{\ldots}(\sigma_1,\sigma_2,\sigma_3,\sigma_4)\,.$$

Six-fermion processes

For the six-fermion contributions the non-vanishing helicity amplitudes read

$$A^+_{\mathrm{dddu}}(-,+,-,+) = \frac{1}{(p_1+p_2)^2}\Big[\frac{\langle k_n p_3\rangle}{(q_\mathrm{W}+p_3)^2}\langle k_l|K_n+K_l+P_3|p_1\rangle\langle p_4 p_2\rangle^* - \frac{\langle k_l p_4\rangle^*}{(q_\mathrm{W}+p_4)^2}\langle p_2|K_n+K_l+P_4|k_n\rangle\langle p_3 p_1\rangle\Big], \tag{8.2.3a}$$

$$A^+_{\mathrm{dddu}}(+,-,-,+) = \frac{1}{(p_1+p_2)^2}\Big[\frac{\langle k_n p_3\rangle}{(q_\mathrm{W}+p_3)^2}\langle k_l|K_n+K_l+P_3|p_2\rangle\langle p_4 p_1\rangle^* - \frac{\langle k_l p_4\rangle^*}{(q_\mathrm{W}+p_4)^2}\langle p_1|K_n+K_l+P_4|k_n\rangle\langle p_3 p_2\rangle\Big], \tag{8.2.3b}$$

$$B^+_{\mathrm{dddu}}(\sigma_1,\sigma_2,\sigma_3,\sigma_4) = (-1)\cdot A^+_{\mathrm{dddu}}(\sigma_1,\sigma_3,\sigma_2,\sigma_4)\big|_{p_2\leftrightarrow p_3}\,, \tag{8.2.3c}$$

for the processes (8.2.1a) and

$$A^+_{\mathrm{uudu}}(\sigma_1,\sigma_2,\sigma_3,\sigma_4) = A^+_{\mathrm{dddu}}(\sigma_1,\sigma_2,\sigma_3,\sigma_4)\,, \tag{8.2.4a}$$

$$B^+_{\mathrm{uudu}}(\sigma_1,\sigma_2,\sigma_3,\sigma_4) = (-1)\cdot A^+_{\mathrm{uudu}}(\sigma_4,\sigma_2,\sigma_3,\sigma_1)\big|_{p_1\leftrightarrow p_4}\,, \tag{8.2.4b}$$

for the processes (8.2.1b), respectively.

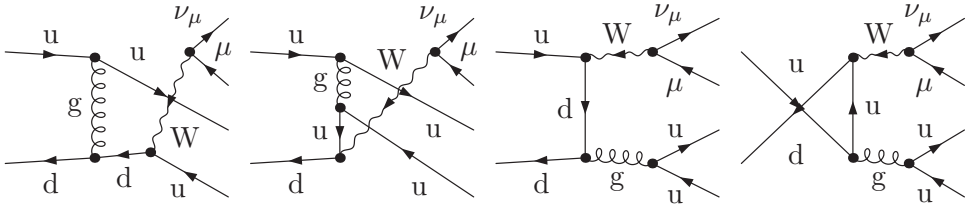

Figure 8.1: Real QCD corrections via the six-fermion process $\mathrm{u}\bar{\mathrm{d}} \to l\nu_l + \mathrm{u}\bar{\mathrm{u}}$.

Processes involving two gluons

For the partonic channels (8.2.1c) involving two gluons we can further simplify the amplitudes and rewrite the $\tilde{G}$-term that emerges from the three-gluon vertex,

$$\mathcal{T}^{\mathrm{R,QCD}}_{0\to W+\mathrm{ggd}_j\bar{\mathrm{u}}_i} = -\frac{g_\mathrm{s}^2 e^2}{s_\mathrm{W}^2(q_\mathrm{W}^2-\mu_\mathrm{W}^2)}\, V_{ij}^* \left[(T^aT^b)_{lk}\, A_{\mathrm{ggdu}} + (T^bT^a)_{lk}\, B_{\mathrm{ggdu}}\right] , \tag{8.2.5}$$

where we have exploited the relation

$$\sum_{c=1}^{N_\mathrm{C}^2-1} f^{abc}T^c_{ij} = -\mathrm{i}[T^a,T^b]_{ij} . \tag{8.2.6}$$

Using WvdW spinor techniques, it is possible to derive compact results for the non-vanishing helicity amplitudes A and B,

$$\begin{aligned}
A^+_{\mathrm{ggdu}}(+,+,-,+) = {}& \frac{2\,\langle p_3 k_n\rangle}{\langle p_3p_1\rangle\langle p_4p_2\rangle\langle p_2p_1\rangle(q_\mathrm{W}+p_3)^2}\Big\{\langle k_l|P_4|p_3\rangle\,[k_n\cdot(k_l+p_3)] \\
& - \langle k_l|K_n|p_3\rangle\left[(q_\mathrm{W}+p_3)^2 + p_4\cdot(p_3+k_l)\right] \\
& + \frac{1}{2}\left[\langle k_l|P_3|p_4\rangle\langle p_4|K_n|p_3\rangle + \langle k_l|K_n|p_4\rangle\langle p_4|K_l|p_3\rangle\right]\Big\} , \qquad (8.2.7a)\\
A^+_{\mathrm{ggdu}}(-,-,-,+) = {}& (A^+_{\mathrm{ggdu}}(+,+,-,+))^*|_{(k_n\leftrightarrow k_l, p_3\leftrightarrow p_4, p_2\leftrightarrow p_1)} , \qquad (8.2.7b)\\
A^+_{\mathrm{ggdu}}(+,-,-,+) = {}& -\frac{\langle p_4p_1\rangle^*\langle k_np_3\rangle}{\langle p_3p_1\rangle\langle p_4p_2\rangle^*\langle p_2p_1\rangle^*(q_\mathrm{W}+p_3)^2} \\
& \times\left[\langle p_4p_1\rangle^*\langle k_np_3\rangle\langle k_lk_n\rangle^* + \frac{\langle p_4|P_2-P_1|p_3\rangle\langle k_l|K_n+P_3|p_2\rangle}{\langle p_2p_1\rangle}\right] \\
& + \text{c.c.}|_{(k_n\leftrightarrow k_l, p_3\leftrightarrow p_4, p_2\leftrightarrow p_1)} , \qquad (8.2.7c)\\
A^+_{\mathrm{ggdu}}(-,+,-,+) = {}& \\
& \frac{1}{(p_1+p_2)^2}\frac{1}{\langle p_3p_1\rangle^*\langle p_4p_2\rangle}\Big\{\frac{\langle k_np_3\rangle}{(q_\mathrm{W}+p_3)^2}\Big[\langle p_3p_2\rangle^*\Big\{\big(2\,(p_1+p_2)^2-(p_1+p_4)^2\big) \\
& \times\langle k_l|P_3+K_n|p_1\rangle + \langle p_2|P_4|p_1\rangle\langle k_l|P_3+K_n|p_2\rangle + 2\,\langle p_4|P_2|p_1\rangle\langle k_l|P_3+K_n|p_4\rangle\Big\} \\
& + \langle p_2|P_1|p_4\rangle\langle p_3p_4\rangle^*\langle k_l|K_n+P_3|p_4\rangle\Big] - (p_1+p_2)^2\langle k_lp_2\rangle^*\langle k_np_1\rangle\Big\} \\
& + \text{c.c.}|_{(k_n\leftrightarrow k_l, p_3\leftrightarrow p_4, p_2\leftrightarrow p_1)} , \qquad (8.2.7d)\\
B^+_{\mathrm{ggdu}}(\sigma_1,\sigma_2,-,+) = {}& A^+_{\mathrm{ggdu}}(\sigma_2,\sigma_1,-,+)|_{p_1\leftrightarrow p_2} , \qquad (8.2.7e)
\end{aligned}$$

where c.c. denotes the complex conjugate of the corresponding expression.

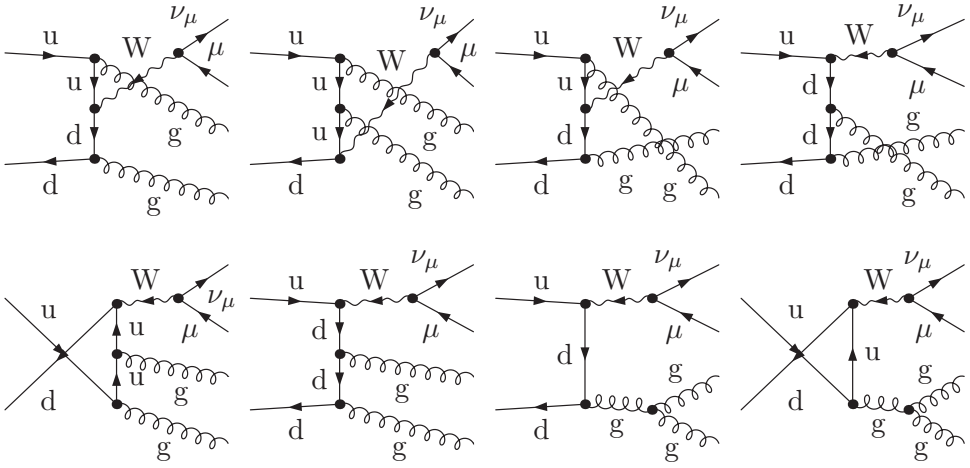

Figure 8.2: Real QCD corrections to the process (6.1.1) via radiation of one additional gluon.

8.2.2 Computation of colour- and CKM structures

In order to calculate the squared matrix elements of the generic processes (8.2.1), care has to be taken when working out the different contributing colour structures. We point out that the construction of the various physical processes from the generic amplitudes via crossing does not change the colour and CKM structure of the underlying mathematical expressions, but it will just modify the kinematics and the helicity structure in A and B. Thus, we can find general expressions for the squared and colour-summed amplitudes for all contributing subprocesses. For the six-fermion processes we find

$$\sum_{\text{col}} \left| \mathcal{T}^{\text{R,QCD}}_{0\to \text{W}+\bar{\text{d}}_i \text{d}_j \text{d}_l \bar{\text{u}}_k} \right|^2 = \frac{4\,(4\pi)^4 \alpha_\text{s}^2 \alpha^2}{|s_\text{W}^2|^2 |(q_\text{W}^2 - \mu_\text{W}^2)|^2} \times \big(\delta_{ij}\, |V_{kl}|^2\, C_{4q}^{AA}\, |A_{\text{dddu}}|^2 + \delta_{il}\, |V_{kj}|^2\, C_{4q}^{BB}\, |B_{\text{dddu}}|^2 + 2\, \delta_{ij}\, \delta_{il}\, |V_{kl}|^2\, C_{4q}^{AB}\, \text{Re}\left[A_{\text{dddu}} B^*_{\text{dddu}} \right] \big)\,, \tag{8.2.8a}$$

$$\sum_{\text{col}} \left| \mathcal{T}^{\text{R,QCD}}_{0\to \text{W}+\bar{\text{u}}_i \text{u}_j \text{d}_l \bar{\text{u}}_k} \right|^2 = \frac{4\,(4\pi)^4 \alpha_\text{s}^2 \alpha^2}{|s_\text{W}^2|^2 |(q_\text{W}^2 - \mu_\text{W}^2)|^2} \times \big(\delta_{ij}\, |V_{kl}|^2\, C_{4q}^{AA}\, |A_{\text{uudu}}|^2 + \delta_{jk}\, |V_{il}|^2\, C_{4q}^{BB}\, |B_{\text{uudu}}|^2 + 2\, \delta_{ij}\, \delta_{kj}\, |V_{il}|^2\, C_{4q}^{AB}\, \text{Re}\left[A_{\text{uudu}} B^*_{\text{uudu}} \right] \big)\,, \tag{8.2.8b}$$

and for the processes involving two gluons, we obtain

$$\sum_{\text{col}} \left| \mathcal{T}^{\text{R,QCD}}_{0\to \text{W}+\text{gg}\text{d}_j \bar{\text{u}}_i} \right|^2 = \frac{(4\pi)^4 \alpha_\text{s}^2 \alpha^2}{|s_\text{W}^2|^2 |(q_\text{W}^2 - \mu_\text{W}^2)|^2}\, |V_{ij}|^2 \left(C_{\text{gg}}^{AA}\, |A_{\text{ggdu}}|^2 + C_{\text{gg}}^{BB}\, |B_{\text{ggdu}}|^2 + 2\, C_{\text{gg}}^{AB}\, \text{Re}\left[A_{\text{ggdu}} B^*_{\text{ggdu}} \right] \right). \tag{8.2.9}$$

In (8.2.8) and (8.2.9), we have omitted the helicity dependences in the notation. The different colour factors are given by

$$C_{4q}^{AA} = T^c_{mn} T^c_{qp} T^d_{nm} T^d_{pq} = [\text{Tr}(T^c T^d)]^2 = (N_\text{C}^2 - 1)\, T_\text{F}^2\,, \tag{8.2.10a}$$

$$C_{4q}^{BB} = T^c_{mn} T^c_{qp} T^d_{nm} T^d_{pq} = [\mathrm{Tr}(T^c T^d)]^2 = (N_\mathrm{C}^2 - 1)\, T_\mathrm{F}^2\,, \tag{8.2.10b}$$

$$C_{4q}^{AB} = T^c_{mn} T^c_{qp} T^d_{pm} T^d_{nq} = \mathrm{Tr}(T^d T^c T^d T^c) = N_\mathrm{C}\, C_\mathrm{F} \left(C_\mathrm{F} - \frac{1}{2} C_\mathrm{A} \right)\,, \tag{8.2.10c}$$

for the four-quark processes, where we assume summation over pairs of identical colour indices. For the colour factors in (8.2.9), we find

$$C_{\mathrm{gg}}^{AA} = \mathrm{Tr}(T^a T^b T^b T^a) = 3 C_\mathrm{F}^2\,, \tag{8.2.11a}$$

$$C_{\mathrm{gg}}^{BB} = \mathrm{Tr}(T^a T^b T^b T^a) = 3 C_\mathrm{F}^2\,, \tag{8.2.11b}$$

$$C_{\mathrm{gg}}^{AB} = \mathrm{Tr}(T^a T^b T^a T^b) = N_\mathrm{C}\, C_\mathrm{F} \left(C_\mathrm{F} - \frac{1}{2} C_\mathrm{A} \right)\,. \tag{8.2.11c}$$

In the numerical evaluation, we have applied the following strategy: For every given subprocess we calculate the expressions $|A|^2$, $|B|^2$, and AB^*, using the adequate crossing prescriptions, and carry out the sum over polarizations. Then we perform a numerical summation over the contributing quark flavours i, j, k, l. Of course, at least the summation of the FS flavours could easily be done analytically, exploiting the unitarity of the CKM matrix (2.1.26). We have tried this approach, but the gain in runtime was negligible. Moreover, doing the flavour summation numerically comprises the important benefit that the complete calculation can be carried out using the general master formulae (8.2.8) and (8.2.9), respectively.

The full squared averaged amplitude for any given partonic channel can be written as

$$\overline{\left| \mathcal{M}^{\mathrm{R,QCD}}_{a_i b_j \to l\nu_l + c_k + d_l} \right|^2} = \frac{1}{F_{ab}} \sum_{\tau_l} \sum_{\sigma_1,\ldots,\sigma_4} \sum_{\mathrm{col}} \left| \mathcal{T}^{\mathrm{R,QCD}}_{0 \to \mathrm{W} + a_i b_j c_l d_k} \right|^2_{a,\,b \text{ crossed into IS}}\,, \tag{8.2.12}$$

where we have to choose the adequate master amplitude from (8.2.8) or (8.2.9). We assume that all partons a, b, c, and d carry flavour indices, which are suppressed in case of gluons. For the relevant averaging factors we find

$$F_{qq} = F_{q\bar{q}} = F_{\bar{q}\bar{q}} = 36\,, \quad F_{qg} = F_{\bar{q}g} = 96\,, \quad F_{\mathrm{gg}} = 256\,. \tag{8.2.13}$$

According to (2.3.4), the corresponding partonic cross sections for the real QCD corrections are then given by

$$\hat{\sigma}^{\mathrm{R,QCD}}_{a_i b_j \to l\nu_l + c_k d_l}(p_a, p_b) = \frac{1}{2\hat{s}} \int \mathrm{d}\Phi_{(l\nu_l + c + d)}\, \frac{1}{1 + \delta_{c_k d_l}}\, \overline{\left| \mathcal{M}^{\mathrm{R,QCD}}_{a_i b_j \to l\nu_l + c_k + d_l} \right|^2}\,, \tag{8.2.14}$$

where the construction of the phase-space integral $\int \mathrm{d}\Phi_{(l\nu_l + c + d)}$ will be discussed in Section 8.4.

8.3 Interferences between EW and QCD diagrams

8.3.1 General structure of the contributions

The purely EW diagrams that contribute to the generic channel (8.2.1a) at the order $\mathcal{O}(\alpha^3)$ (see Section 6.3.3) can be decomposed according to their flavour and colour structure as

$$\mathcal{T}^{\mathrm{R,EW}}_{0 \to \mathrm{W} + \bar{\mathrm{d}}_i \mathrm{d}_j \mathrm{d}_l \bar{\mathrm{u}}_k} = (\delta_{ij} V^*_{kl})\, (\delta_{nm} \delta_{qp})\, T^{A,\mathrm{EW}}_{\mathrm{dddu}} + (\delta_{il} V^*_{kj})\, (\delta_{nq} \delta_{mp})\, T^{B,\mathrm{EW}}_{\mathrm{dddu}}\,, \tag{8.3.1}$$

where we have defined $T^{A,\mathrm{EW}}_{\mathrm{dddu}}$ and $T^{B,\mathrm{EW}}_{\mathrm{dddu}}$ in analogy to A_{dddu} and B_{dddu} in (8.2.2a). Rewriting the corresponding QCD amplitude as

$$\mathcal{T}^{\mathrm{R,QCD}}_{0\to \mathrm{W}+\bar{\mathrm{d}}_i \mathrm{d}_j \mathrm{d}_l \bar{\mathrm{u}}_k} = (\delta_{ij} V^*_{kl}) \sum_a (T^a_{nm} T^a_{pq})\, T^{A,\mathrm{QCD}}_{\mathrm{dddu}} + (\delta_{il} V^*_{kj}) \sum_a (T^a_{pm} T^a_{nq})\, T^{B,\mathrm{QCD}}_{\mathrm{dddu}}\,, \tag{8.3.2}$$

we find that the interference (IF) term

$$\left|\mathcal{T}^{\mathrm{R,IF}}_{0\to \mathrm{W}+\bar{\mathrm{d}}_i \mathrm{d}_j \mathrm{d}_l \bar{\mathrm{u}}_k}\right|^2 = 2\,\mathrm{Re}\left[\mathcal{T}^{\mathrm{R,EW}}_{0\to \mathrm{W}+\bar{\mathrm{d}}_i \mathrm{d}_j \mathrm{d}_l \bar{\mathrm{u}}_k} \left(\mathcal{T}^{\mathrm{R,QCD}}_{0\to \mathrm{W}+\bar{\mathrm{d}}_i \mathrm{d}_j \mathrm{d}_l \bar{\mathrm{u}}_k}\right)^*\right] \tag{8.3.3}$$

contributes at the same order $\mathcal{O}(\alpha^3\alpha_{\mathrm{s}})$ as the genuine EW corrections and thus has to be taken into account within a complete fixed-order calculation.

Looking carefully at the colour structure of (8.3.3), it turns out that the terms with identical flavour structure $\{i,j,k,l\}$ in $\mathcal{T}^{\mathrm{R,EW}}$ and $\mathcal{T}^{\mathrm{R,QCD}}$ vanish, since they include the colour factor $\delta_{mn} T^a_{mn}\, \delta_{qp} T^a_{qp} = [\mathrm{Tr}(T^a)]^2 = 0$, when we sum over colours of the external quarks. Only the terms with different flavour structure survive, yielding the colour factor $\delta_{mn} T^a_{pm} \delta_{pq} T^a_{nq} = \mathrm{Tr}(T^a T^a) = 8\,T_{\mathrm{F}}$. Therefore, we can express the squared colour-summed amplitude (8.3.3) according to

$$\begin{aligned}
&\sum_{\mathrm{col}} \left|\mathcal{T}^{\mathrm{R,IF}}_{0\to \mathrm{W}+\bar{\mathrm{d}}_i \mathrm{d}_j \mathrm{d}_l \bar{\mathrm{u}}_k}\right|^2 \\
&\quad = (8\,T_{\mathrm{F}})\,(\delta_{ij}\delta_{il}|V_{kl}|^2)\,2\,\mathrm{Re}\left[T^{A,\mathrm{EW}}_{\mathrm{dddu}}\left(T^{B,\mathrm{QCD}}_{\mathrm{dddu}}\right)^* + T^{B,\mathrm{EW}}_{\mathrm{dddu}}\left(T^{A,\mathrm{QCD}}_{\mathrm{dddu}}\right)^*\right].
\end{aligned} \tag{8.3.4}$$

8.3.2 Explicit analytical results

For the purely EW contributions, the non-vanishing helicity structures $T^{A,\mathrm{EW}}_{\mathrm{dddu}}$ can be written as

$$T^{A,\mathrm{EW}}_{\mathrm{dddu}} = T^{A,\mathrm{EW}}_{\mathrm{W^+W^-}} + \sum_{V=\gamma,\mathrm{Z}} \left(T^{A,\mathrm{EW}}_{V\mathrm{W^+}} + T^{A,\mathrm{EW}}_{V\mathrm{W^-}} + T^{A,\mathrm{EW}}_{V\mathrm{W^+W^-}}\right), \tag{8.3.5}$$

where the subscripts denote the different vector bosons that appear in the propagators of the underlying diagrams. The subamplitudes that are needed for the calculation explicitly read

$$\begin{aligned}
T^{A,\mathrm{EW}}_{V\mathrm{W^+}}(+,-,-,+) &= \frac{2\,e^4}{s^2_{\mathrm{W}}} \frac{C^-_{V\mathrm{d}\bar{\mathrm{d}}}}{[(p_1+p_2)^2-\mu_V^2](q^2_{\mathrm{W}}-\mu^2_{\mathrm{W}})} \\
&\quad \times \left[C^-_{V\mathrm{u}\bar{\mathrm{u}}} \frac{\langle k_n p_3\rangle}{(q_{\mathrm{W}}+p_3)^2} \langle k_l|K_n+P_3|p_2\rangle \langle p_4 p_1\rangle^* \right. \\
&\qquad \left. - C^-_{V\mathrm{d}\bar{\mathrm{d}}} \frac{\langle k_l p_4\rangle^*}{(q_{\mathrm{W}}+p_4)^2} \langle p_1|K_l+P_4|k_n\rangle \langle p_3 p_2\rangle\right], \\
T^{A,\mathrm{EW}}_{V\mathrm{W^+}}(-,+,-,+) &= \frac{2\,e^4}{s^2_{\mathrm{W}}} \frac{C^+_{V\mathrm{d}\bar{\mathrm{d}}}}{[(p_1+p_2)^2-\mu_V^2](q^2_{\mathrm{W}}-\mu^2_{\mathrm{W}})} \\
&\quad \times \left[C^-_{V\mathrm{u}\bar{\mathrm{u}}} \frac{\langle k_n p_3\rangle}{(q_{\mathrm{W}}+p_3)^2} \langle k_l|K_n+P_3|p_1\rangle \langle p_4 p_2\rangle^* \right. \\
&\qquad \left. - C^-_{V\mathrm{d}\bar{\mathrm{d}}} \frac{\langle k_l p_4\rangle^*}{(q_{\mathrm{W}}+p_4)^2} \langle p_2|K_l+P_4|k_n\rangle \langle p_3 p_1\rangle\right],
\end{aligned} \tag{8.3.6a}$$

$$T^{A,\mathrm{EW}}_{\gamma\mathrm{W}^-}(+,-,-,+) = \frac{2\,e^4}{s^2_\mathrm{W}}\,C_{\gamma\mathrm{d}\bar{\mathrm{d}}}\,C_{\gamma l^- l^+}\,\frac{\langle p_3 k_n\rangle\langle p_4|k_n+p_3|p_2\rangle\langle k_l p_1\rangle^*}{(p_1+p_2)^2[(p_3+p_4)^2-\mu^2_\mathrm{W}](k_n+p_3+p_4)^2}\,,$$
$$T^{A,\mathrm{EW}}_{\gamma\mathrm{W}^-}(-,+,-,+) = \frac{2\,e^4}{s^2_\mathrm{W}}\,C_{\gamma\mathrm{d}\bar{\mathrm{d}}}\,C_{\gamma l^- l^+}\,\frac{\langle p_3 k_n\rangle\langle p_4|k_n+p_3|p_1\rangle\langle k_l p_2\rangle^*}{(p_1+p_2)^2[(p_3+p_4)^2-\mu^2_\mathrm{W}](k_n+p_3+p_4)^2}\,, \tag{8.3.6b}$$

$$\begin{aligned}T^{A,\mathrm{EW}}_{\mathrm{ZW}^-}(+,-,-,+) &= \frac{2\,e^4}{s^2_\mathrm{W}}\,\frac{C^-_{\mathrm{Zd}\bar{\mathrm{d}}}}{[(p_1+p_2)^2-\mu^2_\mathrm{Z}][(p_3+p_4)^2-\mu^2_\mathrm{W}]}\\ &\times\left[C^-_{\mathrm{Z}l^-l^+}\,\frac{\langle p_3 k_n\rangle}{(k_n+p_3+p_4)^2}\langle p_4|K_n+P_3|p_2\rangle\langle k_l p_1\rangle^*\right.\\ &\left.-\,C^-_{\mathrm{Z}\nu_l\bar{\nu}_l}\,\frac{\langle p_4 k_l\rangle^*}{(k_l+p_3+p_4)^2}\langle p_1|K_l+P_4|p_3\rangle\langle k_n p_2\rangle\right],\\ T^{A,\mathrm{EW}}_{\mathrm{ZW}^-}(-,+,-,+) &= \frac{2\,e^4}{s^2_\mathrm{W}}\,\frac{C^+_{\mathrm{Zd}\bar{\mathrm{d}}}}{[(p_1+p_2)^2-\mu^2_\mathrm{Z}][(p_3+p_4)^2-\mu^2_\mathrm{W}]}\\ &\times\left[C^-_{\mathrm{Z}l^-l^+}\,\frac{\langle p_3 k_n\rangle}{(k_n+p_3+p_4)^2}\langle p_4|K_n+P_3|p_1\rangle\langle k_l p_2\rangle^*\right.\\ &\left.-\,C^-_{\mathrm{Z}\nu_l\bar{\nu}_l}\,\frac{\langle p_4 k_l\rangle^*}{(k_l+p_3+p_4)^2}\langle p_2|K_l+P_4|p_3\rangle\langle k_n p_1\rangle\right],\end{aligned} \tag{8.3.6c}$$

$$\begin{aligned}T^{A,\mathrm{EW}}_{V\mathrm{W}^+\mathrm{W}^-}(+,-,-,+) &= -\,\frac{2e^4}{s^2_\mathrm{W}}\,\frac{C_{V\mathrm{W}^+\mathrm{W}^-}\,C^-_{V\mathrm{d}\bar{\mathrm{d}}}}{[(p_1+p_2)^2-\mu^2_V](q^2_\mathrm{W}-\mu^2_\mathrm{W})[(p_3+p_4)^2-\mu^2_\mathrm{W}]}\\ &\times\left[\langle p_1 p_4\rangle^*\langle p_2 p_3\rangle\langle k_l|P_1+P_2|k_n\rangle+\langle p_4 k_l\rangle^*\langle p_3 k_n\rangle\langle p_1|P_3+P_4|p_2\rangle\right.\\ &\left.+\,\langle k_l p_1\rangle^*\langle k_n p_2\rangle\langle p_4|K_l+K_n|p_3\rangle\right],\end{aligned}$$

$$T^{A,\mathrm{EW}}_{V\mathrm{W}^+\mathrm{W}^-}(-,+,-,+) = 0\,, \tag{8.3.6d}$$

$$T^{A,\mathrm{EW}}_{\mathrm{W}^+\mathrm{W}^-}(+,-,-,+) = -\,\frac{2\,e^4}{s^2_\mathrm{W}}C^-_{\mathrm{W}^-\bar{\mathrm{d}}\mathrm{u}}\,C^-_{\mathrm{W}^+\bar{\mathrm{u}}\mathrm{d}}\,\frac{\langle p_4 p_1\rangle^*\langle k_n p_2\rangle\langle k_l|K_n+P_2|p_3\rangle}{(q_\mathrm{W}+p_2)^2(q^2_\mathrm{W}-\mu^2_\mathrm{W})[(p_3+p_4)^2-\mu^2_\mathrm{W}]}\,,$$
$$T^{A,\mathrm{EW}}_{\mathrm{W}^+\mathrm{W}^-}(-,+,-,+) = 0\,, \tag{8.3.6e}$$

where we have adopted the helicity assignment $T^{A,\mathrm{EW}}_{\ldots}(\sigma_1,\sigma_2,\sigma_3,\sigma_4)$. The contributions $T^{B,\mathrm{EW}}_{\ldots}(\sigma_1,\sigma_2,\sigma_3,\sigma_4)$ emerge from (8.3.6) via

$$T^{B,\mathrm{EW}}_{\ldots}(\sigma_1,\sigma_2,\sigma_3,\sigma_4) = (-1)\cdot T^{A,\mathrm{EW}}_{\ldots}(\sigma_1,\sigma_3,\sigma_2,\sigma_4)\Big|_{p_2\leftrightarrow p_3}\,. \tag{8.3.7}$$

The IF contributions for the generic process (8.2.1b) can be deduced in a similar way:

The amplitude for the purely weak contributions reads

$$\mathcal{T}^{\mathrm{R,EW}}_{0\to\mathrm{W}+\bar{\mathrm{u}}_i\mathrm{u}_j\mathrm{d}_l\bar{\mathrm{u}}_k} = (\delta_{ij}V^*_{kl})\,(\delta_{nm}\delta_{qp})\,T^{A,\mathrm{EW}}_{\mathrm{uudu}} + (\delta_{jk}V^*_{il})\,(\delta_{nq}\delta_{mp})\,T^{B,\mathrm{EW}}_{\mathrm{uudu}}\,, \tag{8.3.8}$$

and the QCD amplitude can be written as

$$\mathcal{T}^{\mathrm{R,QCD}}_{0\to\mathrm{W}+\bar{\mathrm{u}}_i\mathrm{u}_j\mathrm{d}_l\bar{\mathrm{u}}_k} = (\delta_{ij}V^*_{kl})\sum_a(T^a_{nm}T^a_{pq})\,T^{A,\mathrm{QCD}}_{\mathrm{uudu}} + (\delta_{jk}V^*_{il})\sum_a(T^a_{pm}T^a_{nq})\,T^{B,\mathrm{QCD}}_{\mathrm{uudu}}\,. \tag{8.3.9}$$

Accordingly, the interference term is given by the expression

$$\begin{aligned}
&\sum_{\text{col}} \left| \mathcal{T}^{\text{R,IF}}_{0\to \text{W}+\bar{\text{u}}_i \text{u}_j \text{d}_l \bar{\text{u}}_k} \right|^2 \\
&\quad = (8\,T_\text{F})\,(\delta_{ij}\delta_{jk}|V_{kl}|^2)\,2\,\text{Re}\left[T^{A,\text{EW}}_{\text{uudu}} \left(T^{B,\text{QCD}}_{\text{uudu}} \right)^* + T^{B,\text{EW}}_{\text{uudu}} \left(T^{A,\text{QCD}}_{\text{uudu}} \right)^* \right] , \quad (8.3.10)
\end{aligned}$$

and the non-vanishing helicity amplitudes $T^{A,\text{EW}}_{\text{uudu}}$ are decomposed according to

$$T^{A,\text{EW}}_{\text{uudu}} = K^{A,\text{EW}}_{\text{W}^+\text{W}^-} + \sum_{V=\gamma,\text{Z}} \left(K^{A,\text{EW}}_{V\text{W}^+} + K^{A,\text{EW}}_{V\text{W}^-} + K^{A,\text{EW}}_{V\text{W}^+\text{W}^-} \right) , \quad (8.3.11)$$

with the explicit expressions

$$\begin{aligned}
K^{A,\text{EW}}_{V\text{W}^+}(+,-,-,+) &= \frac{2\,e^4}{s^2_\text{W}} \frac{C^-_{V\text{u}\bar{\text{u}}}}{[(p_1+p_2)^2-\mu^2_V](q^2_\text{W}-\mu^2_\text{W})} \\
&\quad \times \left[C^-_{V\text{u}\bar{\text{u}}} \frac{\langle k_n p_3\rangle}{(q_\text{W}+p_3)^2} \langle k_l|K_n+P_3|p_2\rangle \langle p_4 p_1\rangle^* \right. \\
&\quad \left. - C^-_{V\text{d}\bar{\text{d}}} \frac{\langle k_l p_4\rangle^*}{(q_\text{W}+p_4)^2} \langle p_1|K_l+P_4|k_n\rangle \langle p_3 p_2\rangle \right] , \\
K^{A,\text{EW}}_{V\text{W}^+}(-,+,-,+) &= \frac{2\,e^4}{s^2_\text{W}} \frac{C^+_{V\text{u}\bar{\text{u}}}}{[(p_1+p_2)^2-\mu^2_V](q^2_\text{W}-\mu^2_\text{W})} \\
&\quad \times \left[C^-_{V\text{u}\bar{\text{u}}} \frac{\langle k_n p_3\rangle}{(q_\text{W}+p_3)^2} \langle k_l|K_n+P_3|p_1\rangle \langle p_4 p_2\rangle^* \right. \\
&\quad \left. - C^-_{V\text{d}\bar{\text{d}}} \frac{\langle k_l p_4\rangle^*}{(q_\text{W}+p_4)^2} \langle p_2|K_l+P_4|k_n\rangle \langle p_3 p_1\rangle \right] , \quad (8.3.12a) \\
K^{A,\text{EW}}_{\gamma\text{W}^-}(+,-,-,+) &= \frac{2\,e^4}{s^2_\text{W}}\, C_{\gamma\text{u}\bar{\text{u}}}\, C_{\gamma l^- l^+} \frac{\langle p_3 k_n\rangle \langle p_4|k_n+p_3|p_2\rangle \langle k_l p_1\rangle^*}{(p_1+p_2)^2[(p_3+p_4)^2-\mu^2_\text{W}](k_n+p_3+p_4)^2} , \\
K^{A,\text{EW}}_{\gamma\text{W}^-}(-,+,-,+) &= \frac{2\,e^4}{s^2_\text{W}}\, C_{\gamma\text{u}\bar{\text{u}}}\, C_{\gamma l^- l^+} \frac{\langle p_3 k_n\rangle \langle p_4|k_n+p_3|p_1\rangle \langle k_l p_2\rangle^*}{(p_1+p_2)^2[(p_3+p_4)^2-\mu^2_\text{W}](k_n+p_3+p_4)^2} , \quad (8.3.12b) \\
K^{A,\text{EW}}_{\text{Z}\text{W}^-}(+,-,-,+) &= \frac{2\,e^4}{s^2_\text{W}} \frac{C^-_{\text{Z}\text{u}\bar{\text{u}}}}{[(p_1+p_2)^2-\mu^2_\text{Z}][(p_3+p_4)^2-\mu^2_\text{W}]} \\
&\quad \times \left[C^-_{\text{Z}l^- l^+} \frac{\langle p_3 k_n\rangle}{(k_n+p_3+p_4)^2} \langle p_4|K_n+P_3|p_2\rangle \langle k_l p_1\rangle^* \right. \\
&\quad \left. - C^-_{\text{Z}\nu_l\bar{\nu}_l} \frac{\langle p_4 k_l\rangle^*}{(k_l+p_3+p_4)^2} \langle p_1|K_l+P_4|p_3\rangle \langle k_n p_2\rangle \right] , \\
K^{A,\text{EW}}_{\text{Z}\text{W}^-}(-,+,-,+) &= \frac{2\,e^4}{s^2_\text{W}} \frac{C^+_{\text{Z}\text{u}\bar{\text{u}}}}{[(p_1+p_2)^2-\mu^2_\text{Z}][(p_3+p_4)^2-\mu^2_\text{W}]} \\
&\quad \times \left[C^-_{\text{Z}l^- l^+} \frac{\langle p_3 k_n\rangle}{(k_n+p_3+p_4)^2} \langle p_4|K_n+P_3|p_1\rangle \langle k_l p_2\rangle^* \right. \\
&\quad \left. - C^-_{\text{Z}\nu_l\bar{\nu}_l} \frac{\langle p_4 k_l\rangle^*}{(k_l+p_3+p_4)^2} \langle p_2|K_l+P_4|p_3\rangle \langle k_n p_1\rangle \right] , \quad (8.3.12c)
\end{aligned}$$

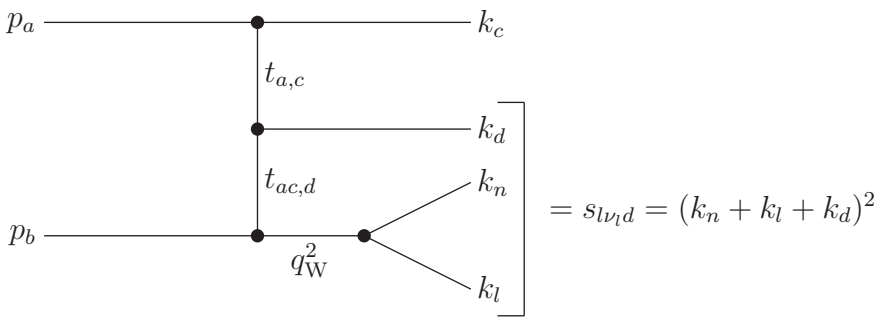

Figure 8.3: Topology for the phase-space construction within the real corrections.

$$
\begin{aligned}
K^{A,\mathrm{EW}}_{V\mathrm{W^+W^-}}(+,-,-,+) = & -\frac{2e^4}{s^2_{\mathrm{W}}}\frac{C_{V\mathrm{W^+W^-}}\; C^{-}_{V\mathrm{u\bar{u}}}}{[(p_1+p_2)^2-\mu^2_V](q^2_{\mathrm{W}}-\mu^2_{\mathrm{W}})[(p_3+p_4)^2-\mu^2_{\mathrm{W}}]} \\
& \times \Big[\langle p_1 p_4\rangle^*\langle p_2 p_3\rangle\langle k_l|P_1+P_2|k_n\rangle + \langle p_4 k_l\rangle^*\langle p_3 k_n\rangle\langle p_1|P_3+P_4|p_2\rangle \\
& \quad + \langle k_l p_1\rangle^*\langle k_n p_2\rangle\langle p_4|K_l+K_n|p_3\rangle\Big]\,, \\
K^{A,\mathrm{EW}}_{V\mathrm{W^+W^-}}(-,+,-,+) = & \; 0\,, \qquad (8.3.12\mathrm{d}) \\
K^{A,\mathrm{EW}}_{\mathrm{W^+W^-}}(+,-,-,+) = & -\frac{2\,e^4}{s^2_{\mathrm{W}}} C^{-}_{\mathrm{W^-\bar{d}u}}\, C^{-}_{\mathrm{W^+\bar{u}d}}\, \frac{\langle k_l p_1\rangle^*\langle p_3 p_2\rangle\langle p_4|p_3+P_2|k_n\rangle}{(q_{\mathrm{W}}+p_1)^2(q^2_{\mathrm{W}}-\mu^2_{\mathrm{W}})[(p_3+p_4)^2-\mu^2_{\mathrm{W}}]}\,, \\
K^{A,\mathrm{EW}}_{\mathrm{W^+W^-}}(-,+,-,+) = & \; 0\,, \qquad (8.3.12\mathrm{e})
\end{aligned}
$$

where we again use the helicity assignment $K^{A,\mathrm{EW}}_{\dots}(\sigma_1,\sigma_2,\sigma_3,\sigma_4)$. Finally, we obtain the contributions $K^{B,\mathrm{EW}}_{\dots}(\sigma_1,\sigma_2,\sigma_3,\sigma_4)$ from (8.3.12) via

$$
K^{B,\mathrm{EW}}_{\dots}(\sigma_1,\sigma_2,\sigma_3,\sigma_4) = (-1)\cdot K^{A,\mathrm{EW}}_{\dots}(\sigma_4,\sigma_2,\sigma_3,\sigma_1)\Big|_{p_1\leftrightarrow p_4}\,. \qquad (8.3.13)
$$

As for the real QCD corrections, the partonic cross sections $\hat{\sigma}^{\mathrm{R,IF}}_{a_i b_j\to l\nu_l + c_k d_l}(p_a,p_b)$ for the interference contributions is computed according to Eqs. (8.2.12) and (8.2.14), respectively.

8.4 Phase-space decomposition for real corrections

In this section we explicitly demonstrate the phase-space parametrization for a four-particle final state, using again the concepts that have been outlined in Appendix B. It turned out to be sufficient to use the same phase-space parametrization for the calculation of the EW corrections, the QCD corrections, and for the computation of the interference effects of EW and QCD diagrams. We consider the process

$$
a(p_a) + b(p_b) \to l^+(k_l) + \nu_l(k_n) + c(k_c) + d(k_d)\,, \qquad (8.4.1)
$$

where c and d denote two massless QCD partons or a parton and a photon, respectively. The phase-space parametrization we use for the calculation of the real corrections reads

$$\int \mathrm{d}\Phi_{(l\nu_l+c+d)}(p_a,p_b;k_l,k_n,k_c,k_d) = \frac{1}{(2\pi)^8}\int_0^{\hat{s}} \mathrm{d}q^2_{\mathrm{W}} \int_{q^2_{\mathrm{W}}}^{\hat{s}} \mathrm{d}s_{l\nu_l c} \times \int \mathrm{d}\Omega_p(p_a,p_b;k_c^2,s_{l\nu_l d}) \int \mathrm{d}\Omega_p(p_a-k_c,p_b;k_d^2,q^2_{\mathrm{W}}) \int \mathrm{d}\Omega_d(q^2_{\mathrm{W}};k_l^2,k_n^2)\,, \quad (8.4.2)$$

where we have defined the time-like invariant $s_{l\nu_l d} = (k_l + k_n + k_d)^2$. Our phase-space decomposition corresponds to the topology depicted in Fig. 8.3. As in the LO case, we list the explicit expressions for the contributing two-particle subspaces,

$$\begin{aligned}
\int \mathrm{d}\Omega_p(p_a,p_b;k_c^2,s_{l\nu_l d}) &= \frac{1}{4\hat{s}}\int_0^{2\pi}\mathrm{d}\phi_c \int_{t_{a,c}^{\min}}^{t_{a,c}^{\max}} \mathrm{d}t_{a,c}\,,\\
\int \mathrm{d}\Omega_p(p_a-k_c,p_b;k_d^2,q^2_{\mathrm{W}}) &= \frac{1}{s_{l\nu_l d}-t_{a,c}}\int_0^{2\pi}\mathrm{d}\phi_d^* \int_{t_{ac,d}^{\min}}^{t_{ac,d}^{\max}} \mathrm{d}t_{ac,d}\,,\\
\int \mathrm{d}\Omega_d(q^2_{\mathrm{W}};k_l^2,k_n^2) &= \frac{1}{8}\int_0^{2\pi}\mathrm{d}\phi_l^{\mathrm{W}} \int_{-1}^{1}\mathrm{d}\cos\theta_l^{\mathrm{W}}\,,
\end{aligned} \quad (8.4.3)$$

where ϕ_d^* is the polar angle of particle d in the rest frame of $p_{a,c} \equiv p_a - k_c$ and p_b. This frame is boosted and rotated with respect to the partonic cm frame. As in (7.3.3a), ϕ_l^{W} and θ_l^{W} span the solid angle of the lepton in the rest frame of the intermediate W boson. The integration boundaries for the t-channel like invariants $t_{a,c} = (p_a - k_c)^2$ and $t_{ac,d} = (p_a - k_c - k_d)^2$ are given by

$$\begin{aligned}
t_{a,c}^{\min} &= -\hat{s} + s_{l\nu_l d}\,, \quad t_{a,c}^{\max} = 0\,,\\
t_{ac,d}^{\min} &= t_{a,c}\frac{q^2_{\mathrm{W}}}{s_{l\nu_l d}}\,, \quad t_{ac,d}^{\max} = q^2_{\mathrm{W}} - s_{l\nu_l d} + t_{a,c}\,.
\end{aligned} \quad (8.4.4)$$

The four-momentum of parton c,

$$k_c^\mu = \frac{\hat{s}-s_{l\nu_l d}}{2\hat{s}}(1,\sin\theta_c\cos\phi_c,\sin\theta_c\sin\phi_c,\cos\theta_c)\,, \quad (8.4.5)$$

with

$$\theta_c = \arccos\left(1+\frac{2\,t_{a,c}}{\hat{s}-s_{l\nu_l d}}\right)\,, \quad (8.4.6)$$

is analogous to (7.3.4). As shown in Section 7.3, the leptonic four-momenta can be obtained from the four-momentum q^μ_{W} of the W boson (7.3.6) and the boost prescriptions (7.3.8). The construction of k_d^μ is more involved. We start with the expression

$$k_d^{*,\mu} = \frac{s_{l\nu_l d}-q^2_{\mathrm{W}}}{2\sqrt{s_{l\nu_l d}}}(1,\sin\theta_d^*\cos\phi_d^*,\sin\theta_d^*\sin\phi_d^*,\cos\theta_d^*) \quad (8.4.7)$$

in the rest frame of $p_{a,c}$ and p_b , where the polar angle θ_d^* is constructed from the integration variables via

$$\cos\theta_d^* = \frac{q^2_{\mathrm{W}}(s_{l\nu_l d}+q^2_{\mathrm{W}})(s_{l\nu_l d}+t_{a,c}) + s_{l\nu_l d}(t_{a,c}-2\,t_{ac,d}-s_{l\nu_l d})}{(q^2_{\mathrm{W}}-s_{l\nu_l d})(s_{l\nu_l d}-t_{a,c})}\,. \quad (8.4.8)$$

To obtain k_d in the partonic cm frame, we have to perform a Lorentz transformation consisting of a rotation and a subsequent boost as defined in (B.19),

$$k_d = \boldsymbol{B}\left[p^0_{a,c} + p^0_b, -(\mathbf{p}_{a,c} + \mathbf{p}_b)\right] \boldsymbol{R}(\tilde{\phi}_d, \cos\tilde{\theta}_d)\, k^*_d\,, \tag{8.4.9}$$

where the boost and rotation matrices are given by (B.16) and (B.20), respectively.

Again, we use a Breit–Wigner mapping as specified in Appendix B.3 to improve the performance of the q^2_{W}-integration in the numerical evaluation, while the remaining integrations in (8.4.2) are worked out applying linear mappings according to (B.23). In the calculation of the interference contributions discussed in Section 8.3, we also use a linear mapping for the q^2_{W}-integration, because these contributions do not contain Breit–Wigner resonances.

Chapter 9

Virtual corrections

In this chapter we discuss the calculation of the virtual EW and QCD corrections to the process $\mathrm{pp}/\mathrm{p\bar{p}} \to l\nu_l + \mathrm{jet} + X$.

9.1 General structure of one-loop corrections

Within the calculation of one-loop corrections to processes with P external legs various *N-point tensor integrals* of the tensor rank n arise that have the general structure

$$\begin{aligned} &T^N_{\mu_1,\dots,\mu_n}(p_1,\dots,p_{N-1},m_0,\dots,m_{N-1}) \\ &\quad = \frac{(2\pi\mu)^{4-d}}{\mathrm{i}\pi^2}\int \mathrm{d}^d q \frac{q_{\mu_1}\cdots q_{\mu_n}}{(q^2-m_0^2+\mathrm{i}\epsilon)\prod_{i=1}^{N-1}[(q+p_i)^2-m_i^2+\mathrm{i}\epsilon]}\,, \end{aligned} \tag{9.1.1}$$

where p_1, $p_2-p_1, p_3-p_2, \dots, -p_{N-1}$ can be identified with the incoming external momenta, $m_0, m_1, m_2, \dots, m_{N-1}$ are the masses of the internal propagators, and $N \leq P$ is valid. To allow for the regularization of UV divergences the tensor integrals are defined via their analytical continuation in d dimensions. To ensure that the integrals retain the correct mass dimension, the reference mass scale μ has been introduced in (9.1.1).

For a consistent treatment of a physical one-loop amplitude in d dimensions all algebraical operations acting on the tensor structure of the amplitude have to be carried out in d dimensions. Additionally, one needs a suitable extension of the Dirac algebra to d dimensions if fermions take part in the considered process. A detailed discussion on the algebraical properties of Lorentz- and Dirac structures in dimensional regularization can e.g. be found in Ref. [105].

The tensor integrals (9.1.1) can be decomposed in terms of a linear combination of all possible covariant structures that can be constructed from the metric and the external momenta, and the coefficient functions that arise during this decomposition into covariants are called tensor coefficients. Those tensor coefficients can be reduced to linear combinations of simpler scalar integrals $T_0^{\{N,N-1,\dots,2\}}$ by means of the Passarino–Veltman reduction algorithm [83]. The explicit expression for the N-point scalar integral is given by

$$\begin{aligned} &T^N_0(p_1,\dots,p_{N-1},m_0,\dots,m_{N-1}) \\ &\quad = \frac{(2\pi\mu)^{4-d}}{\mathrm{i}\pi^2}\int \mathrm{d}^d q \frac{1}{(q^2-m_0^2+\mathrm{i}\epsilon)\prod_{i=1}^{N-1}[(q+p_i)^2-m_i^2+\mathrm{i}\epsilon]}\,. \end{aligned} \tag{9.1.2}$$

For the 2-, 3-, 4- and 5-point functions that appear during the calculation of one-loop corrections the corresponding tensor integrals are conveniently labeled as $T^2 \to B$, $T^3 \to C$, $T^4 \to D$ and $T^5 \to E$ according to the first letters of the alphabet.

9.2 EW contributions

9.2.1 Reduction of 5-point tensor integrals

In scattering processes the external momenta in general become linearly dependent at the phase-space boundary. This means that the determinant $\det(Z)$ of the Gram matrix Z, which is constructed from the external momenta according to

$$Z = \begin{pmatrix} 2p_1p_1 & \dots & 2p_1p_{N-1} \\ \vdots & & \vdots \\ 2p_{N-1}p_1 & \dots & 2p_{N-1}p_{N-1} \end{pmatrix}, \tag{9.2.1}$$

exhibits a zero in these particular phase-space points. In the usual Passarino–Veltman [83] reduction algorithm inverse Gram determinants appear that will lead to zeroes in the denominator if the external momenta become linearly dependent. Although these zeroes are just artefacts of the underlying reduction algorithm and will be compensated by corresponding contributions in the numerator (resulting in a "0/0"-like situation), they might still spoil the accuracy of the numerical phase-space integration.

In $2 \to 2$ scattering processes the singular Gram determinants appear in isolated phase-space points in case of forward or backward scattering, i.e. if the polar angles of the scattered particles approach 0 or π. Thus, the corresponding numerical problems are usually negligible, and the Passarino–Veltman algorithm can safely be adopted.

By contrast, in case of $2 \to 3$ scattering processes the problems of vanishing Gram determinants are more severe and may even jeopardize the reliability of the numerical results. For this reason, we apply the reduction algorithms discussed in Sections 2 and 3 of [106] and in Section 6 of [107] which consistently avoid small Gram determinants within the direct reduction of 5-point tensor integrals to a linear combination of 4-point functions. It is always possible to express 5-point functions in terms of 4-point functions in four space-time dimension, because the integration momentum q can always be written in terms of the four independent external momenta.

9.2.2 Calculation of the EW one-loop corrections

The Feynman diagrams that have to be evaluated for the one-loop EW corrections to the partonic process (6.1.2) are summarized in Fig. 6.3, and the six contributing pentagon diagrams are depicted in Fig. 6.4. The corresponding one-loop amplitude

$$\mathcal{M}^1_{\mathrm{u}_i\mathrm{g}\to l^+\nu_l\mathrm{d}_j} = (V^*_{ij})\,\mathcal{M}^1_{\mathrm{ug}\to l^+\nu_l\mathrm{d}}\,, \tag{9.2.2}$$

where we have factorized the overall LO CKM dependence, can be expressed in terms of standard matrix elements and coefficients, which contain the tensor integrals (following the ideas described in the appendix of Ref. [108]). The tensor integrals are recursively

reduced to master integrals at the numerical level. Scalar and tensor 5-point integrals are directly expressed in terms of 4-point integrals as stated in the previous subsection. For the reduction of the 4- and 3-point tensor coefficients to scalar integrals we use the conventional Passarino–Veltman algorithm. This procedure turned out to be sufficient to allow for a proper numerical evaluation without visible problems due to small Gram determinants. However, one could still improve the numerical efficiency using the sophisticated methods that have been developed in [107] for the treatment of situation where small Gram determinants appear within the reduction of 4- and 3-point tensor integrals.

Since we work in the complex-mass scheme (see Section 2.2.4), all scalar integrals that result from the tensor-reduction procedure are evaluated for complex vector-boson masses, using the methods and results of Refs. [65, 90, 109]. Moreover, one has to compute many scalar integrals that carry IR-singular structures and therefore have to be expanded properly in the corresponding IR limits to allow for a numerically-stable evaluation.

For the recursive numerical reduction of tensor coefficients to scalar integrals, as well as for the analytical evaluation of the scalar integrals we use a *Fortran* implementation[1] of an integral library [110] that has been developed and optimized by Ansgar Denner and Stefan Dittmaier during the last years. This library supports the calculation of scalar integrals with complex vector-boson masses and the correct mass-singular behaviour of such scalar integrals that exhibit IR-singular structures.

The counterterm contribution to process (6.1.2) that emerges from the redefinition of the SM parameters within the complex-mass scheme is given by

$$\mathcal{M}^{\mathrm{CT,EW}}_{\mathrm{ug}\to l^+\nu_l\mathrm{d}} = \delta^{\mathrm{CT,EW}}_{\mathrm{ug}\to l^+\nu_l\mathrm{d}}\, \mathcal{M}^{0}_{\mathrm{ug}\to l^+\nu_l\mathrm{d}}\,, \tag{9.2.3}$$

and the prefactor—which is the same for all partonic processes (6.1.1) – (6.1.3)—explicitly reads

$$\delta^{\mathrm{CT,EW}}_{\mathrm{ug}\to l^+\nu_l\mathrm{d}} = \left[2\left(\delta\mathcal{Z}_e - \frac{1}{2}\Delta r + \frac{\delta s_\mathrm{W}}{s_\mathrm{W}}\right) - \frac{\delta\mu^2_\mathrm{W}}{q^2_\mathrm{W}-\mu^2_\mathrm{W}} + \frac{1}{2}\left(\delta\mathcal{Z}^\mathrm{L}_{u\bar{u}} + \delta\mathcal{Z}^\mathrm{L}_{d\bar{d}} + \mathcal{Z}^\mathrm{L}_{l\bar{l}} + \delta\mathcal{Z}^\mathrm{L}_{\nu_l\bar{\nu}_l}\right)\right], \tag{9.2.4}$$

where the formulae for the renormalization constants can be found in Section 2.2.4. This counterterm is the same for all contributing helicity amplitudes. The parameter Δr (see Eq. (5.3.3)) has to be calculated consequently using complex vector-boson masses. Now, the full renormalized one-loop contribution to the NLO amplitude can be written as

$$\left|\mathcal{M}^{\mathrm{V,EW}}_{\mathrm{ug}\to l^+\nu_l\mathrm{d}}\right|^2 = 2\,\mathrm{Re}\left[\left(\mathcal{M}^{1}_{\mathrm{ug}\to l^+\nu_l\mathrm{d}} + \mathcal{M}^{\mathrm{CT,EW}}_{\mathrm{u\bar{d}}\to l^+\nu_l\mathrm{g}}\right)\left(\mathcal{M}^{0}_{\mathrm{u\bar{d}}\to l^+\nu_l\mathrm{g}}\right)^*\right], \tag{9.2.5}$$

and the virtual corrections to the partonic cross section explicitly read

$$\hat{\sigma}^{\mathrm{V,EW}}_{\mathrm{u}_i\mathrm{g}\to l\nu_l+\mathrm{d}_j}(p_a,p_b) = |V_{ij}|^2\,\frac{1}{2\hat{s}}\int \mathrm{d}\Phi_{(l+\nu_l+\mathrm{d})}\,\overline{\left|\mathcal{M}^{\mathrm{V,EW}}_{\mathrm{ug}\to l^+\nu_l\mathrm{d}}\right|^2}. \tag{9.2.6}$$

[1] As mentioned in Section 6.1.3, in our team we have performed two completely independent calculations of the radiative corrections to W+jet production. Within these calculations, we have also used two different branches of this library, obtaining results that are in mutual agreement.

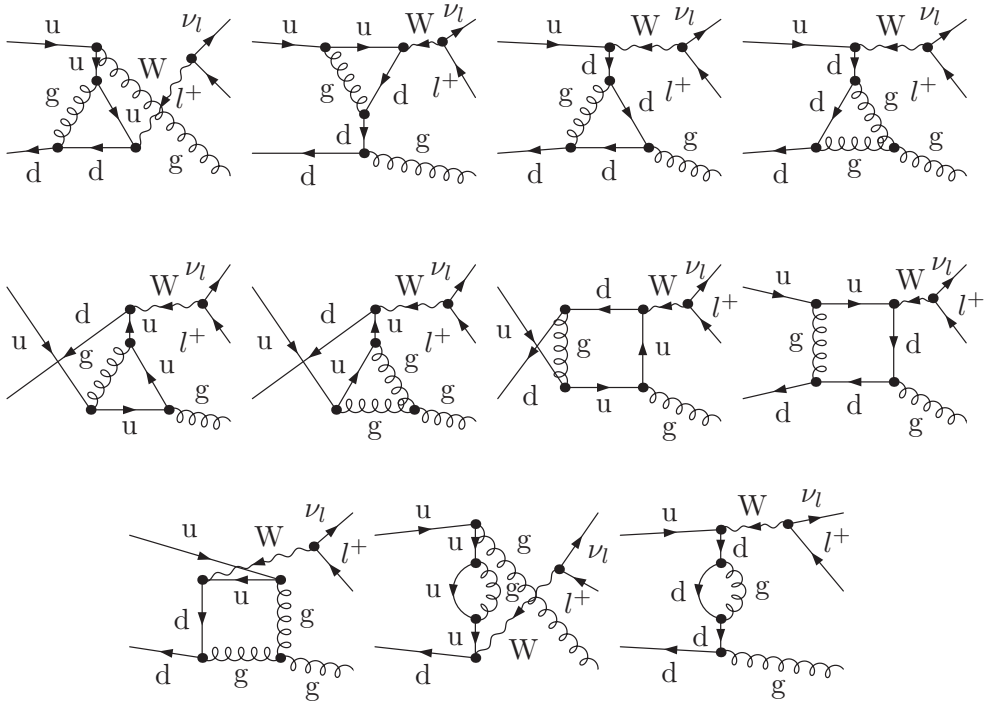

Figure 9.1: Virtual QCD corrections to the process (6.1.1).

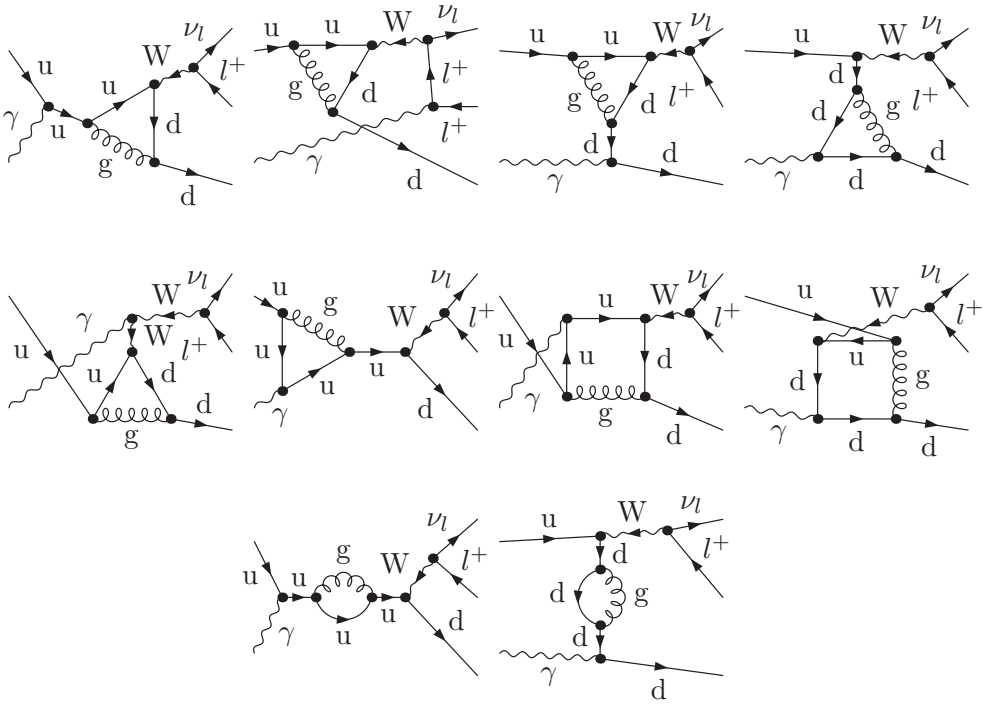

Figure 9.2: Virtual QCD corrections to the photon-induced process (6.1.5).

9.3 One-loop QCD corrections

The calculation of the virtual QCD corrections includes self-energies, triangles, and box diagrams. For completeness, we list all contributing Feynman diagrams for channel (6.1.1) in Fig. 9.1. The diagrams are consistently calculated in dimensional regularization, i.e. all light quark masses are exactly zero, and then reduced algebraically to scalar integrals according to the Passarino–Veltman algorithm, again using the library [110].

The counterterm that has to be added to the bare one-loop corrections for a proper cancellation of UV singularities reads

$$\mathcal{M}^{\mathrm{CT,QCD}}_{\mathrm{u\bar{d}}\to l^+\nu_l \mathrm{g}} = \delta^{\mathrm{CT,QCD}}_{\mathrm{u\bar{d}}\to l^+\nu_l \mathrm{g}}\, \mathcal{M}^{0}_{\mathrm{u\bar{d}}\to l^+\nu_l \mathrm{g}}\,, \tag{9.3.1}$$

with

$$\delta^{\mathrm{CT,QCD}}_{\mathrm{u\bar{d}}\to l^+\nu_l \mathrm{g}} = \frac{1}{2}\left(\delta Z_{\alpha_\mathrm{s}} + \delta Z_G + \delta Z_{u\bar{u}} + \delta Z_{d\bar{d}}\right)\,, \tag{9.3.2}$$

where we have adopted an on-shell renormalization prescription for the external fields of the QCD partons. We perform an $\overline{\mathrm{MS}}$ renormalization of the strong coupling constant, where the contribution from the massive top-quark loop in the gluon self-energy is subtracted at zero momentum transfer, so that the running of α_s is driven by the $n_f = 5$ light flavours. The renormalization constants for $n_f = 5$ massless quark flavours explicitly read

$$\delta Z_G = \frac{\alpha_\mathrm{s}}{\pi}\left(\frac{5}{4} - \frac{n_f}{6}\right) B_0(0,0,0) - \frac{\alpha_\mathrm{s}}{6\pi} B_0(0, m_\mathrm{t}^2, m_\mathrm{t}^2)\,, \tag{9.3.3}$$

$$\delta Z_{\alpha_\mathrm{s}} = -\frac{\alpha_\mathrm{s}}{\pi}\left(\frac{11}{4} - \frac{n_f}{6}\right)\left(\Delta^{\mathrm{UV}} + \ln\frac{\mu^2}{{\mu_\mathrm{R}}^2}\right) + \frac{\alpha_\mathrm{s}}{6\pi} B_0(0, m_\mathrm{t}^2, m_\mathrm{t}^2)\,, \tag{9.3.4}$$

$$\delta Z_{q\bar{q}} = -\frac{\alpha_\mathrm{s}}{3\pi} B_0(0,0,0)\,, \tag{9.3.5}$$

where

$$\Delta^{\mathrm{UV}} = \frac{1}{\epsilon}\frac{(4\pi)^\epsilon}{\Gamma(1-\epsilon)}\,, \quad d = 4 - 2\epsilon\,, \tag{9.3.6}$$

contains the UV divergence, and the contributing scalar 2-point integrals are given by

$$B_0(0, m_\mathrm{t}, m_\mathrm{t}) = \Delta^{\mathrm{UV}} - \ln\frac{m_\mathrm{t}^2}{\mu^2}\,, \quad B_0(0,0,0) = \Delta^{\mathrm{UV}} - \Delta_1^{\mathrm{IR}}\,, \tag{9.3.7}$$

with Δ_1^{IR} from (3.3.2), i.e. the scale-free integral $B_0(0,0,0)$ does not vanish if we use different regulators for IR and UV singularities. The prefactor (9.3.2) is the same for all partonic channels (6.1.1) – (6.1.3), and the contribution that has to be added to the one-loop QCD corrections to process (6.1.1) is given by $2\,\delta^{\mathrm{CT,QCD}}_{\mathrm{u\bar{d}}\to l^+\nu_l \mathrm{g}}\,|V_{ij}|^2\,\overline{|\mathcal{M}^{0}_{\mathrm{u\bar{d}}\to l^+\nu_l \mathrm{g}}|^2}$ when the cross section for the virtual corrections is computed according to (4.4.9). Note that we have evaluated the renormalization constants and the loop integrals using a real top-quark mass m_t.

9.4 One-loop QCD corrections to photon-induced processes

The loop diagrams that contribute to the process (6.1.5) are shown in Fig. 9.2. Since the corresponding amplitude does not contain the strong coupling constant, we simply have

to perform a renormalization of the external quark fields, resulting in the counterterm contribution

$$\mathcal{M}^{\mathrm{CT,QCD}}_{\mathrm{u}\gamma\to l\nu_l\mathrm{d}} = \frac{1}{2}\left(\delta Z_{u\bar{u}} + \delta Z_{d\bar{d}}\right)\mathcal{M}^{0}_{\mathrm{u}\gamma\to l\nu_l\mathrm{d}}\,, \tag{9.4.1}$$

that has to be added to the one-loop amplitude $\mathcal{M}^{1}_{\mathrm{u}\gamma\to l\nu_l\mathrm{d}}$.

Chapter 10

Hadronic cross sections

10.1 Definition of hadronic observables

10.1.1 Recombination

For the experimental identification of the process $\mathrm{pp}/\mathrm{p\bar{p}} \to \mathrm{W}^+ + \mathrm{jet} \to l^+\nu_l + \mathrm{jet} + X$ we recombine FS partons and photons to IR-safe pseudo-particles and impose a set of phase-space cuts as detailed now.

To define the recombination procedure and the separation cuts, we use the variable

$$R_{ij} = \sqrt{(y_i - y_j)^2 + \phi_{ij}^2}\,, \tag{10.1.1}$$

to quantify the separation of particles i and j in phase space. In (10.1.1), y_i denotes the rapidity

$$y = \frac{1}{2}\ln\frac{p^0 + p_\mathrm{L}}{p^0 - p_\mathrm{L}} \tag{10.1.2}$$

of particle i and ϕ_{ij} is the azimuthal angle in the transverse plane between the particles i and j. In the definition of the rapidity, p^0 denotes the particle's energy and $p_\mathrm{L} = p^3$ the momentum along the beam axis. The recombination procedure, where we simply add four-momenta to form a pseudo-particle, works as follows:

1. For observables with bare muons we do not recombine photons and leptons. Alternatively, a photon and an electron are recombined for $R_{\gamma l} < 0.1$ to define IR safe inclusive observables.

2. A photon and a parton a (quark or gluon) are recombined for $R_{\gamma a} < 0.5$. In this case, we use the energy fraction of the photon inside the jet, $z_\gamma = \frac{p_\gamma^0}{p_\gamma^0 + p_a^0}$, to distinguish between $\mathrm{W} + \mathrm{jet}$ and $\mathrm{W} + \gamma$ production. If $z_\gamma > 0.7$, the event is regarded as a part of $\mathrm{W} + \gamma$ production and rejected because it lacks any other hard jet at NLO. This event definition is not collinear safe and requires the usage of a quark-to-photon fragmentation function to include the non-perturbative part of the quark–photon splitting (see Section 3.7 for details).

3. Two QCD partons c and d in the final state are recombined for $R_{cd} < 0.5$. For our simple FS configurations, this procedure is equivalent to the Tevatron Run II k_T-algorithm [70] for jet reconstruction with resolution parameter $D = 0.5$.

Technically, we perform a possible photon–lepton recombination before the photon–parton recombination. This procedure is IR safe because the triple-soft/collinear situation that a photon should have been first recombined with a parton, but was by mistake first recombined with a lepton, is excluded by our basic cuts.

10.1.2 Basic event-selection cuts

A W+jet event is defined by the following basic requirements:

1. A partonic object (after a possible recombination) is called a jet if its transverse momentum
$$p_{\mathrm{T}} = \sqrt{(p^1)^2 + (p^2)^2} \tag{10.1.3}$$
is larger than 25 GeV. Events are required to include at least one jet.

2. We demand a charged lepton with transverse momentum $p_{\mathrm{T}} > 25$ GeV and a missing momentum (i.e. the transverse momentum of the FS neutrino) $\not{p}_{\mathrm{T}} > 25$ GeV.

3. The events have to be central, i.e. the lepton and at least one jet have to be produced in the rapidity range $|y| < y_{\max} = 2.5$.

4. The lepton has to be isolated, i.e. the event is discarded if the distance between the lepton and a jet $R_{l\mathrm{jet}}$ is smaller than 0.5.
(The lepton–jet separation is also required for jets with $|y| > y_{\max}$. It is important to apply a lepton–jet separation procedure only to visible jets (not to low-p_{T} partons), since otherwise observables would not be IR safe.)

While the EW corrections differ for FS electrons and muons without photon recombination, the corrections become universal in the presence of photon recombination, since the lepton-mass logarithms cancel in this case, in accordance with the KLN theorem. In Chapter 11, numerical results will be presented for photon recombination and for bare muons.

10.2 LO contributions

The total hadronic cross section at LO is given by

$$\begin{aligned}
&\sigma_{AB}^{\mathrm{LO}}(p_A, p_B; \mu_{\mathrm{F}}^2) \\
&= \int_0^1 \mathrm{d}x_a \mathrm{d}x_b \Bigg\{ \Bigg[\sum_{i=1}^{2} \sum_{j=1}^{3} \mathcal{L}_{AB}^{\mathrm{u}_i \bar{\mathrm{d}}_j}(x_a, x_b) \hat{\sigma}^0_{\mathrm{u}_i \bar{\mathrm{d}}_j \to l^+ + \nu_l + \mathrm{g}}(p_a, p_b; k_l, k_n, k_c) \\
&\quad + \sum_{i=1}^{2} \mathcal{L}_{AB}^{\mathrm{u}_i(\mathrm{g}/\gamma)}(x_a, x_b) \sum_{j=1}^{3} \hat{\sigma}^0_{\mathrm{u}_i(\mathrm{g}/\gamma) \to l^+ + \nu_l + \mathrm{d}_j}(p_a, p_b; k_l, k_n, k_c) \\
&\quad + \sum_{j=1}^{3} \mathcal{L}_{AB}^{\bar{\mathrm{d}}_j(\mathrm{g}/\gamma)}(x_a, x_b) \sum_{i=1}^{2} \hat{\sigma}^0_{\bar{\mathrm{d}}_j(\mathrm{g}/\gamma) \to l^+ + \nu_l + \bar{\mathrm{u}}_i}(p_a, p_b; k_l, k_n, k_c) \Bigg] \\
&\qquad + \Big[\ldots \Big]_{a \leftrightarrow b} \Bigg\} F_J^{(l^+ + \nu_l + 1\,\mathrm{jet})}(k_l, k_n, k_c; p_a, p_b) \,,
\end{aligned} \tag{10.2.1}$$

where

$$\mathcal{L}^{ab}_{\mathrm{pp}}(x_a,x_b) \equiv f_{a/\mathrm{p}}(x_a,\mu_{\mathrm{F}}^2) f_{b/\mathrm{p}}(x_b,\mu_{\mathrm{F}}^2)\,, \quad \mathcal{L}^{ab}_{\mathrm{p\bar{p}}}(x_a,x_b) \equiv f_{a/\mathrm{p}}(x_a,\mu_{\mathrm{F}}^2) f_{b/\bar{\mathrm{p}}}(x_b,\mu_{\mathrm{F}}^2)\,, \quad (10.2.2)$$

denote the experimentally determined parton luminosities for the LHC or the Tevatron. Although it is formally part of the partonic cross section, we have made the jet function $F_J^{(l^+ + \nu_l + 1\,\mathrm{jet})}$ explicit that includes the basic event-selection cuts described in Section 10.1.2. The partonic cross sections $\hat{\sigma}^0_{a\,(b/\gamma)\to l^+\nu_l c}$ are defined in (7.3.1). Equation (10.2.1) covers the dominant QCD enhanced contributions (6.1.1) – (6.1.3) as well as the photon-induced processes (6.1.5) and (6.1.6).

10.2.1 Numerical integration of the hadronic variables

For the numerical implementation of the convolutive integrations $\int_0^1 \mathrm{d}x_a \mathrm{d}x_b \equiv \int_0^1 \mathrm{d}x_a \int_0^1 \mathrm{d}x_b$ we first transform the integrals (2.3.8) according to

$$\int_0^1 \mathrm{d}x_a \mathrm{d}x_b\, \mathcal{F}(x_a,x_b) \to \int_{\tau_{\min}}^1 \mathrm{d}\tau \int_\tau^1 \frac{\mathrm{d}x_b}{x_b}\, \mathcal{F}(\tau/x_b, x_b)\,, \quad (10.2.3)$$

where $\tau \equiv x_a x_b$, and the choice of $\tau_{\min} = 9\,p^2_{\mathrm{T,min}}/s$ corresponds to the minimal cm energy $\hat{s}_{\min} = \tau_{\min} s$ that is necessary to produce a jet, a lepton, and a neutrino with a minimal transverse momentum $p_{\mathrm{T,min}}$, as demanded by our basic cuts. To cancel the overall $1/\hat{s}$ dependence that appears in any phase-space integral, the hadronic integrations (10.2.3) are mapped to the unit square $\mathbf{r} = (r_1, r_2)$ via

$$\int_{\tau_{\min}}^1 \mathrm{d}\tau \int_\tau^1 \frac{\mathrm{d}x_b}{x_b} = \int_0^1 \mathrm{d}^2\mathbf{r}\, [\tau(\mathbf{r}) \ln\tau(\mathbf{r}) \ln\tau_0]\, \mathcal{F}(x_a(\mathbf{r}), x_b(\mathbf{r}))\,, \quad (10.2.4)$$

with $\tau = \tau_{\min}^{r_1}$ and $x_b = \tau^{r_2}$.

10.3 EW corrections

The partonic expressions for the EW NLO corrections are given by the sum of the virtual corrections $\hat{\sigma}^{\mathrm{V,EW}}$, the collinear counterterm $\hat{\sigma}^{\mathrm{C,EW}}$ that arises from the replacement (3.4.1) in the LO cross section, and the bremsstrahlung contributions $\hat{\sigma}^{\mathrm{R,EW}}$,

$$\hat{\sigma}^{\mathrm{NLO,\,EW}}_{ab\to l^+\nu_l c(+\gamma)}(p_a,p_b;\mu_{\mathrm{F}}^2) = \hat{\sigma}^{\mathrm{V,EW}}_{ab\to l^+\nu_l c}(p_a,p_b) + \hat{\sigma}^{\mathrm{C,EW}}_{ab\to l^+\nu_l c}(p_a,p_b;\mu_{\mathrm{F}}^2) + \hat{\sigma}^{\mathrm{R,EW}}_{ab\to l^+\nu_l c+\gamma}(p_a,p_b)\,, \quad (10.3.1)$$

where the explicit expressions for the partonic contributions $\hat{\sigma}^{\mathrm{R,EW}}_{ab\to l^+\nu_l c+\gamma}$ and $\hat{\sigma}^{\mathrm{V,EW}}_{ab\to l^+\nu_l c}$ are given by Eqs. (8.1.7) and (9.2.6), respectively. The full hadronic contribution simply emerges from (10.2.1) via the replacement[1]

$$\hat{\sigma}^0_{ab\to l^+\nu_l c}(p_a,p_b) \to \hat{\sigma}^{\mathrm{NLO,EW}}_{ab\to l^+\nu_l c(+\gamma)}(p_a,p_b;\mu_{\mathrm{F}}^2)\,, \quad (10.3.2)$$

[1]For a consistent NLO calculation, one also has to replace the LO PDFs by adequate PDFs defined at NLO. However, since the `MRSTQED2004` PDF set we use in our calculation is only available at NLO accuracy, we employ those NLO PDFs for the LO as well as for the NLO computation.

but one has to keep in mind that the bremsstrahlung cross section is defined on a four-particle phase space, implying the necessity of introducing the jet function $F_J^{(l^+ + \nu_l + 1\,\mathrm{jet} + \gamma)}$ that properly accounts for the recombination of photons and light fermions in the final state as detailed in Section 10.1.1,

$$\begin{aligned}
&\sigma_{AB}^{\mathrm{NLO,EW}}(p_A, p_B; \mu_\mathrm{F}^2) \\
&= \int_0^1 \mathrm{d}x_a \mathrm{d}x_b \Bigg\{ \Bigg[\sum_{i=1}^{2} \sum_{j=1}^{3} \mathcal{L}_{AB}^{\mathrm{u}_i \bar{\mathrm{d}}_j}(x_a, x_b) \hat{\sigma}^{\mathrm{NLO,EW}}_{\mathrm{u}_i \bar{\mathrm{d}}_j \to l^+ + \nu_l + \mathrm{g}(+\gamma)}(p_a, p_b; k_l, k_n, k_c(, k_\gamma)) \\
&\qquad + \sum_{i=1}^{2} \mathcal{L}_{AB}^{\mathrm{u}_i \mathrm{g}}(x_a, x_b) \sum_{j=1}^{3} \hat{\sigma}^{\mathrm{NLO,EW}}_{\mathrm{u}_i \mathrm{g} \to l^+ + \nu_l + \mathrm{d}_j(+\gamma)}(p_a, p_b; k_l, k_n, k_c(, k_\gamma)) \\
&\qquad + \sum_{j=1}^{3} \mathcal{L}_{AB}^{\bar{\mathrm{d}}_j \mathrm{g}}(x_a, x_b) \sum_{i=1}^{2} \hat{\sigma}^{\mathrm{NLO,EW}}_{\bar{\mathrm{d}}_j \mathrm{g} \to l^+ + \nu_l + \bar{\mathrm{u}}_i(+\gamma)}(p_a, p_b; k_l, k_n, k_c(, k_\gamma)) \Bigg] \\
&\qquad + \Big[\dots \Big]_{a \leftrightarrow b} \Bigg\} F_J^{(l^+ + \nu_l + 1\,\mathrm{jet}(+\gamma))}(k_l, k_n, k_c(, k_\gamma); p_a, p_b)\,.
\end{aligned} \tag{10.3.3}$$

In (10.3.3), all bremsstrahlung corrections are calculated using the dipole subtraction technique discussed in Sections 4.1 and 4.2, applying formula (4.2.1),

$$\begin{aligned}
&\int \mathrm{d}\Phi_{(l\nu_l + c + \gamma)} \left| \mathcal{M}^{\mathrm{R,EW}}_{ab \to l\nu_l + c + \gamma} \right|^2 \\
&= \int \mathrm{d}\Phi_{(l\nu_l + c + \gamma)} \left(\left| \mathcal{M}^{\mathrm{R,EW}}_{ab \to l\nu_l + c + \gamma} \right|^2 - |\mathcal{M}_{\mathrm{sub}}|^2 \right) + \int \mathrm{d}\tilde{\Phi}_{(l\nu_l + c)} \otimes \left(\int [\mathrm{d}k]\, |\mathcal{M}_{\mathrm{sub}}|^2 \right),
\end{aligned} \tag{10.3.4}$$

with $|\mathcal{M}_{\mathrm{sub}}|^2$ from Eq. (4.2.2), for the safe numerical evaluation of the squared bremsstrahlung amplitudes. Since the corresponding expressions are a bit lengthy, we explicitly list the contributing dipoles and the integrated counterparts that have to be readded to the virtual corrections in Appendix C.

10.4 QCD corrections

10.4.1 Real radiation processes

After summing over all IS and FS quark flavours according to (2.3.8) and (4.4.8), we can still distinguish twelve different partonic contributions that have to be convoluted with the proper parton luminosities and afterwards summed incoherently to obtain the final hadronic result. The four contributions arising from the generic process (8.2.1c) add up to

$$\begin{aligned}
&\sigma_{AB}^{\mathrm{R,\,(W+ggdu)}}(p_A, p_B; \mu_\mathrm{F}^2) \\
&= \int_0^1 \mathrm{d}x_a\, \mathrm{d}x_b \Bigg\{ \Bigg[\frac{1}{2}\, \mathcal{L}_{AB}^{\mathrm{gg}}(x_a, x_b) \sum_{i=1}^{2} \sum_{j=1}^{3} \hat{\sigma}^{\mathrm{R,QCD}}_{\mathrm{gg} \to \mathrm{W} + \bar{\mathrm{u}}_i \mathrm{d}_j}(p_a, p_b; k_l, k_n, k_c, k_d)
\end{aligned}$$

$$
\begin{aligned}
&+\sum_{i=1}^{2}\mathcal{L}_{AB}^{\mathrm{g u}_i}(x_a,x_b)\sum_{j=1}^{3}\hat{\sigma}^{\mathrm{R,QCD}}_{\mathrm{g u}_i\to \mathrm{W+g d}_j}(p_a,p_b;k_l,k_n,k_c,k_d)\\
&+\sum_{j=1}^{3}\mathcal{L}_{AB}^{\mathrm{g}\bar{\mathrm{d}}_j}(x_a,x_b)\sum_{i=1}^{2}\hat{\sigma}^{\mathrm{R,QCD}}_{\mathrm{g}\bar{\mathrm{d}}_j\to \mathrm{W+g}\bar{\mathrm{u}}_i}(p_a,p_b;k_l,k_n,k_c,k_d)\\
&+\sum_{i=1}^{2}\sum_{j=1}^{3}\mathcal{L}_{AB}^{\mathrm{u}_i\bar{\mathrm{d}}_j}(x_a,x_b)\hat{\sigma}^{\mathrm{R,QCD}}_{\mathrm{u}_i\bar{\mathrm{d}}_j\to \mathrm{W+gg}}(p_a,p_b;k_l,k_n,k_c,k_d)\Bigg]\\
&\qquad+\Big[\dots\Big]_{a\leftrightarrow b}\Bigg\}F_J^{(l^+\!+\nu_l+2\text{ jets})}(k_l,k_n,k_c,k_d;p_a,p_b)\,,
\end{aligned}
\tag{10.4.1}
$$

where the corresponding parton luminosities for the LHC and the Tevatron are defined in the $\overline{\mathrm{MS}}$ factorization scheme w.r.t. IS QCD corrections. In (10.4.1) we have used the prescription (8.2.14) to calculate the partonic QCD cross sections. Note that it is important to boost the FS momenta to the hadronic cm frame according to (2.3.13) before calculating the cut function $F_J^{(l^+\!+\nu_l+2\text{ jets})}$ that summarizes the recombination and cut procedure discussed in Section 10.1. The hadronic contributions arising from the processes (8.2.1a) read

$$
\begin{aligned}
&\sigma_{AB}^{\mathrm{R,\,(W+dddu)}}(p_A,p_B;\mu_{\mathrm{F}}^2)\\
&=\int_0^1\mathrm{d}x_a\,\mathrm{d}x_b\,\Bigg\{\Bigg[\sum_{i,j=1}^{3}\mathcal{L}_{AB}^{\mathrm{d}_i\bar{\mathrm{d}}_j}(x_a,x_b)\sum_{l=1}^{3}\sum_{k=1}^{2}\hat{\sigma}^{\mathrm{R,QCD}}_{\mathrm{d}_i\bar{\mathrm{d}}_j\to \mathrm{W+}\bar{\mathrm{u}}_k\mathrm{d}_l}(p_a,p_b;k_l,k_n,k_c,k_d)\\
&\quad+\sum_{i=1}^{3}\sum_{k=1}^{2}\mathcal{L}_{AB}^{\mathrm{d}_i\mathrm{u}_k}(x_a,x_b)\sum_{j=1}^{3}\sum_{l=j}^{3}\hat{\sigma}^{\mathrm{R,QCD}}_{\mathrm{d}_i\mathrm{u}_k\to \mathrm{W+d}_j\mathrm{d}_l}(p_a,p_b;k_l,k_n,k_c,k_d)\\
&\quad+\sum_{j=1}^{3}\sum_{k=1}^{2}\mathcal{L}_{AB}^{\bar{\mathrm{d}}_j\mathrm{u}_k}(x_a,x_b)\sum_{i,l=1}^{3}\hat{\sigma}^{\mathrm{R,QCD}}_{\bar{\mathrm{d}}_j\mathrm{u}_k\to \mathrm{W+}\bar{\mathrm{d}}_i\mathrm{d}_l}(p_a,p_b;k_l,k_n,k_c,k_d)\\
&\quad+\left(\frac{1}{1+\delta_{jl}}\right)\sum_{j=1}^{3}\sum_{l=j}^{3}\mathcal{L}_{AB}^{\bar{\mathrm{d}}_j\bar{\mathrm{d}}_l}(x_a,x_b)\sum_{i=1}^{3}\sum_{k=1}^{2}\hat{\sigma}^{\mathrm{R,QCD}}_{\bar{\mathrm{d}}_j\bar{\mathrm{d}}_l\to \mathrm{W+}\bar{\mathrm{d}}_i\bar{\mathrm{u}}_k}(p_a,p_b;k_l,k_n,k_c,k_d)\Bigg]\\
&\qquad+\Big[\dots\Big]_{a\leftrightarrow b}\Bigg\}F_J^{(l^+\!+\nu_l+2\text{ jets})}(k_l,k_n,k_c,k_d;p_a,p_b)\,,
\end{aligned}
\tag{10.4.2}
$$

where the parton luminosities are defined in the same way as in (10.2.2). Finally, we also list the hadronic contributions that emerge from the generic processes (8.2.1b),

$$
\begin{aligned}
&\sigma_{AB}^{\mathrm{R,\,(W+uudu)}}(p_A,p_B;\mu_{\mathrm{F}}^2)\\
&=\int_0^1\mathrm{d}x_a\,\mathrm{d}x_b\,\Bigg\{\Bigg[\sum_{i,j=1}^{2}\mathcal{L}_{AB}^{\mathrm{u}_i\bar{\mathrm{u}}_j}(x_a,x_b)\sum_{l=1}^{3}\sum_{k=1}^{2}\hat{\sigma}^{\mathrm{R,QCD}}_{\mathrm{u}_i\bar{\mathrm{u}}_j\to \mathrm{W+}\bar{\mathrm{u}}_k\mathrm{d}_l}(p_a,p_b;k_l,k_n,k_c,k_d)\\
&\quad+\left(\frac{1}{1+\delta_{ik}}\right)\sum_{i=1}^{2}\sum_{k=j}^{2}\mathcal{L}_{AB}^{\mathrm{u}_i\mathrm{u}_k}(x_a,x_b)\sum_{j=1}^{2}\sum_{l=1}^{3}\hat{\sigma}^{\mathrm{R,QCD}}_{\mathrm{u}_i\mathrm{u}_k\to \mathrm{W+u}_j\mathrm{d}_l}(p_a,p_b;k_l,k_n,k_c,k_d)\\
&\quad+\sum_{j=1}^{2}\sum_{k=1}^{2}\mathcal{L}_{AB}^{\bar{\mathrm{u}}_j\mathrm{u}_k}(x_a,x_b)\sum_{i=1}^{2}\sum_{l=1}^{3}\hat{\sigma}^{\mathrm{R,QCD}}_{\bar{\mathrm{u}}_j\mathrm{u}_k\to \mathrm{W+}\bar{\mathrm{u}}_i\mathrm{d}_l}(p_a,p_b;k_l,k_n,k_c,k_d)
\end{aligned}
$$

$$+\sum_{j=1}^{2}\sum_{l=1}^{3}\mathcal{L}_{AB}^{\bar{\mathrm{u}}_j\bar{\mathrm{d}}_l}(x_a,x_b)\sum_{i=1}^{2}\sum_{k=i}^{2}\hat{\sigma}^{\mathrm{R,QCD}}_{\bar{\mathrm{u}}_j\bar{\mathrm{d}}_l\to\mathrm{W}+\bar{\mathrm{u}}_i\bar{\mathrm{u}}_k}(p_a,p_b;k_l,k_n,k_c,k_d)\Big]$$
$$+\quad\Big[\ldots\Big]_{a\leftrightarrow b}\Big\}F_J^{(l^+\nu_l+2\text{ jets})}(k_l,k_n,k_c,k_d;p_a,p_b)\,. \tag{10.4.3}$$

As mentioned before, the complete result for the real corrections to the hadronic cross section is given by the sum

$$\begin{aligned}&\sigma_{AB}^{\mathrm{R,\,QCD}}(p_A,p_B;\mu_\mathrm{F}^2)\\&\quad=\sigma_{AB}^{\mathrm{R,\,(W+uudu)}}(p_A,p_B;\mu_\mathrm{F}^2)+\sigma_{AB}^{\mathrm{R,\,(W+dddu)}}(p_A,p_B;\mu_\mathrm{F}^2)+\sigma_{AB}^{\mathrm{R,\,(W+ggdu)}}(p_A,p_B;\mu_\mathrm{F}^2)\,,\end{aligned} \tag{10.4.4}$$

where we implicitly assume that all partonic contributions are calculated according to

$$\hat{\sigma}_{ab}^{\mathrm{R,QCD}}=\int\Big(\mathrm{d}\hat{\sigma}_{ab}^{\mathrm{R,QCD}}-\mathrm{d}\hat{\sigma}_{ab}^{\mathrm{A}}\Big)+\int\mathrm{d}\hat{\sigma}_{ab}^{\mathrm{A}}\,, \tag{10.4.5}$$

using the proper subtraction formulae (4.4.15) and (4.4.16). We will now discuss the structure of the subtraction contributions $\mathrm{d}\hat{\sigma}^{\mathrm{A}}$ in some detail.

Subtraction contributions $\hat{\sigma}^{\mathrm{A}}$

Since the focus of this thesis is not on the calculation of the QCD corrections, we will not list all contributing subtraction terms and all corresponding readded counterparts explicitly, but we will outline the general procedure by means of the example process

$$\mathrm{u}_i(p_a)\,\mathrm{u}_k(p_b)\to\mathrm{W}(q_\mathrm{W})+\mathrm{u}_j(k_c)+\mathrm{d}_l(k_d)\,. \tag{10.4.6}$$

However, since we have provided a formal discussion of the calculation of NLO QCD corrections in Section 4.4, the general procedure of the calculation should become sufficiently clear.

Calculating the subtraction terms for the partonic processes in (10.4.1), (10.4.2), and (10.4.3), the flavour structure of the involved quarks has to be respected carefully. For the channels involving two external gluons, this task is trivial, since the overall flavour factor $|V_{ij}|^2$ can be factorized, and the computation is straight-forward, applying Eq. (4.4.16).

For the channels with four external quarks, however, the subtraction kernels have to be composed according to the flavour structure of the squared amplitudes as discussed in Section 8.2. Since the kinematical configurations that lead to IR singularities during the phase-space integration are entirely contained in the factors $|A|^2$ and $|B|^2$ in (8.2.8), the flavour structure of the adequate subtraction terms can be expressed as

$$\hat{\sigma}^{\mathrm{A}}_{(\mathrm{dddu})}=\delta_{ij}\,|V_{kl}|^2\,|\mathcal{A}^{\mathrm{sub}}_{\mathrm{dddu}}|^2+\delta_{il}\,|V_{kj}|^2\,|\mathcal{B}^{\mathrm{sub}}_{\mathrm{dddu}}|^2\,, \tag{10.4.7a}$$
$$\hat{\sigma}^{\mathrm{A}}_{(\mathrm{uudu})}=\delta_{ij}\,|V_{kl}|^2\,|\mathcal{A}^{\mathrm{sub}}_{\mathrm{uudu}}|^2+\delta_{jk}\,|V_{il}|^2\,|\mathcal{B}^{\mathrm{sub}}_{\mathrm{uudu}}|^2\,, \tag{10.4.7b}$$

for all partonic channels in (10.4.2) and (10.4.3).

The subtraction function for our example process (10.4.6) is given by

$$\begin{aligned}\hat{\sigma}^{\mathrm{A}}_{\mathrm{u}_i\mathrm{u}_k\to\mathrm{W}+\mathrm{u}_j\mathrm{d}_l}&=\frac{1}{4}\int\mathrm{d}\Phi_{(l^+\nu_l+c+d)}\\&\times\Big\{\delta_{ij}\,|V_{kl}|^2[\mathcal{D}^{\mathrm{u}_i\mathrm{u}_j,\mathrm{u}_k}+\mathcal{D}^{\mathrm{u}_i\mathrm{u}_j}_{\mathrm{d}_l}]_{\mathrm{gu}\to l\nu_l\mathrm{d}}+\delta_{kj}\,|V_{il}|^2\,[\mathcal{D}^{\mathrm{u}_k\mathrm{u}_j,\mathrm{u}_i}+\mathcal{D}^{\mathrm{u}_k\mathrm{u}_j}_{\mathrm{d}_l}]_{\mathrm{ug}\to l\nu_l\mathrm{d}}\Big\}\,,\end{aligned} \tag{10.4.8}$$

where the first two subtraction kernels will compensate for the IS collinear singularity that arises from the $\mathrm{u}_i(p_a) \to \mathrm{g}^*(\tilde{p}_{ac})\,\mathrm{u}_i(k_c)$ splitting in the initial state, and the last two terms cancel the singular contributions originating from the collinear splitting $\mathrm{u}_j(p_b) \to \mathrm{g}^*(\tilde{p}_{bc})\,\mathrm{u}_j(k_c)$. The lower subscripts denote the LO contributions that have to be used in the calculation of the dipoles (4.4.17).

10.4.2 Calculation of the hadronic V + A + C contributions

Now we will briefly discuss the hadronic contributions that result from the sum of virtual corrections V, the readded subtraction terms A, and the collinear counterterm C in (4.4.15).

To obtain the hadronic virtual contributions and the corrections due to the $\boldsymbol{I}$-operator corresponding to the second line of (4.4.15), it is sufficient to simply replace the LO expression in (10.2.1) according to

$$\mathrm{d}\hat{\sigma}^0_{ab}(p_a,p_b) \to \mathrm{d}\hat{\sigma}^{\mathrm{V,QCD}}_{ab}(p_a,p_b;\epsilon) + \mathrm{d}\hat{\sigma}^0_{ab}(p_a,p_b)\boldsymbol{I}_{ab}(\epsilon), \tag{10.4.9}$$

for processes with two QCD partons in the initial state. The $\boldsymbol{I}$-operator contains all singularities related to soft-gluon radiation, and it covers all singular structures that arise if the collinear FS splittings $\mathrm{g}^* \to \mathrm{gg}$ and $\mathrm{g}^* \to q_i\bar{q}_i$ are integrated analytically. This is always assumed, because we only consider IR-safe jet observables, i.e. two partons that are sufficiently collinear are always recombined to a jet.

The convolutive contributions to the readded counterparts that contain the collinear counterterm C and the finite parts of the collinear IS splittings are obtained by replacing all partonic radiative contributions $\hat{\sigma}^{\mathrm{R}}_{ab}$ in (10.4.1), (10.4.2), and (10.4.3) by the adequate expressions given by the last two lines of (4.4.15). Doing so, care has to be taken to account for the different flavour structures properly. For instance, the convolutive expression for our partonic example process (10.4.6) explicitly reads

$$\begin{aligned}\hat{\sigma}^{\mathrm{A+C}}_{\mathrm{u}_i\mathrm{u}_k\to\mathrm{W}+\mathrm{u}_j\mathrm{d}_l}\bigg|_{\mathrm{conv.}} = \int_0^1 \mathrm{d}x\, \Bigg\{ &\Big(\boldsymbol{K}^{q,g}(x) + \boldsymbol{P}^{q,g}(xp_a,x;\mu_{\mathrm{F}}^2)\Big)\, \hat{\sigma}^0_{\mathrm{gu}\to l^+\nu_l+\mathrm{d}}(xp_a,p_b)\;\delta_{ij}\,|V_{kl}|^2 \\ &+ \Big(\boldsymbol{K}^{q,g}(x) + \boldsymbol{P}^{q,g}(xp_b,x;\mu_{\mathrm{F}}^2)\Big)\, \hat{\sigma}^0_{\mathrm{ug}\to l^+\nu_l+\mathrm{d}}(p_a,xp_b)\;\delta_{kj}\,|V_{il}|^2 \Bigg\},\end{aligned} \tag{10.4.10}$$

i.e. there are convolutive contributions from the collinear $\mathrm{u}_i \to \mathrm{g}^*\mathrm{u}_i$ splitting connected to the incoming momentum p_a as well as from the splitting $\mathrm{u}_k \to \mathrm{g}^*\mathrm{u}_k$ connected to the reverse incoming momentum p_b. In (10.4.10), we have factorized the CKM dependence of the LO cross sections according to

$$\hat{\sigma}^0_{\mathrm{u}_i\mathrm{g}\to l^+\nu_l+\mathrm{d}_j} = |V_{ij}|^2\,\hat{\sigma}^0_{\mathrm{ug}\to l^+\nu_l\mathrm{d}}\,. \tag{10.4.11}$$

10.4.3 Real corrections to photon-induced processes

Here we list the explicit formulae that are needed to calculate the real radiative corrections (6.3.13) – (6.3.15) to the photon-induced processes (6.1.5) and (6.1.6) within the dipole subtraction formalism. In this section we omit the CKM structure in all expression, since it is always given by the same overall factor $|V_{ij}|^2$.

Initial-state QED singularities

The channels

$$\gamma(p_a) + q(p_b) \to l^+(k_l) + \nu_l(k_n) + q'(k_c) + \mathrm{g}(k_d)\,, \tag{10.4.12}$$

which are formally part of the real QCD corrections to the photon-induced processes, exhibit a collinear QED singularity due to the splitting $\gamma \to q'\bar{q}'^*$ in the initial state. Following the notation of Section 4.3, the function that has to be subtracted from the averaged squared amplitude to compensate for this singularity reads

$$\overline{|\mathcal{M}_{\mathrm{sub}}|}^2 = Q_{q'}^2\, e^2\, h_{\mathrm{g}}^{\gamma q'}(p_a, k_c, k_d) \overline{\left|\mathcal{M}^0_{\bar{q}'q\to l\nu_l\mathrm{g}}(\tilde{p}_a, p_b, \tilde{k}_d)\right|}^2\,, \tag{10.4.13}$$

where we have chosen the gluon as FS spectator, and the function $h_{\mathrm{g}}^{\gamma q'}$ was defined in (4.3.21). The integrated contribution containing the singularity in terms of quark-mass logarithms is given by

$$\hat{\sigma}^{\mathrm{sub}}_{\gamma q\to l\nu_l q'\mathrm{g}} = N_{\mathrm{C}} \frac{Q_{q'}\alpha}{2\pi} \int_0^1 \mathrm{d}x\, \mathcal{H}_{\mathrm{g}}^{\gamma q'}(P_{da}^2, x)\, \hat{\sigma}^0_{\bar{q}'q\to l\nu_l\mathrm{g}}(xp_a, p_b)\,, \tag{10.4.14}$$

with $P_{da}^2 = (k_d(x) - xp_a)^2$, and $\mathcal{H}_{\mathrm{g}}^{\gamma q'}$ from (4.3.33). After adding the collinear counterterm that arises through the redefinition of the PDFs (see Section 3.4), the renormalized integrated counterpart that has to be added to the hadronic cross section is

$$\begin{aligned}\tilde{\sigma}^{\mathrm{sub}}_{AB,(\gamma q\to l\nu_l q'\mathrm{g})} &= \int_0^1 \mathrm{d}x_a \mathrm{d}x_b\, \mathcal{L}_{AB}^{\gamma q}(x_a, x_b) \\ &\times \int_0^1 \mathrm{d}x\, \frac{\alpha}{2\pi} N_{\mathrm{C}} Q_{q'}^2 \left\{ P_{f\gamma}(x) \ln\left[\frac{P_{da}^2(x-1)}{x\mu_{\mathrm{F}}^2}\right] + 2x(1-x) - C_{f\gamma}^{\mathrm{DIS}}(x) \right\} \hat{\sigma}^0_{\bar{q}'q\to l\nu_l q'\mathrm{g}}(xp_a, p_b)\,,\end{aligned} \tag{10.4.15}$$

where we have applied Eqs. (3.4.1) and (4.3.32). Note that (10.4.15) shows an explicit dependence on the factorization scale μ_{F}. The analogous calculation for the channels with a photon and a gluon in the initial state should be obvious.

Subtraction for gluon radiation

For the QCD subtraction term that cancels the soft and collinear singularities in (10.4.12) that are related to gluon radiation, we obtain

$$\hat{\sigma}^{\mathrm{A}}_{\gamma q\to \mathrm{W}+q'\mathrm{g}} = \frac{1}{4} \int \mathrm{d}\Phi_{(l^+\nu_l+c+d)}\, [\mathcal{D}^q_{q'\mathrm{g}} + \mathcal{D}^{qg}_{q'}]_{\gamma q\to \mathrm{W}+q'}\,, \tag{10.4.16}$$

where we have applied (4.4.19). The readded counterpart (see Eq. (4.4.20)) after the renormalization of the quark PDF is given by

$$\begin{aligned}\hat{\sigma}^{\mathrm{A+C}}_{\gamma q\to \mathrm{W}+q'\mathrm{g}} &= \boldsymbol{I}_{\gamma q}(\epsilon)\hat{\sigma}^0_{\gamma q\to \mathrm{W}+q'}(p_a, p_b) \\ &\quad + \int_0^1 \mathrm{d}x \left(\boldsymbol{K}^{q,q}(x) + \boldsymbol{P}^{q,q}(x, p_b, \mu_{\mathrm{F}}^2) \right) \hat{\sigma}^0_{\gamma q\to \mathrm{W}+q'}(p_a, xp_b)\,.\end{aligned} \tag{10.4.17}$$

The operators $\boldsymbol{I}$, $\boldsymbol{K}$, and $\boldsymbol{P}$ in this case explicitly read

$$\begin{aligned}
\boldsymbol{I}_{\gamma q}(\epsilon) &= \left(\frac{\alpha_\mathrm{s}}{2\pi}\right)\, 2C_\mathrm{F}\left[\Delta_2^\mathrm{IR}\left(\frac{\mu^2}{2\,(p_b k_d)}\right)^\epsilon + \frac{3}{2}\Delta_1^\mathrm{IR}\left(\frac{\mu^2}{2\,(p_b k_d)}\right)^\epsilon - \frac{\pi^2}{2} + 5\right], \\
\boldsymbol{P}^{q,q}(x, p_b, \mu_\mathrm{F}^2) &= -\left(\frac{\alpha_\mathrm{s}}{2\pi}\right) P^{qq}(x) \ln\left(\frac{\mu_\mathrm{F}^2}{2x\,(p_b k_c)}\right), \\
\boldsymbol{K}^{q,q}(x) &= \left(\frac{\alpha_\mathrm{s}}{2\pi}\right)\left\{\overline{K}^{qq}(x) - \frac{3}{2}C_\mathrm{F}\left[\left(\frac{1}{1-x}\right)_+ + \delta(1-x)\right]\right\}. \qquad (10.4.18)
\end{aligned}$$

Here we used

$$\Delta_2^\mathrm{IR} = \frac{1}{\epsilon^2}\frac{(4\pi)^\epsilon}{\Gamma(1-\epsilon)}, \qquad (10.4.19)$$

that includes the overlapping soft and collinear singularities, and Δ_1^IR from (3.3.2). The explicit expression for the regularized Altarelli–Parisi splitting function in four dimensions $P^{qq}(x)$ and for $\overline{K}^{qq}(x)$ can be found in Appendix C of [66].

The real QCD corrections to the photon-induced processes comprise the γg channel

$$\gamma(p_a) + \mathrm{g}(p_b) \to \mathrm{W}^+(q_\mathrm{W}) + \bar{\mathrm{u}}(k_c) + \mathrm{d}(k_d), \qquad (10.4.20)$$

that is absent at LO. The collinear QCD singularities related to the IS $\mathrm{g} \to qq^*$ splittings are subtracted from the corresponding integrand using the local counterterm

$$\hat{\sigma}^\mathrm{A}_{\gamma\mathrm{g}\to\mathrm{W}+\bar{\mathrm{u}}\mathrm{d}} = \frac{1}{4}\int \mathrm{d}\Phi_{(l^+\nu_l+c+d)}\, \left(\mathcal{D}_\mathrm{d}^{\mathrm{g}\bar{\mathrm{u}}}\big|_{\gamma\mathrm{u}\to\mathrm{W}+\mathrm{d}} + \mathcal{D}_{\bar{\mathrm{u}}}^{\mathrm{g}\mathrm{d}}\big|_{\gamma\bar{\mathrm{d}}\to\mathrm{W}+\bar{\mathrm{u}}}\right), \qquad (10.4.21)$$

and the corresponding readded counterpart reads

$$\begin{aligned}
\hat{\sigma}^{\mathrm{A+C}}_{\gamma\mathrm{g}\to\mathrm{W}+\bar{\mathrm{u}}\mathrm{d}} = \int_0^1 \mathrm{d}x \Big[&\Big(\boldsymbol{P}^{\mathrm{g},\mathrm{u}}(x, p_b, \mu_\mathrm{F}^2) + \boldsymbol{K}^{\mathrm{g},\mathrm{u}}(x)\Big)\hat{\sigma}^0_{\gamma\mathrm{u}\to\mathrm{W}+\mathrm{d}}(p_a, xp_b) \\
&+ \Big(\boldsymbol{P}^{\mathrm{g},\bar{\mathrm{d}}}(x, p_b, \mu_\mathrm{F}^2) + \boldsymbol{K}^{\mathrm{g},\bar{\mathrm{d}}}(x)\Big)\hat{\sigma}^0_{\gamma\bar{\mathrm{d}}\to\mathrm{W}+\bar{\mathrm{u}}}(p_a, xp_b)\Big]. \qquad (10.4.22)
\end{aligned}$$

The operators $\boldsymbol{K}$ and $\boldsymbol{P}$ in this case are given by

$$\boldsymbol{K}^{\mathrm{g},(\mathrm{u}/\bar{\mathrm{d}})}(x) = \left(\frac{\alpha_\mathrm{s}}{2\pi}\right)\, \overline{K}^{gq}(x), \qquad (10.4.23)$$

and

$$\begin{aligned}
\boldsymbol{P}^{\mathrm{g},\mathrm{u}}(x, p_b, \mu_\mathrm{F}^2) &= -\frac{\alpha_\mathrm{s}}{2\pi}\, P^{gq}(x) \ln\left(\frac{\mu_\mathrm{F}^2}{2x\,(p_b k_d)}\right), \\
\boldsymbol{P}^{\mathrm{g},\bar{\mathrm{d}}}(x, p_b, \mu_\mathrm{F}^2) &= -\frac{\alpha_\mathrm{s}}{2\pi}\, P^{gq}(x) \ln\left(\frac{\mu_\mathrm{F}^2}{2x\,(p_b k_c)}\right). \qquad (10.4.24)
\end{aligned}$$

Again, the expressions for $P^{gq}(x)$ and $\overline{K}^{gq}(x)$ can be found in Appendix C of [66].

10.5 Interference contributions of EW and QCD diagrams

The calculation of the hadronic cross sections for the interference contributions discussed in Section 8.3 is carried out using Eqs. (10.4.2) and (10.4.3), where the partonic expressions $\mathrm{d}\hat{\sigma}^{\mathrm{R,QCD}}_{ab\to \mathrm{W}+cd}$ have to be replaced by the corresponding contributions of $\mathrm{d}\hat{\sigma}^{\mathrm{R,IF}}_{ab\to \mathrm{W}+cd}$. Note that no regularization procedure has to be applied within the calculation of the interference contributions, since those corrections are IR (and of course also UV) finite by construction.

Chapter 11

$\mathrm{pp/p\bar{p}} \to l^+\nu_l + \mathrm{jet}(+\gamma/\mathrm{jet})$: Numerical Results

11.1 Input parameters and setup

The relevant SM input parameters are

$$\begin{aligned}
&G_\mathrm{F} = 1.16637 \times 10^{-5}\,\mathrm{GeV}^{-2}, && \Lambda_\mathrm{QCD} = 239\,\mathrm{MeV}, && \alpha_\mathrm{s}(M_\mathrm{Z}) = 0.11899,\\
&M_\mathrm{W}^\mathrm{OS} = 80.398\,\mathrm{GeV}, && \Gamma_\mathrm{W}^\mathrm{OS} = 2.141\,\mathrm{GeV}, &&\\
&M_\mathrm{Z}^\mathrm{OS} = 91.1876\,\mathrm{GeV}, && \Gamma_\mathrm{Z}^\mathrm{OS} = 2.4952\,\mathrm{GeV}, && M_\mathrm{H} = 120\,\mathrm{GeV},\\
&m_\mathrm{e} = 0.510998910\,\mathrm{MeV}, && m_\mu = 105.658367\,\mathrm{MeV}, && m_\mathrm{t} = 172.6\,\mathrm{GeV},\\
&|V_\mathrm{ud}| = |V_\mathrm{cs}| = 0.974, && |V_\mathrm{us}| = |V_\mathrm{cd}| = \sqrt{1-|V_\mathrm{cs}|^2}, &&
\end{aligned} \tag{11.1.1}$$

which essentially follow Ref. [4]. The CKM matrix is included via global factors in the partonic cross sections for the different possible quark flavours. Within loops the CKM matrix is set to unity, because its effect is negligible there.

Using the complex-mass scheme that was outlined in Section 2.2.4, we employ a fixed width in the W- and Z-boson propagators in contrast to the approach used at LEP and Tevatron to fit the W and Z resonances, where running widths are taken. Therefore, we have to convert the "on-shell" (OS) values of M_V^OS and Γ_V^OS ($V = \mathrm{W}, \mathrm{Z}$), resulting from LEP and Tevatron, to the "pole values" denoted by M_V and Γ_V. The relation between the two sets of values is given by [111]

$$M_V = M_V^\mathrm{OS}/\sqrt{1+(\Gamma_V^\mathrm{OS}/M_V^\mathrm{OS})^2}, \qquad \Gamma_V = \Gamma_V^\mathrm{OS}/\sqrt{1+(\Gamma_V^\mathrm{OS}/M_V^\mathrm{OS})^2}, \tag{11.1.2}$$

leading to

$$\begin{aligned}
M_\mathrm{W} &= 80.370\ldots\,\mathrm{GeV}, & \Gamma_\mathrm{W} &= 2.1402\ldots\,\mathrm{GeV},\\
M_\mathrm{Z} &= 91.153\ldots\,\mathrm{GeV}, & \Gamma_\mathrm{Z} &= 2.4943\ldots\,\mathrm{GeV}.
\end{aligned} \tag{11.1.3}$$

We make use of these mass and width parameters in the numerics discussed below, although the difference between using M_V or M_V^OS would be hardly visible.

As mentioned in Section 6.1, we adopt the G_F scheme, where the electromagnetic coupling α is set to α_{G_F}. In this scheme the electric-charge renormalization constant does not contain logarithms of the light-fermion masses, in contrast to the $\alpha(0)$ scheme, so that the results become independent of the light-quark masses.

The $\mathcal{O}(\alpha)$-improved `MRSTQED2004` set of PDFs [78] is used throughout implying the value of $\alpha_\mathrm{s}(M_\mathrm{Z})$ stated above. We use standard two-loop running of the strong coupling constant in the 5-flavour scheme,

$$\alpha_\mathrm{s}^{(5),\mathrm{NLO}}(\mu_\mathrm{R}^2) = \alpha_\mathrm{s}^{(5),\mathrm{LO}}(\mu_\mathrm{R}^2) \left[1 - \frac{\beta_1^{(5)}}{\left(\beta_0^{(5)}\right)^2} \frac{\ln\left(\ln \mu_\mathrm{R}^2/(\Lambda_\mathrm{QCD}^{(5)})^2\right)}{\ln \mu_\mathrm{R}^2/(\Lambda_\mathrm{QCD}^{(5)})^2}\right], \tag{11.1.4}$$

where $\alpha_\mathrm{s}^{(n_f),\mathrm{LO}}(\mu_\mathrm{R}^2)$ denotes the one-loop running (5.4.2), $\beta_1^{(n_f)} = 102 - 38/3\, n_f$ for $N_\mathrm{C} = 3$, and $\Lambda_\mathrm{QCD}^{(5)} = 239\,\mathrm{MeV}$. Since the `MRSTQED2004` PDF set has been released, there have been considerable improvements for PDFs, in particular with respect to the heavy-flavour treatment. Since recent PDF sets do not include QED effects we stick to `MRSTQED2004` for theoretical consistency. Hence, all the absolute values for cross sections lack the recent PDF improvements. However, the presented relative corrections should be more stable with respect to variations in the PDFs than absolute predictions.

The QCD and QED factorization scales as well as the renormalization scale are always identified. For low-p_T jets, the scale of the process is given by the invariant mass of the leptons which in turn peaks around M_W for resonant W-boson production. Hence, one natural choice is the W-boson mass, i.e. $\mu_\mathrm{R} = \mu_\mathrm{F} = M_\mathrm{W}$. For high-$p_\mathrm{T}$ jets, well beyond the W-boson scale, however, the relevant scale is certainly larger, and the QCD emission from the initial state is best modelled by the p_T of the jet itself (see e.g. Ref. [112]). To interpolate between the two regimes, we alternatively use

$$\mu = \mu_\mathrm{R} = \mu_\mathrm{F} = \sqrt{M_\mathrm{W}^2 + (p_\mathrm{T}^\mathrm{had})^2}\,, \tag{11.1.5}$$

where $p_\mathrm{T}^\mathrm{had}$ is given by the p_T of the summed four-momenta of all partons, i.e. quarks and/or gluons in the final state. At LO, $p_\mathrm{T}^\mathrm{had}$ is simply the p_T of the one FS jet. We present results for both scale choices.

11.2 Results on cross sections

We first consider W^+ production in association with a jet at the LHC, i.e. a pp initial state with a cm energy of $\sqrt{s} = 14\,\mathrm{TeV}$.

11.2.1 LHC results

We present the LO cross section σ_0 and various types of corrections δ, defined relative to the LO cross section by $\sigma = \sigma_0 \times (1 + \delta)$. Concerning the EW corrections, we distinguish the cross section $\sigma_\mathrm{EW}^{\mu^+\nu_\mu}$ for bare muons and $\sigma_\mathrm{EW}^\mathrm{rec}$ for which lepton–photon recombination is employed as defined above. Accordingly, the corresponding corrections are labelled $\delta_\mathrm{EW}^{\mu^+\nu_\mu}$

and $\delta_{\text{EW}}^{\text{rec}}$, respectively. An additional label specifies which renormalization and factorization scale is used. Either we use the fixed scale ($\mu = M_{\text{W}}$) or we determine the scale on an event-by-event basis by the kinematical configuration of the final state (var), as specified in (11.1.5). For the EW corrections the difference is not expected to be large, since the LO and the NLO results depend on the renormalization scale for α_{s} and the QCD factorization scale in the same way. However, for the QCD part a sensible scale choice can be crucial for the stability of the perturbative series. Accordingly, the QCD corrections are labelled $\delta_{\text{QCD}}^{\mu=M_{\text{W}}}$ for a fixed scale choice and $\delta_{\text{QCD}}^{\text{var}}$ for the scale choice defined in (11.1.5).

As shown below, the QCD corrections become larger and larger with increasing p_{T} of the leading jet.[1] The increase in the cross section results from a new kinematical configuration which is available for the $\text{W} + 2\,\text{jets}$ final state. The large p_{T} of the leading jet is not balanced by the leptons, as required at LO, but by the second jet. Hence, we encounter the production of 2 jets where one of the quark lines radiates a relatively soft W boson. This part of the cross section, which does not really correspond to a true NLO correction to $\text{W} + \text{jet}$ production, can be separated by employing a veto against a second hard jet in real-emission events. Hence, we present NLO QCD corrections with a jet veto, ($\delta_{\text{QCD,veto}}^{\mu=M_{\text{W}}}$, $\delta_{\text{QCD,veto}}^{\text{var}}$), and without a jet veto, ($\delta_{\text{QCD}}^{\mu=M_{\text{W}}}$, $\delta_{\text{QCD}}^{\text{var}}$).

Using a jet veto based on a fixed p_{T} value for the second jet is not well suited. It will either cut away relatively collinear emission events in the high-p_{T} tails of the leading-jet distribution (leading to large negative corrections) or it has to be chosen too large to be effective in the intermediate-p_{T} parts of the distribution. Hence, we veto any sub-leading jet with $p_{\text{T}} > p_{\text{T,j}_1}/2$, where $p_{\text{T,j}_1}$ denotes the p_{T} of the leading jet. As shown below, this jet veto indeed effectively removes events with back-to-back kinematics.

We also investigate the impact of the photon-induced tree-level processes (6.1.5) and (6.1.6) and the corresponding NLO QCD corrections including the real-emission processes (6.3.13), (6.3.14), and (6.3.15). Since even the LO photon-induced cross section is a small effect, we show its relative impact $\delta_{\gamma,\text{Born}}$ with respect to the LO cross section where initial states with photons are not taken into account. Including the NLO QCD corrections, the relative impact of the full NLO cross section is denoted by $\delta_{\gamma,\text{NLO}}$. The impact of the interference contribution introduced at the end of Section 6.3 is denoted by δ_{IF}. Additional labels again indicate the scale choice and the application of a jet veto.

Table 11.1 shows the LO predictions and the above corrections for different cuts on the p_{T} of the charged lepton p_{T,l^+}. All other cuts and the corresponding event selection follow our default choice as introduced in Section 10.1. All integrated cross sections and, hence, the corrections are dominated by events close to the lowest accepted p_{T,l^+}, as can be seen by the rapid decrease of the integrated cross section when increasing the p_{T,l^+} cut.

Tables 11.2 and 11.3 show the analogous results for a variation of cuts on the transverse mass of the FS leptons, defined by

$$M_{\text{T},l\nu_l} = \sqrt{2 p_{\text{T},l^+} \not{p}_{\text{T}} (1 - \cos\phi_{l\nu_l})}\,, \tag{11.2.1}$$

and the p_{T} of the leading jet $p_{\text{T,jet}}$, respectively. The transverse mass and the p_{T,l^+} distributions are particularly relevant for the measurement of the W-boson mass at hadron colliders. For this measurement, W-boson events without or with very little additional jet

[1] The leading jet is defined as the jet with highest p_{T}.

$pp \to l^+\nu_l \text{ jet} + X$ at $\sqrt{s} = 14\,\text{TeV}$

p_{T,l^+} / GeV	$25 - \infty$	$50 - \infty$	$100 - \infty$	$200 - \infty$	$500 - \infty$	$1000 - \infty$
$\sigma^{\mu=M_\text{W}}_\text{Born}$ / fb	508560(50)	163680(20)	130900(10)	1484.2(2)	44.461(6)	1.3784(2)
$\sigma^{\text{var}}_\text{Born}$ / fb	501770(50)	159450(20)	114800(10)	1124.62(7)	25.873(4)	0.6433(1)
$\delta^{\mu^+\nu_\mu,\text{var}}_\text{EW}$ / %	−3.048(9)	−5.376(6)	−8.948(9)	−14.762(7)	−25.73(3)	−36.46(5)
$\delta^{\text{rec},\text{var}}_\text{EW}$ / %	−2.08(2)	−3.16(2)	−6.51(2)	−11.63(1)	−21.51(4)	−31.17(9)
$\delta^{\mu=M_\text{W}}_\text{QCD}$ / %	48.2(1)	34.4(1)	50.3(1)	30.3(1)	−15.7(1)	−60.4(4)
$\delta^{\text{var}}_\text{QCD}$ / %	47.5(1)	33.8(1)	54.7(1)	46.43(7)	27.58(6)	6.10(4)
$\delta^{\text{var}}_{\gamma,\text{Born}}$ / %	0.3978(3)	0.5869(5)	1.669(1)	2.650(2)	4.049(4)	4.882(5)
$\delta^{\text{var}}_{\gamma,\text{NLO}}$ / %	0.3761(4)	0.5626(7)	1.660(3)	2.642(3)	4.068(4)	4.973(6)
$\delta^{\text{var}}_\text{IF}$ / %	0.0491(3)	0.0176(5)	0.0238(7)	0.0039(8)	−0.050(1)	−0.135(1)

Table 11.1: Integrated cross sections for different cuts on the lepton transverse momentum at the LHC. We show the LO results for both a variable and a constant scale. The relative EW corrections δ_EW are given with and without lepton–photon recombination. The QCD corrections δ_QCD are presented for a fixed as well as a variable scale. The corrections due to photon-induced processes δ_γ, and the contributions from interference terms δ_IF are presented for a variable scale. The error from the Monte Carlo integration for the last digit(s) is given in parentheses.

activity are selected. Nevertheless, the calculation of the EW corrections in the presence of an additional jet supplies a handle to quantify how well the interplay of QCD and EW corrections is understood.

Note that for a given $p_{\text{T,jet}}$ both leptons share the recoil since they stem from a boosted W boson and are therefore preferably emitted in the same direction. Consequently, the LO cross section for a given cut on p_{T,l^+} is smaller than for the same cut on $p_{\text{T,jet}}$, because on average the required cm energy is larger. In other words, there is a kinematic and an additional PDF suppression of events with a cut on the lepton p_T compared to events with the same cut on the jet p_T. For large values of $M_{\text{T},l\nu_l}$, the W boson is necessarily produced far off shell so that the cross section is further suppressed. The presented cut values for $M_{\text{T},l\nu_l}$ are chosen because one finds $M_{\text{T},l\nu_l} = 2p_{\text{T},l}$ for back-to-back leptons in the rest frame of the decaying W boson.

For the most-inclusive cross section (left columns in Table 11.1 or Table 11.3) the EW corrections are at the percent level and negative. The difference in scale choice is not important, and due to the recombination procedure $\delta^\text{rec}_\text{EW}$ is slightly smaller in absolute size. With increasing p_{T,l^+} cut, the relevant cm energies rise, and the well-known Sudakov logarithms in the virtual EW corrections start to dominate the total corrections as expected. For $p_{\text{T},l^+} > 1000$ GeV, the EW corrections reach the level of −30%. This behaviour is generic and also holds true for the cross sections with varying cuts on the transverse

$pp \to l^+\nu_l \text{ jet} + X$ at $\sqrt{s} = 14\,\text{TeV}$

$M_{\text{T},l\nu_l}$ / GeV	$50-\infty$	$100-\infty$	$200-\infty$	$500-\infty$	$1000-\infty$	$2000-\infty$
$\sigma_{\text{Born}}^{\mu=M_{\text{W}}}$ / fb	450720(50)	71030(1)	752.2(1)	53.301(7)	5.0645(8)	0.24029(4)
$\sigma_{\text{Born}}^{\text{var}}$ / fb	446080(50)	69370(1)	714.9(1)	48.618(7)	4.4510(7)	0.20231(4)
$\delta_{\text{EW}}^{\mu^+\nu_\mu,\text{var}}$ / %	−3.126(6)	−5.190(8)	−8.24(1)	−14.79(1)	−22.42(1)	−32.89(3)
$\delta_{\text{EW}}^{\text{rec},\text{var}}$ / %	−2.119(8)	−3.665(7)	−6.784(5)	−12.805(8)	−19.90(1)	−29.28(3)
$\delta_{\text{QCD}}^{\mu=M_{\text{W}}}$ / %	47.7(1)	30.1(2)	11.5(1)	−15.8(1)	−40.5(1)	−69.90(6)
$\delta_{\text{QCD}}^{\text{var}}$ / %	47.2(2)	30.5(2)	14.5(1)	−8.9(1)	−30.4(1)	−56.07(6)
$\delta_{\gamma,\text{Born}}^{\text{var}}$ / %	0.3547(3)	0.3427(8)	0.4464(8)	0.4698(8)	0.4081(6)	0.3307(3)
$\delta_{\gamma,\text{NLO}}^{\text{var}}$ / %	0.3333(4)	0.331(1)	0.431(1)	0.452(1)	0.3912(8)	0.3128(4)
$\delta_{\text{IF}}^{\text{var}}$ / %	0.0575(4)	0.008(1)	−0.0461(6)	−0.0819(5)	−0.0855(3)	−0.0685(1)

Table 11.2: Integrated cross sections for different cuts on the transverse mass of the W at the LHC.

mass or $p_{\text{T,jet}}$. We compare the EW corrections for $p_{\text{T,jet}}$ with previous results obtained in the on-shell approximation of Chapter 5 together with the differential distributions in Section 11.3.

Turning to the NLO QCD results, the corrections $\delta_{\text{QCD}}^{\text{var}}$ for different cuts on p_{T,l^+}, as shown in Table 11.1, are sizable and reach the 50% level for intermediate cut values. For low cut values, $\delta_{\text{QCD}}^{\mu=M_{\text{W}}}$ is practically the same. However, for large cut values, the corrections for a fixed scale differ significantly. Here, $\delta_{\text{QCD}}^{\mu=M_{\text{W}}}$ grows large and negative to compensate for the overestimated LO cross section, which is larger by more than a factor of two with respect to σ_0^{var}. This is expected, since the hard jet recoiling against the high-p_{T} lepton should be reflected in the scale choice. Including the NLO QCD corrections, the difference between the results obtained with our two scale choices is significantly reduced.

For small cut values on the transverse mass, as shown in Table 11.2, the corrections are quite similar to the ones of the corresponding cuts on p_{T,l^+}. However, for large $M_{\text{T},l\nu_l}$, both scale choices fail to reflect the kinematical situation, since the production of a far off-shell W boson is dominated by the region near the threshold set by the cut on $M_{\text{T},l\nu_l}$. In this region the W boson decays mainly to back-to-back leptons with relatively soft jet activity. Hence, $\delta_{\text{QCD}}^{\mu=M_{\text{W}}}$ as well as $\delta_{\text{QCD}}^{\text{var}}$ become large and negative. A scale choice based on the cm energy of the event would be more adequate.

As discussed above, the integrated NLO QCD cross sections for large $p_{\text{T,jet}}$ cuts, as shown in Table 11.3, contain large contributions from a completely different class of events for which two jets recoil against each other. Hence, the corrections are huge. The correction $\delta_{\text{QCD}}^{\mu=M_{\text{W}}}$ is smaller than $\delta_{\text{QCD}}^{\text{var}}$ because it is defined relative to a larger LO cross section. In absolute size, they are similar. Using the jet veto proposed above, the corrections are reduced and $\delta_{\text{QCD}}^{\text{var}}$ rises only to the 50% level for large cut values. The fixed scale choice

$pp \to l^+\nu_l \text{ jet} + X$ at $\sqrt{s} = 14\,\text{TeV}$

$p_{\text{T,jet}}$/ GeV	$25 - \infty$	$50 - \infty$	$100 - \infty$	$200 - \infty$	$500 - \infty$	$1000 - \infty$
$\sigma^{\mu=M_W}_{\text{Born}}$/ fb	508560(50)	182460(10)	49700(5)	8096.1(8)	315.07(1)	11.675(1)
$\sigma^{\text{var}}_{\text{Born}}$/ fb	501770(50)	176090(10)	45312(4)	6488.5(6)	184.73(2)	4.7809(3)
$\delta^{\mu^+\nu_\mu,\text{var}}_{\text{EW}}$/%	−3.048(9)	−3.36(1)	−4.66(1)	−8.52(1)	−18.08(3)	−28.30(2)
$\delta^{\text{rec},\text{var}}_{\text{EW}}$/%	−2.08(2)	−2.59(2)	−4.21(2)	−8.33(2)	−17.93(1)	−28.19(2)
$\delta^{\mu=M_W}_{\text{QCD}}$/%	48.1(1)	64.8(1)	80.71(9)	115.20(9)	188.6(1)	270.3(1)
$\delta^{\text{var}}_{\text{QCD}}$/%	47.5(1)	65.58(9)	85.9(1)	135.14(9)	270.3(1)	495.7(2)
$\delta^{\mu=M_W}_{\text{QCD,veto}}$/%	21.7(1)	18.2(1)	22.5(1)	24.36(8)	5.51(8)	−26.09(9)
$\delta^{\text{var}}_{\text{QCD,veto}}$/%	22.5(1)	20.9(1)	29.91(9)	42.92(8)	52.56(7)	59.29(7)
$\delta^{\text{var}}_{\gamma,\text{Born}}$/%	0.3978(3)	0.7520(6)	1.298(1)	2.039(1)	3.420(2)	5.249(4)
$\delta^{\text{var}}_{\gamma,\text{NLO}}$/%	0.3761(4)	0.7006(8)	1.181(1)	1.877(2)	3.274(3)	5.223(6)
$\delta^{\text{var}}_{\gamma,\text{NLO,veto}}$/%	0.3453(4)	0.6420(7)	1.104(1)	1.765(2)	3.048(3)	4.751(5)
$\delta^{\text{var}}_{\text{IF}}$/%	0.0491(3)	0.1289(5)	0.5076(7)	1.884(1)	11.490(7)	49.85(3)
$\delta^{\text{var}}_{\text{IF,veto}}$/%	0.0102(3)	0.0298(4)	0.1133(5)	0.4034(9)	1.630(2)	4.729(5)

Table 11.3: Integrated cross sections for different cuts on the p_T of the leading jet at the LHC. Corrections with a second jet in real-emission events are shown with and without a jet veto.

leads to even smaller corrections $\delta^{\mu=M_W}_{\text{QCD}}$ in absolute size. However, varying the exact definition of the jet veto, the variable scale turns out to be more robust. We have also verified that our simple jet veto indeed removes mainly events with back-to-back jets from the event selection. If we only veto events with $\cos\phi_{jj} < -0.99$, where ϕ_{jj} is the azimuthal angle in the transverse plane between the two jets, $\delta^{\text{var}}_{\text{QCD}}$ for example is still reduced from 495% to 172% for $p_{\text{T,jet}} > 1000\,\text{GeV}$. Events with $\cos\phi_{jj} > 0$ do not have any noticeable effect.

The contribution δ_γ from the photon-induced processes are small and only reach up to 5% for large cuts on p_{T,l^+} or $p_{\text{T,jet}}$ where the EW and QCD corrections to the dominating tree-level processes are by far larger. The NLO corrections to the photon-induced processes are phenomenologically completely irrelevant.

The corrections δ_{IF} due to the interference between EW and QCD diagrams also turn out to be unimportant. They only increase together with the NLO QCD corrections for large $p_{\text{T,jet}}$. Once a sensible jet veto is applied, they disappear again.

$p\bar{p} \to l^+\nu_l$ jet $+ X$ at $\sqrt{s} = 1.96\,\text{TeV}$

p_{T,l^+} / GeV	$25-\infty$	$50-\infty$	$75-\infty$	$100-\infty$	$200-\infty$	$300-\infty$
$\sigma_{\text{Born}}^{\mu=M_\text{W}}$ / fb	37342(4)	10563(1)	1007.2(2)	263.50(6)	7.242(2)	0.3901(1)
$\sigma_{\text{Born}}^{\text{var}}$ / fb	36061(4)	10052(1)	863.4(2)	209.52(5)	4.834(1)	0.23644(9)
$\delta_{\text{EW}}^{\mu^+\nu_\mu,\text{var}}$ / %	−2.827(5)	−5.39(1)	−6.81(1)	−8.19(1)	−13.15(2)	−17.46(4)
$\delta_{\text{EW}}^{\text{rec},\text{var}}$ / %	−1.88(4)	−2.84(2)	−3.99(3)	−5.15(3)	−9.00(4)	−12.39(9)
$\delta_{\text{QCD}}^{\mu=M_\text{W}}$ / %	33.4(1)	23.9(1)	27.4(1)	18.08(9)	−6.5(1)	−22.34(7)
$\delta_{\text{QCD}}^{\text{var}}$ / %	35.8(1)	27.3(1)	39.6(1)	36.6(1)	28.0(1)	21.4(1)
$\delta_{\gamma,\text{Born}}^{\text{var}}$ / %	0.3762(3)	0.4983(6)	1.144(1)	1.398(2)	1.467(3)	1.283(1)
$\delta_{\gamma,\text{NLO}}^{\text{var}}$ / %	0.3706(4)	0.4909(8)	1.174(2)	1.432(3)	1.525(3)	1.355(2)
$\delta_{\text{IF}}^{\text{var}}$ / %	−0.0994(8)	−0.110(1)	−0.229(2)	−0.262(3)	−0.189(9)	−0.128(5)

Table 11.4: Integrated cross sections for different cuts on the lepton transverse momentum at the Tevatron.

$p\bar{p} \to l^+\nu_l$ jet $+ X$ at $\sqrt{s} = 1.96\,\text{TeV}$

$M_{\text{T},l\nu_l}$ / GeV	$50-\infty$	$100-\infty$	$150-\infty$	$200-\infty$	$400-\infty$	$600-\infty$
$\sigma_{\text{Born}}^{\mu=M_\text{W}}$ / fb	34425(4)	434.5(1)	80.35(1)	27.602(7)	1.2539(3)	0.08821(3)
$\sigma_{\text{Born}}^{\text{var}}$ / fb	33362(4)	415.7(1)	76.03(1)	25.930(6)	1.1572(3)	0.08048(2)
$\delta_{\text{EW}}^{\mu^+\nu_\mu,\text{var}}$ / %	−2.89(1)	−5.02(1)	−6.44(1)	−7.95(1)	−12.65(2)	−16.70(3)
$\delta_{\text{EW}}^{\text{rec},\text{var}}$ / %	−1.92(2)	−3.32(2)	−4.84(1)	−6.12(2)	−9.96(3)	−13.25(2)
$\delta_{\text{QCD}}^{\mu=M_\text{W}}$ / %	33.3(1)	20.9(1)	12.3(1)	7.7(1)	−4.9(2)	−13.2(1)
$\delta_{\text{QCD}}^{\text{var}}$ / %	35.7(1)	24.1(1)	16.8(1)	12.4(1)	1.5(2)	−6.2(1)
$\delta_{\gamma,\text{Born}}^{\text{var}}$ / %	0.3500(3)	0.2343(5)	0.1775(3)	0.1435(2)	0.0743(1)	0.04771(6)
$\delta_{\gamma,\text{NLO}}^{\text{var}}$ / %	0.3432(4)	0.2336(8)	0.1775(3)	0.1438(3)	0.0741(2)	0.04737(8)
$\delta_{\text{IF}}^{\text{var}}$ / %	−0.0963(8)	−0.110(2)	−0.107(1)	−0.0994(8)	−0.073(1)	−0.0442(2)

Table 11.5: Integrated cross sections for different cuts on the transverse mass of the W at the Tevatron.

$p\bar{p} \to l^+\nu_l \text{ jet} + X$ at $\sqrt{s} = 1.96\,\text{TeV}$

$p_{\text{T,jet}}$/ GeV	$25 - \infty$	$50 - \infty$	$75 - \infty$	$100 - \infty$	$200 - \infty$	$300 - \infty$
$\sigma_{\text{Born}}^{\mu=M_W}$/ fb	37342(4)	8849(1)	3115.1(3)	1231.7(1)	54.559(8)	3.6279(6)
$\sigma_{\text{Born}}^{\text{var}}$/ fb	36061(4)	8094(1)	2685.9(3)	998.3(1)	34.990(5)	1.8965(3)
$\delta_{\text{EW}}^{\mu^+\nu_\mu,\text{var}}$/%	−2.827(5)	−2.922(7)	−3.179(7)	−3.704(9)	−6.48(2)	−9.17(3)
$\delta_{\text{EW}}^{\text{rec},\text{var}}$/%	−1.88(4)	−2.12(2)	−2.55(1)	−3.18(2)	−6.18(2)	−9.01(6)
$\delta_{\text{QCD}}^{\mu=M_W}$/%	33.4(1)	31.6(1)	25.2(1)	20.7(1)	6.1(1)	−8.2(1)
$\delta_{\text{QCD}}^{\text{var}}$/%	36.10(6)	39.5(1)	39.4(1)	41.8(1)	56.3(1)	70.6(1)
$\delta_{\text{QCD,veto}}^{\mu=M_W}$/%	20.8(1)	7.2(1)	1.3(1)	−3.8(1)	−24.2(2)	−43.7(1)
$\delta_{\text{QCD,veto}}^{\text{var}}$/%	23.6(1)	15.3(1)	15.1(1)	16.0(1)	19.5(1)	21.1(1)
$\delta_{\gamma,\text{Born}}^{\text{var}}$/%	0.3762(3)	0.8024(7)	1.152(1)	1.421(1)	1.997(2)	2.317(2)
$\delta_{\gamma,\text{NLO}}^{\text{var}}$/%	0.3706(4)	0.768(1)	1.074(1)	1.306(2)	1.824(4)	2.154(3)
$\delta_{\gamma,\text{NLO,veto}}^{\text{var}}$/%	0.3545(4)	0.732(1)	1.039(1)	1.270(2)	1.784(3)	2.102(2)
$\delta_{\text{IF}}^{\text{var}}$/%	−0.0994(8)	−0.386(1)	−0.580(1)	−0.778(2)	−1.972(4)	−3.500(4)
$\delta_{\text{IF,veto}}^{\text{var}}$/%	−0.0364(6)	−0.131(1)	−0.266(1)	−0.356(1)	−0.725(2)	−1.092(1)

Table 11.6: Integrated cross sections for different cuts on the p_{T} of the leading jet at the Tevatron. Corrections with a second jet in real-emission events are shown with and without a jet veto.

11.2.2 Tevatron results

The qualitative features of the corrections at the Tevatron, where protons and antiprotons collide at $\sqrt{s} = 1.96\,\text{TeV}$, are very similar to those at the LHC. At the Tevatron the high-energy, Sudakov regime is not as accessible as at the LHC but the onset of the Sudakov dominance is nevertheless visible as can be seen for the different observables in Tables 11.4 – 11.6. We have adapted the range for the different integrated cross sections to the kinematic reach of the Tevatron.

11.3 Results on momentum and transverse-mass distributions

In Figs. 11.1 – 11.6 we show for various observables the LO distribution and the distribution including the full set of corrections, i.e. the EW corrections δ_{EW}, the contribution of the photon-induced processes $\delta_{\gamma,\text{NLO}}$, interference contribution δ_{IF}, and the QCD corrections δ_{QCD}. The various contributions to the corrections are also shown separately relative to the LO.

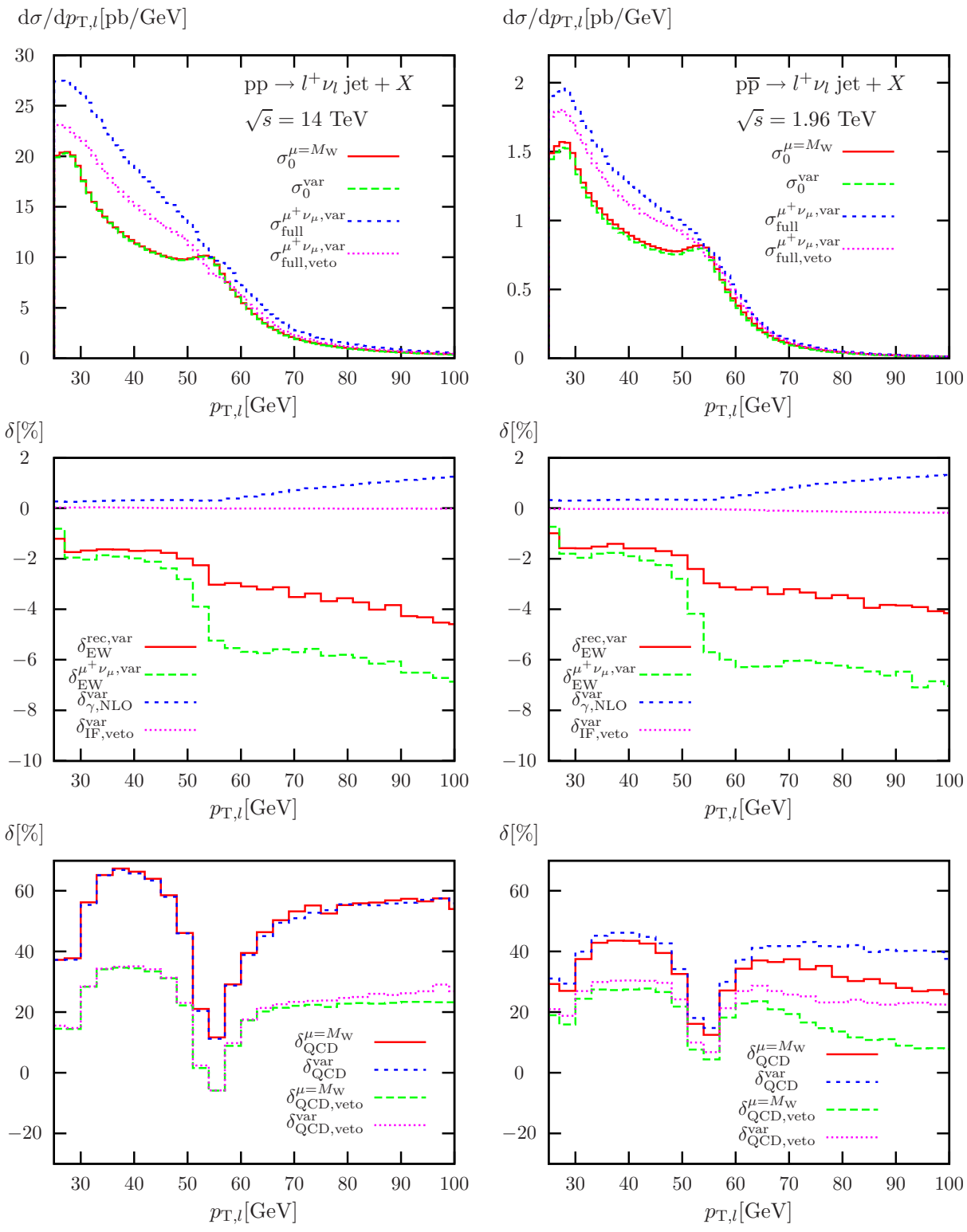

Figure 11.1: LO and fully corrected distribution (top), corresponding relative EW, photon-induced, and interference corrections (middle), and relative QCD corrections (bottom) for the transverse momentum of the charged lepton at the LHC (left) and the Tevatron (right).

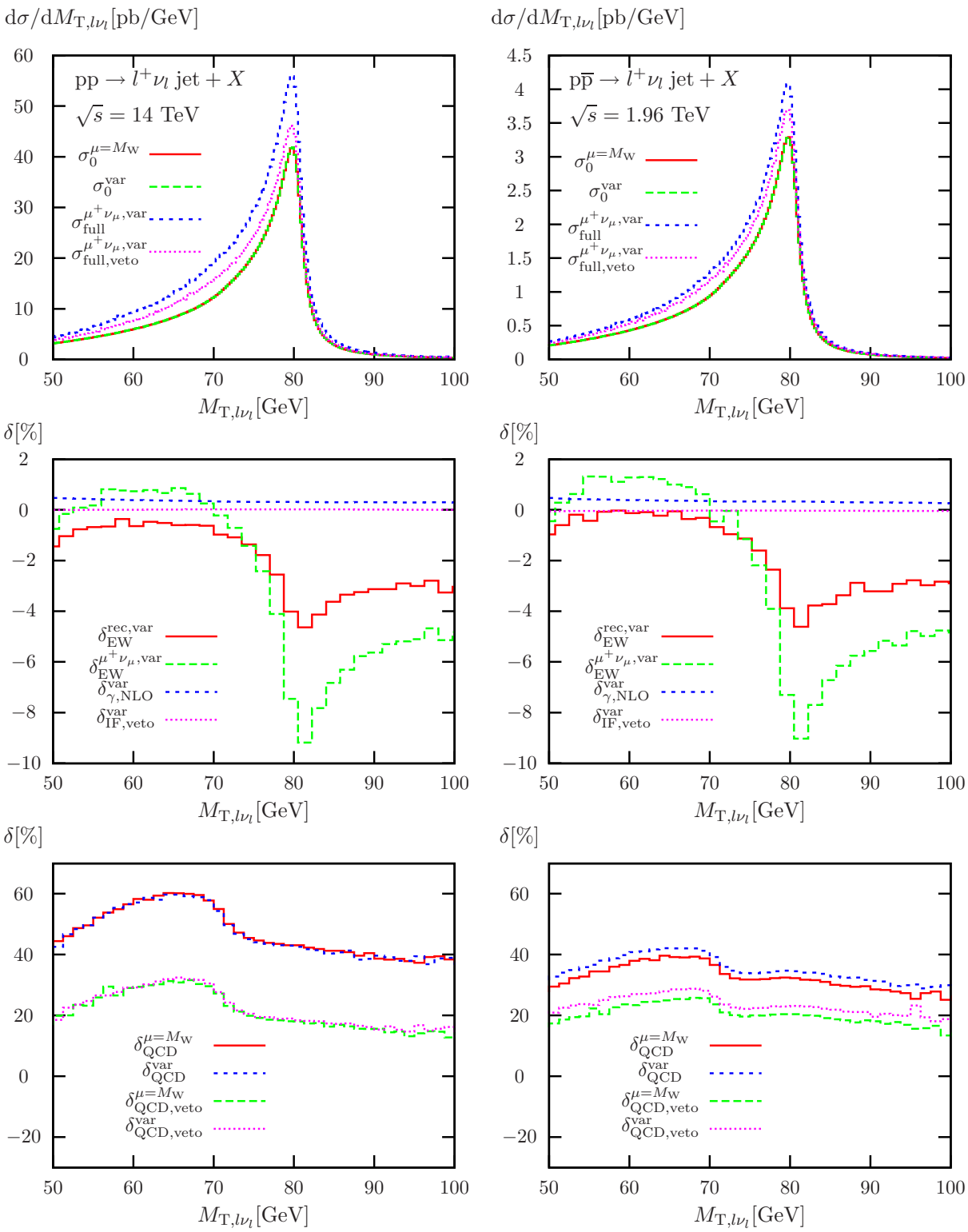

Figure 11.2: LO and fully corrected distribution (top), corresponding relative EW, photon-induced, and interference corrections (middle), and relative QCD corrections (bottom) for the W-boson transverse mass at the LHC (left) and the Tevatron (right).

While the corrections to the integrated cross sections are quite similar for a given p_{T,l^+} and an $M_{\mathrm{T},l\nu_l}$ cut of similar size, the differential distributions in Fig. 11.1 and Fig. 11.2 are significantly different. The EW corrections for the $M_{\mathrm{T},l\nu_l}$ distributions resemble the corrections for the inclusive W-boson sample for which no additional jet is required (see, e.g., Figure 2 in Ref. [22]). This result is expected since the definition (11.2.1) of the transverse mass is boost invariant to first order in the boost velocity and therefore insensitive to a boost of the intermediate W boson. The p_{T,l^+} distribution, in contrast, is sensitive to these boosts, and neither the LO prediction nor the NLO EW corrections resemble the inclusive result (see, e.g., Figure 1 in Ref. [22]).

As expected, the corrections for bare muons are larger since photons, being radiated collinearly to the charged lepton, carry away transverse momentum. Hence, events that are enhanced by muon-mass logarithms are shifted to lower bins in the distributions and to some extent do not survive the basic cuts. As a result, the corrections are dominated by negative virtual corrections that are not compensated by positive bremsstrahlung contributions. This is particularly evident around the peak of the differential cross section with respect to the W-boson transverse mass in Fig. 11.2 and also for the peaks in the transverse-momentum distribution of the charged leptons near $(M_{\mathrm{W}} \pm p_{\mathrm{T,jet}}^{\mathrm{cut}})/2$ in Fig. 11.1.

In Fig. 11.3 we show the differential cross sections with respect to $p_{\mathrm{T,jet}}$ and the corresponding corrections. As expected, the increasing size of the EW corrections with $p_{\mathrm{T,jet}}$ due to the EW Sudakov logarithms can be observed. This observable has also been accessible in calculations using the approximations of a stable, on-shell W boson as worked out in Chapter 5. A comparison of our numerical results to former results for on-shell $\mathrm{W}+\mathrm{jet}$ production [37, 38, 39] has to face the problem that we apply various event-selection cuts to the leptonic final state, while in the previous calculations the degrees of freedom related to the decaying W boson are implicitly integrated out. Nevertheless, the relative EW corrections at high momentum transfer are dominated by Sudakov logarithms [98] of the form $\ln^2(\hat{s}/M_{\mathrm{W}}^2)$ that, at least at the one-loop level, give rise to large process-independent contributions and therefore are expected to show a similar behaviour for both the on- and off-shell case. Comparing our results for the leading-jet $p_{\mathrm{T,jet}}$ (Fig. 11.3) with Fig. 5 in Ref. [39], we in fact find reasonable agreement within 2%. The results for the EW corrections to the integrated cross sections with different cuts on $p_{\mathrm{T,jet}}$ given in Table 11.3 also agree within 1% with the results presented in Fig. 5.9(b) in Chapter 5 for cut values larger than 200 GeV. This figure shows the relative corrections for the sum of W^+- and W^- production at the LHC, but the relative EW corrections to the on-shell W^+ and W^- production rates turn out to be very similar, as can e.g. be seen in Fig. 10 of Ref. [39]. Comparing the EW corrections at the Tevatron given in Table 6 to the on-shell results of Fig. 5.9(a), we observe slightly larger deviations, because the universal Sudakov-like contributions are not dominant at typical Tevatron energy scales.

Turning again to the NLO QCD results, the corrections to p_{T,l^+} and $M_{\mathrm{T},l\nu_l}$ distributions, also displayed in Figs. 11.1 and 11.2, show quite different features. The corrections to the $M_{\mathrm{T},l\nu_l}$ distribution are rather flat, reflecting the well-known fact that the transverse mass is less sensitive to additional QCD radiation. In contrast, the corrections δ_{QCD} for p_{T,l^+} show pronounced dips where the LO cross section has peaks, indicating that the real corrections do not particularly populate the regions of the distributions that are enhanced due to the particular LO kinematics. The QCD corrections to the differential distribution for $p_{\mathrm{T,jet}}$

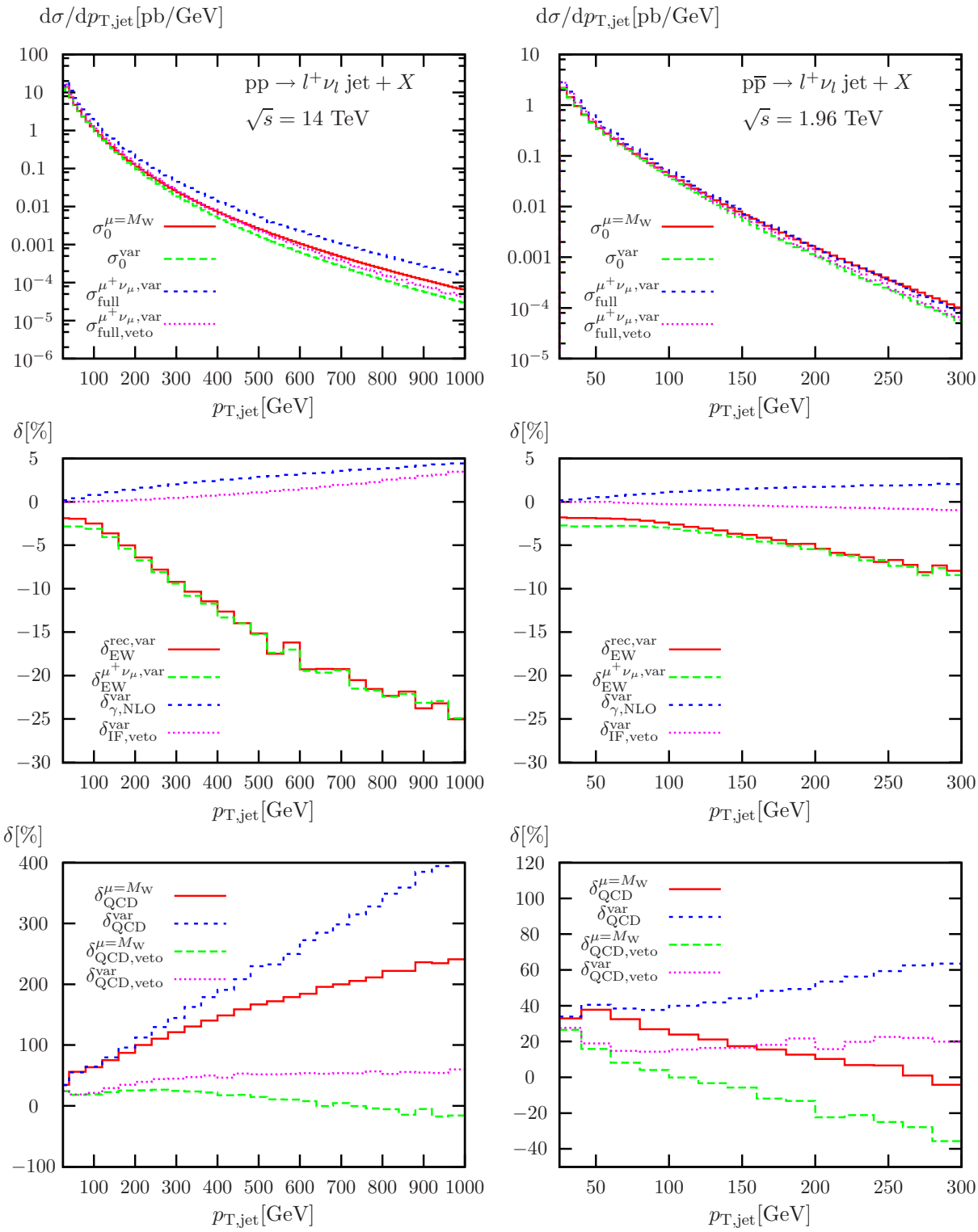

Figure 11.3: LO and fully corrected distribution (top), corresponding relative EW, photon-induced, and interference corrections (middle), and relative QCD corrections (bottom) for the transverse momentum of the leading jet at the LHC (left) and the Tevatron (right).

show exactly the same features which have already been discussed for the integrated cross sections (see Table 11.3), as can be seen in Fig. 11.3.

At the Tevatron, the shapes of the EW and QCD corrections to distributions (see Figs. 11.1 – 11.3) are very similar to the respective results for the LHC. For the p_{T} distribution of the leading jet (see Fig. 11.3), the jet veto again stabilizes the perturbative result. However, using the variable scale choice, the increase in cross section without jet veto is not as pronounced as at the LHC. On the other hand, as expected, the fixed scale choice together with a jet veto leads to large negative corrections. A fixed scale choice without a jet veto accidentally leads to small corrections at the Tevatron.

11.4 Results on rapidity and angular distributions

In Fig. 11.4, we analyse the rapidity distribution for the charged lepton. While the EW corrections are flat, the NLO QCD corrections are larger at large rapidities and, hence, tend to populate the forward and backward regions with more events. Concerning the rapidity of the leading jet at the LHC, both EW and NLO QCD corrections do not disturb the LO shapes of the distribution, as can be seen in Fig. 11.5.

At the Tevatron, the rapidity distributions show the expected asymmetry between the forward and backward direction due to the antiproton in the initial state. This asymmetry is also reflected by asymmetric NLO QCD corrections for the rapidity of the leading jet.

Another interesting observable is the angle between the charged lepton and missing p_{T} in the transverse plane (Fig. 11.6). For W production without jet activity the two leptons are always back-to-back in the transverse plane. Here, with one jet at LO, the distribution is still peaked at large angles. However, back-to-back events are suppressed as shown in Fig. 11.6. While the EW corrections only slightly disturb the shape of the distribution, the NLO QCD corrections tend to distribute events more equally with respect to the investigated angle. However, the dip in the NLO distributions at the LO peak might indicate that higher orders are necessary for an accurate prediction of this observable. The shapes of the relative QCD corrections reflect the large impact of real corrections induced by $\mathrm{W} + 2\,\mathrm{jets}$ configurations where two hard jets are nearly back-to-back while the W boson receives only a small transverse momentum. Such events cause the large positive corrections for $\phi_{l\nu_l} \to 180°$, which are sensitive to the application of the jet veto.

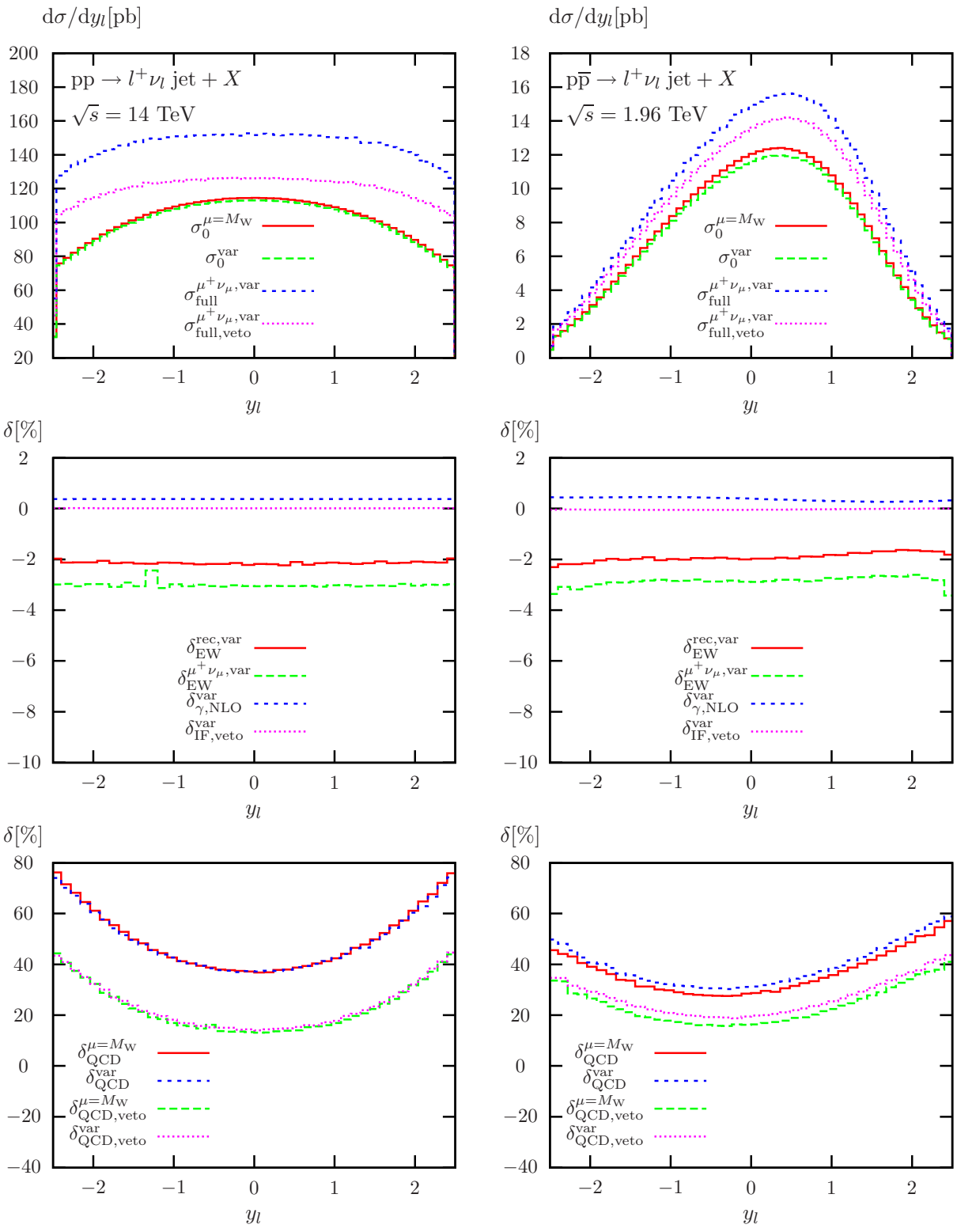

Figure 11.4: LO and fully corrected distribution (top), corresponding relative EW, photon-induced, and interference corrections (middle), and relative QCD corrections (bottom) for the rapidity of the charged lepton at the LHC (left) and the Tevatron (right).

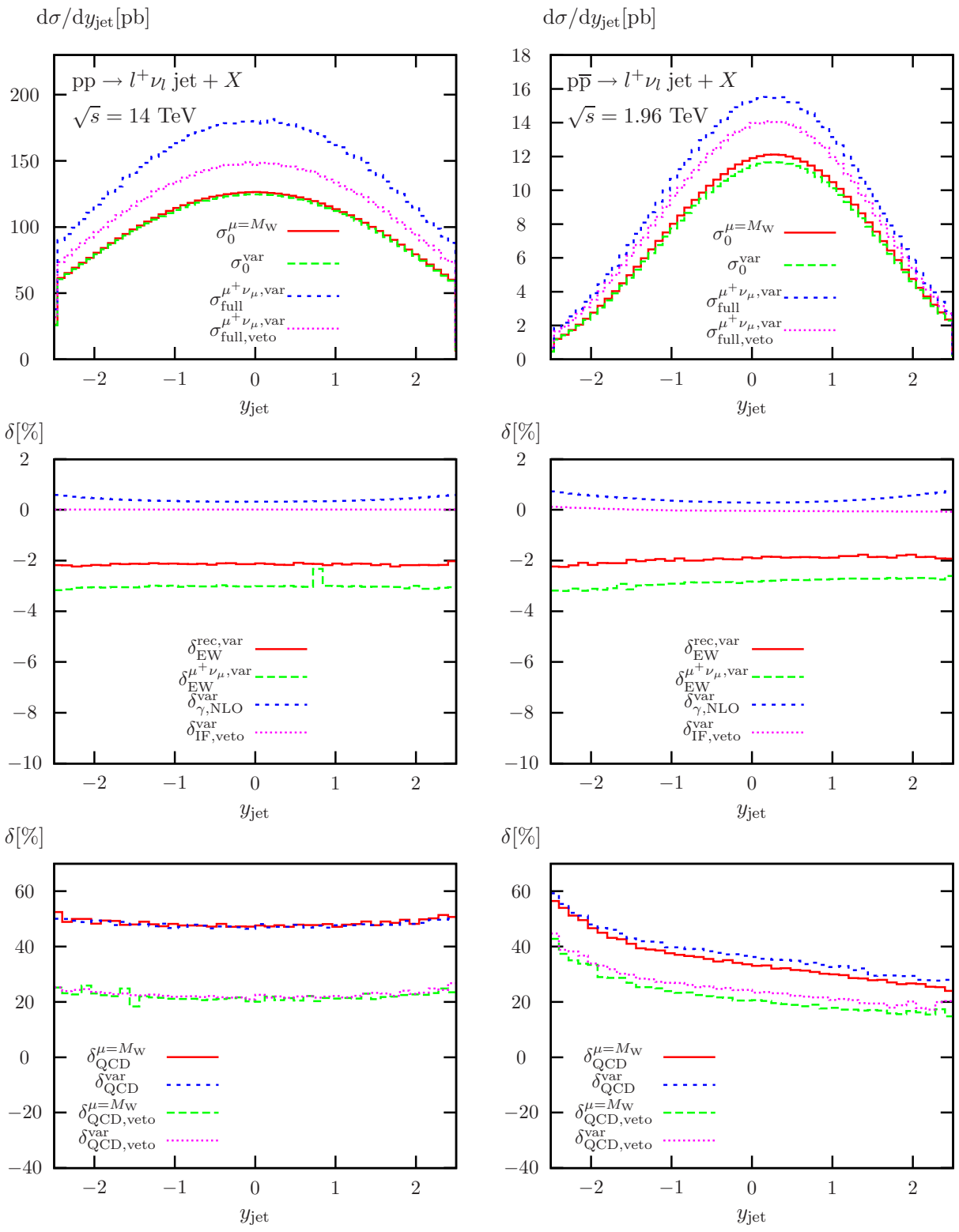

Figure 11.5: LO and fully corrected distribution (top), corresponding relative EW, photon-induced, and interference corrections (middle), and relative QCD corrections (bottom) for the rapidity of the leading jet at the LHC (left) and the Tevatron (right).

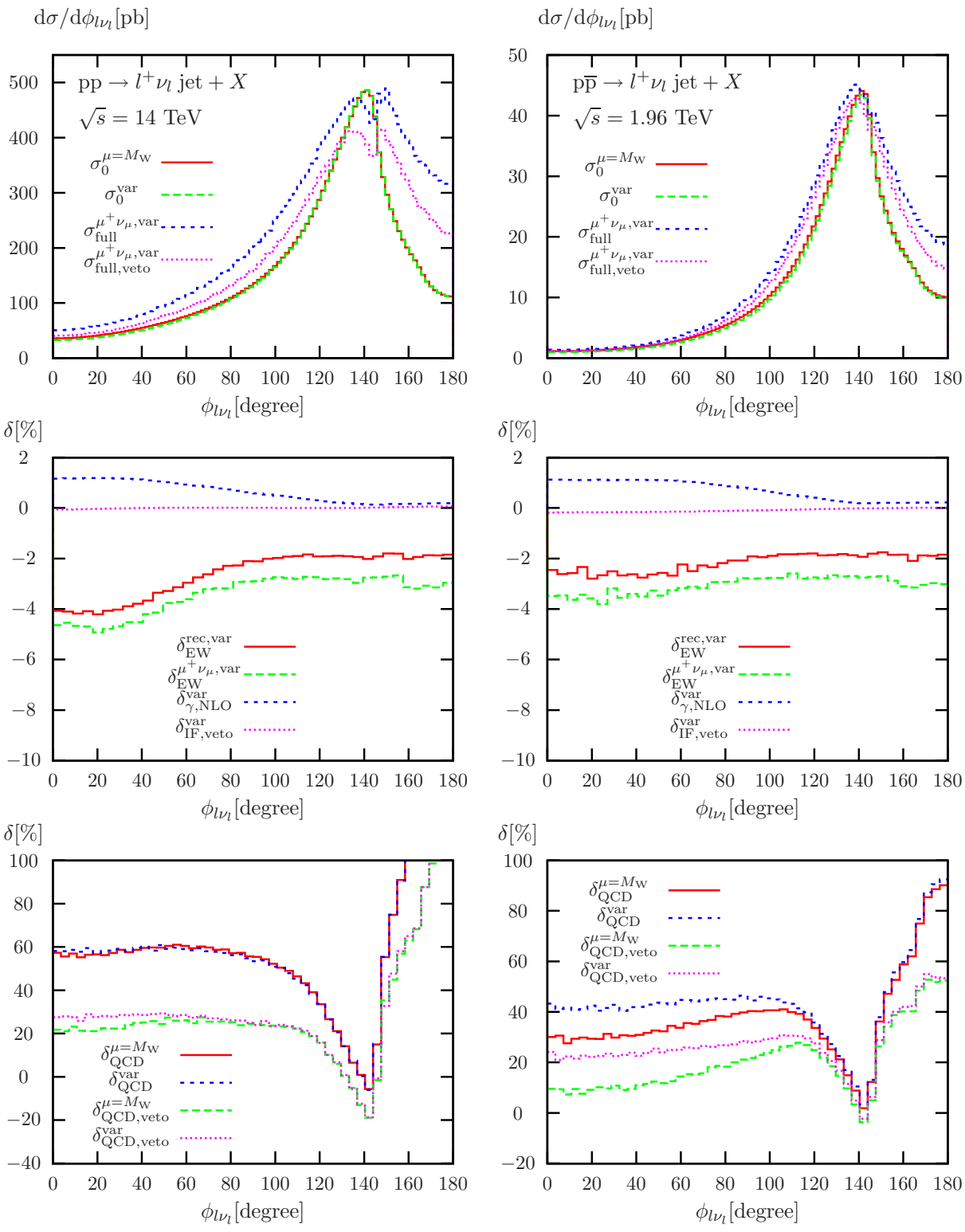

Figure 11.6: LO and fully corrected distribution (top), corresponding relative EW, photon-induced, and interference corrections (middle), and relative QCD corrections (bottom) for the azimuthal angle in the transverse plane between the charged lepton and the neutrino (missing p_T) at the LHC (left) and the Tevatron (right).

Chapter 12

Summary and outlook

In this work we have presented the calculation of radiative corrections to the hadroproduction of a W boson and one associated jet at the LHC and the Tevatron. In a first simpler approach, we have considered a stable W boson that is produced on its mass shell. In a second step, the leptonic decay of the W boson has been included in the calculation, where finite-width effects are consistently accounted for using the complex-mass scheme. We have extended the dipole subtraction method to non-collinear-safe observables in order to enable the computation of radiative corrections related to collinear photon radiation off muons in the final state.

In Chapter 5 we have studied the effect of electroweak radiative corrections at first order on the cross section of the inclusive hadroproduction of single on-shell W bosons with finite values of p_{T}, i.e. accompanied by one hard QCD jet, putting special emphasis on the notion of IR-safe observables with a common treatment of hadron jets initiated by (anti)quarks and gluons.

To circumvent the soft-gluon singularity in the channel $\mathrm{u\bar{d}} \to l\nu_l + \mathrm{g} + \gamma$ after applying a jet algorithm, we additionally include the $\mathcal{O}(\alpha_{\mathrm{s}})$ correction to $\mathrm{W} + \gamma$ production along with the $\mathcal{O}(\alpha)$ correction to $\mathrm{W} + \mathrm{jet}$ production in our calculation that both contribute at absolute order $\mathcal{O}(\alpha^2\alpha_{\mathrm{s}})$ to the cross section. We also consider the contribution from events where one of the colliding hadrons interacts via a real photon, which is of absolute order $\mathcal{O}(\alpha^3)$, if one assumes that the photon PDF within the hadron is suppressed by one order of α. The hadron can then either stay intact (elastic scattering) or be destroyed (inelastic scattering), both contributions were calculated, and the elastic part turned out to be negligible.

Within the on-shell calculation, the UV singularities are extracted using dimensional regularization and removed by renormalization in the on-shell scheme. The IR soft and collinear singularities are regularized by means of an infinitesimal photon or gluon mass λ, and light quark masses m_u and m_d, respectively. We use the phase-space slicing method, with technical slicing cuts on the photon and gluon energies and on the separation angles in the initial and final states, respectively, to isolate the soft and collinear singularities within the corrections from real particle radiation. The cancellation of λ, m_u, and m_d is achieved analytically, and we ensure that the numerical results are insensitive to variations of the slicing cuts within wide ranges.

We have presented theoretical predictions for the total cross sections with a minimum-p_{T} cut and for the p_{T} distributions to be measured in $\mathrm{p\overline{p}}$ collisions with $\sqrt{s} = 1.96$ TeV

at run II at the Tevatron and in pp collisions with $\sqrt{s} = 14$ TeV at the LHC, and estimate the theoretical uncertainties from the scale setting ambiguities. As expected, the renormalization-scale dependence of about 10% in the LO cross section that originates from the strong coupling constant α_s is not significantly reduced after adding the NLO EW corrections. We find that considerably less than 1% of all $W + X$ events contain a prompt photon. The EW corrections considered turn out to be negative and to increase in magnitude with the value of p_T. While the reduction is moderate at the Tevatron, reaching about -4% at $p_T = 200$ GeV, it can be quite sizeable at the LHC, of order -30% at $p_T = 2$ TeV, which is due to the well-known enhancement by Sudakov logarithms. It is an interesting new finding that the photoproduction contribution is considerably larger than expected from the formal order of couplings. In fact, at very high values of p_T, it compensates an appreciable part of the reduction due to the $\mathcal{O}(\alpha^2\alpha_s)$ correction. Nevertheless, taking NLO QCD corrections into account, one finds that the photon-induced contributions are still small compared to those contributions.

As an extension of the on-shell calculation, we have also computed the EW NLO corrections to W + jet production within the SM including the decay of the W boson into a lepton and a neutrino to mimic a realistic experimental scenario as good as possible. Doing so, we are able to apply event-selection cuts to the decay products of the W boson and to provide differential cross sections for leptonic observables that have to be known at high precision in order to allow for an accurate experimental determination of the mass and width of the W boson. As opposed to the procedure in Chapter 5, we use the dipole subtraction method exposed in Chapter 4 to enable the calculation of mass singularities within real corrections both for the EW and the QCD contributions. Thus, to afford a flexible treatment of collinear photons and muons in the final state, we establish the dipole subtraction method for non-collinear-safe observables to account for experimental situations in which collinear photon–muon or photon–quark pairs are not recombined to a new quasi-particle.

Our results have been implemented in a flexible Monte Carlo code which can model the experimental event definition at the NLO parton level. In contrast to the approach presented in Chapter 5, a distinction of W + jet and $W + \gamma$ production is consistently assumed by making use of the measured quark-to-photon fragmentation function that absorbs the residual quark-mass dependence that arises if collinear quark–photon pairs are not recombined properly. We have recalculated the NLO QCD corrections supporting a phase-space dependent scale choice that is better suited to describe events that happen at a high momentum transfer. Interference contributions of EW and QCD diagrams as well as photon-induced processes, contributing at the same order $\mathcal{O}(\alpha^3\alpha_s)$ as the purely EW corrections, are included but—compared with the size of the genuine QCD corrections—turn out to be phenomenologically unimportant.

In Chapter 11 we have presented integrated cross sections for different phase-space cuts and various distributions of differential cross sections. The EW corrections to the transverse mass of the W boson exhibit the same enhancement as for a W boson without jet activity, reaching -10% for corrections without photon–muon recombination at the peak of the LO distribution which is dominated by resonant W bosons. For large transverse mass, i.e. in the off-shell tail of the distribution, we find large negative corrections, dominated by the well-known EW Sudakov logarithms. The EW corrections to the p_T distributions of the lepton and the jet in the final state are rather flat and at the percent level for

small values of p_{T} and also become more and more negative owing to contributions from Sudakov logarithms. In this Sudakov-dominated regime, we find good agreement with the results for the on-shell approximations presented in Chapter 5. The QCD corrections have a typical size of 50%. However, they can become extremely large (hundreds of percent) at large jet p_{T} if one does not apply a sensible jet veto.

The precise prediction for W-boson production at the Tevatron and the LHC is an important task. Our results extend the theoretical effort to associated production with a hard jet. As part of a full NNLO prediction of the mixed EW and QCD corrections for inclusive W production our results can provide a handle for a better understanding of the interplay between EW and QCD corrections in the charged-current Drell–Yan process. Moreover, they establish a flexible precision calculation for one of the most important background processes for BSM-physics searches. In the range of intermediate and large transverse momenta of the additional hard jet our calculation delivers state-of-the-art predictions. For small transverse momenta, however, the pure NLO calculation should of course be improved by dedicated QCD resummations.

Since our calculation includes all relevant fixed-order NLO contribution to the $\mathrm{W}+\mathrm{jet}$ final state and, additionally, provides maximal flexibility, we hope that our results will find their way into the analysis of physical data once the LHC era has started. In the future, the calculation should be supplemented by the inclusion of QCD parton showers or by the inclusion of soft-gluon resummations to improve the reliability of the QCD predictions in the low-p_{T} regime. As an advance on the EW side, we will first tackle the calculation of the EW corrections also for $\mathrm{W}^-+\mathrm{jet}$ production to study in detail the W-boson charge asymmetry given in Eq. (1.0.3). Moreover, we plan to work out the NLO corrections for associated $\mathrm{Z}^0+\mathrm{jet}$ production at the LHC and the Tevatron with a leptonically decaying Z^0 boson. For this purpose, the same techniques can be applied that have been discussed in this thesis, and we expect the calculation to be straight-forward.

Appendix

A Conventions and notation

A.1 General conventions

In this thesis we use the following conventions. The components of a covariant four-vector

$$k^\mu = (k^0, k^1, k^2, k^3) \tag{A.1}$$

are denoted by upper indices, and its spatial part

$$\mathbf{k} = (k^1, k^2, k^3) \tag{A.2}$$

is indicated by a bold symbol. The Lorentz-invariant scalar product of two four-vectors p^μ and k^ν is given by

$$pk \equiv p \cdot k = p^0 k^0 - \mathbf{p} \cdot \mathbf{k} \,. \tag{A.3}$$

Introducing the metric tensor in its canonical definition,

$$g_{\mu\nu} = \mathrm{diag}(1, -1, -1, -1) \,, \tag{A.4}$$

the scalar product can be expresses via

$$pk = g_{\mu\nu} p^\mu k^\nu \,, \tag{A.5}$$

where summation over identical indices is implicitly assumed. The covariant derivative ∂_μ is defined via

$$\partial_\mu k^\mu = \frac{\partial k^0}{\partial x^0} - \boldsymbol{\nabla} \cdot \mathbf{k} \,, \tag{A.6}$$

where the three-dimensional gradient is given by

$$\boldsymbol{\nabla} = \left(\frac{\partial}{\partial x^1}, \frac{\partial}{\partial x^2}, \frac{\partial}{\partial x^3} \right)^{\mathrm{T}} \,. \tag{A.7}$$

Moreover, we introduce the convenient shorthand notation

$$\not{k} = g_{\mu\nu} k^\mu \gamma^\nu \tag{A.8}$$

for the contraction of a four-vector with the Dirac matrices γ^μ.

We use the Feynman rules and coupling parameters arranged in Appendix A of Ref. [47] for the EW part of the SM to express physical scattering amplitudes that are always assigned by caligraphic letters $\mathcal{M}$ or $\mathcal{T}$, respectively. The QCD Feynman rules are taken from Section 2.4.2 of Ref. [48]. All Feynman rules can be translated into the Weyl–van-der-Waerden formalism as explained in Section 4 of Ref. [100].

A.2 Basic definitions for Lie algebras and gauge groups

Since the Standard Model of particle physics is formulated as a gauge theory[1] with the underlying symmetry group

$$\mathrm{U}(1) \times \mathrm{SU}(2) \times \mathrm{SU}(3)\,, \tag{A.9}$$

it is reasonable to discuss some basic definitions of SU(N) gauge groups.

The fundamental representation of the local internal symmetry group SU(N) of any gauge theory is generated via exponentiation by a set of N^2-1 traceless and hermitian $N \times N$ matrices $\boldsymbol{Q}^a$,

$$\boldsymbol{U}(x) = \exp\left[-\mathrm{i}\sum_a \theta^a(x)\boldsymbol{Q}^a\right], \quad a = 1, \ldots, N^2-1\,, \tag{A.10}$$

with adequate group parameters $\theta^a(x)$, where the unitary matrix $\boldsymbol{U}(x)$ is an element of SU(N), i.e. any symmetry transformation of a multiplet $\boldsymbol{\phi}(x)$ in the fundamental representation of SU(N) can be written according to

$$\boldsymbol{\phi}(x) \to \boldsymbol{\phi}'(x) = \boldsymbol{U}(x)\boldsymbol{\phi}(x)\,. \tag{A.11}$$

The matrices $\boldsymbol{Q}^a$ live in the fundamental representation of the Lie algebra $\mathfrak{su}(N)$ that can be defined via its total-antisymmetric structure functions f^{abc} according to

$$[Q^a, Q^b]_{ij} = \mathrm{i}\, f^{abc}\, Q^c_{ij}\,, \tag{A.12}$$

where summation over c is assumed. The *Dynkin index* T_F of the fundamental representation of $\mathfrak{su}(N)$ is defined via

$$\mathrm{Tr}(Q^a Q^b) = \delta^{ab} T_\mathrm{F}, \tag{A.13}$$

with $T_\mathrm{F} = 1/2$. The *Casimir operator* C_F in the fundamental representation of $\mathfrak{su}(N)$ is diagonal,

$$\sum_{a=1}^{N^2-1}\sum_j (Q^a_{ij} Q^a_{jk}) = \delta_{ij} C_\mathrm{F}\,, \tag{A.14}$$

and takes the value

$$C_\mathrm{F} = \frac{N^2-1}{2N}\,. \tag{A.15}$$

The $(N^2-1) \times (N^2-1)$ matrices

$$(Q^a_\mathrm{adj})_{bc} = \mathrm{i} f^{abc}\,, \tag{A.16}$$

that also satisfy the commutation relations (A.12) define the *adjoint representation* of $\mathfrak{su}(N)$, where Dynkin index and Casimir operator are given by $T_\mathrm{A} = C_\mathrm{A} = N$.

[1] A theory that is invariant under continuous local transformations of a given symmetry group is called a gauge theory.

Gauge groups in the SM

- In case of the weak-isospin group SU(2), the three generators are given by the 2×2 matrices
$$I_{ij}^a = \tau_{ij}^a/2\,, \quad a = 1,2,3\,, \tag{A.17}$$
where τ^a denote the three Pauli matrices, and the structure functions ϵ^{abc} are identical to the total-antisymmetric Levi–Civita tensor, i.e. the commutator (A.12) is given by
$$[\tau^a, \tau^b]_{ij} = \mathrm{i}\epsilon^{abc}\tau_{ij}^c\,. \tag{A.18}$$
- The gauge group of QCD, SU(3), is generated by the eight 3×3 matrices
$$T_{ij}^a = \lambda_{ij}^a/2\,, \quad a = 1,\ldots,8\,, \tag{A.19}$$
with the eight Gell-Mann matrices λ_{ij}^a and the non-vanishing structure functions
$$\begin{aligned} &f^{123} = +1\,, \quad f^{458} = f^{678} = \frac{\sqrt{3}}{2}\,, \\ &f^{147} = -f^{156} = f^{246} = f^{257} = f^{345} = -f^{367} = \frac{1}{2}\,. \end{aligned} \tag{A.20}$$

B Techniques for phase-space generation

B.1 Monte Carlo integrators

In general, the integral (2.3.4) is too involved to be worked out analytically owing to the complicated structure of $|\mathcal{M}|^2$. Therefore, Monte Carlo computer techniques are used to compute cross sections numerically by sampling the $m = (3n-4)$-dimensional integrand using m-dimensional tuples of random numbers $\mathbf{r} = (r_1, \ldots, r_m)$ with $0 < r_i < 1$. This is done in the following way.

A given $(3n-4)$-dimensional phase-space integral of the form (2.3.4) can always be expressed via
$$I_n = \int_\Phi \mathrm{d}\sigma_{ab\to f} = \int \mathrm{d}^{3n-4}\boldsymbol{\phi}\; \rho\left(k_i(\boldsymbol{\phi})\right) f\left(k_i(\boldsymbol{\phi})\right)\,, \tag{B.1}$$
where $\boldsymbol{\phi} = (\phi_1, \ldots, \phi_m)$ is a proper parametrization of the phase space $\mathrm{d}\Phi_{(n)}$, $\rho\left(k_i(\boldsymbol{\phi})\right)$ denotes the so-called phase-space density, and
$$f\left(k_i(\boldsymbol{\phi})\right) = \frac{1}{2\hat{s}}\overline{|\mathcal{M}_{ab\to f}(p_a, p_b; k_1(\boldsymbol{\phi}), \ldots, k_n(\boldsymbol{\phi}))|^2}\,. \tag{B.2}$$
The integral (B.1) is now mapped to the $(3n-4)$-dimensional hypercube $\mathbf{r}$ via the transformation $\boldsymbol{\phi} = \mathbf{h}(\mathbf{r})$,
$$\int_{\Phi(\boldsymbol{\phi})} \mathrm{d}^{3n-4}\boldsymbol{\phi}\; \rho\left(k_i(\boldsymbol{\phi})\right) f\left(k_i(\boldsymbol{\phi})\right) = \int_0^1 \mathrm{d}^{3n-4}\mathbf{r}\; \frac{f\left(k_i(\mathbf{h}(\mathbf{r}))\right)}{g\left(k_i(\mathbf{h}(\mathbf{r}))\right)}\,, \tag{B.3}$$
where g denotes the probability density of events generated in phase-space,
$$\frac{1}{g\left(k_i(\boldsymbol{\phi})\right)} = \rho\left(k_i(\boldsymbol{\phi})\right) \left|\frac{\partial \mathbf{h}((r))}{\partial \mathbf{r}}\right|_{\mathbf{r}=\mathbf{h}^{-1}(\boldsymbol{\phi})}\,. \tag{B.4}$$

If one generates N $(3n-4)$-tuples $\mathbf{r}_k$, $k = 1, \ldots, N$, the integral I_n can be approximated by the finite sum

$$\bar{I}_n(N) = \frac{1}{N} \sum_{k=1}^{N} \frac{f\left(k_i(\mathbf{h}(\mathbf{r}_k))\right)}{g\left(k_i(\mathbf{h}(\mathbf{r}_k))\right)} \,. \tag{B.5}$$

Of course, N should be chosen as large as possible, since the statistical deviation of $\bar{I}_n(N)$ from the true result I_n,

$$\delta I_n = \sqrt{\frac{\overline{I_n^2}(N) - \overline{I}_n^2(N)}{N}} \,, \tag{B.6}$$

will decrease $\propto 1/\sqrt{N}$ for large N.

B.2 Generic phase-space decomposition

Appendix C of [113] provides a detailed discussion of the generic construction of phase-space parametrizations. It is shown how different phase-space parametrizations can be built from universal sub-entities, allowing for a proper numerical integration of in principle arbitrarily complicated multi-particle phase-space structures by means of multi-channel integration techniques. In this approach, different phase-space parametrizations are used at the same time to optimally adapt the phase-space weight to the potentially complicated structure of the considered integrand that may result from the various different propagator structures in the underlying S-matrix elements. Moreover, specific mappings are suggested that facilitate to efficiently and generically smooth certain "peaks" in the integrand that arise as a result of s– and t–channel propagators and Breit–Wigner-like structures connected to unstable particles. We will not discuss all these topics in detail, since in this thesis we do not use a sophisticated multi-channel approach. Nevertheless, it is convenient to stress the most important concepts of the generic phase-space generation procedure.

Consider a $2 \to n$ particle scattering process

$$a(p_a) + b(p_a) \to c_1(k_1) \ldots c_n(k_n) \tag{B.7}$$

with the incoming four-momenta p_a^μ and p_b^μ and the outgoing four-momenta k_i^μ, $i = 1, \ldots, n$. According to (2.3.5), the differential phase space for the n-particle final state in four dimensions reads

$$\mathrm{d}\Phi_{(2\to n)} = (2\pi)^{4-3n} \left[\prod_{i=1}^{n} \mathrm{d}^4 k_i \, \delta(k_i^2 - m_i^2)\theta(k_i^0)\right] \delta^{(4)}\left(p_a + p_b - \sum_{i=1}^{n} k_i\right) \,, \tag{B.8}$$

where the $m_i = \sqrt{k_i^2}$ denote the masses of the FS particles. The IS particles are assumed massless. As shown in [113, 114] the phase-space integral $\int \mathrm{d}\Phi_{(2\to n)}$ can be constructed by proper combinations of three generic building blocks. These blocks are

- integrations of s–channel-like variables,
- phase-space integrations $\int \mathrm{d}\Omega_d$ of $1 \to 2$ particle decay processes $i(p_{12}) \to f_1(k_1) + f_2(k_2)$, and

- phase-space integrations $\int \mathrm{d}\Omega_p$ of t–channel-like $2 \to 2$ particle scattering processes $i_1(p_1) + i_2(p_2) \to f_1(k_1) + f_2(k_2)$.

Defining $s_{12} = (k_1 + k_2)^2$, the corresponding analytic expressions for the last two contributions are given by

$$\begin{aligned}
&\int \mathrm{d}\Omega_d(s_{12}; k_1^2, k_2^2) \equiv (2\pi)^2 \int \mathrm{d}\Phi_{(1\to 2)}(p_{12}; k_1, k_2) \\
&= \int \mathrm{d}^4k_1 \, \left[\delta(k_1^2 - m_1^2)\theta(k_1^0)\right] \, \mathrm{d}^4k_2 \, \left[\delta(k_2^2 - m_2^2)\theta(k_2^0)\right] \, \delta^{(4)}(p_{12} - k_1 - k_2)\,, \qquad \text{(B.9)} \\
&\int \mathrm{d}\Omega_p(p_1, p_2; k_1^2, k_2^2) \equiv (2\pi)^2 \int \mathrm{d}\Phi_{(2\to 2)}(p_a, p_b; k_1, k_2) \\
&= \int \mathrm{d}^4k_1 \, \left[\delta(k_1^2 - m_1^2)\theta(k_1^0)\right] \, \mathrm{d}^4k_2 \, \left[\delta(k_2^2 - m_2^2)\theta(k_2^0)\right] \delta^{(4)}(p_1 + p_2 - k_1 - k_2)\,. \qquad \text{(B.10)}
\end{aligned}$$

The δ-functions in $\int \mathrm{d}\Omega_d$ and $\int \mathrm{d}\Omega_p$ can be integrated out analytically, in each case resulting in a residual two-fold non-trivial integration. It turns out to be convenient to parametrize the phase space of the particle decay (B.9) by the azimuthal angle ϕ^* and the polar angle θ^* of particle f_1 in the rest frame of particle i, leading to the explicit form

$$\int \mathrm{d}\Omega_d(s_{12}; k_1^2, k_2^2) = \frac{\lambda^{1/2}\,(s_{12}, k_1^2, k_2^2)}{8\, s_{12}} \int_0^{2\pi} \mathrm{d}\phi^* \int_{-1}^{1} \mathrm{d}\cos\theta^*\,, \qquad \text{(B.11)}$$

where we have introduced the kinematical Kaellen function

$$\lambda(x, y, z) = x^2 + y^2 + z^2 - 2(xy + xz + yz)\,. \qquad \text{(B.12)}$$

The four-vector $k_1^{\mu,*}$ in the rest frame of i is given by

$$k_1^{\mu,*} = (k_1^0, |\mathbf{k}_1^*|\sin\theta^*\cos\phi^*, |\mathbf{k}_1^*|\sin\theta^*\sin\phi^*, |\mathbf{k}_1^*|\cos\theta^*) \qquad \text{(B.13)}$$

where the energy and the absolute value of the three-momentum of the particle read

$$k_1^{0,*} = \frac{s_{12} + k_1^2 - k_2^2}{2\sqrt{s_{12}}}, \quad |\mathbf{k}_1^*| = \frac{\lambda^{1/2}(s_{12}, k_1^2, k_2^2)}{2\sqrt{s_{12}}}\,. \qquad \text{(B.14)}$$

Since the momenta k_1 and k_2 are defined in the rest frame of i, they have to be boosted to the laboratory frame (i.e. the partonic cm frame) via a proper Lorentz transformation, resulting in

$$k_1 = \boldsymbol{B}\,[p_{12}, -\mathbf{p}_{12}]\, k_1^*, \quad k_2 = p_{12} - k_1\,. \qquad \text{(B.15)}$$

The boost matrix $\boldsymbol{B}(Q^0, \mathbf{Q})$ transforms any given four-vector k^μ into the rest frame of Q^μ assigned by $\mathbf{Q} = 0$. Defining $m = \sqrt{Q^2}$ and $\gamma = p^0/m$, one finds

$$\mathbf{k}^* = \mathbf{k} + \left(\frac{\mathbf{Q}\cdot\mathbf{k}}{m^2(\gamma+1)} - \frac{k^0}{m}\right)\mathbf{Q}\,, \qquad \text{(B.16a)}$$

$$k^{*,0} = \frac{1}{m}(Q^0 k^0 - \mathbf{Q}\cdot\mathbf{k}) = \frac{Q\cdot k}{m} \qquad \text{(B.16b)}$$

for the components of the boosted four-vector $k^{*,\mu} = \boldsymbol{B}(Q^0, \mathbf{Q})\, k^\mu$. The inverse transformation $k^\mu = \boldsymbol{B}(Q^0, -\mathbf{Q})\, k^{*,\mu}$ is obtained by inverting the signs of the spatial parts of Q^μ.

The phase-space integral of the t–channel-like scattering process (B.10) should preferably be parametrized explicitly using the variable $t = (p_1 - k_1)^2$, yielding

$$\int \mathrm{d}\Omega_p(p_1, p_2; k_1^2, k_2^2) = \frac{1}{4\,\lambda^{1/2}\,(s_{12}, p_1^2, p_2^2)} \int_0^{2\pi} \mathrm{d}\phi^* \int_{t^-}^{t^+} \mathrm{d}t\,. \tag{B.17}$$

The four-vector k_1^* in the rest frame of $p_1 + p_2$ is given by (B.13), and its polar angle is related to the integration variable t via

$$t = k_1^2 + p_1^2 - \frac{(s_{12} + k_1^2 - k_2^2)(s_{12} + p_1^2 - p_2^2) - \lambda^{1/2}(s_{12}, k_1^2, k_2^2)\lambda^{1/2}(s_{12}, p_1^2, p_2^2)\cos\theta^*}{2\,s_{12}}\,. \tag{B.18}$$

The vector k_1 in the laboratory frame is obtained applying a Lorentz transformation that consists of a rotation and a subsequent boost,

$$k_1 = \boldsymbol{B}\left[p_1^0 + p_2^0, -(\mathbf{p}_1 + \mathbf{p}_2)\right] \boldsymbol{R}(\tilde{\phi}, \cos\tilde{\theta})\, k_1^*, \quad k_2 = p_1 + p_2 - k_1\,. \tag{B.19}$$

The rotation matrix $\boldsymbol{R}(\phi, \cos\theta)$ is given by

$$\boldsymbol{R}(\phi, \cos\theta) = \begin{pmatrix} 1 & 0 & 0 & 0 \\ 0 & \cos\phi & -\sin\phi & 0 \\ 0 & \sin\phi & \cos\phi & 0 \\ 0 & 0 & 0 & 1 \end{pmatrix} \begin{pmatrix} 1 & 0 & 0 & 0 \\ 0 & \cos\theta & 0 & \sin\theta \\ 0 & 0 & 1 & 0 \\ 0 & -\sin\theta & 0 & \cos\theta \end{pmatrix}, \tag{B.20}$$

corresponding to an anti-clockwise θ-rotation around the x^2-axis followed by an anti-clockwise ϕ-rotation around the x^3-axis which in our case coincides with the beam axis. The explicit expressions for the angles $\tilde{\theta}$ and $\tilde{\phi}$ have to be calculated from the incoming momentum $\tilde{p}_1 = \boldsymbol{B}(p_1^0 + p_2^0, \mathbf{p}_1 + \mathbf{p}_2)\, p_1$ according to

$$\tilde{\phi} = \begin{cases} \arctan\left(\frac{\tilde{p}_1^2}{\tilde{p}_1^1}\right) & \text{if} \quad \tilde{p}_1^1 > 0 \\ \arctan\left(\frac{\tilde{p}_1^2}{\tilde{p}_1^1}\right) + \pi & \text{if} \quad \tilde{p}_1^1 < 0 \end{cases}, \quad \cos\tilde{\theta} = \frac{\tilde{p}_1^3}{|\tilde{\mathbf{p}}_1|}\,. \tag{B.21}$$

Finally, the limits

$$t^\pm = k_1^2 + p_1^2 - \frac{(s_{12} + k_1^2 - k_2^2)(s_{12} + p_1^2 - p_2^2) \pm \lambda^{1/2}(s_{12}, k_1^2, k_2^2)\lambda^{1/2}(s_{12}, p_1^2, p_2^2)}{2\,s_{12}} \tag{B.22}$$

of the t-integration are set by simple geometrical constraints, restricting the cosine of θ^* between -1 and 1.

B.3 Breit–Wigner mappings

The integral transformation (B.3) can always be carried out easily using an iterative linear mapping $\boldsymbol{\phi} = \mathbf{h}_l(\mathbf{r})$,

$$\begin{aligned}
\phi_1 &\to \phi_{1,\min} + r_1(\phi_{1,\max} - \phi_{1,\min})\,, \\
\phi_2 &\to \phi_{2,\min}(\phi_1(r_1)) + r_2(\phi_{2,\max}(\phi_1(r_1)) - \phi_{2,\min}(\phi_1(r_1)))\,, \\
&\vdots \\
\phi_m &\to \phi_{m,\min}(\{\phi_i(r_j)\}) + r_m(\phi_{m,\max}(\{\phi_i(r_j)\}) - \phi_{m,\min}(\{\phi_i(r_j)\}))\,,
\end{aligned} \tag{B.23}$$

with $i \leq j < m$, and

$$g_l(\mathbf{h}_l(\mathbf{r})) = \prod_{i=1}^{m}(\phi_{i,\max}(\mathbf{r}) - \phi_{i,\min}(\mathbf{r}))\,, \tag{B.24}$$

but one should keep in mind that this naive procedure does not at all take into account the structure of the integrand, possibly resulting in an inefficient numerical integration. In particular, severe problems can arise if processes including resonances are considered.

If an unstable particle (for instance the weak bosons W or Z) of mass m and width Γ appears in a propagator, the partonic cross section will in general comprise dominating terms of the form

$$\sigma \propto \frac{1}{|p^2 - m^2 + \mathrm{i}m\Gamma|^2} \tag{B.25}$$

(see Section 2.2) that lead to sharp resonance peaks of the integrand when the incoming momentum p is timelike, i.e. $p^2 > 0$. In such situations, a naive numerical integration without adequate phase-space mappings will be very inefficient and maybe even provide wrong results, since only very few random numbers $\mathbf{r}$ will eventually hit the important region $p^2 \sim m^2$ where the cross section is large. This problem can be cured by introducing a so-called Breit–Wigner resonance mapping. If one chooses the timelike invariant p^2 flowing through the problematic propagator as integration variable, the phase-space integral will contain the expression $\int_{p^2_{\min}}^{p^2_{\max}} \mathrm{d}p^2$, with the limits $p^2_{\min\,/\,\max}$. Applying the substitution

$$p^2 \to h(r, m^2, -\mathrm{i}m\Gamma, 2, p^2_{\min}, p^2_{\max}) = m\,\Gamma\,\tan[y_1 + (y_2 - y_1)r] + m^2\,, \tag{B.26}$$

with

$$y_{1/2} = \arctan\left(\frac{p^2_{\min\,/\,\max} - m^2}{m\Gamma}\right) \tag{B.27}$$

and $0 < r < 1$ will mediate a transformation of the integral that is given by

$$\int_{p^2_{\min}}^{p^2_{\max}} \mathrm{d}p^2 \to \int_0^1 \frac{\mathrm{d}r}{g_s(p^2(r), m^2, 2, p^2_{\min}, p^2_{\max})}, \tag{B.28}$$

where the phase-space probability density

$$\begin{aligned}
g_s(p^2(r), m^2, 2, p^2_{\min}, p^2_{\max}) &\equiv \left[\frac{\mathrm{d}h(r, m^2, -\mathrm{i}m\Gamma, 2, p^2_{\min}, p^2_{\max})}{\mathrm{d}r}\right]^{-1} \\
&= \frac{m\Gamma}{(y_1 - y_2)[(p^2(r) - m^2)^2 + m^2\Gamma^2]}
\end{aligned} \tag{B.29}$$

will exactly cancel the problematic denominator (B.25), leaving a smooth function that can be sampled with good efficiency. The procedure of manipulating the integrand in such a way that more random numbers are sampled in phase-space regions where the integrand is large is known as *importance sampling*.

C Dipole subtraction for photonic bremsstrahlung processes

In this appendix we list the explicit formulae for the subtraction functions for the bremsstrahlung corrections to the processes (6.1.1) – (6.1.3). We also present the contributions that have to be readded to the cross section. We follow the notation of [35, 36], and Section 4.2 where we always use the formulae for light emitters and massless spectators. The momenta are always assigned according to (8.0.1), i.e. the incoming partons carry the momenta p_a and p_b, while the momentum of the outgoing QCD parton is denoted by k_c. In the following, we use the shorthand notation $\Phi_\gamma \equiv \Phi_{(ab\to l\nu_l+c+\gamma)}$ to denote the bremsstrahlung phase space. Moreover, we introduce the notation $\tilde{\Phi}_{0,AB}$ for the LO phase space $\Phi_{(ab\to l\nu_l+c)}$ of the auxiliary momenta $\{\tilde{k}_j\}$ that enter the squared LO amplitudes $|\mathcal{M}_{ab\to l\nu_l+c}(\{\tilde{k}_j\})|^2$ within the subtraction kernels which are constructed from an emitter A and a spectator B, respectively. The cut function $F_J^{(l^+\!+\nu_l+c+\gamma)}$ will be denoted as Θ_{cut} in the following.

C.1 Subtraction contributions

Subtraction terms for the channel $\mathrm{u\bar{d}} \to l^+\nu_l \mathrm{g}\gamma$

We first present the two dipoles that have to be constructed with an IS emitter and an IS spectator.

The corresponding auxiliary variables are defined through the momenta of the full bremsstrahlung phase space,

$$x_{\mathrm{u\bar{d}}} = \frac{p_a p_b - p_a k_\gamma - p_b k_\gamma}{p_a p_b}\,, \quad x_{\bar{\mathrm{d}}\mathrm{u}} = x_{\mathrm{u\bar{d}}}\,, \quad y_{\mathrm{u\bar{d}}} = \frac{p_a k_\gamma}{p_a p_b}\,, \quad y_{\bar{\mathrm{d}}\mathrm{u}} = \frac{p_b k_\gamma}{p_a p_b}\,, \tag{C.1}$$

where the momentum assignment of (8.0.1) was used. The two contributing dipoles are given by

$$g^{(\mathrm{sub})}_{\mathrm{u\bar{d}}}(p_a, p_b, k_\gamma) = \frac{1}{(p_a k_\gamma) x_{\mathrm{u\bar{d}}}}\left[\frac{2}{1-x_{\mathrm{u\bar{d}}}} - 1 - x_{\mathrm{u\bar{d}}}\right], \tag{C.2}$$

$$g^{(\mathrm{sub})}_{\bar{\mathrm{d}}\mathrm{u}}(p_b, p_a, k_\gamma) = \frac{1}{(p_b k_\gamma) x_{\bar{\mathrm{d}}\mathrm{u}}}\left[\frac{2}{1-x_{\bar{\mathrm{d}}\mathrm{u}}} - 1 - x_{\bar{\mathrm{d}}\mathrm{u}}\right], \tag{C.3}$$

and the auxiliary IS momenta which enter the LO matrix elements are constructed according to

$$\mathrm{u\bar{d}\ case}: \quad \tilde{p_a}^\mu = x_{\mathrm{u\bar{d}}} p_a^\mu\,, \quad \tilde{P}^\mu_{\mathrm{u\bar{d}}} = x_{\mathrm{u\bar{d}}} p_a^\mu + p_b^\mu\,, \quad P^\mu_{\mathrm{u\bar{d}}} = p_a^\mu + p_b^\mu - k_\gamma^\mu\,, \quad \tilde{p_b}^\mu = p_b^\mu, \tag{C.4}$$

$$\bar{\mathrm{d}}\mathrm{u}\ \mathrm{case}: \quad \tilde{p_b}^\mu = x_{\bar{\mathrm{d}}\mathrm{u}} p_b^\mu\,, \quad \tilde{P}^\mu_{\bar{\mathrm{d}}\mathrm{u}} = x_{\bar{\mathrm{d}}\mathrm{u}} p_b^\mu + p_a^\mu\,, \quad P^\mu_{\bar{\mathrm{d}}\mathrm{u}} = p_b^\mu + p_a^\mu - k_\gamma^\mu\,, \quad \tilde{p_a}^\mu = p_a^\mu, \tag{C.5}$$

for the $\mathrm{u}\bar{\mathrm{d}}$ and the $\bar{\mathrm{d}}\mathrm{u}$ cases, respectively. All remaining FS momenta $\{k_i\}$ that are used to calculate the physical observables are modified by a Lorentz transformation,

$$\tilde{k}_i^\mu = \Lambda^\mu{}_\nu\, k_i^\nu\,, \quad \Lambda^\mu{}_\nu = g^\mu{}_\nu - \frac{(P_{qq'}+\tilde{P}_{qq'})^\mu (P_{qq'}+\tilde{P}_{qq'})_\nu}{P_{qq'}^2 + (P_{qq'}\tilde{P}_{qq'})} + \frac{2\tilde{P}^\mu_{qq'} P_{qq',\nu}}{P^2_{qq'}}\,, \tag{C.6}$$

where qq' denotes the two different contributions $\mathrm{u}\bar{\mathrm{d}}$ and $\bar{\mathrm{d}}\mathrm{u}$.

We find four contributing dipoles that are built from an IS emitter and a FS spectator, and vice versa. The auxiliary variables that are needed to construct the subtraction kernels read

$$x_{l\mathrm{u}} = \frac{p_a k_l + p_a k_\gamma - k_l k_\gamma}{p_a k_l + p_a k_\gamma}\,, \quad z_{l\mathrm{u}} = \frac{p_a k_l}{p_a k_l + p_a k_\gamma}\,, \tag{C.7}$$

$$x_{l\bar{\mathrm{d}}} = \frac{p_b k_l + p_b k_\gamma - k_l k_\gamma}{p_b k_l + p_b k_\gamma}\,, \quad z_{l\bar{\mathrm{d}}} = \frac{p_b k_l}{p_b k_l + p_b k_\gamma}\,, \tag{C.8}$$

and the dipoles are given by

$$g_{\mathrm{ul}}^{(\mathrm{sub})}(p_a, k_l, k_\gamma) = \frac{1}{(p_a k_\gamma) x_{lu}}\left[\frac{2}{2 - x_{lu} - z_{lu}} - 1 - x_{lu}\right], \tag{C.9}$$

$$g_{l\mathrm{u}}^{(\mathrm{sub})}(k_l, p_a, k_\gamma) = \frac{1}{(k_l k_\gamma) x_{lu}}\left[\frac{2}{2 - x_{lu} - z_{lu}} - 1 - z_{lu}\right], \tag{C.10}$$

$$g_{\bar{\mathrm{d}}l}^{(\mathrm{sub})}(p_b, k_l, k_\gamma) = \frac{1}{(p_b k_\gamma) x_{ld}}\left[\frac{2}{2 - x_{ld} - z_{ld}} - 1 - x_{ld}\right], \tag{C.11}$$

$$g_{l\bar{\mathrm{d}}}^{(\mathrm{sub})}(k_l, p_b, k_\gamma) = \frac{1}{(k_l k_\gamma) x_{ld}}\left[\frac{2}{2 - x_{ld} - z_{ld}} - 1 - z_{ld}\right]. \tag{C.12}$$

The auxiliary momenta that enter the LO matrix elements are constructed from the original bremsstrahlung momenta via

$$\tilde{k_l}^\mu = k_l^\mu + k_\gamma^\mu - (1 - x_{l\mathrm{u}}) p_a^\mu\,, \quad \tilde{p_a}^\mu = x_{l\mathrm{u}} p_a^\mu\,, \tag{C.13}$$

for the ul case, and

$$\tilde{k_l}^\mu = k_l^\mu + k_\gamma^\mu - (1 - x_{l\bar{\mathrm{d}}}) p_b^\mu\,, \quad \tilde{p_b}^\mu = x_{l\bar{\mathrm{d}}} p_b^\mu\,, \tag{C.14}$$

for the $\bar{\mathrm{d}}l$ case. All other momenta remain unchanged. Exploiting momentum conservation, we define the momenta

$$P_{l\mathrm{u}}^\mu = k_l^\mu + k_\gamma^\mu - p_a^\mu = \tilde{k_l}^\mu - \tilde{p_a}^\mu\,, \tag{C.15}$$

$$P_{l\bar{\mathrm{d}}}^\mu = k_l^\mu + k_\gamma^\mu - p_b^\mu = \tilde{k_l}^\mu - \tilde{p_b}^\mu\,, \tag{C.16}$$

that will be needed in the calculation of the readded counterparts. In case of photon radiation off FS leptons we are also interested in calculating non-collinear-safe observables, which means that the photon and the emitting fermion are not considered as one quasi particle in the collinear cone and that cuts are imposed solely on the bare lepton. For this purpose we have to reconstruct the photon momentum and the antilepton momentum from the auxiliary momentum $\tilde{k_l}^\mu$ via

$$k_\gamma'^\mu = (1 - z_{l\{\mathrm{u},\bar{\mathrm{d}}\}})\,\tilde{k_l}^\mu\,, \quad k_l'^\mu = z_{l\{\mathrm{u},\bar{\mathrm{d}}\}}\,\tilde{k_l}^\mu\,. \tag{C.17}$$

These reconstructed momenta then enter the cut function of the hard bremsstrahlung process.

According to Eq. (4.2.2), the local counterterm that has to be subtracted from the squared bremsstrahlung amplitude is given by

$$
\begin{aligned}
&|\mathcal{M}_{\text{sub}}(\Phi_\gamma)|^2 \\
&\quad = -e^2 \Big[Q_u \sigma_u Q_d \sigma_d \; g_{\text{u}\bar{\text{d}}}^{(\text{sub})}(p_a, p_b, k_\gamma) \left| \mathcal{M}^0_{\text{u}\bar{\text{d}}\to l^+\nu_l \text{g}} \left(\tilde{\Phi}_{0,\text{u}\bar{\text{d}}} \right) \right|^2 \Theta_{\text{cut}}(\tilde{p}_a, \tilde{p}_b; \tilde{k}_l, \tilde{k}_n, \tilde{k}_c, 0) \\
&\qquad + Q_d \sigma_d Q_u \sigma_u \; g_{\bar{\text{d}}\text{u}}^{(\text{sub})}(p_b, p_a, k_\gamma) \left| \mathcal{M}^0_{\text{u}\bar{\text{d}}\to l^+\nu_l \text{g}} \left(\tilde{\Phi}_{0,\bar{\text{d}}\text{u}} \right) \right|^2 \Theta_{\text{cut}}(\tilde{p}_a, \tilde{p}_b; \tilde{k}_l, \tilde{k}_n, \tilde{k}_c, 0) \\
&\qquad + Q_u \sigma_u Q_l \sigma_l \; g_{\text{u}l}^{(\text{sub})}(p_a, k_l, k_\gamma) \left| \mathcal{M}^0_{\text{u}\bar{\text{d}}\to l^+\nu_l \text{g}} \left(\tilde{\Phi}_{0,\text{u}l} \right) \right|^2 \Theta_{\text{cut}}(\tilde{p}_a, p_b; \tilde{k}_l, k_n, k_c, 0) \\
&\qquad + Q_d \sigma_d Q_l \sigma_l \; g_{\bar{\text{d}}l}^{(\text{sub})}(p_b, k_l, k_\gamma) \left| \mathcal{M}^0_{\text{u}\bar{\text{d}}\to l^+\nu_l \text{g}} \left(\tilde{\Phi}_{0,\bar{\text{d}}l} \right) \right|^2 \Theta_{\text{cut}}(p_a, \tilde{p}_b; \tilde{k}_l, k_n, k_c, 0) \\
&\qquad + Q_l \sigma_l Q_u \sigma_u \; g_{l\text{u}}^{(\text{sub})}(k_l, p_a, k_\gamma) \left| \mathcal{M}^0_{\text{u}\bar{\text{d}}\to l^+\nu_l \text{g}} \left(\tilde{\Phi}_{0,l\text{u}} \right) \right|^2 \Theta_{\text{cut}}(\tilde{p}_a, p_b; k'_l, k_n, k_c, k'_\gamma) \\
&\qquad + Q_l \sigma_l Q_d \sigma_d \; g_{l\bar{\text{d}}}^{(\text{sub})}(k_l, p_b, k_\gamma) \left| \mathcal{M}^0_{\text{u}\bar{\text{d}}\to l^+\nu_l \text{g}} \left(\tilde{\Phi}_{0,l\bar{\text{d}}} \right) \right|^2 \Theta_{\text{cut}}(p_a, \tilde{p}_b; k'_l, k_n, k_c, k'_\gamma) \Big] .
\end{aligned}
\tag{C.18}
$$

Note that the squared LO amplitude in every single subtraction contribution is always defined on the reduced phase-space $\tilde{\Phi}_{0,AB}$ that is spanned by the corresponding auxiliary momenta. The same momenta also have to be used to calculate physical observables to impose event-selection cuts, i.e. every subtraction kernel has to be multiplied with the cut function Θ_{cut} that acts on the corresponding momenta defined on the auxiliary phase space $\tilde{\Phi}_{0,AB}$. In case of non-collinear-safe photon radiation off FS leptons, the momenta of the photon and the lepton have to be reconstructed according to (C.17) from the auxiliary momenta entering the underlying process without photon radiation. As suggested by (4.2.4), those reconstructed momenta are then used to compute the observables that are treated in a non-collinear-safe way.

Subtraction terms for the channel ug $\to l^+\nu_l$dγ

Instead of pairs of an IS emitter and an IS spectator we are now also confronted with the situation where emitter and spectator (namely quark and lepton, or vice versa) are both FS particles. Defining the auxiliary variables

$$
y_{\text{d}l} = \frac{k_c k_\gamma}{k_c k_l + k_c k_\gamma + k_l k_\gamma} , \quad z_{\text{d}l} = \frac{k_c k_l}{k_c k_l + k_l k_\gamma} , \tag{C.19}
$$

and

$$
y_{l\text{d}} = \frac{k_l k_\gamma}{k_c k_l + k_l k_\gamma + k_c k_\gamma} , \quad z_{l\text{d}} = \frac{k_c k_l}{k_c k_l + k_c k_\gamma} , \tag{C.20}
$$

we obtain the subtraction functions

$$
g_{\text{d}l}^{(\text{sub})} = \frac{1}{(k_c k_\gamma)(1 - y_{\text{d}l})} \left[\frac{2}{1 - z_{\text{d}l}(1 - y_{\text{d}l})} - 1 - z_{\text{d}l} \right] , \tag{C.21}
$$

$$
g_{l\text{d}}^{(\text{sub})} = \frac{1}{(k_l k_\gamma)(1 - y_{l\text{d}})} \left[\frac{2}{1 - z_{l\text{d}}(1 - y_{l\text{d}})} - 1 - z_{l\text{d}} \right] . \tag{C.22}
$$

For the ld case, the auxiliary momenta that enter the LO subprocess are given by

$$\tilde{k_l}^{\mu} = k_l^{\mu} + k_\gamma^{\mu} - \frac{y_{l\mathrm{d}}}{1-y_{l\mathrm{d}}} k_c^{\mu}\,, \quad \tilde{k_c}^{\mu} = \frac{1}{1-y_{l\mathrm{d}}} k_c^{\mu}\,, \tag{C.23}$$

and for the dl case, they read

$$\tilde{k_c}^{\mu} = k_c^{\mu} + k_\gamma^{\mu} - \frac{y_{\mathrm{d}l}}{1-y_{\mathrm{d}l}} k_l^{\mu}\,, \quad \tilde{k_l}^{\mu} = \frac{1}{1-y_{\mathrm{d}l}} k_l^{\mu}\,. \tag{C.24}$$

All other FS momenta remain unchanged. To treat the lepton–photon pair or the quark–photon pair exclusively, the corresponding momenta have to be reconstructed from the adequate auxiliary momenta according to

$$k_\gamma'^{\mu} = (1-z_{l\mathrm{d}})\tilde{k_l}^{\mu}, \quad k_l'^{\mu} = z_{l\mathrm{d}}\,\tilde{k_l}^{\mu}\,, \tag{C.25}$$

in the ld-case and

$$k_\gamma'^{\mu} = (1-z_{\mathrm{d}l})\tilde{k_c}^{\mu}, \quad k_c'^{\mu} = z_{\mathrm{d}l}\,\tilde{k_c}^{\mu}\,, \tag{C.26}$$

for the collinear quark-photon splitting. Momentum conservation now implies

$$\begin{aligned} P_{l\mathrm{d}}^{\mu} &= k_l^{\mu} + k_c^{\mu} + k_\gamma^{\mu} = \tilde{k_l}^{\mu} + \tilde{k_c}^{\mu}\,, \\ P_{\mathrm{d}l}^{\mu} &= P_{l\mathrm{d}}^{\mu}\,. \end{aligned} \tag{C.27}$$

The full subtraction contribution for the bremsstrahlung process $\mathrm{ug} \to l^+\nu_l \mathrm{d}\gamma$ is given by

$$\begin{aligned} &|\mathcal{M}_{\mathrm{sub}}(\Phi_\gamma)|^2 \\ &\quad = -e^2\Big[Q_u\sigma_u Q_d\sigma_d\; g_{\mathrm{ud}}^{(\mathrm{sub})}(p_a,k_c,k_\gamma)\left|\mathcal{M}^0_{\mathrm{ug}\to l^+\nu_l\mathrm{d}}\left(\tilde{\Phi}_{0,\mathrm{ud}}\right)\right|^2\Theta_{\mathrm{cut}}(\tilde{p}_a,p_b;k_l,k_n,\tilde{k}_c,0) \\ &\qquad + Q_d\sigma_d Q_u\sigma_u\; g_{\mathrm{du}}^{(\mathrm{sub})}(k_c,p_a,k_\gamma)\left|\mathcal{M}^0_{\mathrm{ug}\to l^+\nu_l\mathrm{d}}\left(\tilde{\Phi}_{0,\mathrm{du}}\right)\right|^2\Theta_{\mathrm{cut}}(\tilde{p}_a,p_b;k_l,k_n,k_c',k_\gamma') \\ &\qquad + Q_u\sigma_u Q_l\sigma_l\; g_{\mathrm{ul}}^{(\mathrm{sub})}(p_a,k_l,k_\gamma)\left|\mathcal{M}^0_{\mathrm{ug}\to l^+\nu_l\mathrm{d}}\left(\tilde{\Phi}_{0,\mathrm{ul}}\right)\right|^2\Theta_{\mathrm{cut}}(\tilde{p}_a,p_b;\tilde{k}_l,k_n,k_c,0) \\ &\qquad + Q_d\sigma_d Q_l\sigma_l\; g_{\mathrm{dl}}^{(\mathrm{sub})}(k_c,k_l,k_\gamma)\left|\mathcal{M}^0_{\mathrm{ug}\to l^+\nu_l\mathrm{d}}\left(\tilde{\Phi}_{0,\mathrm{dl}}\right)\right|^2\Theta_{\mathrm{cut}}(p_a,p_b;\tilde{k}_l,k_n,k_c',k_\gamma') \\ &\qquad + Q_l\sigma_l Q_u\sigma_u\; g_{l\mathrm{u}}^{(\mathrm{sub})}(k_l,p_a,k_\gamma)\left|\mathcal{M}^0_{\mathrm{ug}\to l^+\nu_l\mathrm{d}}\left(\tilde{\Phi}_{0,l\mathrm{u}}\right)\right|^2\Theta_{\mathrm{cut}}(\tilde{p}_a,p_b;k_l',k_n,k_c,k_\gamma') \\ &\qquad + Q_l\sigma_l Q_d\sigma_d\; g_{l\mathrm{d}}^{(\mathrm{sub})}(k_l,k_c,k_\gamma)\left|\mathcal{M}^0_{\mathrm{ug}\to l^+\nu_l\mathrm{d}}\left(\tilde{\Phi}_{0,l\mathrm{d}}\right)\right|^2\Theta_{\mathrm{cut}}(p_a,p_b;k_l',k_n,\tilde{k}_c,k_\gamma')\Big]\,, \end{aligned} \tag{C.28}$$

where the contributions $g_{\mathrm{ud}}^{(\mathrm{sub})}$ and $g_{\mathrm{du}}^{(\mathrm{sub})}$ are obtained analogously to the expressions $g_{\mathrm{ul}}^{(\mathrm{sub})}$ and $g_{l\mathrm{u}}^{(\mathrm{sub})}$ in (C.1). The subtraction function for the process $\bar{\mathrm{d}}\mathrm{g} \to l^+\nu_l\bar{\mathrm{u}}$ emerges from (C.28) via the replacement $\mathrm{u} \to \bar{\mathrm{d}}$ and $\mathrm{d} \to \bar{\mathrm{u}}$.

C.2 Readded Counterparts

Convolution terms for the channel $\mathrm{u\bar{d}} \to l^+\nu_l \mathrm{g}\gamma$

In case of the $\mathrm{u\bar{d}}$- and the $\bar{\mathrm{d}}\mathrm{u}$-parts of the subtraction function the analytically-integrated counterparts that have to be added to the result read

$$\begin{aligned}
\int \mathrm{d}\Phi_\gamma |\mathcal{M}_{\mathrm{sub},\mathrm{u\bar{d}}}|^2 &= -\frac{\alpha}{2\pi} Q_u \sigma_u Q_d \sigma_d \int_0^1 \mathrm{d}x \Big\{ \left[\mathcal{G}^{(\mathrm{sub})}_{\mathrm{u\bar{d}}}(\hat{s},x)\right]_+ + G^{(\mathrm{sub})}_{\mathrm{u\bar{d}}}(\hat{s})\delta(1-x) \Big\} \\
&\quad \times \frac{1}{x} \int \mathrm{d}\tilde{\Phi}_{0,\mathrm{u\bar{d}}}(\hat{s},x) |\mathcal{M}_{\mathrm{u\bar{d}}\to l^+\nu_l \mathrm{g}}(xp_a, p_b, \tilde{k}_l, \tilde{k}_n, \tilde{k}_c)|^2 \Theta_{\mathrm{cut}}(xp_a, p_b; \tilde{k}_l, \tilde{k}_n, \tilde{k}_c, 0)\,, \\
\int \mathrm{d}\Phi_\gamma |\mathcal{M}_{\mathrm{sub},\bar{\mathrm{d}}\mathrm{u}}|^2 &= -\frac{\alpha}{2\pi} Q_u \sigma_u Q_d \sigma_d \int_0^1 \mathrm{d}x \Big\{ \left[\mathcal{G}^{(\mathrm{sub})}_{\bar{\mathrm{d}}\mathrm{u}}(\hat{s},x)\right]_+ + G^{(\mathrm{sub})}_{\bar{\mathrm{d}}\mathrm{u}}(\hat{s})\delta(1-x) \Big\} \\
&\quad \times \frac{1}{x} \int \mathrm{d}\tilde{\Phi}_{0,\bar{\mathrm{d}}\mathrm{u}}(\hat{s},x) |\mathcal{M}_{\mathrm{u\bar{d}}\to l^+\nu_l \mathrm{g}}(p_a, xp_b, \tilde{k}_l, \tilde{k}_n, \tilde{k}_c)|^2 \Theta_{\mathrm{cut}}(p_a, xp_b; \tilde{k}_l, \tilde{k}_n, \tilde{k}_c, 0)\,, \qquad \text{(C.29)}
\end{aligned}$$

where the kernels containing the singularities are given by

$$\mathcal{G}^{(\mathrm{sub})}_{ab}(\hat{s},x) = P_{ff}(x)\left[\ln\left(\frac{\hat{s}}{m_a^2}\right) - 1\right] + 1 - x\,, \qquad \text{(C.30)}$$

$$G^{(\mathrm{sub})}_{ab}(\hat{s}) = \mathcal{L}(\hat{s}, m_a^2) - \frac{\pi^2}{3} + 2\,, \qquad \text{(C.31)}$$

with the abbreviation from (4.2.17),

$$\mathcal{L}(P^2, m^2) = \ln\left(\frac{m^2}{P^2}\right)\ln\left(\frac{\lambda^2}{P^2}\right) + \ln\left(\frac{\lambda^2}{P^2}\right) - \frac{1}{2}\ln^2\left(\frac{m^2}{P^2}\right) + \frac{1}{2}\ln\left(\frac{m^2}{P^2}\right). \qquad \text{(C.32)}$$

Here, λ is a small photon mass to regularize the soft singularity occurring at $x = 1$, and $\lambda^2 \ll m^2 \ll |P^2|$ is valid. In (C.29), the LO momenta that enter $|\mathcal{M}_{\mathrm{u\bar{d}}\to l^+\nu_l \mathrm{g}}|^2$ are defined on the LO phase-space sets $\tilde{\Phi}_{0,\mathrm{u\bar{d}}}$ and $\tilde{\Phi}_{0,\bar{\mathrm{d}}\mathrm{u}}$ that are constructed using the incoming momenta xp_a and p_b in the $\mathrm{u\bar{d}}$ case or p_a and xp_b in the $\bar{\mathrm{d}}\mathrm{u}$ case, respectively. Note that two independent phase-space sets have to be generated, one set for $x < 1$ and one for $x = 1$.

For the contributions corresponding to an IS emitter and a FS spectator we obtain

$$\begin{aligned}
\int \mathrm{d}\Phi_\gamma |\mathcal{M}_{\mathrm{sub},\mathrm{u}l}|^2 &= -\frac{\alpha}{2\pi} Q_u \sigma_u Q_l \sigma_l \int_0^1 \mathrm{d}x \Big\{ \left[\mathcal{G}^{(\mathrm{sub})}_{\mathrm{u}l}(P^2_{\mathrm{u}l},x)\right]_+ + G^{(\mathrm{sub})}_{\mathrm{u}l}(P^2_{\mathrm{u}l})\delta(1-x) \Big\} \\
&\quad \times \frac{1}{x} \int \mathrm{d}\tilde{\Phi}_{0,\mathrm{u}l}(P^2_{\mathrm{u}l},x) |\mathcal{M}_{\mathrm{u\bar{d}}\to l^+\nu_l \mathrm{g}}(xp_a, p_b; \tilde{k}_l, \tilde{k}_n, \tilde{k}_c)|^2 \\
&\qquad \times \Theta_{\mathrm{cut}}(xp_a, p_b; \tilde{k}_l, \tilde{k}_n, \tilde{k}_c, 0)\,, \\
\int \mathrm{d}\Phi_\gamma |\mathcal{M}_{\mathrm{sub},\bar{\mathrm{d}}l}|^2 &= -\frac{\alpha}{2\pi} Q_d \sigma_d Q_l \sigma_l \int_0^1 \mathrm{d}x \Big\{ \left[\mathcal{G}^{(\mathrm{sub})}_{\bar{\mathrm{d}}l}(P^2_{\bar{\mathrm{d}}l},x)\right]_+ + G^{(\mathrm{sub})}_{\bar{\mathrm{d}}l}(P^2_{\bar{\mathrm{d}}l})\delta(1-x) \Big\} \\
&\quad \times \frac{1}{x} \int \mathrm{d}\tilde{\Phi}_{0,\bar{\mathrm{d}}l}(P^2_{\bar{\mathrm{d}}l},x) |\mathcal{M}_{\mathrm{u\bar{d}}\to l^+\nu_l \mathrm{g}}(p_a, xp_b; \tilde{k}_l, \tilde{k}_n, \tilde{k}_c)|^2 \\
&\qquad \times \Theta_{\mathrm{cut}}(p_a, xp_b; \tilde{k}_l, \tilde{k}_n, \tilde{k}_c, 0)\,, \qquad \text{(C.33)}
\end{aligned}$$

where the momenta that are used to calculate $|\mathcal{M}_{\mathrm{u\bar{d}}\to l^+\nu_l \mathrm{g}}|^2$ are defined on the phase-space sets $\tilde{\Phi}_{0,\mathrm{u}l}$ and $\tilde{\Phi}_{0,\bar{\mathrm{d}}l}$ that are constructed from the incoming momenta xp_a and p_b in the ul

case or p_a and xp_b in the $\bar{\mathrm{d}}l$ case, respectively. The universal kernels $\mathcal{G}_{ai}$ and G_{ai} for an IS emitter a and a FS spectator i are given by

$$\mathcal{G}_{ai}^{(\mathrm{sub})}(P_{ia}^2,x) = P_{ff}(x)\left[\ln\left(\frac{|P_{ia}^2|}{m_a^2 x}\right)-1\right] - \frac{2}{1-x}\ln(2-x) + (1+x)\ln(1-x) + 1 - x\,, \tag{C.34}$$

$$G_{ai}^{(\mathrm{sub})}(P_{ia}^2) = \mathcal{L}(|P_{ia}^2|,m_a^2) + \frac{\pi^2}{6} - 1\,, \tag{C.35}$$

where the four-vector

$$P_{ia}^{\mu}(x) = \tilde{k}_i^{\mu}(x) - xp_a^{\mu} \tag{C.36}$$

is constructed from the four-momenta of the underlying process and thus implicitly depends on x. In the endpoint of the $[\ldots]_+$ distribution in (C.33), however, one has to use $P_{ia}^2(1)$ that is evaluated from the phase-space set generated for $x = 1$.

Finally, the readded counterparts for the two contributions with the antilepton as FS emitter and one light quark as IS spectator are given by

$$\begin{aligned}
&\int \mathrm{d}\Phi_\gamma |\mathcal{M}_{\mathrm{sub},l\mathrm{u}}(\Phi_\gamma)|^2 = -\frac{\alpha}{2\pi} Q_l\sigma_l Q_u\sigma_u \int_0^1 \mathrm{d}x \int \mathrm{d}\tilde{\Phi}_{0,l\mathrm{u}}(P_{l\mathrm{u}}^2,x) \int_0^1 \mathrm{d}z \\
&\times \Theta_{\mathrm{cut}}\big(xp_a,p_b;k_l' = z\tilde{k}_l,\tilde{k}_n,\tilde{k}_c,k_\gamma' = (1-z)\tilde{k}_l\big) \\
&\times \frac{1}{x}\Big\{ G_{lu}^{(\mathrm{sub})}(P_{l\mathrm{u}}^2)\delta(1-x)\delta(1-z) + \big[\mathcal{G}_{l\mathrm{u}}^{(\mathrm{sub})}(P_{l\mathrm{u}}^2,x)\big]_+\delta(1-z) + \big[\bar{\mathcal{G}}_{l\mathrm{u}}^{(\mathrm{sub})}(P_{l\mathrm{u}}^2,z)\big]_+\delta(1-x) \\
&\qquad + \big[\bar{g}_{lu}^{(\mathrm{sub})}(x,z)\big]_+^{(x,z)}\Big\} \Big|\mathcal{M}_{\mathrm{u}\bar{\mathrm{d}}\to l^+\nu_l\mathrm{g}}\big(xp_a,p_b;\tilde{k}_l,\tilde{k}_n,\tilde{k}_c\big)\Big|^2\,,
\end{aligned} \tag{C.37a}$$

$$\begin{aligned}
&\int \mathrm{d}\Phi_\gamma |\mathcal{M}_{\mathrm{sub},l\bar{\mathrm{d}}}(\Phi_\gamma)|^2 = -\frac{\alpha}{2\pi} Q_l\sigma_l Q_d\sigma_d \int_0^1 \mathrm{d}x \int \mathrm{d}\tilde{\Phi}_{0,l\bar{\mathrm{d}}}(P_{l\bar{\mathrm{d}}}^2,x) \int_0^1 \mathrm{d}z \\
&\times \Theta_{\mathrm{cut}}\big(p_a,xp_b;k_l' = z\tilde{k}_l(x),\tilde{k}_n,\tilde{k}_c,k_\gamma' = (1-z)\tilde{k}_l\big) \\
&\times \frac{1}{x}\Big\{ G_{l\bar{\mathrm{d}}}^{(\mathrm{sub})}(P_{l\bar{\mathrm{d}}}^2)\delta(1-x)\delta(1-z) + \big[\mathcal{G}_{l\bar{\mathrm{d}}}^{(\mathrm{sub})}(P_{l\bar{\mathrm{d}}}^2,x)\big]_+\delta(1-z) + \big[\bar{\mathcal{G}}_{l\bar{\mathrm{d}}}^{(\mathrm{sub})}(P_{l\bar{\mathrm{d}}}^2,z)\big]_+\delta(1-x) \\
&\qquad + \big[\bar{g}_{l\bar{\mathrm{d}}}^{(\mathrm{sub})}(x,z)\big]_+^{(x,z)}\Big\} \Big|\mathcal{M}_{\mathrm{u}\bar{\mathrm{d}}\to l^+\nu_l\mathrm{g}}\big(p_a,xp_b;\tilde{k}_l,\tilde{k}_n,\tilde{k}_c\big)\Big|^2\,,
\end{aligned} \tag{C.37b}$$

where we have used the iterated (+)-distribution (4.2.28). The kernels in (C.37) explicitly read

$$\bar{g}_{ia}^{(\mathrm{sub})}(x,z) = \frac{1}{1-x}\Big(\frac{2}{2-x-z} - 1 - z\Big)\,, \tag{C.38}$$

$$\mathcal{G}_{ia}^{(\mathrm{sub})}(P_{ia}^2,x) = \frac{1}{1-x}\Big[2\ln\Big(\frac{2-x}{1-x}\Big) - \frac{3}{2}\Big]\,, \tag{C.39}$$

$$\bar{\mathcal{G}}_{ia}^{(\mathrm{sub})}(P_{ia}^2,z) = P_{ff}(z)\Big[\ln\Big(\frac{-P_{ia}^2 z}{m_i^2}\Big) - 1\Big] - \frac{2\ln(2-x)}{1-z} + (1+z)\ln(1-z) + 1 - z\,, \tag{C.40}$$

$$G_{ia}^{(\mathrm{sub})}(P_{ia}^2) = \mathcal{L}(|P_{ia}^2|,m_i^2) - \frac{\pi^2}{2} + \frac{3}{2}\,. \tag{C.41}$$

In (C.37) the momenta of the photon and the FS lepton that enter the cut function have to be reconstructed from the lepton momentum of the underlying hard process.

Convolution terms for the channel ug $\to l^+\nu_l \mathrm{d}\gamma$

Additionally, one now has to cover the situation with a FS emitter and a FS spectator. In this case, the readded counterpart reads

$$\begin{aligned}\int \mathrm{d}\Phi_\gamma |\mathcal{M}_{\mathrm{sub},l\mathrm{d}}(\Phi_\gamma)|^2 &= -\frac{\alpha}{2\pi} Q_l \sigma_l Q_d \sigma_d \int \mathrm{d}\tilde{\Phi}_{0,l\mathrm{d}}(P^2_{l\mathrm{d}}) \int_0^1 \mathrm{d}z \\ &\times \left\{ G^{(\mathrm{sub})}_{l\mathrm{d}}(P^2_{l\mathrm{d}})\delta(1-z) + \left[\bar{\mathcal{G}}^{(\mathrm{sub})}_{l\mathrm{d}}(P^2_{l\mathrm{d}}, z)\right]_+ \right\} \\ &\times \left| \mathcal{M}_{\mathrm{ug}\to l^+\nu_l \mathrm{d}}(p_a, p_b; \tilde{k}_l, \tilde{k}_n, \tilde{k}_c) \right|^2 \Theta_{\mathrm{cut}}\big(p_a, p_b; k'_l = z\tilde{k}_l, \tilde{k}_n, \tilde{k}_c, k'_\gamma = (1-z)\tilde{k}_l\big)\,, \end{aligned} \tag{C.42}$$

$$\begin{aligned}\int \mathrm{d}\Phi_\gamma |\mathcal{M}_{\mathrm{sub},\mathrm{d}l}(\Phi_\gamma)|^2 &= -\frac{\alpha}{2\pi} Q_d \sigma_d Q_l \sigma_l \int \mathrm{d}\tilde{\Phi}_{0,\mathrm{d}l}(P^2_{\mathrm{d}l}) \int_0^1 \mathrm{d}z \\ &\times \left\{ G^{(\mathrm{sub})}_{\mathrm{d}l}(P^2_{\mathrm{d}l})\delta(1-z) + \left[\bar{\mathcal{G}}^{(\mathrm{sub})}_{\mathrm{d}l}(P^2_{\mathrm{d}l}, z)\right]_+ \right\} \\ &\times \left| \mathcal{M}_{\mathrm{ug}\to l^+\nu_l \mathrm{d}}(p_a, p_b; \tilde{k}_l, \tilde{k}_n, \tilde{k}_c) \right|^2 \Theta_{\mathrm{cut}}\big(p_a, p_b; \tilde{k}_l, \tilde{k}_n, k'_c = z\tilde{k}_c, k'_\gamma = (1-z)\tilde{k}_c\big)\,, \end{aligned} \tag{C.43}$$

where the LO phase-space sets $\tilde{\Phi}_{0,l\mathrm{d}}$ and $\tilde{\Phi}_{0,\mathrm{d}l}$ are generated using the IS momenta p_a and p_b. The kernels containing the collinear and soft singularities are given by

$$\bar{\mathcal{G}}^{(\mathrm{sub})}_{ij}(P^2_{ij}, z) = P_{ff}(z)\left[\ln\left(\frac{P^2_{ij} z}{m_i^2}\right) - 1\right] + (1+z)\ln(1-z) + 1 - z\,, \tag{C.44}$$

$$G^{(\mathrm{sub})}_{ij}(P^2_{ij}, z) = \mathcal{L}(P^2_{ij}, m_i^2) - \frac{\pi^2}{3} + \frac{3}{2}\,, \tag{C.45}$$

where we have used the four-vector

$$P^\mu_{ij} = \tilde{k}^\mu_i + \tilde{k}^\mu_j\,, \tag{C.46}$$

which again has to be constructed from the four-momenta of the underlying process and therefore is a dynamical quantity.

Bibliography

[1] N. Besson, M. Boonekamp, E. Klinkby, T. Petersen and S. Mehlhase [ATLAS Collaboration], Eur. Phys. J. C **57** (2008) 627 [arXiv:0805.2093 [hep-ex]].

[2] C. E. Gerber *et al.* [TeV4LHC Top and Electroweak Working Group], "Tevatron-for-LHC report: Top and electroweak physics," arXiv:0705.3251 [hep-ph].

[3] J. Alcaraz *et al.* [LEP Collaborations and ALEPH Collaboration and DELPHI Collaboration an], arXiv:0712.0929 [hep-ex].

[4] C. Amsler *et al.* [Particle Data Group], Phys. Lett. B **667**, 1 (2008).

[5] S. Haywood *et al.*, arXiv:hep-ph/0003275.

[6] D. Froidevaux and V. A. Mitsou, J. Phys. Conf. Ser. **171**, 012021 (2009) [arXiv:0905.0258 [hep-ex]].

[7] V. Büscher *et al.* [TeV4LHC Landscape Working Group], "Tevatron-for-LHC report: Preparations for discoveries," hep-ph/0608322.

[8] G. Aad *et al.* [The ATLAS Collaboration], arXiv:0901.0512 [hep-ex].

[9] T. Aaltonen *et al.* [CDF Collaboration], Phys. Rev. D **78** (2008) 032008 [arXiv:0803.3493 [hep-ex]].

[10] K. Jakobs, Eur. Phys. J. C **59** (2009) 463.

[11] W. L. van Neerven and E. B. Zijlstra, Nucl. Phys. B **382** (1992) 11 [Erratum-ibid. B **680** (2004) 513];
R. V. Harlander and W. B. Kilgore, Phys. Rev. Lett. **88** (2002) 201801 [hep-ph/0201206];
C. Anastasiou, L. J. Dixon, K. Melnikov and F. Petriello, Phys. Rev. Lett. **91** (2003) 182002 [hep-ph/0306192];
C. Anastasiou, L. J. Dixon, K. Melnikov and F. Petriello, Phys. Rev. D **69** (2004) 094008 [hep-ph/0312266];
S. Catani, L. Cieri, G. Ferrera, D. de Florian and M. Grazzini, arXiv:0903.2120 [hep-ph].

[12] S. Moch and A. Vogt, Phys. Lett. B **631** (2005) 48 [hep-ph/0508265];
E. Laenen and L. Magnea, Phys. Lett. B **632**, 270 (2006) [hep-ph/0508284];
A. Idilbi, X. d. Ji, J. P. Ma and F. Yuan, Phys. Rev. D **73**, 077501 (2006) [hep-ph/0509294];

V. Ravindran and J. Smith, Phys. Rev. D **76**, 114004 (2007) [arXiv:0708.1689 [hep-ph]].

[13] S. Frixione and B. R. Webber, hep-ph/0612272.

[14] C. Balazs and C. P. Yuan, Phys. Rev. D **56** (1997) 5558 [hep-ph/9704258];
R. K. Ellis and S. Veseli, Nucl. Phys. B **511** (1998) 649 [hep-ph/9706526];
A. Kulesza and W. J. Stirling, JHEP **0001** (2000) 016 [hep-ph/9909271].

[15] S. Frixione and M. L. Mangano, JHEP **0405** (2004) 056 [hep-ph/0405130].

[16] V. A. Zykunov, Eur. Phys. J. direct C **3** (2001) 1 [hep-ph/0107059].

[17] S. Dittmaier and M. Krämer, Phys. Rev. D **65** (2002) 073007 [hep-ph/0109062].

[18] U. Baur and D. Wackeroth, Phys. Rev. D **70** (2004) 073015 [hep-ph/0405191];
A. Arbuzov, D. Bardin, S. Bondarenko, P. Christova, L. Kalinovskaya, G. Nanava and R. Sadykov, Eur. Phys. J. C **46** (2006) 407 [Erratum-ibid. C **50** (2007) 505] [hep-ph/0506110].

[19] C. M. Carloni Calame, G. Montagna, O. Nicrosini and A. Vicini, JHEP **0612** (2006) 016 [hep-ph/0609170].

[20] C. M. Carloni Calame, G. Montagna, O. Nicrosini and M. Treccani, Phys. Rev. D **69** (2004) 037301 [hep-ph/0303102].

[21] W. Placzek and S. Jadach, Eur. Phys. J. C **29** (2003) 325 [hep-ph/0302065];
C. M. Carloni Calame, S. Jadach, G. Montagna, O. Nicrosini and W. Placzek, Acta Phys. Polon. B **35** (2004) 1643 [hep-ph/0402235].

[22] S. Brensing, S. Dittmaier, M. Krämer and A. Mück, Phys. Rev. D **77** (2008) 073006 [arXiv:0710.3309 [hep-ph]].

[23] S. Dittmaier and M. Krämer, in
C. Buttar *et al.*, *"Les Houches physics at TeV colliders 2005, standard model, QCD, EW, and Higgs working group: Summary report,"* hep-ph/0604120.

[24] A. B. Arbuzov and R. R. Sadykov, arXiv:0707.0423 [hep-ph].

[25] Q. H. Cao and C. P. Yuan, Phys. Rev. Lett. **93** (2004) 042001 [hep-ph/0401026];
B. F. L. Ward, C. Glosser, S. Jadach and S. A. Yost, Int. J. Mod. Phys. A **20** (2005) 3735 [hep-ph/0411047];
B. F. L. Ward and S. A. Yost, Acta Phys. Polon. B **38** (2007) 2395 [arXiv:0704.0294 [hep-ph]].

[26] G. Balossini *et al.*, arXiv:0907.0276 [hep-ph].

[27] W. T. Giele, E. W. N. Glover and D. A. Kosower, Nucl. Phys. B **403** (1993) 633 [hep-ph/9302225].

[28] J. M. Campbell and R. K. Ellis, Phys. Rev. D **65** (2002) 113007 [hep-ph/0202176].

[29] C. F. Berger *et al.*, arXiv:0907.1984 [hep-ph].

[30] R. K. Ellis, K. Melnikov and G. Zanderighi, JHEP **0904** (2009) 077 [arXiv:0901.4101 [hep-ph]];
C. F. Berger *et al.*, arXiv:0902.2760 [hep-ph].

[31] T. Kasprzik, *"Electroweak corrections to the hadroproduction of W bosons and jets. (In German)"*, Diploma Thesis, Hamburg 2006.

[32] A. Denner, S. Dittmaier, M. Roth and D. Wackeroth, Nucl. Phys. B **560** (1999) 33 [hep-ph/9904472].

[33] A. Denner, S. Dittmaier, M. Roth and L. H. Wieders, Nucl. Phys. B **724** (2005) 247 [hep-ph/0505042].

[34] D. Buskulic *et al.* [ALEPH Collaboration], Z. Phys. C **69** (1996) 365.

[35] S. Dittmaier, Nucl. Phys. B **565** (2000) 69 [hep-ph/9904440].

[36] S. Dittmaier, A. Kabelschacht and T. Kasprzik, Nucl. Phys. B **800** (2008) 146 [arXiv:0802.1405 [hep-ph]].

[37] W. Hollik, T. Kasprzik and B. A. Kniehl, Nucl. Phys. B **790** (2008) 138 [arXiv:0707.2553 [hep-ph]].

[38] J. H. Kühn, A. Kulesza, S. Pozzorini and M. Schulze, Phys. Lett. B **651** (2007) 160 [hep-ph/0703283].

[39] J. H. Kühn, A. Kulesza, S. Pozzorini and M. Schulze, Nucl. Phys. B **797** (2008) 27 [arXiv:0708.0476 [hep-ph]].

[40] G. J. Gounaris, J. Layssac and F. M. Renard, Phys. Rev. D **77** (2008) 013003 [arXiv:0709.1789 [hep-ph]].

[41] A. Denner, S. Dittmaier, T. Kasprzik and A. Mück, arXiv:0906.1656 [hep-ph].

[42] O. W. Greenberg, Phys. Rev. Lett. **13**, 598 (1964).

[43] M. Y. Han and Y. Nambu, Phys. Rev. **139**, B1006 (1965).

[44] H. Fritzsch, M. Gell-Mann and H. Leutwyler, Phys. Lett. B **47**, 365 (1973).

[45] P. W. Higgs, Phys. Lett. **12**, 132 (1964);
P. W. Higgs, Phys. Rev. Lett. **13**, 508 (1964);
P. W. Higgs, Phys. Rev. **145**, 1156 (1966);
F. Englert and R. Brout, Phys. Rev. Lett. **13**, 321 (1964);
T. W. B. Kibble, Phys. Rev. **155**, 1554 (1967).

[46] V. N. Popov and L. D. Faddeev, In *"Lai, C. H. (ed.): Gauge Theory Of Weak and Electromagnetic Interactions"* , 213-233 and Kiev Inst. Theor. Phys. Acad. Sci. - ITF-67-036 (67,REC.APR.68) 28 P. (803533) (SEE BOOK INDEX).

[47] A. Denner, Fortsch. Phys. **41**, 307 (1993) [arXiv:0709.1075 [hep-ph]].

[48] M. Böhm, A. Denner and H. Joos, *"Gauge theories of the Strong and Electroweak Interaction,"* Stuttgart, Germany: Teubner (2001) 784 p.

[49] S. L. Glashow, Nucl. Phys. **22** (1961) 579;
S. Weinberg, Phys. Rev. Lett. **19** (1967) 1264;
S. L. Glashow, J. Iliopoulos and L. Maiani, Phys. Rev. D **2**, 1285 (1970);
A. Salam, Originally printed in *"Svartholm: Elementary Particle Theory, Proceedings Of The Nobel Symposium Held 1968 At Lerum, Sweden"*, Stockholm 1968, 367-377.

[50] G. 't Hooft and M. J. G. Veltman, Nucl. Phys. B **44**, 189 (1972).

[51] C. G. Bollini and J. J. Giambiagi, Phys. Lett. B **40**, 566 (1972).

[52] G. 't Hooft, Nucl. Phys. B **33**, 173 (1971).

[53] G. 't Hooft, Nucl. Phys. B **35**, 167 (1971).

[54] D. A. Ross and J. C. Taylor, Nucl. Phys. B **51**, 125 (1973) [Erratum-ibid. B **58**, 643 (1973)].

[55] A. Denner, S. Dittmaier and T. Hahn, Phys. Rev. D **56**, 117 (1997) [arXiv:hep-ph/9612390].

[56] A. Sirlin, Phys. Rev. Lett. **67**, 2127 (1991).

[57] P. Gambino and P. A. Grassi, Phys. Rev. D **62**, 076002 (2000) [arXiv:hep-ph/9907254].

[58] A. Denner and S. Dittmaier, Nucl. Phys. Proc. Suppl. **160** (2006) 22 [hep-ph/0605312].

[59] R. P. Feynman, Phys. Rev. Lett. **23**, 1415 (1969).

[60] J. D. Bjorken and E. A. Paschos, Phys. Rev. **185**, 1975 (1969).

[61] J. C. Collins, D. E. Soper and G. Sterman, Adv. Ser. Direct. High Energy Phys. **5**, 1 (1988) [arXiv:hep-ph/0409313].

[62] R. K. Ellis, W. J. Stirling and B. R. Webber, Camb. Monogr. Part. Phys. Nucl. Phys. Cosmol. **8** (1996) 1.

[63] S. Dittmaier, Nucl. Phys. B **675**, 447 (2003) [arXiv:hep-ph/0308246].

[64] F. Bloch and A. Nordsieck, Phys. Rev. **52** (1937) 54.

[65] G. 't Hooft and M. J. G. Veltman, Nucl. Phys. B **153**, 365 (1979).

[66] S. Catani and M. H. Seymour, Nucl. Phys. B **485** (1997) 291 [Erratum-ibid. B **510** (1998) 503] [arXiv:hep-ph/9605323].

[67] T. Kinoshita, J. Math. Phys. **3** (1962) 650;
T. D. Lee and M. Nauenberg, Phys. Rev. **133** (1964) B1549.

[68] K. P. Diener, S. Dittmaier and W. Hollik, Phys. Rev. D **72** (2005) 093002 [hep-ph/0509084].

[69] S. Catani, Y. L. Dokshitzer, M. H. Seymour and B. R. Webber, Nucl. Phys. B **406**, 187 (1993);
S. V. Chekanov, arXiv:hep-ph/0211298;
G. P. Salam, arXiv:0705.2696 [hep-ph];
M. Cacciari, G. P. Salam and G. Soyez, JHEP **0804**, 063 (2008) [arXiv:0802.1189 [hep-ph]];
G. Soyez, arXiv:0807.0021 [hep-ph];
S. D. Ellis and D. E. Soper, Phys. Rev. D **48**, 3160 (1993) [arXiv:hep-ph/9305266].

[70] G. C. Blazey *et al.*, arXiv:hep-ex/0005012.

[71] S. Catani and M. H. Seymour, Phys. Lett. B **378** (1996) 287 [hep-ph/9602277].

[72] E. W. N. Glover and A. G. Morgan, Z. Phys. C **62** (1994) 311.

[73] R. K. Ellis, D. A. Ross and A. E. Terrano, Nucl. Phys. B **178** (1981) 421;
S. D. Ellis, Z. Kunszt and D. E. Soper, Phys. Rev. D **40** (1989) 2188;
M. L. Mangano, P. Nason and G. Ridolfi, Nucl. Phys. B **373** (1992) 295;
Z. Kunszt and D. E. Soper, Phys. Rev. D **46** (1992) 192;
S. Frixione, Z. Kunszt and A. Signer, Nucl. Phys. B **467** (1996) 399 [hep-ph/9512328];
Z. Nagy and Z. Trócsányi, Nucl. Phys. B **486** (1997) 189 [hep-ph/9610498];
J. M. Campbell, M. A. Cullen and E. W. N. Glover, Eur. Phys. J. C **9** (1999) 245 [hep-ph/9809429].

[74] L. Phaf and S. Weinzierl, JHEP **0104** (2001) 006 [hep-ph/0102207].

[75] S. Catani, S. Dittmaier, M. H. Seymour and Z. Trócsányi, Nucl. Phys. B **627** (2002) 189 [hep-ph/0201036].

[76] B. A. Kniehl, Phys. Lett. B **254**, 267 (1991).

[77] M. Glück, M. Stratmann and W. Vogelsang, Phys. Lett. B **343**, 399 (1995).

[78] A. D. Martin, R. G. Roberts, W. J. Stirling and R. S. Thorne, Eur. Phys. J. C **39**, 155 (2005) [arXiv:hep-ph/0411040].

[79] S. Dittmaier, *"Gauge-boson production in electron - photon collisions,"* Phd Thesis, Würzburg, 1993.

[80] J. Küblbeck, M. Böhm and A. Denner, Comput. Phys. Commun. **60** (1990) 165;
H. Eck and J. Küblbeck, *Guide to FeynArts 1.0*, University of Würzburg, 1992.

[81] T. Hahn, Comput. Phys. Commun. **140** (2001) 418 [hep-ph/0012260];
T. Hahn and C. Schappacher, Comput. Phys. Commun. **143** (2002) 54 [hep-ph/0105349].

[82] T. Hahn and M. Perez-Victoria, Comput. Phys. Commun. **118** (1999) 153 [hep-ph/9807565].

[83] G. Passarino and M. J. G. Veltman, Nucl. Phys. B **160** (1979) 151.

[84] R. Mertig, M. Bohm and A. Denner, Comput. Phys. Commun. **64**, 345 (1991).

[85] T. Hahn, Acta Phys. Polon. B **30**, 3469 (1999) [arXiv:hep-ph/9910227];
T. Hahn, Nucl. Phys. Proc. Suppl. **89**, 231 (2000) [arXiv:hep-ph/0005029];
T. Hahn and M. Rauch, Nucl. Phys. Proc. Suppl. **157**, 236 (2006) [arXiv:hep-ph/0601248].

[86] G. J. van Oldenborgh, Comput. Phys. Commun. **66**, 1 (1991).

[87] G. P. Lepage, "Vegas: An Adaptive Multidimensional Integration Program", Cornell preprint CLNS 80-447, March 1980.

[88] T. Hahn, Nucl. Instrum. Meth. A **559**, 273 (2006) [arXiv:hep-ph/0509016];
T. Hahn, Comput. Phys. Commun. **168**, 78 (2005) [arXiv:hep-ph/0404043].

[89] A. Sirlin, Phys. Rev. D **22**, 971 (1980).

[90] W. Beenakker and A. Denner, Nucl. Phys. B **338**, 349 (1990).

[91] U. Baur, S. Keller and D. Wackeroth, Phys. Rev. D **59**, 013002 (1999) [arXiv:hep-ph/9807417].

[92] K. P. O. Diener, S. Dittmaier and W. Hollik, Phys. Rev. D **69** (2004) 073005 [arXiv:hep-ph/0310364];
K. P. O. Diener, S. Dittmaier and W. Hollik, Nucl. Phys. Proc. Suppl. **135**, 183 (2004).

[93] K. Fabricius, I. Schmitt, G. Kramer and G. Schierholz, Z. Phys. C **11**, 315 (1981);
G. Kramer and B. Lampe, Fortsch. Phys. **37**, 161 (1989).

[94] R. Kleiss, Z. Phys. C **33**, 433 (1987).

[95] G. Altarelli and G. Parisi, Nucl. Phys. B **126**, 298 (1977).

[96] W. M. Yao *et al.* [Particle Data Group], J. Phys. G **33**, 1 (2006).

[97] J. Pumplin, D. R. Stump, J. Huston, H. L. Lai, P. M. Nadolsky and W. K. Tung, JHEP **0207**, 012 (2002) [arXiv:hep-ph/0201195].

[98] P. Ciafaloni and D. Comelli, Phys. Lett. B **446** (1999) 278 [hep-ph/9809321];
V. S. Fadin, L. N. Lipatov, A. D. Martin and M. Melles, Phys. Rev. D **61** (2000) 094002 [hep-ph/9910338];
A. Denner and S. Pozzorini, Eur. Phys. J. C **18** (2001) 461 [hep-ph/0010201];
W. Beenakker and A. Werthenbach, Nucl. Phys. B **630** (2002) 3 [hep-ph/0112030];
A. Denner, M. Melles and S. Pozzorini, Nucl. Phys. B **662** (2003) 299 [hep-ph/0301241].

[99] A. Denner, S. Dittmaier, T. Gehrmann and C. Kurz, arXiv:0906.0372 [hep-ph].

[100] S. Dittmaier, Phys. Rev. D **59**, 016007 (1999) [arXiv:hep-ph/9805445].

[101] E. Accomando, A. Denner and C. Meier, Eur. Phys. J. C **47** (2006) 125 [arXiv:hep-ph/0509234].

[102] S. Dittmaier and M. Roth, Nucl. Phys. B **642** (2002) 307 [arXiv:hep-ph/0206070].

[103] A. Bredenstein, A. Denner, S. Dittmaier and S. Pozzorini, JHEP **0808**, 108 (2008) [arXiv:0807.1248 [hep-ph]].

[104] M. L. Ciccolini, S. Dittmaier and M. Krämer, Phys. Rev. D **68** (2003) 073003 [arXiv:hep-ph/0306234].

[105] M. J. G. Veltman, Nucl. Phys. B **319**, 253 (1989).

[106] A. Denner and S. Dittmaier, Nucl. Phys. B **658** (2003) 175 [hep-ph/0212259].

[107] A. Denner and S. Dittmaier, Nucl. Phys. B **734** (2006) 62 [hep-ph/0509141].

[108] A. Denner, S. Dittmaier, M. Roth and M.M. Weber, Nucl. Phys. B **660** (2003) 289 [hep-ph/0302198].

[109] A. Denner, U. Nierste and R. Scharf, Nucl. Phys. B **367** (1991) 637.

[110] A. Denner and S. Dittmaier, in preparation.

[111] D. Y. Bardin, A. Leike, T. Riemann and M. Sachwitz, Phys. Lett. B **206**, 539 (1988).

[112] C. W. Bauer and B. O. Lange, arXiv:0905.4739 [hep-ph].

[113] M. Roth, *"Precise predictions for four-fermion production in electron positron annihilation"*, Phd Thesis, Zürich 1999, arXiv:hep-ph/0008033.

[114] S. Kallweit, *"Precision Calculations for Gauge-Boson Pair Production with a Hadronic Jet at Hadron Colliders"*, Phd Thesis, LMU München 2008.

Acknowledgments

First of all, I am grateful to Stefan Dittmaier for providing such a productive working atmosphere and for three years of continuous great support in theoretical and practical questions, allowing me to benefit from his profound experience and knowledge. Special thanks also go to Alexander Mück for a motivating and fruitful collaboration and many instructive and helpful discussions about our project and the manuscript of my thesis.

I am thankful to my officemate Thomas Hahn for an enjoyable time and many interesting conversations. Of course, I also have to thank him for helping me with various computer problems.

Many thanks are given to all my colleagues in the MPI theory group for the great atmosphere and the free and open discussion culture. Especially, I have profited from stimulating and clarifying discussions with Max Huber, Stefan Kallweit, Marina Billoni, Maike Trenkel, Edoardo Mirabella, Jan Germer, and Ananda Landwehr. In particular I would like to thank Max Huber, Marina Billoni, and Ananda Landwehr for reading parts of the manuscript.

I am also much obliged to all the people who contributed to the nice and illustrative conversations during the countless interesting afternoon coffee breaks at the MPI. Moreover, I have to thank my fellow PhD students for many unforgettable common activities and a great time in Munich.

Finally, I want to thank all my friends who continuously supported me and—if necessary—cheered me up during the last years. I am especially indebted to my parents for their patience, encouragement, understanding, and of course also their financial support during my studies.

List of publications

1. W. Hollik, T. Kasprzik and B. A. Kniehl,
   "Electroweak corrections to W-boson hadroproduction at finite transverse momentum," Nucl. Phys. B **790**, 138 (2008) [arXiv:0707.2553 [hep-ph]].

2. S. Dittmaier, A. Kabelschacht and T. Kasprzik,
   "Polarized QED splittings of massive fermions and dipole subtraction for non-collinear-safe observables," Nucl. Phys. B **800**, 146 (2008) [arXiv:0802.1405 [hep-ph]].

3. A. Denner, S. Dittmaier, T. Kasprzik and A. Mück,
   "Electroweak corrections to W + jet hadroproduction including leptonic W-boson decays," arXiv:0906.1656 [hep-ph], to appear in JHEP.

Lebenslauf

Tobias Kasprzik

MPI für Physik,
Werner-Heisenberg-Institut
Föhringer Ring 6
80805 München
Tel.: 32354 - 300

Ickstattstrasse 7
80469 München
mobil: 0179 37 25 961
tobiask@mppmu.mpg.de

Personendaten

Geburtsdatum	05. 03. 1980
Geburtsort	Hamburg
Staatsangehörigkeit	Deutsch
Familienstand	ledig

Schulausbildung

1986 - 1990	Grundschule Königsländer Schule Hamburg
1990 - 1999	Charlotte-Paulsen-Gymnasium Hamburg
17. 06. 1999	Abschluß Abitur

Wehrdienst/Zivildienst/Soziales Jahr

1999 - 2000	Zivildienst am Allgemeinen Krankenhaus Barmbek in Hamburg

Universitätsausbildung

2000 - 2002	Physikstudium an der Universität Hamburg
25. 10. 2002	Vordiplom in Physik
2002 - 2006	Physikstudium an der Universität Hamburg
16. 06. 2006	Hauptdiplom in Physik

Promotion

Seit 01. 09. 2006	Promotion am MPI für Physik in München
15. 10. 2009	Verteidigung der Dissertation an der Albert-Ludwigs-Universität Freiburg im Breisgau

Freiburg, den 31. August 2009